UNIVERSITA' DEGLI STUDI DI PADOVA

Dipartimento di Scienze Farmaceutiche

Scuola di Dottorato in Scienze Molecolari

Indirizzo Scienze Farmaceutiche

XXII Ciclo

Struttura e Funzione dei Fattori della Coagulazione

Trombina, β2-Glicoproteina I e Fattore di von Willebrand

Direttore della Scuola: Ch.mo Prof. Maurizio CASARIN

Coordinatore di indirizzo: Ch.mo Prof.ssa Adriana CHILIN

Supervisore: Ch.mo Prof. Vincenzo DE FILIPPIS

Dottorando: Dr. Nicola POZZI

UNIVERSITY OF PADOVA

Department of Pharmaceutical Sciences

Ph.D. School in Molecular Sciences

Pharmaceutical Sciences Curriculum

XXII Cycle

Structure and Function of Coagulation Factors in Health and Disease:

Thrombin, β2-Glycoprotein I and von Willebrand Factor

School Director: Prof. Maurizio CASARIN

Curriculum Coordinator: Prof. Adriana CHILIN

Supervisor: Prof. Vincenzo DE FILIPPIS

Ph.D. Student: Nicola POZZI

Alla Vita

Nulla si ottiene senza sacrificio e senza coraggio. Se si fa una cosa apertamente, si può anche soffrire di più, ma alla fine l'azione sarà più efficace. Chi ha ragione ed è capace di soffrire alla fine vince.

(Mahatma Gandhi)

Contents

RIASSUNTO

Oggigiorno le malattie cardiovascolari rappresentano la principale causa di morte nel mondo. Secondo i dati riportati dall'Organizzazione Mondiale della Sanità (OMS), il 30% di tutti i decessi è dovuto alle malattie cardiovascolari, mentre solamente il 10-15% è dovuto alle malattie oncologiche. Tale percentuale assume maggiore rilevanza se si considera che il numero di decessi è in aumento anno dopo anno, non solo nei paesi industrializzati ad elevato reddito ma anche nei paesi in via di sviluppo dove il benessere sta lentamente alterando le abitudini alimentari e sociali dei popoli.

Il termine malattie cardiovascolari rappresenta un'ampia serie di patologie che, in modo generico, si possono ricondurre ad una disfunzione vascolare o cardiaca, quale ad esempio aterosclerosi, trombosi, ipertensione arteriosa, angina pectoris e malattie cardiache congenite. Molto spesso le malattie cardiovascolari hanno un decorso molto lungo e nel tempo invalidano gravemente la funzione non solo del distretto anatomico coinvolto, ma di tutto l'organismo.

Nell'ambito delle malattie cardiovascolari, la trombosi — ovvero un fenomeno patologico spontaneo che porta alla coagulazione del sangue —rappresenta in assoluto la prima causa di morte. La trombosi arteriosa improvvisa è di fatto la principale causa di disfunzione e di infarto del miocardio, mentre il tromboembolismo venoso è la terza causa di morte. Un'importante complicazione che riguarda lo studio delle malattie cardiovascolari consiste nella diversa morfologia ed eziogenesi dei fenomeni di trombosi arteriosa e/o venosa. Tale diversità si riflette anche sul tipo di terapia utilizzata nella pratica clinica in cui i trombi arteriosi vengono preferenzialmente trattati con antiaggreganti piastrinici mentre quelli venosi, di norma, vengono trattati con farmaci anticoagulanti. Tuttavia, molto spesso, il decorso clinico dei pazienti genera un quadro terapeutico molto più complesso in cui le strategie utilizzate devono seguire percorsi integrati e trasversali. I farmaci ad ora utilizzati, pur essendo molto efficaci nel ridurre gli episodi di trombosi nei pazienti con malattie cardiovascolari, sono limitati nel loro impiego terapeutico poiché portano frequentemente ad episodi emorragici fatali. Per ridurre l'incidenza di tale effetto collaterale e migliore pertanto la loro finestra terapeutica è necessario studiare nei dettagli l'eziogenesi di tali patologie e quindi ottenere nuovi e più efficaci strumenti terapeutici e/o di prevenzione.

Durante il mio dottorato di ricerca la mia attenzione è stata focalizzata sullo studio della struttura e della funzione di alcuni fattori della coagulazione e di loro inibitori (i.e., trombina, irudina, emadina, nexina 1, beta2-glicoproteina I, ADAMTS-13 e fattore di von Willebrand), utilizzando metodi chimici (sintesi di peptidi in fase solida, spettrometria di massa), biochimici (cinetica enzimatica e ELISA) e biofisici (fluorescenza, dicroismo circolare e SPR). In particolare in questa Tesi di Dottorato gli argomenti di studio sono stati trattati singolarmente, distinguendo i lavori in capitoli indipendenti. Brevemente nel capitolo 2 è stato indagato il rapporto struttura-funzione della trombina, una proteasi

serinica cruciale nella cascata emocoagulativa, considerando dapprima la sua natura allosterica e quindi sfruttando le informazioni ottenute come base per lo sviluppo di nuovi possibili farmaci anticoagulanti ed antiaggreganti piastrinici. Nel capitolo 3, l'attenzione è stata trasferita alla β2-glicoptoteina I (β_2GpI), una glicoproteina plasmatica che è stata recentemente identificata come il principale target di autoanticorpi coinvolti nella sindrome antifosfolipidica (APS). Lo studio della β_2GpI ha contribuito ad individuare un dominio della proteina quale epitopo conformazionale riconosciuto dagli autoanticorpi, evidenziando così la possibilità di nuovi approcci terapeutici e diagnostici nella sindrome antifosfolipidica. Infine, nel capitolo 4, è stato riportato uno studio sull'effetto dell'ossidazione mediata da perossinitrito a carico del fattore di von Willebrand (VWF). Il fattore di von Willebrand è una glicoproteina plasmatica estremamente complessa le cui dimensioni contribuiscono a regolare l'equilibrio emostatico. Nello studio di seguito riportato è stato proposto e dimostrato come l'ossidazione di un residuo di metionina situato nel dominio A2 della glicoproteina impedisca il taglio proteolitico da parte di ADAMTS-13, promuovendo uno stato protrombotico nei pazienti sottoposti ad un elevato stress ossidativo.

ABSTRACT

Cardiovascular disease (CVD) is the leading cause of death globally. According to the World Health Organization (WHO), it was responsible for 30% of all deaths in 2005 with respect, for instance, to cancer related diseases that cover only the 10-15%. Unfortunately this scenario is dramatically evolving year after year, not only in the high-income countries where risk factors such as smoking, diet and pollution are elevated but also in some developing nations where the wellness and industrialisation are changing the lifestyle and the mores of the people.

Cardiovascular disease usually stems from vascular dysfunction or heart failure which can be the result of atherosclerosis, thrombosis, high blood pressure, angina pectoris and congenital cardiovascular defects. Generally the cardiovascular disease is a long term treated disease that during time compromises not only the single district where the injury takes place but the overall organism leading to death.

Among all cardiovascular diseases, thrombosis — localized pathological clotting of the blood — can occur in the arterial or the venous circulation and has a major medical impact. Acute arterial thrombosis is the proximal cause of most cases of myocardial infarction (heart attack) and of about 80% of strokes, collectively the most common cause of death in the developed world. Venous thromboembolism is the third leading cause of cardiovascular-associated death. A great complication regarding the study of the CVD is the multiplicity and the heterogeneous system that has to be consider. For instance the pathophysiology of arterial thrombosis totally differs from that of venous thrombosis, as reflected by the different ways in which they are treated. In broad terms, arterial thrombosis is treated with drugs that target platelets, and venous thrombosis is treated with drugs that target proteins of the coagulation cascade. The available antithrombotic drugs are effective at reducing arterial thrombosis and venous thrombosis in patients with cardiovascular disease. However, the main side effect of these drugs is bleeding, which limits their use. To develop a new generation of safe and effective antithrombotic drugs with larger therapeutic windows (that is, a larger difference between the dose that prevents thrombosis and the dose that induces bleeding), a better understanding of the pathogenic processes that lead to thrombotic occlusion of blood vessels is needed.

During my Ph.D. course my efforts have been devoted to investigate specific aspects of the structure and function of blood coagulation factors and their inhibitors (i.e., thrombin, hirudin, haemadin, protease nexin-1, beta2-glycoprotein-I, ADAMTS-13 protease and von Willebrand factor) using chemical (solid-phase peptide synthesis, mass spectrometry), biochemical (enzyme kinetics) and biophysical (fluorescence, circular dichroism, surface plasmon resonance, calorimetry) techniques. Herein reported in my Ph.D. Thesis, the different treated subjects are divided into independent chapters each containing a single case study. Briefly in chapter 2 it has been proposed the study on the structure

and function of thrombin, a serine protease that exerts a pivotal role in blood coagulation. In particular it was investigated the allosteric nature of thrombin and information obtained about the enzyme was further applied to propose a rational model to finally design new possible antiaggregant and anticoagulant agents. In chapter 3 it has been reported the study on the β2-Glycoprotein I (β_2GpI), a plasma glycoprotein that has been recently recognized as the primary target for some autoantibodies (aPL) found in the autophospholipid syndrome (APS). In this study we contributed to identify a conformational epitope, corresponding to the first domain of the full-length protein, that was efficiently recognized by the plasma autoantibodies of the patients. Starting form these considerations we further propose a new therapeutic and diagnostic approach for the antiphospholipid syndrome. Finally in chapter 4, it has been reported a study concerning the effect of the oxidation mediated by peroxynitrite on von Willebrand factor. Von Willebrand factor is a plasma glycoprotein extremely complex whose dimensions play a pivotal role in maintaining haemostasis. Since peroxynitrite oxidizes a single residue of methionine in the A2 domain of VWF, protease ADAMTS-13 results unable to process the full-length VWF leading to a multimer accumulation and consequently to a prothrombotic event. Notably this mechanism has been demonstrated in vitro and, more interestingly, in patients possessing an elevated oxidative stress conditions, such as diabetes mellitus type 2.

1. INTRODUCTION

CHAPTER 1.1.

Cardiovascular Disease

Cardiovascular disease (CVD) is the leading cause of death globally: more people die annually from CVD than from any other cause. According to the World Health Organization (WHO), an estimated 17.1 million people died from CVD in 2005, representing the 30% of all global deaths. Looking forward to the next future, this scenario will become more and more alarming considering that in 2030 almost 23.6 million people will die from CVD. In fact although CVD is typically considered diseases of high-income countries, its incidence is seriously increasing in the developing world.

Considering the huge number of patients involved and the extremely world wide distribution, the attention for CVD is not only restricted to the medical practise but assumes relevant socio-economic implications. For instance the cost of cardiovascular disease in the United States in 2009 is estimated to be 475.3 billion dollars *(American Heart Association 2009)* and at least 29 billion pounds per year in UK *(University of Oxford 2009)*. Also in Italy, the 23.5% of the Italian pharmaceutical cost — calculated as 1.34% of the PIL — is spent for cardiovascular disease drugs *(ISTAT 2002)*.

Cardiovascular disease usually stems from vascular dysfunction — for example, as a result of atherosclerosis, thrombosis or high blood pressure — which then compromises organ function. Most notably, the heart and brain can be affected, as occurs in myocardial infarction and stroke, respectively. Of the overall 17.1 million deaths reported previously, an estimated 7.2 million were due to coronary heart disease and 5.7 million were due to stroke. For heart disease in particular, a wide range of underlying pathologies can lead to defective functioning of the heart muscle. In the past few decades, major improvements have been made in treating some types of cardiovascular diseases. In the case of coronary heart disease, for example, therapies such as the administration of statins and the insertion of stents have reduced death rates. However, new treatment options are urgently needed for all types of cardiovascular diseases. Moreover, improving diagnosis is crucial, because by detecting the early stages of disease, the focus of therapy could be shifted from treatment to prevention.

CHAPTER 1.2.

Treatments and New Targets for Thrombosis

Thrombosis — localized clotting of the blood — can occur in the arterial or the venous circulation and has a major medical impact. Acute arterial thrombosis is the proximal cause of most cases of myocardial infarction (heart attack) and of about 80% of strokes, collectively the most common cause of death in the developed world. Venous thromboembolism is the third leading cause of cardiovascular-associated death. The pathogenic changes that occur in the blood vessel wall and in the blood itself resulting in thrombosis are not fully understood. Understanding these processes is crucial for developing safer and more effective antithrombotic drugs.

The pathophysiology of arterial thrombosis differs from that of venous thrombosis, as reflected by the different ways in which they are treated. In broad terms, arterial thrombosis is treated with drugs that target platelets, and venous thrombosis is treated with drugs that target proteins of the coagulation cascade. The available antithrombotic drugs are effective at reducing arterial thrombosis and venous thrombosis in patients with cardiovascular disease. However, the main side effect of these drugs is bleeding, which limits their use. To develop a new generation of safe and effective antithrombotic drugs with larger therapeutic windows (that is, a larger difference between the dose that prevents thrombosis and the dose that induces bleeding), a better understanding of the pathogenic processes that lead to thrombotic occlusion of blood vessels is needed.

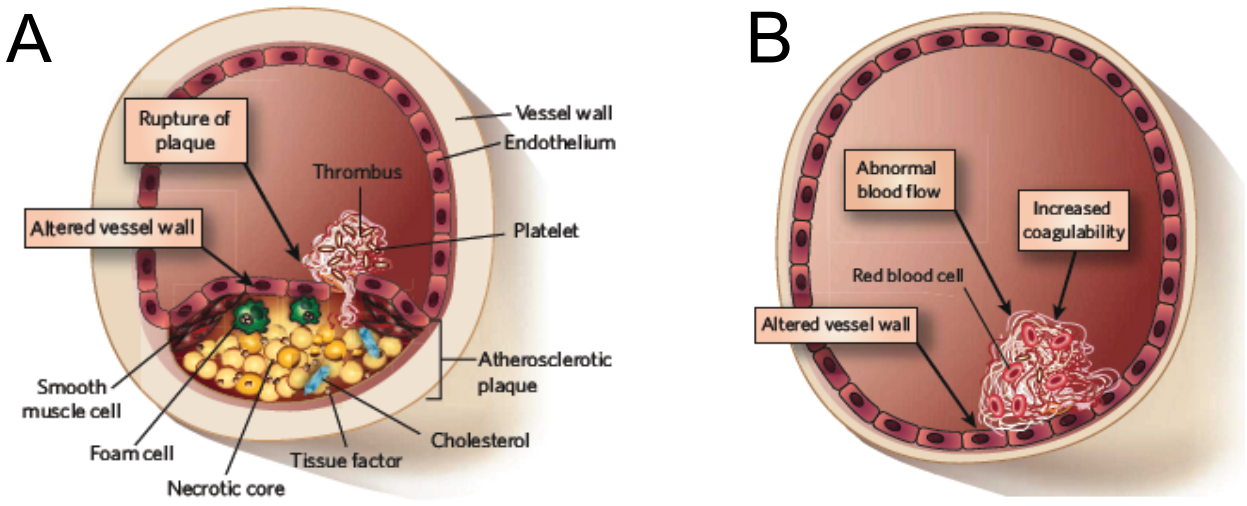

Fig. 1. Triggers of arterial and venous thrombosis. (A) Artery. The primary event that triggers to arterial thrombosis is the rupture of the atherosclerotic plaque. **(B) Vein.** By contrast in vein thrombosis the endothelium remains intact but can be converted from a surface with anticoagulants properties to one with procoagulant properties. *(Adapted form Mackman N. , Nature 2008)*

The primary trigger for arterial thrombosis is the rupture of an atherosclerotic plaque (Fig. 1A), which develops through the accumulation of lipid deposits and lipid-laden macrophages (foam cells) in the artery wall. The thrombi that form at ruptured plaques are rich in platelets, which are small (about 1 μm in diameter) anucleate cells produced by megakaryocytes in the bone marrow. These disc-shaped cells circulate in the blood as sentinels of vascular integrity and rapidly form a primary haemostatic plug at sites of vascular injury (1). When an atherosclerotic plaque ruptures, platelets are rapidly recruited to the site, through the interaction of specific platelet cell-surface receptors with collagen and von Willebrand factor (2). After this adhesion to the vessel wall, platelets aggregate each other leading to a rapid growth of the thrombus. Platelets also become activated at this stage promoting the release of their granule contents, which further promote platelet recruitment, adhesion, aggregation and activation. The major pathway of activation involves the cleavage of the platelet receptor PAR1 (protease-activated receptor 1) by thrombin (3) which is a serine protease generated at the end of the blood coagulation cascade. The blood coagulation cascade is the sequential process by which coagulation factors interact and are activated. The cascade starts immediately either in arterial and in venous injuries when vascular endothelial cells loose their correct morphology and function. Usually the coagulation cascade immediately starts following the exposure of an integral transmembrane receptor known as tissue factor (TF). In the case of arterial thrombosis, the TF is over expressed in the atherosclerotic plaques (4) then the rapture of the plaques trigger a massive activation of coagulation factors and finally thrombin formation. Once generated, thrombin activates platelets and catalyzes the cleavage of soluble fibrinogen into insoluble fibrin, the main protein component of the final thrombus, indicated as secondary haemostatic plug.

In the case of acute thrombotic events, drugs that reduce the growth of a thrombus can be administered. The main target of these drugs is platelets. Antiplatelet drugs are also used prophylactically to reduce the incidence of arterial thrombosis in patients with cardiovascular disease (5). The primary targets of antiplatelet therapy are molecules involved in platelet activation and aggregation, such as cyclooxigenase inhibitors (i.e. Aspirin), ADP-receptors antagonists (i.e. Clopidorgel), PAR-1 inhibitors (i.e. E5555 and SCH 530348) and $\alpha_{IIb}\beta_3$ inhibitors (i.e. Abiciximab and Eptifibatide). At present, there are no drugs in clinical use that block the binding of platelets to collagen and von Willebrand factor and hence their adhesion to the blood vessel wall. In theory, inhibition of this early step in thrombus formation is more likely to disrupt the primary role of platelets in normal blood clotting (haemostasis) and therefore to increase the risk of bleeding. Nevertheless, such inhibitors are in development. Another important treatment for acute thrombotic events is the degradation of fibrin, which stabilizes the structure of a thrombus, by using activators of the fibrinolytic system: namely ‘clot busters’, such as tissue plasminogen activator and streptokinase. However, the success of such treatment depends crucially on the timing of intervention, with earlier intervention generally having a better outcome. In the past few years, studies identifying platelet receptors and signalling mechanisms have

yielded a trove of new targets for antiplatelet therapy. For example, recent studies have shown that several cell-surface receptor– ligand interactions occur on close contact between platelets, such as the binding of the ligand semaphorin 4D to its receptors, CD72 and plexin B1 (6). Finally, the complexities of 'outside-in' and 'inside-out' signalling in platelets (that is, signalling that originates extracellularly or intracellularly, respectively) have begun to be unravelled. However, redundancy in signalling pathways makes it difficult to identify therapeutic targets.

Deep vein thrombosis and pulmonary embolism are collectively referred to as venous thromboembolism, which is the third leading cause of cardiovascular-associated death, after myocardial infarction and stroke. Deep vein thrombosis occurs most often in the large veins of the legs. Pulmonary embolism is a complication of deep vein thrombosis that can occur if part of the thrombus breaks away, travels to the lungs and lodges in a pulmonary artery, resulting in the disruption of blood flow. Thrombi that form in veins are rich in fibrin and trapped red blood cells and are referred to as red clots (as opposed to the platelet-rich thrombi that form in arteries, which are referred to as white clots) (Fig. 1B). Deep vein thrombosis mainly occurs as a result of changes in the composition of the blood that promote thrombosis, changes that reduce or abolish blood flow, and/or changes to the vessel wall. Both genetic and environmental factors can increase the risk of thromboembolism (7). In inherited venous thrombotic disease, there can be increased activity or abundance of proteins that promote coagulation and/or decreased abundance of proteins that inhibit coagulation (i.e. Factor V Leiden, Haemophilia A and B, prothrombin mutations, etc). Acquired risk factors for venous thromboembolism include cancer, obesity and major surgery. Increased amounts of circulating tissue factor, which sits at the apex of the coagulation cascade, might also trigger venous thrombosis (8). Anticoagulants are used to treat a wide variety of conditions that involve arterial or venous thrombosis, including prevention of venous thromboembolism and long-term prevention of ischaemic stroke in patients with atrial fibrillation. The two main classes of anticoagulant drug are vitamin K antagonists and heparins, which target multiple proteases in the coagulation cascade. As is the case for antiplatelet drugs, the main side effect of anticoagulant therapy is bleeding.

When targeting factors in the coagulation cascade, it is important to consider that the sequential activation of factors by proteolytic cleavage results in an amplification of each step. Therefore, a drug that targets an upstream component of the cascade, such as tissue factor, might be more potent than one that targets a downstream component, such as thrombin. However, the tissue factor and factor VIIa complex, which initiates the coagulation cascade, is essential for haemostasis, and inhibition of this complex can lead to considerable bleeding (9). It is also important to consider that the coagulation cascade can be subdivided into three pathways: the extrinsic pathway (tissue factor and factor VIIa), which is the primary activator of the cascade; the intrinsic pathway (factor XIIa, factor XIa, factor IXa and factor VIIIa), which amplifies the cascade; and the common pathway (factor Xa, factor Va and thrombin), which generates thrombin and fibrin. In contrast to the critical nature of the extrinsic

pathway, mice can survive without components of the intrinsic pathway (10). Humans deficient in factor VIII, factor IX or factor XI have mild haemostatic defects, whereas those deficient in factor XII have normal haemostasis (11). Intrinsic-pathway components might therefore be usefully targeted for therapy. Factor XIIa is of particular interest in this regard. A recent study with factor-XII-deficient mice confirmed that factor XIIa is not required for haemostasis; however, it was shown to be important for thrombosis and thus seems an inviting target for antithrombotic therapy (12). Factor IXa, part of the intrinsic pathway, has also been proposed as a target (13). Despite the possibility that the risk of bleeding is lower after inhibition of components of the intrinsic pathway than of the common coagulation pathway, most pharmaceutical companies have chosen to focus on inhibition of factor Xa and thrombin (14,15). This might be because inhibition of the intrinsic pathway is expected to have less impact on ongoing thrombosis than would inhibition of the downstream proteases. An important concern about antithrombotic drugs is how to reverse their effects in the event of bleeding. A new approach that addresses this concern uses aptamers, which are composed of modified oligonucleotides. The first aptamer developed as an anticoagulant was targeted to thrombin and was shown to inhibit the activity of clot-bound thrombin and to reduce the formation of platelet-rich arterial thrombi (16). The aptamer modulates thrombin activity exploiting the multi-tasking and allosteric nature of the enzyme. More recently, an RNA aptamer that inhibits factor IXa has been developed (17). By elegant design, an 'antidote' oligonucleotide was also developed, to reverse the anti coagulant activity of the inhibitory aptamer rapidly in the event of bleeding.

REFERENCES

1. Ruggeri, Z. M. & Mendolicchio, G. L. Adhesion mechanisms in platelet function. *Circ. Res.* 100, 1673–1685 (2007).
2. Savage, B., Almus-Jacobs, F. & Ruggeri, Z. M. Specific synergy of multiple substrate–receptor interactions in platelet thrombus formation under flow. *Cell* 94, 657–666 (1998).
3. Coughlin, S. R. Protease-activated receptors in hemostasis, thrombosis and vascular biology. *J. Thromb. Haemost.* 3, 1800–1814 (2005).
4. Denis, C. V. & Wagner, D. D. Platelet adhesion receptors and their ligands in mouse models of thrombosis. *Arterioscler. Thromb. Vasc. Biol.* 27, 728–739 (2007).
5. Meadows, T. A. & Bhatt, D. L. Clinical aspects of platelet inhibitors and thrombus formation. *Circ. Res.* 100, 1261–1275 (2007).
6. Brass, L. F., Zhu, L. & Stalker, T. J. Minding the gaps to promote thrombus growth and stability. *J. Clin. Invest.* 115, 3385–3392 (2005).

7. Heit, J. A. Venous thromboembolism: disease burden, outcomes and risk factors. *J. Thromb. Haemost.* 3, 1611–1617 (2007).
8. Tesselaar, M. E. *et al.* Microparticle-associated tissue factor activity: a link between cancer and thrombosis? *J. Thromb. Haemost.* 5, 520–527 (2007).
9. Snyder, L. A. *et al.* Expression of human tissue factor under the control of the mouse tissue factor promoter mediates normal hemostasis in knock-in mice. *J. Thromb. Haemost.* 6, 306–314 (2008).
10. Mackman, N. Tissue-specific hemostasis in mice. *Arterioscler. Thromb. Vasc. Biol.* 25, 2273–2281 (2005).
11. Bolton-Maggs, P. H. & Pasi, K. J. Haemophilias A and B. *Lancet* 361, 1801–1809 (2003).
12. Galiani, D. & Renne, T. The intrinsic pathway of coagulation: a target for treating thromboembolic disease? *J. Thromb. Haemost.* 5, 1106–1112 (2007).
13. Howard, E. L., Becker, C. D., Rusconi, C. P. & Becker, R. C. Factor IXa inhibitors as novel anticoagulants. *Arterioscler. Thromb. Vasc. Biol.* 27, 722–727 (2007).
14. Turpie, A. G. Oral, direct factor Xa inhibitors in development for the prevention and treatment of thromboembolic diseases. *Arterioscler. Thromb. Vasc. Biol.* 27, 1238–1247 (2007).
15. Weitz, J. I. & Buller, H. R. Direct thrombin inhibitors in acute coronary syndromes: present and future. *Circulation* 105, 1004–1011 (2002).
16. Li, W. X., Kaplan, A. V., Grant, G. W., Toole, J. J. & Leung, L. L. A novel nucleotide-based thrombin inhibitor inhibits clot-bound thrombin and reduces arterial platelet thrombus formation. *Blood* 83, 677–682 (1994).
17. Rusconi, C. P. *et al.* RNA aptamers as reversible antagonists of coagulation factor IXa. *Nature* 419, 90–94 (2002).

2. HUMAN α-THROMBIN

CHAPTER 2.1.

Structure and Function of Thrombin

Function of Thrombin

Thrombin is the final protease generated in the coagulation cascade, and it is the only factor capable of cleaving soluble fibrinogen into insoluble fibrin then promoting clot formation. Once generated from its inactive precursor prothombin (FII) by prothrombinase complex (FXa-FVa-Ca^{2+}-membrane phospholipids), it can diffuse freely to encounter a large number of potential substrates both procoagulant and anticoagulant (Fig.1). For instance, thrombin promotes positive feedback amplification of the coagulation pathway, leading to its own generation by proteolitically converting FXI to FXIa (a serine protease of the intrinsic pathway), as well as FVIII and FV (cofactors in the generation of FXa and thrombin, respectively) (1). In addition thrombin activates platelets through the cleavage of two protease platelet receptors, PAR-1 and PAR-4, promoting platelets aggregation (2).

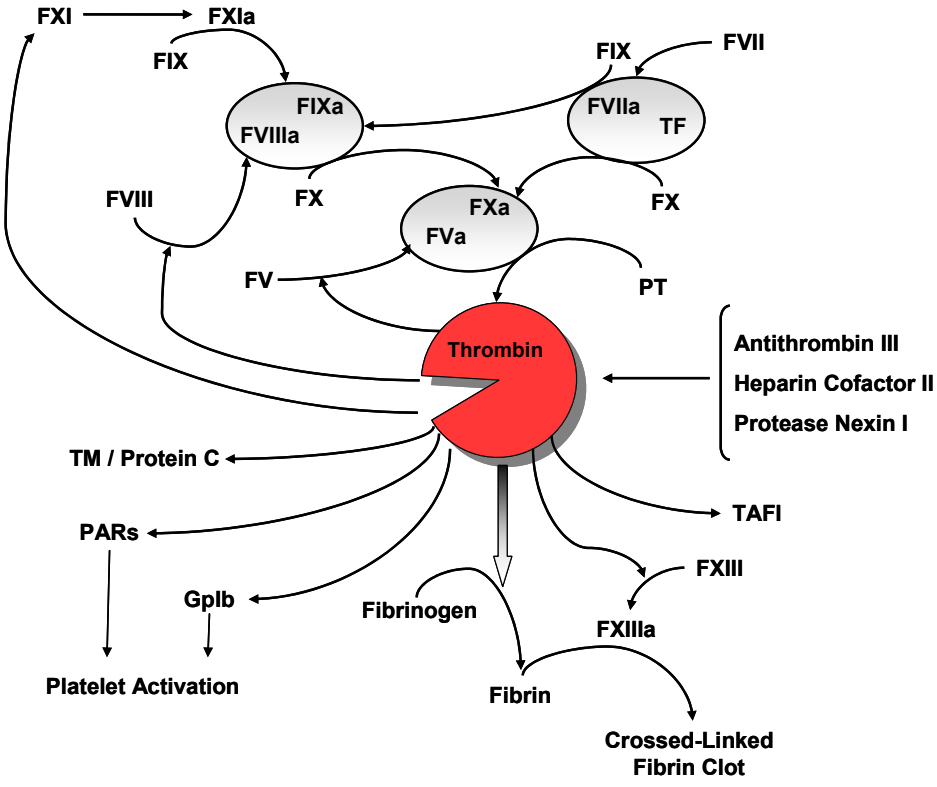

Figure 1. The central role of thrombin in haemostasis. Thrombin is the final protease generated in the coagulation cascade. Once generated in the bloodstream it experts either procoagulant and anticoagulant functions.

By contrast thrombin promotes its own down-regulation by activating the protein C pathway. Upon contact with thrombomodulin (TM), which is an integral membrane protein present on the vascular

endothelial cells, the specificity of the enzyme toward the zymogen protein C is enhanced greater than thousand-fold. The reaction is further enhanced by the presence of a specific endothelial cell protein C receptor (3). Activated protein C (aPC) cleaves and inactivates FVa and FVIIIa, two essential cofactors of coagulation, and FXa and FIXa that are required for thrombin generation, thereby down-regulating both the amplification and progression of the coagulation cascade. Hijacking of thrombin by thrombomodulin and activation of protein C in the microcirculation constitute the natural anticoagulant pathway that prevents massive intravascular conversion of fibrinogen into a soluble clot upon thrombin generation.

In addition to its direct role in promoting and regulating clot formation, thrombin elicits numerous cellular responses in cells other than platelets, many of which can be ascribed to its activation of PARs. Thrombin stimulates a variety of responses by endothelial cells, including cell surface expression and secretion of cellular adhesion molecules as well as the production of growth factors and cytokines. Thrombin also promotes cytokine elaboration by smooth muscle cells and stimulates the proliferation of both smooth muscle cells and fibroblasts.

Efficient regulation of thrombin activity is essential to prevent excessive or improperly localized clot formation. Certain members of the serine protease inhibitor (serpin) superfamily inhibit the catalytic activity of thrombin, and this reaction is greatly accelerated in the presence of glycosamminoglycans such as heparin, heparan sulphate, and dermatan sulphate. The most important serpins responsible for thrombin inhibition are antithrombin (originally called antithrombin III), heparin cofactor II (HCII), and protease nexin I (PNI) (4). Antithrombin is abundant in the blood (2.3 μM), inhibits a variety of serine proteases involved in blood coagulation, and appears to be the main inhibitor limiting intravascular clot formation. In contrast, HCII is highly specific for thrombin and appears to regulate thrombin activity in extravascular tissues following vascular injury, whereas PNI is likely to inhibit thrombin at or near the surface of a variety of cell types but especially in tha brain (5). In addition to this endogenous thrombin inhibitors, several potent thrombin inhibitors have been isolated from hematophagous organisms, including hirudin and haemadin from the leeches *Hirudo medicinalis* and *Haemadipsa sylvestris,* respectively.

It's now sufficiently clear that thrombin function is not only limited to the conversion of the fibrinogen into fibrin but it absolutely plays a pivotal role in maintaining haemostasis. However the fundamental question about thrombin regards how a single protease domain possesses the determinants to specifically recognize such a large number of substrates. The answer requires an understanding of the unique structural features of thrombin.

Structure of Thrombin

Human α-thrombin is a serine protease belonging to the chymotrypsin family, with which show a high degree of similarity (~49%). Consequently thrombin sequence numbering follows the numeration of chymotrypsynogen (see Appendix B). Thrombin is composed of two polypeptide chains of 36 (A chain) and 259 (B chain) residues that are covalently linked through a disulfide bond (6). The B chain carries the functional epitopes of the enzyme and has the typical fold of serine proteases, with two sixstranded β-barrels of similar structure that pack together asymmetrically to accommodate the residues of the catalytic triad H57, D102 and S195 at their interface (Fig. 2). The catalytic triad polarizes the side chain of the active site S195 for a nucleophilic attack on the C atom in the scissile bond of the substrate. The C atom is converted into a tetrahedral intermediate in the transition state, which is stabilized by hydrogen bonds between the charged carbonyl O atom of the peptide group of the scissile bond and the amide hydrogen atoms of G193 and S195 which form the oxyanion hole. The substrate is then acylated by the Oγ atom of S195 after transfer of a proton to H57 and its C-terminal fragment is released. Nucleophilic attack by a water molecule catalyses deacylation, releasing the carboxylic acid product and the N terminal fragment of the substrate, which restores the state of the catalytic triad. D102 anchors H57 in the correct orientation for proton transfer from and to S195, which compensates for the developing positive charge (7).

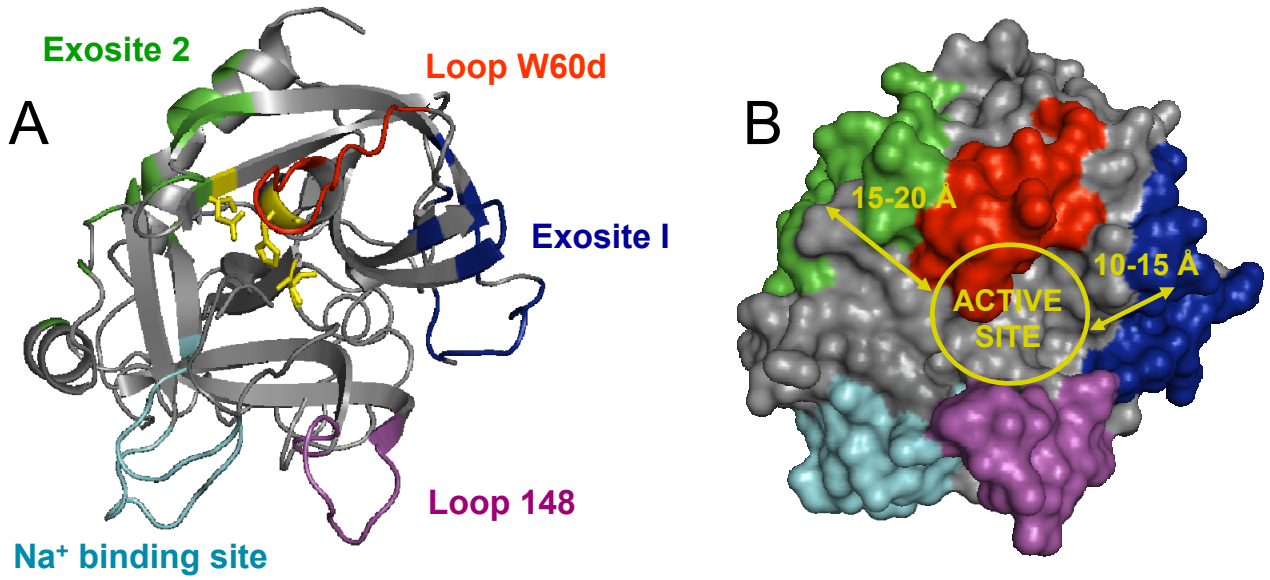

Figure 2. Thrombin Structure. Thrombin (1PPb.pdb) is shown in the standard Bode orientation. The active site containing the catalytic triad (H57, D102, S195, yellow) is covered by the hydrophobic loop W60d (red) and by the hydrophilic loop 148 (magenta). Exosite 1 (blue) and 2 (green) are two electropositive patches that flank the active site and coordinate substrates/inhibitors recruitment. As for exosites, the Na^+-binding site (cyan) is located about 15-20 Å away from the catalytic triad, too.

Active-site cleft and direct substrate/inhibitor interactions

Numerous insertions are present in thrombin, relative to trypsin and chymotrypsin, shaped as loops connecting β-strands in the B chain. Two such insertions shape and narrow the access to the active site. The W60d loop defines the upper rim of the active site and screens H57 and S195 from the solvent. The loop contains an insertion of nine residues, from Y60a to I60i, and protrudes into the solvent with the bulky side chain of W60d providing most of the steric hindrance (8). Opposite to the W60d loop, the autolysis 148-loop forms the lower rim of the active-site cleft. The 148-loop is strategically positioned in thrombin (6) and is crucial for fibrinogen recognition (8). It is characterized by high intrinsic conformational heterogeneity, but it is still unclear whether the different structural modes observed for the 148-loop represent real responses to different ligands or if they result from crystal-packing effects. Notably Na^+ binding to thrombin stabilizes the enzyme into a more open and rigid conformation, locking and therefore protecting the 148-loop from the cleavage by subtilisin (9).

In between the two insertion loops, the active-site residues are nestled in the centre of a narrow cleft framed. The trypsin-like specificity for basic residues at P1 (based on the nomenclature of Schechter and Berger, 1967) is conferred to thrombin by the presence of D189 at the S1 site occupying the bottom of the catalytic pocket. However, differently from trypsin pocket, thrombin increased flexibility allows accommodation of more hydrophobic or even uncharged P1 groups and confers a strong preference for P1-R over K residues (4). Relatively unique to thrombin is the acidic E192 residue positioned at the entrance to this pocket. Its negatively charged side chain is not compensated by hydrogen bonds or ion pair interactions with neighbour residues. The uncompensated charge of E192 plays an important role in discriminating against substrates carrying acidic groups near the scissile bond, like protein C and the thrombin receptor 1 (PAR-1) (10). Based on the W215 indole moiety, a hydrophobic surface groove extends on top of the S1 pocket, which is partially delimited by the 60 loop. The conjunction of hydrophobic residues together with the pavement of the active-site forms an apolar binding site, which is subdivided into the S2 cavity and the aryl binding site/S4 groove. This latter site hosts P4 side chain of all L-amino acids substrates, whereas the P3 side chain extends alongside E192, away from the active site. The S1’ site of thrombin positioned to the right of the active site is limited in size by the K60f side chain, and therefore particularly suited to accommodate small polar P1’ side chain. The S2’ subsite is of medium size and mainly hydrophobic, so that bulky hydrophobic P2’ residues are preferred. The S3’ site is open and slightly acidic, resulting in a weak preference for basic P3’ side chains and an aversion for acidic residues (Table 1).

Table 1: Cleavage Sequences of Thrombin Substrates or Inhibitors Around the Scissile Peptide Bond and the Reactive-Centre Loop, respectively

	P4	P3	P2	P1	P1'	P2'	P3'	Cofactor and Exosite
Fibrinogen A	Gly	Gly	Val	Arg	Gly	Pro	Arg	1
Fibrinogen B	Phe	Ser	Ala	Arg	Gly	His	Arg	1
FV (709)	Leu	Gly	Ile	Arg	Ser	Phe	Arg	1 and 2
FV (1018)	Leu	Ser	Pro	Arg	Thr	Phe	His	1 and 2
FV (1545)	Trp	Tyr	Leu	Arg	Ser	Asn	Asn	1 and 2
FVIII (372)	Ile	Gln	Ile	Arg	Ser	Val	Ala	1 and 2
FVIII (740)	Ile	Glu	Pro	Arg	Ser	Phe	Ser	1 and 2
FVIII (1689)	Gln	Ser	Pro	Arg	Ser	Phe	Gln	1 and 2
FXIII	Gly	Val	Pro	Arg	Gly	Val	Asn	None
PAR-1	Leu	Asp	Pro	Arg	Ser	Phe	Leu	1
PAR-4	Pro	Ala	Pro	Arg	Gly	Tyr	Pro	None
FXI	Ile	Lys	Pro	Arg	Ile	Val	Gly	1
PC	Val	Asp	Pro	Arg	Ile	Val	Gly	TM (1)
TAFI	Val	Ser	Pro	Arg	Ala	Ser	Ala	TM (1)
AT	Ile	Ala	Gly	Arg	Ser	Leu	Asn	Heparin (2)
HCII	Phe	Met	Pro	Leu	Ser	Yhr	Gln	1 and Heparin (2)

AT, antithrombin; F, factor, HC, heparin cofactor, TAFI, thrombin-activable fibrinolysis inhibitor

On these basis, a P4 to P3' consensus sequence of an optimal thrombin polypeptide substrate should contain a P4-F/L, any P3 residue, a P2-P/V, a P1-R, a P1'-S/G, a P2'-F, and a P3'-R residue. Although the majority of thrombin natural substrates follows the consensus scheme proposed, important exceptions are found with fibrinogen Aα (FAα), factor XIII, protein C, and HCII. Therefore it must be admitted the presence of other features that support and govern the substrates/inhibitors presentation to active site. Notably in thrombin structure the active site is flanked by two electropositive patches called exosites, which make additional favorable contacts with substrates/inhibitors (Fig.2). All relevant physiological substrates/inhibitors interact with thrombin by contacting exosite 1 or/and exosite 2 (Table 1 and Fig. 3). Therefore the maintenance of an high grade of specificity towards substrates/inhibitors in thrombin is guaranteed by exosites.

Exosite 1 or ABE-1

The prominent loop centered around K70 is called exosite 1 and is homologous to the Ca^{2+} binding loop of the cognate proteases trypsin and chymotrypsin (11). In these pancreatic proteases Ca^{2+} stabilizes the fold and confers increased resistance to proteolytic digestion. In thrombin the need for Ca^{2+} is eliminated by the insertion of K70, the side chain of which mimics the bound Ca^{2+} and obliterates the cavity available for binding this cation. In fact, thrombin does not bind Ca^{2+} up to mM concentrations. Exosite 1 is located about 10-15 Å away from the active site and is mainly placed on the R67 to I82 loop and bordered by the 37-loop and segment K109-K110. In this domain, four charged residues (R67, K70, E77, and E80) form a salt bridge cluster, which is buried well below the surface of the exosite, substantially contributing to the rigidity of the loop (6). Over this buried charged spot, several not compensated cationic residues, R73, R75, R77a, form a strong electropositive field.

Electrostatic forces generated by the exosite 1's charges have an important influence on the biomolecular association of thrombin with some ligands. The exosite 1, in fact, represents the recognition site for many macromolecular ligands, such as fibrin(ogen), thrombomodulin, PAR-1, heparin cofactor II, hirudin, coagulation factor V, VIII and XIII (12-19). It is hypothesized that the exosite 1's electrical field could pre-orient the enzyme for a productive interaction ("electrostatic steering") so that the hydrophobic stacking components can subsequently stabilized the various adducts.

Exosite 1 also serves as an extended primed recognition site that can communicate changes to the catalytic moiety of the enzyme. In fact, peptides derived from the physiological inhibitor heparin cofactor II (20), the thrombin receptor 1 (21) or the hirudin C-terminal domain (22) influence the active site of thrombin allosterically.

Exosite 2 or ABE-2

On the other side of the enzyme, opposite exosite 1, a prominent C-terminal helix hosts a number of positively charged residues that provide the anion binding exosite 2. Exosite 2 is the template for interaction with polyanionic ligands such as heparin and glycosaminoglycans. At this surface, a small hydrophobic L234-based groove is surrounded (in clockwise order) by basic residues R93, R101, R165, R233, R126, K236, K235, K240, and H91, with most of their side chain charges not compensated by adjacent negative charges. This assignment was confirmed with exosite 2 mutants by measuring the heparin-catalyzed thrombin inhibition by ATIII (23), and crystallographically by a structure of the α-thrombin complex with an eight unit heparin fragment, in which each octasaccharide chain is sandwiched between two adjacent thrombin molecules (24). Exosite 2 is also the locale for thrombin interaction with the platelet receptor GpIbα and the acidic moiety of the fibrinogen γ' chain (25,26).

Moreover because the helix packs tightly against the domain supporting the catalytic D102, it is conceivable that binding to exosite 2 could influence allosterically the catalytic activity of the enzyme by affecting the position of the side chain of D102.

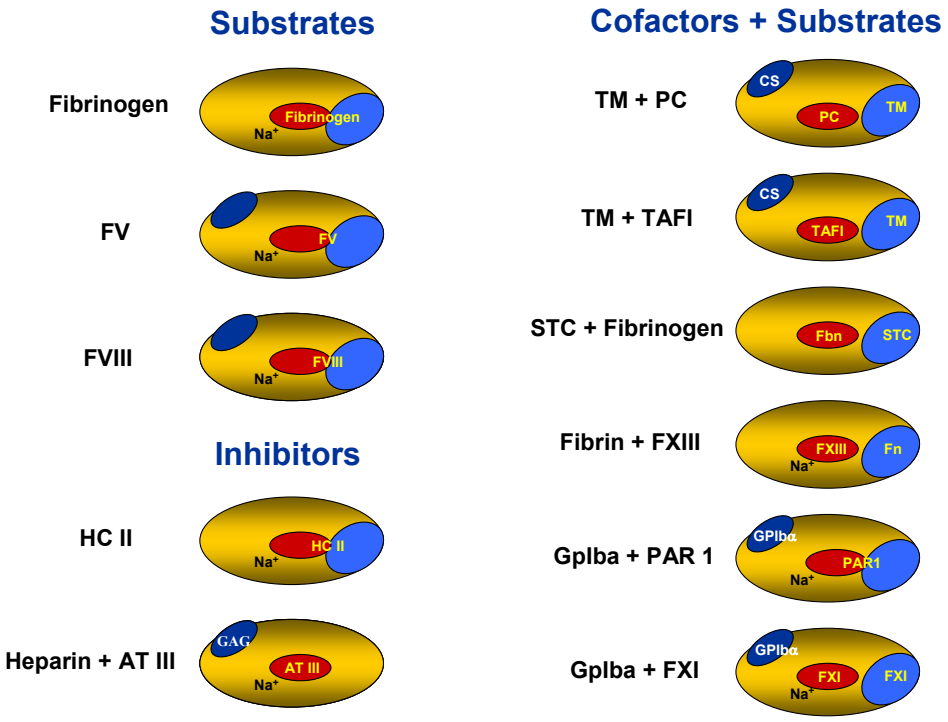

Figure 3. Schematic interaction of thrombin (represented as a large ellipsoid) **and the different surface regions that bind substrates, inhibitors, carbohydrate, and cofactors.** AT, antithrombin; F, factor; Gp, glycoprotein; HC, heparin cofactor; PAR, protease-activated receptor; PC, protein C; TAFI, thrombin-activable fybrinolysis inhibitor; STC, staphylocoagulase; TM, thrombomodulin.

Na^+ binding site and allosteric effect

Sodium has been found to be an important allosteric modulator of α-thrombin. The binding of this monovalent cation to thrombin plays a relevant role in the allosteric control of the protease activities, as it causes a conformational transition from a Na+-free form, referred to as slow, to a Na+-bound form, referred to as fast. The slow and fast forms are significantly (2:3 ratio) populated under physiologic conditions because the Kd for Na+ binding is 110 mM at 37°C and physiologic NaCl concentration (140 mM) is not sufficient for saturation. The two forms exhibit different relative activities toward macromolecular substrates. The fast thrombin form cleaves fibrinogen and PARs more efficiently and displays procoagulant, prothrombotic, and prosignaling properties. The slow form preferentially cleaves protein C, exhibiting more anticoagulant properties (Table 2).

The Na+ binding site has been confined to a site in the center of the 222 loop situated in a solvent-filled cavity behind the S1 specificity pocket located near D189. The bound Na+ ion, located more than 15 Å away from the catalytic triad, is coordinated octaedrically by the carbonyl oxigens of R221a and K224 and by four internal water molecules, and is further stabilized by the negative charges of D221

and D222. In a recent study, which combined comprehensive mutational experiments with crystallographic results, Di Cera and co-workers identified residues D189, E217, D222, and Y225 clustering around the Na+ site as being energetically linked to Na+ binding and responsible for transducing Na+ binding into enhanced catalytic activity. The authors suggested that Na+ binding reorients the R221a carbonyl group to form the R187-D222 salt bridge, thereby favourably orienting the side chains of D189, E192, and S195 and the connecting water network. The structural movements of these residues are relatively small but nevertheless functionally important, namely in the range of usual crystal packing effects. However, these movements may be limited due to the constraints of the crystal packing effects.

Table 2. Effect of Na+ on the catalytic activity of thrombin towards some relevant physiological substrates

	k_{cat}/K_m (μM^{-1} s^{-1})		r
	Fast	**Slow**	
(D)FPR-pNA	88.9 ± 4	3.5 ± 0.5	26
Fibrinopeptide A release	35 ± 4	1.5 ± 0.1	23
Fibrinopeptide B release	17 ± 1	0.73 ± 0.03	23
PAR-1[a]	54 ± 2	1.4 ± 0.1	39
Protein C	0.21 ± 0.001	0.32 ± 0.01	0.7

All measures were performed in buffer that stabilized either the fast (0.2 M NaCl) or the slow (0.2M ChCl) form. Kinetic constants were obtained by Di Cera et al., 1997.

Larger structural changes observed with a human S195A thrombin mutant devoid of any active-site or exosite contacts, as well as in a E217K mutant with match residues fibrinogenase activity but similar protein C cleavage capacity, were suggested to be typical for the slow form of thrombin. These crystal structures indicated an allosteric switch mechanism, according to which the Na+ removal induces flipping of the C168-C182 disulfide bridge and the aromatic side chains of F227, W215, and W60d, resulting in the constriction of the active site cleft, limiting access of substrates. Although many reported observations regarding the perturbations in the vicinity of aromatic residues of the S2 to S4 subsites agree with considering these structures as representing the slow thrombin form, the main problem with these conclusions is that they have Na+ bound or are not capable of binding Na+, respectively. Nevertheless, these structures display the enormous plasticity of the substrates interaction surface of thrombin and its capability to propagate binding effects to distal regions allosterically.

Currently available data suggest that Na+-bound (fast) thrombin form is more stable and exhibits a more open accessible and rigid active site cleft, whereas the Na+-free (slow) form possesses a more closed, flexible substrate binding region (9). Thus the fast from of thrombin would be a better template for productive binding of the inherently flexible cleavage segment of fibrinogen and PAR-1 to its active

centre, such that the scissile peptide bonds are optimally presented to the S195 Oγ and the oxyanion hole. Importantly, thrombin substrate complexes in the presence or absence of Na+ go through transition states that are short-lived, making the structural characterization of these states difficult. Several naturally occurring mutations of the prothrombin gene, like prothrombin Frankfurt, Salakta, Greenville, Scranton, Copenhagen and Saint Denis, affect residues linked to Na+ binding and are often associated with bleeding (27).

REFERENCES

1. Davie, E.W., and Kulman, J.D. (2006) An overview of the structure and function of thrombin. *Sem. Thromb. Haemost.* 32, Suppl. 1, 3-15.
2. Coughlin, S. R. Protease-activated receptors in hemostasis, thrombosis and vascular biology. *J. Thromb. Haemost.* 3, 1800–1814 (2005).
3. Esmon, C.T. (1989) The roles of protein C and thrombomodulin in the regulation in the regulation of blood coagulation. *J. Biol. Chem.* 264, 4743-4746.
4. Johnson, D.J.D., Adams, T.E., Li, W., and Huntington, J.A. (2005) Crystal structure of wild-type human thrombin in the Na+-free state. *Biochem. J.* 392, 21-28.
5. Arcone R, Chinali A, Pozzi N, Parafati M, Maset F, Pietropaolo C, De Filippis V. Conformational and biochemical characterization of a biologically active ratrecombinant Protease Nexin-1 expressed in E. coli. *Biochim Biophys Acta*. 2009;1794:602-14.
6. Bode, W., Turk, D., and Karshikov, A. (1992) The refined 1.9-Å X-ray crystal structure of D-Phe-Pro-Arg-chloromethylketone-inhibited human α-thrombin: Structure analysis, overall structure, electrostatic properties, detailed active-site geometry, and structure-function relationships. *Protein Sci.* 1, 426-471.
7. Warshel A, Naray-Szabo G, Sussman F, Hwang JK. How do serine proteases really work? *Biochemistry*. 1989 2;28:3629-37. Review.
8. Di Cera, E., Dang, Q.D., and Ayala, Y.M. (1997) Molecular mechanisms of thrombin function. *Cell Mol. Life Sci.* 53, 701-730.
9. De Filippis, V., De Dea, E., Lucatello, F., and Frasson, R. (2005) Effect of Na+ binding on the conformation, stability, and molecular recognition properties of thrombin. *Biochem. J.* 390, 485-492.
10. Guinto ER, Vindigni A, Ayala YM, Dang QD, Di Cera E. Identification of residues linked to the slow-->fast transition of thrombin. *Proc Natl Acad Sci U SA*. 1995 Nov 21;92:11185-9.

11. Bartunik HD, Summers LJ, Bartsch HH. Crystal structure of bovine beta-trypsin at 1.5 A resolution in a crystal form with low molecular packing density. Active site geometry, ion pairs and solvent structure. *J Mol Biol.* 1989 Dec 20;210:813-28.
12. Stubbs, M.T., Oschkinat, H., Mayr, I., Huber, R., Angliker, H., Stone, S.R., and Bode, W. (1992) The interaction of thrombin with fibrinogen: A structural basis for its specificity. *Eur. J. Biochem.* 206, 187-195.
13. Steen M, Dahlbäck B. Thrombin-mediated proteolysis of factor V resulting in gradual B-domain release and exposure of the factor Xa-binding site. *J Biol Chem.* 2002 11;277:38424-30.
14. Esmon, C.T., and Lollar, P. (1996) Involvement of thrombin anionbinding exosites 1 and 2 in the activation of factor V and factor VIII. *J Biol Chem* 271, 13882–13887.
15. Sadasivan, C., Yee, V.C. (2000) Interaction of the factor XIII activation peptide with alpha-thrombin. Crystal structure of its enzyme-substrate analog complex. *J. Biol. Chem.* 275, 36942–36948.
16. Hall, S.W., Nagashima, M., Zhao, L., Morser, J., and Leung, L.K. (1999) Thrombin interacts with thrombomodulin, protein C, and thrombin-activable fibrinolysis inhibitor via specific and distinct domains. *J. Biol. Chem.* 274, 25510-25516.
17. Myles, T., Le Bonniec, B.F., and Stone, S.R. (2001) The dual role of thrombin's anion-binding exosite-I in the recognition and cleavage of the protease-activated receptor 1. *Eur. J. Biochem.* 268, 70-77.
18. Myles, T., Church, F.C., Whinna, H.C., Monard, D., and Stone, S.R. (1998) Role of thrombin anion-binding exosite-I in the formation of thrombin-serpin complexes. *J. Biol. Chem.* 273, 31203-31208.
19. Hall SW, Gibbs CS, Leung LL. Identification of critical residues on thrombin mediating its interaction with fibrin. *Thromb Haemost.* 2001;86:1466-74.
20. 1: Hortin GL, Trimpe BL. Allosteric changes in thrombin's activity produced by peptides corresponding to segments of natural inhibitors and substrates. *J Biol Chem.* 1991 15;266:6866-71.
21. Liu, L.W., Rezaie, A.R., Carson, C.W., Esmon. N.L., and Esmon, C.T. (1994) Occupancy of anion binding exosite 2 on thrombin determines Ca^{2+} dependence of protein C activation. *J. Biol. Chem.* 269, 11807-11812.
22. Jackman, M. P., Parry, M. A. A., Hofsteenge, J. and Stone S. R. (1992). Intrinsic Fluorescence Change and Rapid Kinetics of the Reaction of Thrombin with Hirudin. *J. Biol. Chem.* 267, 15375-15383
23. Gan, Z.R., Li., Y., Chen, Z., Lewis, S.D., and Shafer, J.A. (1994) Identification of basic amino acid residues in thrombin essential for heparin-catalyzed inactivation by antithrombin III. *J. Biol. Chem.* 269, 1301-1305.
24. Carter, W.J., Cama, E., Huntington, J.A. (2005) Crystal structure of thrombin bound to heparin. *J. Biol. Chem.* 280, 2745-2749.

25. De Cristofaro, R., De Candia, E., Landolfi, R., Rutella, S., and Scott W. Hall, S.W. (2001) Structural and functional mapping of the thrombin domain involved in the binding to the platelet glycoprotein Ib. *Biochemistry.* 40, 13268-13273.
26. Lancellotti, S., Rutella, S., De Filippis, V., Pozzi, N., and Rocca, B. (2008) Fibrinogen-elongated γ chain inhibits thrombin-induced platelet response, hindering the interaction with different receptors. *J. Biol. Chem.* 283, 30193-30204.
27. Di Cera E. Thrombin: a paradigm for enzymes allosterically activated by monovalent cations. *C R Biol.* 2004;327:1065-76. Review.

CHAPTER 2.2.

Structural Effect of Mutating the Catalytic Asp102 in Human α-Thrombin

Nicola Pozzi [1], Enrico Di Cera[2] and Vincenzo De Filippis [1]

[1] *Department of Pharmaceutical Sciences, University of Padua, via F. Marzolo 5, I-35131 Padua, Italy*

[2] *Department of Biochemistry and Molecular Biophysics, Washington University School of Medicine, St. Louis Missouri 63110*

INTRODUCTION

Na+ ion is an allosteric modulator of thrombin activity in solution and it triggers a conformational transition in thrombin from a low activity Na+-free (slow) form to a high-activity Na+-bound (fast) form. The slow form displays selective loss of specificity for the procoagulant substrates fibrinogen and PAR-1, while it essentially retains the activity of the fast form for the anticoagulant substrate protein C. The results of crystallographic and kinetic studies accumulated so far are consistent with the following biphasic mechanism: S* ⇔ S ⇔ F, in which a low populated (< 5%) and essentially incative slow form (S*) exists in equilibrium with the highly polulated and active slow form (S). In a second step, the binding of Na+ converts the S form into the fully active F form (1,2).

The putative structure of the S and F forms, without inhibiotrs bound, have been solved by X-ray crystallography. Both crystal structures contain two thrombin molecules in the asymmetric unit, and show only subtle, but nevertheless functionally important, structural differences in the catalytic pocket, in the primary specificity site, and in the Na+-binding site. More recently, the crystallographic structure of a thrombin mutant in which the catalytic Asp102 was replaced by Asn (D102N) has been reported and assigned to the low populated inactive S* form (4). The structure of D102N shows a single thrombin molecule in the asymmetric unit and it is in a self-inhibited conformation, with Trp-215 and Arg-221a occluding the active site and the primary specificity pocket, and Arg-187 filling the empty Na+-binding site (Fig.1). Importantly, it was proposed that the structural features of the D102N mutant represent genuine properties of the inactive slow form (S*), captured during the crystallization process.

In order to discriminate whether the unique structure of the D102N mutant pertains to the inactive slow form of the wild type thrombin (S*) or is the unexpected results of the mutation D102N, the overall conformational and stability properties of the mutant were investigated by circular dichroism and fluorescence spectroscopy, whereas the structure of the specificity sites and exosite-1 was probed by

different inhibitors, like PABA, hirudin HM2 and its fragments Hir(1-47), analogue Hir(1-47)S2R and Hir(48-64). In particular, PABA interacts selectively in the S1 site of the enzime, Hir(1-47) covers the catlytic pocket and penetrates the S2 and S3 sites whereas analogue Hir(1-47)S2R makes an extra-interaction respect to Hir(1-47) with S1 site. Finally the acidic C-terminal tail Hir(48-64) binds to the exosite-1. Changes in the affinity of these ligands for D102N mutant are expected to provide key information on the conformational state of their putative binding sites in the mutant structure.

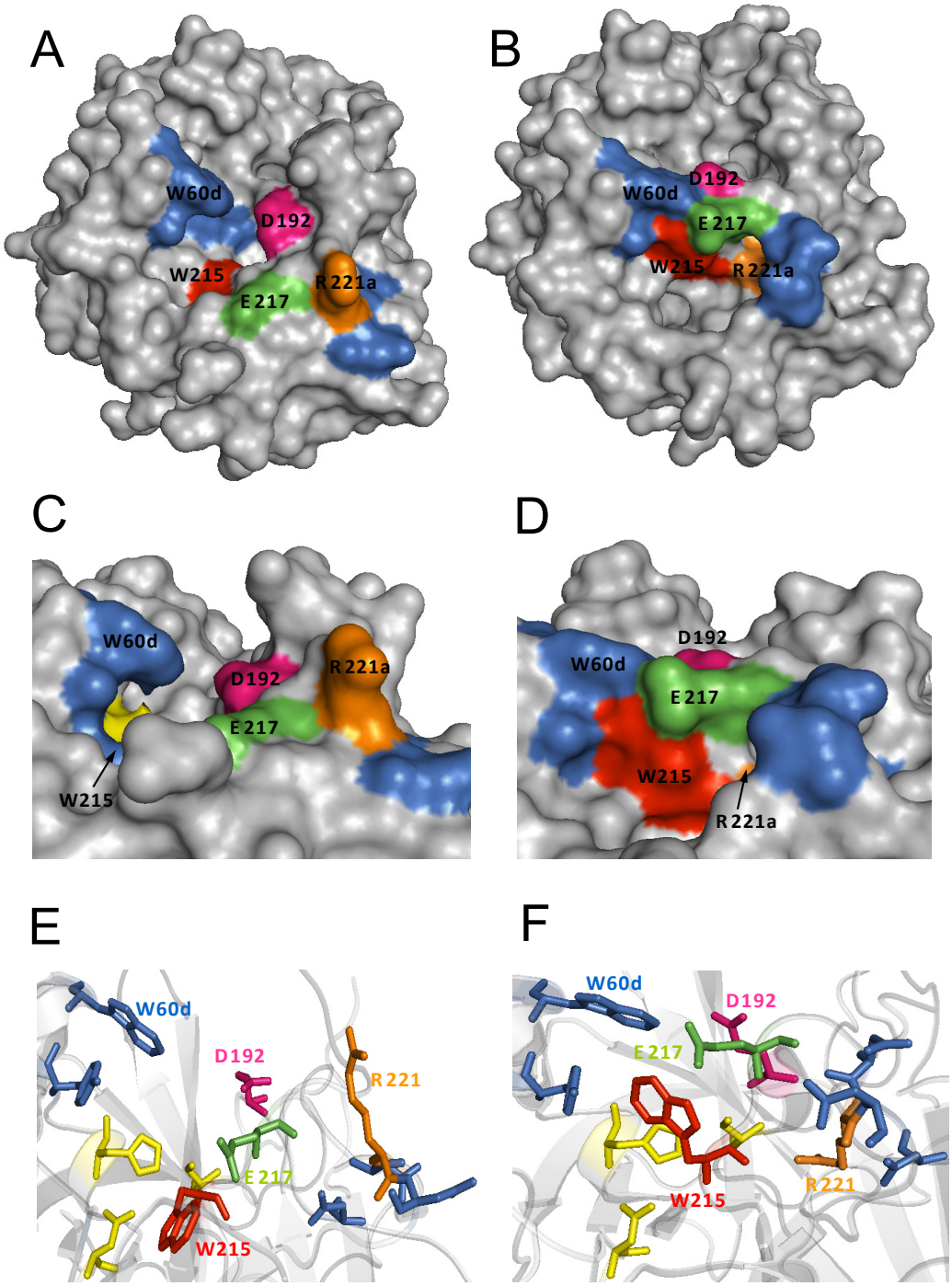

Figure 1. Comparison between human alpha-thrombin wild-type (1SHH, A-C-E) and mutant D102N (2GP9, B-D-F). In D102N mutant 215-217 strand is collapsed deep down the active site and this structural rearrangement leads to a more closed and locked conformation of the enzyme. Pictures E and F show the aminoacids that are major involved in this reorganization

MATERIALS AND METHODS

Materials. Wild-type α-thrombin from human plasma was obtained from Haematologic Technologies (Essex Junction, VT) in 50% water:glycerol solution. Aliquots (0.4-0.7 mg) of commercial thrombin were loaded onto a fast flow HiTrap column (1.6 x 2.5 cm) from Pharmacia (Uppsala, Sweden), eluted at a flow rate of 1 ml/min with 5 mM Tris-HCl buffer, pH 8.0, containing 0.1% (w/v) PEG 8000, at the desires chloride salt concentration, as indicated. The thrombin mutant D102N was expressed, purified and tested for activity as described previously (3,4). It was a generous gift of Prof. Enrico Di Cera (Washington School of Medicine, St. Luois, MO). Recombinant hirudin variant HM2 was a generous gift of Dr. Gaetano Orsini (Farmitalia Carlo-Erba, Milan, Italy).
The chromogenic substrate FPR was synthesized as previously described (5). The peptides Hir(1-47) and Hir(48-64) were obtained by limeted proteolysis of hirudin HM2 with trypsin, as detailed elsewhere (6), or by solid-phase synthesis, using standard Fmoc-chemistry (7) on a model PS3 automated synthesizer from Protein Technologies (Tucson, AZ), as previously described (8,9). The peptides were purified by RP-HPLC and their chemical identity carefully established enzymatic fingerprint analysis and high-resolution mass spectrometry on a Mariner ESI-TOF instrument from Perseptive Biosystems (Stafford, TX). N□-Fmoc protected amino acids, solvents and reagents for peptide synthesis were purchased from Applied Biosystems (Foster City, CA) or Bachem AG (Bubendorf, Switzerland). PABA, deuterated water, and trypsin were from Sigma. Buffers, urea and organic solvents were of analytical grade and purcahsed from or Fluka.

Spectroscopic measurements. Unless otherwise specified, all measurements were carried out at 25 ± 0.1 °C in 5 mM Tris-HCl buffer, pH 8.0, containing 0.1% (w/v) PEG-8000 and 0.2 M NaCl, for the fast form, or choline chloride (ChCl), for the slow form. Temperature correction was applied for Tris buffer (10). All measurements were carried out at least in duplicate and the spectra were subtracted for the corresponding base lines.

Protein concentration. Protein concentration was determined by UV absorption at 280 nm (11) on a Lambda-2 spectrophotometer from Perkin-Elmer (Norwalk, CT) using a molar absorptivity value of 65770 $M^{-1}\cdot cm^{-1}$ for natural α-thrombin and mutant D102N, and 2920 $M^{-1}\cdot cm^{-1}$ for full-length hirudin HM2 and fragment Hir(1-47). The concentration of Hir(48-64), having only one aromatic chromophore in the sequence (i.e., Phe-54), was taken as 200 $M^{-1}\cdot cm^{-1}$ at 257 nm. The active-site concentration of natural α-thrombin solutions was also determined by titration with hirudin HM2 in the presence of FPR as a chromogenic substrate, using a procedure similar to that reported elsewhere (12), and found identical (within 5% error) to that determined by UV absorption. The concentration of PABA stock solutions was determined using a molar absorptivity value of 15000 at 293 nm (13).

Far-UV CD spectra. Far-UV CD spectra were recorded on a Jasco (Tokyo, Japan) model J-810 spectropolarimeter equipped with a water-jacketed cell holder, connected to a model RTE-111 (NesLab) water-circulating bath. The spectra were recorded in a 1-mm cell, at a scan-speed of 10 nm/min, with a response time of 16 sec, and resulted from the average of four accumulations. CD data were expressed as mean the residue ellipticity $[\theta] = \theta_{obs} \cdot MRW/(10 \cdot l \cdot c)$, where θ_{obs} is the observed signal in degrees, MRW is the mean residue weight taken as 114.6 Da, l is the cuvette pathlength in cm, and c is the protein concentration in g/ml. Fluorescence spectra were recorded at a scan speed of 200 nm/min in a 1-cm pathlength cuvette (2 ml internal volume) on a Jasco model FP-6500 spectropolarimeter, equipped with Peltier model ETC-273T temperature control system from Jasco. Protein samples (5 – 50 nM) were excited at 280 or 295 nm, using excitation and emission slits of 5 and 10 nm, respectively.

Stability measurements. Urea-mediated denaturation of human α-thrombin and mutant D102N was carried out at 25 ± 0.1 °C, at pH 8.0 and 6.5, in the presence of 0.2 M chloride salts, as described (14,15). After 1-hour incubation at the specified urea concentration, protein samples (2 ml, 50 nM) were excited at 280 or 295 nm and the fluorescence intensity was recorded at 334 nm. At each urea concentration, the fluorescence signal was subtracted for that of the corresponding base line. Reversibility of the denaturation process was evaluated by measuring the recovery of the fluorescence intensity or λ_{max} value upon 20-fold dilution of enzyme stock solutions (3 μM) in 7-M urea with non-denaturing buffer at either pH 8.0 or 6.5. When denaturation was only partially reversible (i.e., at pH 8.0), the value of $[urea]_{1/2}$ was estimated as reported (16), whereas when the unfolding was almost fully reversible (i.e., at pH 6.5), the data were analyzed within the framework a two-state process by fitting fluorescence data to the equation (14)

$$F = \{F_{0,N} + \alpha_N [D] + (F_{0,U} + \alpha_U [D]) \times \exp [m ([D] - [D]_{1/2})/RT]\}/\{1 + \exp[m ([D] - [D]_{1/2})/RT]\} \quad \text{(eq. 1)}$$

where F is the observed spectroscopic signal at the specified denaturant concentration, [D], $F_{0,N}$ and $F_{0,U}$ are the signal characteristic of the native, N, or unfolded, U, state; α_N and α_U are the baseline slopes for the pre- and post-transition regions and $[D]_{1/2}$ is the urea concentration at which the protein is half unfolded, m is the slope of the denaturation curve in the transition region. The error on the estimation of $[D]_{1/2}$ was always less than 0.1 M urea.

Ligand binding to thrombin. The affinity of different ligands [i.e., Na^+, hirudin HM2 and its proteolytic fragments Hir(1-47) and Hir(48-64)] for natural thrombin and mutant D102N was determined at 25 ± 0.1 °C in 5 mM Tris-HCl buffer, pH 8.0, containing 0.1% (w/v) PEG-8000 and the specified Na+concentration, by exciting the protein samples at 280 or 295 nm and measuring the

increase of fluorescence intensity at 334 nm as a function of ligand concentration. Under all conditions tested, the optical density of the solution was always much lower than 0.02 units both at λ_{ex} and λ_{em} and therefore no inner filter effect was observed (17). Aliquots (2-5 µl) of ligand stock solutions were added, under gentle magnetic stirring, to a thrombin solution (5-50 nM, 2 ml) in a 1-cm pathlength cuvette. After stirring (30 s) was stopped, the solution was allowed to equilibrate for 2 min and the signal intensity was recorded at 334 nm. Fluorescence data were corrected for sample dilution, that was always lower than 2% at the and of the titration. Photobeaching was reduced to less than 2%, even after prolonged light exposure, by using a 1-cm pathlength quartz cuvette (2 ml internal volume) with two opaque walls that are able to diffuse the incident light inside the sample, thus preventing photodegradation of Trp-residues. For low-affinity binders, like Na+ and Hir(48-64), fluorescence data were fitted to the equation describing a simple one-site binding mechanism) R + L $\Leftrightarrow$ RL (17),

$$\Delta F/\Delta F_{max} = [RL]/[R] = [L]/(K_d + [L]) \qquad \text{(eq. 2)}$$

where the fluorescence intensity, F, of the receptor, R, at a given concentration of ligand, L, is linearly related to the concentration of the complex [RL], according to the equation $F = [RL]\cdot F_{bound} + [R]_{free}\cdot F_{free}$. $\Delta F = F\text{-}F°$ is the change in thrombin fluorescence in the absence, F°, and presence, F, of the ligand, ΔF_{max} is the maximum signal change at infinite concentration of ligand, $[L]_\infty$, and K_d is the dissociation constant of the complex, RL. The data were interpolated using the program Origin 7.0 (MicroCal Inc., Northampton, MA) to obtain the fitting parameters ΔF_{max} and K_d.

Equation 2 assumes the simplification that at equilibrium $[L]_{free} \cong [L]_{tot}$ and thus it is valid only when $K_d >> [R]$. For tight binders, like full-length hirudin and Hir(1-47), $K_d \cong [R]$ and equation 2 is no longer valid. In these cases, fluorescence data were fitted to the rigorous equation of tight binding (18),

$$\Delta F/\Delta F_{max} = [RL]/[R] = \{([R] + [L] + K_d) - \{([R] + [L] + K_d)^2 - 4\cdot[R][L]\}^{1/2}\}/2\cdot[R]. \qquad \text{(eq. 3)}$$

For Na+ binding to thrombin, a solution containing 50 nM enzyme in 5 mM Tris-HCl, pH 8.0, 0.1% PEG 8000 and 400 mM NaCl was incrementally added to a solution containing 50 nM thrombin in 5 mM Tris-HCl, pH 8.0, 0.1% PEG 8000 and 400 mM ChCl. The ionic strength and enzyme concentration were held constant, while the Na+ concentration was increased (19).

PABA binding. The interaction of PABA with thrombin was monitored by adding, under gentle magnetic stirring in a 1 cm pathlength cuvette, aliquots (2-10 µl) of PABA stock solution (12.5-50 mM) to a solution of thrombin (1.4 ml, 376 nM). At each PABA concentration, thrombin sample was equilibrated for 2 min at 37 ± 0.2 °C and excited at 335 nm, using an excitation/emission slit of 5 and 10

nm, respectively. The increase in fluorescence intensity of PABA in the presence of the enzyme was recorded at the 376 nm as a function of PABA concentration. Fluorescence data were corrected for IFE, since fluorescence intensity is only proportional to the absorbance of the sample up to an optical density of 0.05 units, both at λ_{ex} and λ_{em} (18,19)The following equation was used:

$$F_{corr} = F_{obs} \cdot 10^{[(\Delta Aex + \Delta Aem)/2]} \quad \text{(eq. 4)}$$

where ΔA_{ex} and ΔA_{em} are the observed additional absorbance at the excitation (λ_{ex} = 335 nm) and emission (λem = 376 nm) wavelengths. Fluorescence data were then corrected for sample dilution (< 10% of the final volume) and finally expressed as $\Delta F = F\text{-}F°$, where F° and F is the fluorescence of PABA in the presence and absence of thrombin, respectively.

For a simple one-site binding mechanism R + L ↔RL (also see below) data were interpolated with equation 2, using the program Origin 7.5 (MicroCal Inc., Northampton, MA) to obtain the fitting parameters ΔF_{max} and K_d:

$$\Delta F = F\text{-}F° = (\Delta F_{max} \cdot [L])/(K_d + [L]) \quad \text{(eq. 5)}$$

where K_d is the dissociation constant of the complex, RL, and ΔFmax is the maximum fluorescence change at infinite concentration of ligand, $[L]\infty$. Equation 2 assumes that at equilibrium $[L]_{free} \approx [L]_{tot}$ and thus it is valid only when $K_d >> [R]$, as usually observed for PABA complexes.

Thrombin Inhibition Assays. K_d values of recombinant hirudin HM2 and Hir(1-47) were also estimated by classical competitive inhibition experiments of thrombin-mediated substrate hydrolysis, according to the tight-binding inhibition model (18) as previously detailed (5). The inhibitor was incubated at 25 ± 0.2 °C for one hour with 100 pM thrombin in 5 mM Tris, pH 8.0, containing 0.1% (w/v) PEG-8000 and 0.2 M NaCl or ChCl. The reaction was started by addition of FPR (20 μM) and the release of *p*-nitroaniline (*p*NA) was determined by recording the absorbance increase at 405 nm. The ionic strength was kept constant at 200 mM with NaCl for the fast form or with ChCl when the slow form was being studied. Thrombin inhibition data were fitted to the equation,

$$v_i/v_0 = 1\text{-}\{([E]+[I]+K_I^{app})\text{-}\{([E]+[I]+K_I^{app})^2\text{-}4\cdot[E][I]\}^{1/2}\}/2\cdot[E] \quad \text{(eq.6)}$$

to obtain the apparent inhibition constant, K_I^{app}. [E] and [I] are the total enzyme and inhibitor concentrations and v_i and v_0 are the steady-state velocities of substrate hydrolyisis by thrombin, in the presence (v_i) or absence (v_0) of the inhibitor. K_I^{app} values were corrected for substrate concentration and

for the K_m value of FPR for thrombin under fast and slow conditions (5,20), according to the following equation

$$K_I = K_I^{app}/[1+([S]/K_m)] \quad \text{(eq. 7)}$$

where K_I is equal to the dissociation constant, K_d, of the enzyme-inhibitor complex (18).

RESULTS

Comparison between X-ray structures of thrombin wild-type and mutant D102N. To compare the three-dimensional structures of human alpha-thrombin and mutant D102N we used 1PPB.pdb (21) and 2GP9.pbd (2) files, respectively. In D102N structure the specificity sites, especially the primary specificity site (S1, Asp189) and the Na+-binding site result heavily compromised. In fact the 215-219 strand collapses into the primary specificity pocket and forces the indole ring to pack against the hydrophobic pocket in the active site formed by Trp60d, Tyr60d, His57 and Leu99. In this conformation Trp215 occupies the same position as the Pro ring of the active site inhibitor PPACK. Downstream of the 215-219 strand, the twist in the backbone caused by the collapse of Trp215 moves the entire 220-loop upward changing the orientation of several residues and in particular of Arg221a, that penetrated in the S1 site (Fig.2). The movement of the entire 220-loop makes free the side chain of Arg187 that penetrates into the protein core and into the Na+-binding site, with the guanidium group positioned within 1Å from where sodium would bind (Fig.2). These rearrangements produce a singular thrombin structure, defined by the authors as self-inhibited which theoretically devoid of any sodium and ligand binding properties (4).

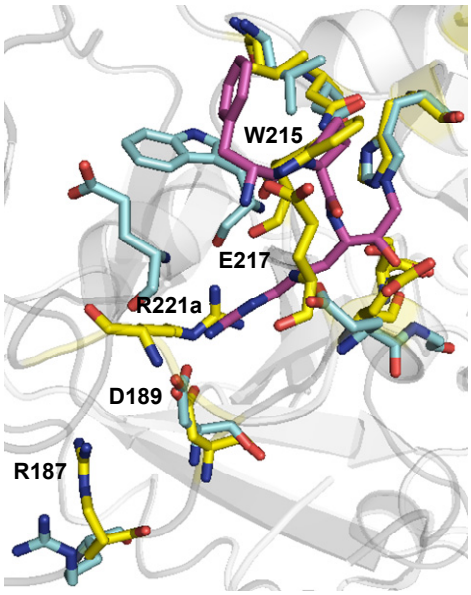

Figure 2. Stereo view of the overlay of the structures of D102N (CPK, with C in yellow) and the PPACK inhibited Na_-bound form (CPK, with C in cyan) reveals the molecular basis of self-inhibition in the D102N structure. Trp-215 and Arg-221a of D102N produce a self-inhibited conformation of the enzyme by occupying positions analogous to Pro and Arg of PPACK (stick model, magenta) in the fast form**.**

Conformational and stability properties of the thrombin mutant D102N. The conformation, stability and the sodium binding properties of thrombin mutant D102N were principally investigated using circular dichroism and fluorescence spectroscopy. When Na+ was removed, to maintain the ionic strength constant, we used Ch+ as a neutral cation. It is widely accepted, in fact, that Ch+ ion has an hydrodynamic radius too large to efficiently interacts with thrombin (22).

The intensity and the shape of the far-UV CD spectra in the absence or in the presence of Na+ (0.2M NaCl) showed how the overall solution structure of D102N was different when compared to the structure of thrombin wild-type (Fig. 3A and 3B). Of note, thrombin wild-type had two minima centred at 210 and 225 nm with a maximum intensity of -4.5x10^3 deg·cm^2·dmol^{-1}, whereas D102N had two minima centred at 209 and 229 nm with a maximum intensity of -3.1x10^3 deg·cm^2·dmol^{-1}. Moreover in the presence of Na+, the dichroic spectrum of D102N did not move significantly, suggesting a compromised signal transmission between the Na+ binding site and the active site of the mutant. In fact Na+ binding to thrombin wild-type strongly reduced the intensity and altered the shape of the CD spectrum (Fig. 2A) and this effect reflected conformational changes likely to occur in the environment of some aromatic amino acids clustered within the S2 and S3 sites of thrombin. These effects become more important for those proteins displaying low signal intensity and are most prominent in systems where aromatic groups are clustered in the protein structure, such as thrombin (15).

Also fluorescence spectroscopy reported relevant differences between thrombin wild-type and mutant D102N. Even if the λ_{max} values did not change between the species, in the absence of Na+ the fluorescence quantum yield (λ_{ex} 280 nm) of the mutant was slightly increased with respect to the wild-type enzyme. Notably this difference was not registered when the samples were excited at 295 nm. Because at 295 nm only tryptophan residues of the protein were excited, the effect observed at 280 nm could be attributed either to a more efficient tyrosine-tryptophan energy transfer in the mutant or more likely to a different chemical environment, more rigid and hydrophobic, experimented by some fluorophores (14). Residue Trp215, in fact, is the main actor in changing fluorescence since its indole ring is flipped of 130° into the active site, becoming less accessible to the solvent. When Na+ (0.2 M) bound to mutant D102N the fluorescence intensity increased up to 7%, about an half of that observed for the wild-type (i.e., 14%) (Fig. 2B) (15) in the same experimental conditions. This incomplete effect found a reasonable explanation by a 6-fold reduced affinity of D102N for the monovalent cation. The Na+ dissociation constant for the wild-type enzyme was calculated as 20 mM whereas it increased to 120 mM for mutant D102N, at 25°C. Interestingly this result was in part unexpected because in the crystallographic structure of D102N the Na+-binding site is occupied by the guanidium group of Arg187 and therefore inaccessible to Na+. However at high concentrations of the cation it's reasonable that Na+ filled its loop and displaced Arg187 triggering a drastic rearrangement of the structure as a whole.

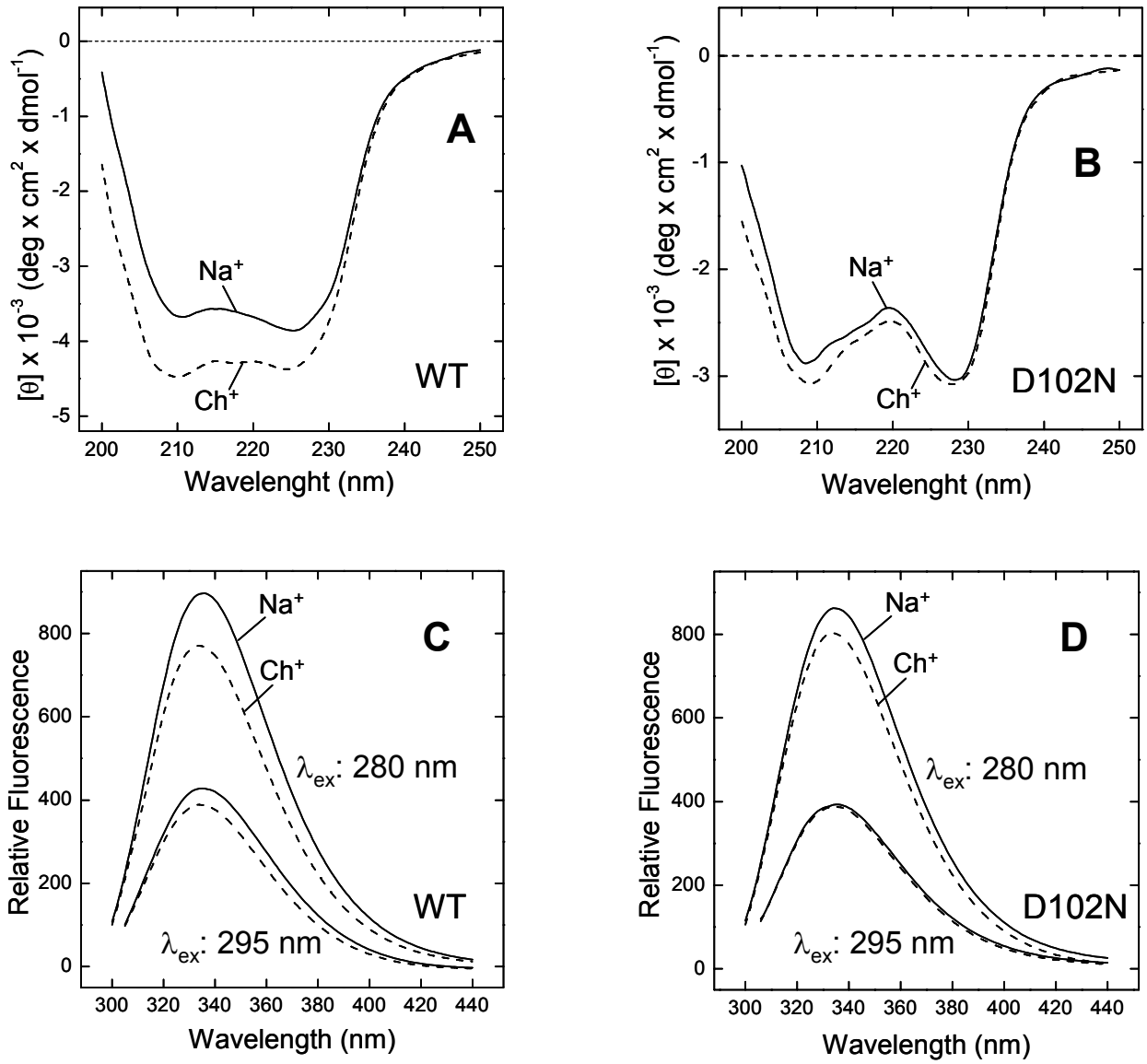

Figure 3. Spectroscopic properties of natural α-thrombin (WT) and mutant D102N. Far-UV CD spectra of natural thrombin (**A**) and D102N (**B**) were obtained at a protein concentration of 6.8 and 5.2 μM in a 1-mm pathlength cuvette. Fluorescence spectra of natural thrombin (**C**) and D102N (**D**) were obtained by exciting the protein sample (2 ml, 50 nM) at 280 or 295 nm. All spectra were taken at 25 ± 0.1°C in 5 mM Tris-HCl buffer, pH 8.0, containing 0.1% PEG-8000, in the presence of 0.2 M NaCl (—) or ChCl (----), as indicated.

Since generally the binding of monovalent and divalent cations increases the thermal and chemical stability of the enzymes, we expected a reduced stability for the mutant D102N. To investigate this, we performed thrombin denaturation experiments at pH 8.0 and 6.5 exciting the sample at 280 and 295 nm (Figures 3A and 3B). In all cases, a single sharp transition was observed, suggestive of a highly co-operative unfolding process. Very interestingly we observed that in the absence of Na+, D102N was more stable to urea-induced denaturation, both at pH 6.5 and 8.0, (Fig. 4) and in particular the $[urea]_{1/2}$ (the concentration of urea inducing the 50% effect) value changed from 2.6 for the wild-type thrombin to 3.1 for the mutant D102N. However in the presence of Na+ (0.2M), both thrombins presented almost the same stability ($[urea]_{1/2}$ = 3.1 ± 0.1M). These results indicate that Na+ efficiently stabilized the

structure of thrombin wild-type (i.e, $\Delta[urea]_{1/2}$ = 0.5M, corresponding to -2.1 kcal mol^{-1}) (15), whereas basically did not influence the stability of the mutant (i.e, $\Delta[urea]_{1/2}$ = 0.1M) that assumed a more closed and locked conformation even in the absence of Na+.

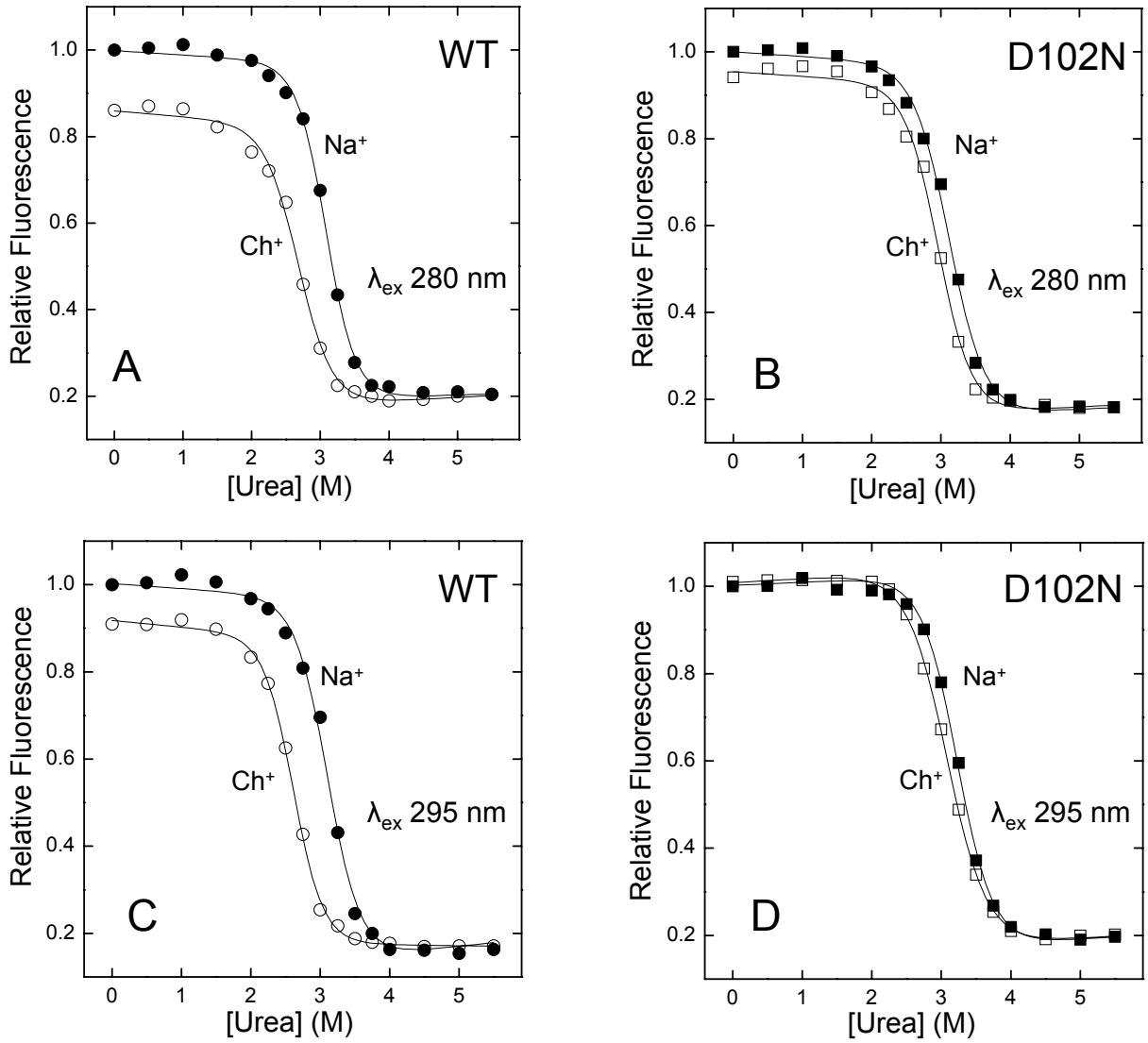

Figure 4. Effect of 0.2 M NaCl on the stability of natural thrombin **(A-C)** and mutant D102N **(B-D)** to urea-induced denaturation. Protein samples (50 nM) were excited at 295 nm and the fluorescence intensity was recorded at 334 nm, as a function of urea concentration. Denaturation experiments were carried out at 25 ± 0.1°C in 5 mM Tris-HCl buffer, pH 8.0, containing 0.1% PEG-8000, in the presence of 0.2 M NaCl (●,■) or ChCl (○,□). Continuous lines represent the best fit of the data points to equation 1, yielding the following [urea]1/2 values: WT, 3.1 and 2.6 M urea , with or without Na+; D102N, 3.2 and 3.1 M urea, with or without Na+.

Binding of PABA to the thrombin mutant D102N. To selectively map the S1 site of thrombin we used PABA (p-aminobenzamidine) as a probe (13). In the absence or at low concentrations of Na+ (0.2M), PABA was not able to efficiently interact with the primary specificity site of D102N. As clearly shown in figure 2 the acidic moiety of Asp189 makes a single salt-bridge within Nζ of the guanidium group of Arg221a. However the ionic bond between Asp189 and Arg221a is less stable respect to Asp189 and Arg1' of the PPACK because of the orientation (2 salt bridges for the PPACK and only one

for D102N) and the distance (2.65Å vs. 2.73Å) between the two polar side chains. Consequently, when we increased the concentration of Na+ up to 0.8M, mutant D102N became able to bind PABA (Fig. 5A), even if with a dissociation constant of 7 and 2 times higher with respect to Na+-bound and Na+-free forms of the wild-type enzyme (Table 1), respectively. Of note the effect of Na+ for the mutant D102N was extremely specific and not a generic scaling up of the ionic strength, since in the presence of 0.8M ChCl PABA had been resulted unable to interact with D102N (Fig. 5B). Data herein proposed suggest and confirm that the S1 site of D102N is partially compromised and less accessible to PABA as basically expected from the crystal details. However when an allosteric modulator such as Na+ interacts with the enzyme, it evokes a more open and accessible conformation. In particular we speculated about a pronounced re-organisation of the residues forming the Na+-binding loop (Asp220-Arg221a, Asp222 and Arg187) that return to complex sodium and consequently free Asp189.

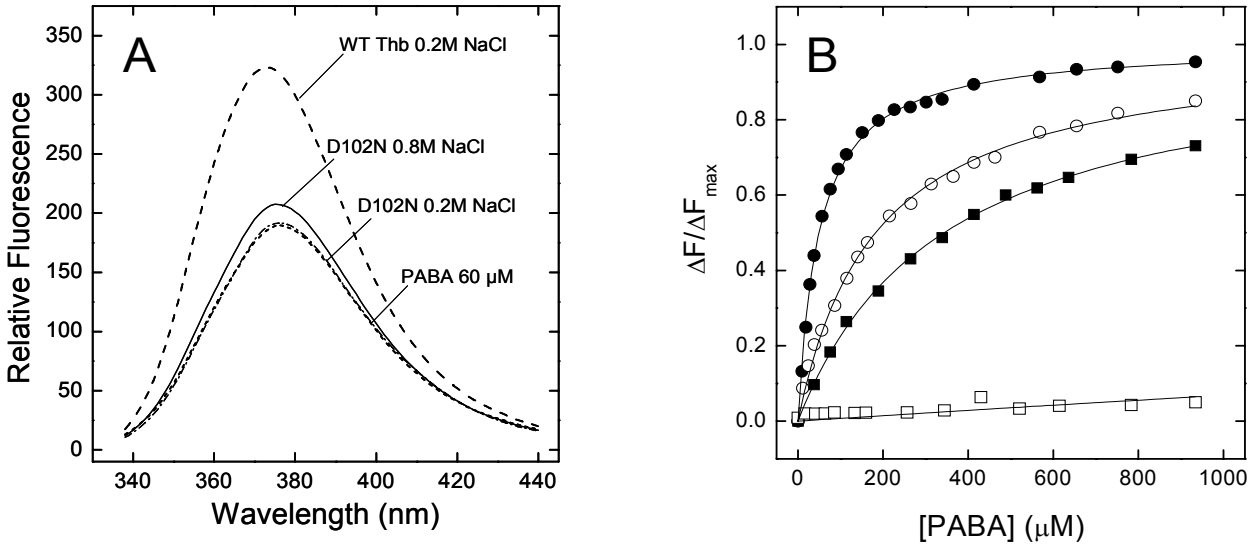

Figure 5. Probing the primary specificity site S1 of natural thrombin and mutant D102N by binding of PABA. (A) To a solution of PABA (60 mM) in 5 mM Tris-HCl buffer, pH 8.0, 0.1% PEG-8000, containing 0.2 or 0.8 M NaCl was added an aliquot (10-20 µl) of natural thrombin or mutant D102N, to a final concentration of 200 nM. Spectra were taken at 25 ± 0.1 °C in a 1-cm pathlength quartz cuvette (0.5 ml internal volume) by exciting the protein samples at 325 nm. **(B)** The interaction of thrombin wild type (●,○) or D102N (■,□) with PABA in the absence (○,□) or in the presence of saturing concentrations of Na+ (●,■) was monitored by adding to a thrombin solution (1.5 ml, 376 nM) aliquots of a stock solution of PABA. Samples were exciting at 335 nm and the fluorescence signal was recorded at 376 nm. Raw data were corrected for the IFE (eq. 4) and subtracted for the corresponding base line due to the PABA solution only (see Materials and Methods).

Table 1. Binding of PABA to Wild-Type Thrombin and Mutant D102N

Thrombin Wild-Type		**Mutant D102N**	
K_d (µM)		K_d (µM)	
0.8 M NaCl	0.8M ChCl	0.8M NaCl	0.8M ChCl
49 ± 2	182 ± 5	354 ± 9	n.d.

All measurements were carried out at 25°C in 5 mM Tris, pH 8.0 containing 0.1% PEG-8,000 in the presence of 800 mM NaCl for the fast form or 800 mM ChCl when the slow form was being studied. Raw data have been corrected for IFE (Inner Filter Effect).

Structural mapping of the thrombin mutant D102N by hirudin HM2 and its fragments Hir(1-47) and Hir(48-64). Hirudin (HM2), a small leech-derived protein composed by 64 residues, binds thrombin with a K_d in the pM range and covers more than 20% of water accessible surface area of the enzyme (15). The high affinity of interaction and the widespread contacts with the active site, through its N-terminal domain (1-47), and exosite 1, through its C-terminal domain (48-64), of thrombin, make hirudin and its fragments an excellent probe to map in detail the conformation of mutant D102N.

All dissociation constants were obtained exploiting the increment of the tryptophan fluorescence signal that gave rise upon the complex formation. In particular, in agreement with previously reported data (23), we observed a fluorescence increase of 35, 23 and 10% with HM2, Hir(1-47) and Hir(48-64), respectively. Exceptionally the interaction of thrombin wild-type with HM2 was estimated by kinetic inhibition assay, because of the very low dissociation constant of the system. When we performed fluorescence studies, in fact, we merely obtained information about the stoichiometry of the interaction (i.e., 1:1) and the concentration of the active site of the enzyme (Fig. 6A) (i.e, represented by the intersection point in between the two lines).

D102N bound full-length hirudin (HM2) 300-fold lower than the wild-type, in the absence of Na+ (Table 2) (Fig. 6B). This drastic decrease in affinity points out that the structure of D102N and more likely its active site, is globally closer and less accessible to inhibitors and substrates but at same time reports how D102N conserves all the correct specificity sites characteristics of the fully active thrombin wild-type. This latter observations is further confirmed taking into account that in the presence of Na+ (0.2M NaCl) the dissociation constant of HM2 for D102N became low, making it undetectable in the experimental conditions used; a similar situation has been described for the wild-type enzyme (Fig. 6A). Moreover, since the concentration of the mutant in solution was as low as 5 nM (Fig. 6B) the expected dissociation constant would be at least 10-50 times lower than the concentration of the enzyme used.

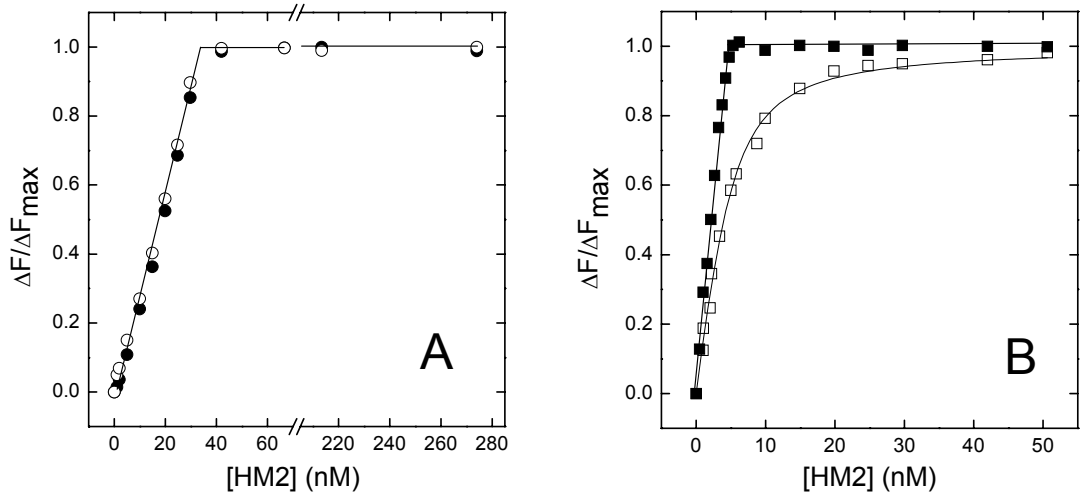

Figure 6. Binding of hirudin HM2 to wild-type thrombin and mutant D102N under fast and slow salt conditions. Fluorescence data were taken at 25 ± 0.1 °C in 5 mM Tris-HCl buffer, pH 8.0, 0.1% PEG-8000, containing 0.2 M NaCl or ChCl. **(A)** Binding of full-length hirudin HM2 to the wild-type enzyme (30 nM) under fast (●) and slow (○) salt conditions. (**B**) Binding of full-length hirudin HM2 to the mutant D102N (5 nM) under fast (■) and slow (□) salt conditions. Excitation wavelength was settled at 280 nm.

With the aim to better understand the basis of such impaired affinity between mutant D102N and HM2, we cut full-length hirudin into its N-terminal domain Hir(1-47), which selectively interacts with the active site of the enzyme, and into its C-terminal domain Hir(48-64), which interacts with the exosite 1. The interaction of Hir(1-47) was seriously compromised reporting a net loss of affinity of 600 times, a value similar to what observed with the full length hirudin. Since Hir(1-47) generally penetrates the active site and interacts with S2 and S3 sites of the enzyme, and since the S2 site of mutant seems to be conserved, it's reasonable to affirm that the failure of affinity is due to the movement of the 215-219 strand, which contains the S3 site, deep down into the active site pocket. By contrary the binding of Hir(48-64) to exosite 1 of D102N was only 3.5 times higher with respect to the wild-type, indicating that the exosite 1 is almost conserved.

Table 2: Structural mapping of the thrombin mutant D102N by hirudin HM2 and its fragments Hir(1-47) and Hir(48-64)

Thrombin Wild-Type			
	0.2 M NaCl	**0.2 M ChCl**	**r**
HM2	0.20 ± 0.03 pM	5.5 ± 0.6 pM	27.5
Hir(1-47)	40 ± 2 nM	1440 ± 20 nM	34.3
Hir(48-64)	0.8 ± 0.1 μM	8.0 ± 0.3 μM	10
Hir(1-47) +Hir(48-64)	37 ± 2 nM	140 ± 10 nM	3.9
Mutant D102N			
	0.2 M NaCl	**0.2 M ChCl**	**r**
HM2	< 0.1 nM	1.6 ± 0.2 nM	-
Hir(1-47)	24 ± 2 μM	154[a] ± 40 μM[a]	6.4
Hir(48-64)	1.9 ± 0.1 μM	19.3 ± 0.9 μM	10.1
Hir(1-47) +Hir(48-64)	2.9 ± 0.1 μM	120[a] ± 30 μM[a]	41.4

All measurements were carried out at 25°C in 5 mM Tris, pH 8.0 containing 0.1% PEG-8,000 in the presence of 200 mM NaCl or 200 mM ChCl. [a]Dissociation constants were extrapolated at 0 M NaCl using a linkage equation reported previously by Arosio et al., 2000.

In summary the isosteric substitution Asp→Asn principally altered the region of the active site making it less accessible towards substrates and inhibitors. Nevertheless, contrary with the idea proposed for the S* form of thrombin, mutant D102N is not a dead enzyme devoid of any ligand binding properties. D102N in fact interacts with some active site probes in the micromolar range and most notably these interactions can be positively modulated by the presence of allosteric effectors either Na+ or exosite 1 binders, such as Hir(48-64) (Fig. 7 and Fig.8).

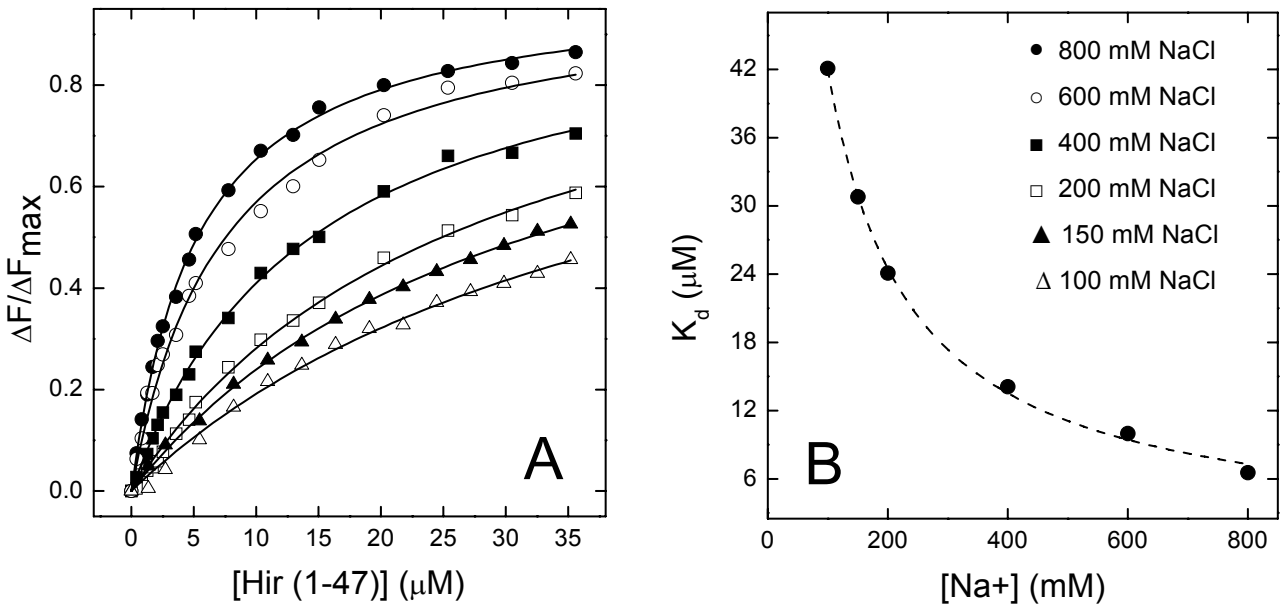

Figure 7. Binding of Hir(1-47) to thrombin mutant D102N as a function of [Na+]. (A) Fluorescence data were taken at 25 ± 0.1 °C in 5 mM Tris-HCl buffer, pH 8.0, 0.1% PEG-8000, containing increasing concentrations of NaCl, as indicated. To a solution of D102N (40 nM) was added aliquots (1-10 μl) of Hir(1-47) to a final concentration of 35 μM. Spectra were taken at 25 ± 0.1 °C in a 1-cm pathlength quartz cuvette (3 ml internal volume) by exciting the protein samples at 280 nm. **(B)** The dissociation constants of Hir(1-47) for D102N were plotted as a function of Na+. The linkage equation used to fit the data permitted us to obtain the extrapolated value of Kd for Hir(1-47) at 0M NaCl (see table 2) and the dissociation constant of Na+ for mutant D102N (i.e. = 80 mM), constant that is in close agreement with that obtained previously by direct fluorescence measurements.

As reported in figure 7 the affinity of the mutant D102N for Hir(1-47) increased as a function of sodium concentration following a saturable behaviour (Fig.7B). This is clearly shown by plotting the dissociation constants obtained from each single binding experiment as a function of sodium. The linkage equation used to fit the data permitted us to obtain the extrapolated value of K_d for Hir(1-47) at 0M NaCl (Table 2) and the dissociation constant of Na+ for mutant D102N (i.e., 80 mM), constant that is in close agreement with that obtained previously by direct fluorescence measurements (i.e., 120 mM). Most notably at 0.8M NaCl the dissociation constant of Hir(1-47) was reduced up to 4 times, indicating that the sodium binding site and S2 and S3 sites are thermodynamically related. Similar considerations have been made for the S1 site. Also the perturbation of exosite 1 positively modulates the active site and thus in the presence of saturing concentrations of Hir(48-64) the dissociation constant for Hir(1-47) dropped down to 10 times, exactly form 24 to 2.9 μM (Table 2). Very interestingly this allosteric effect was more pronounced in the presence of sodium, exactly the opposite respect to thrombin wild-type. The binding of Hir(48-64) to the Na+-free form of the native enzyme is, in fact, sufficient to trigger the enzyme into a more open and accessible species likely because the extreme structural plasticity of thrombin whereas it's not sufficient to evoke in D102N a new conformation in solution. Since D102N assumes a more closed, rigid and stable conformation, we speculated that D102N could represent a locked form of an enzyme that has to walk through an higher activation barrier in order to transform.

Consequently the binding of a singular allosteric modulator results unable to unlock the structure, that is definitely free when more effectors act together, sinergically.

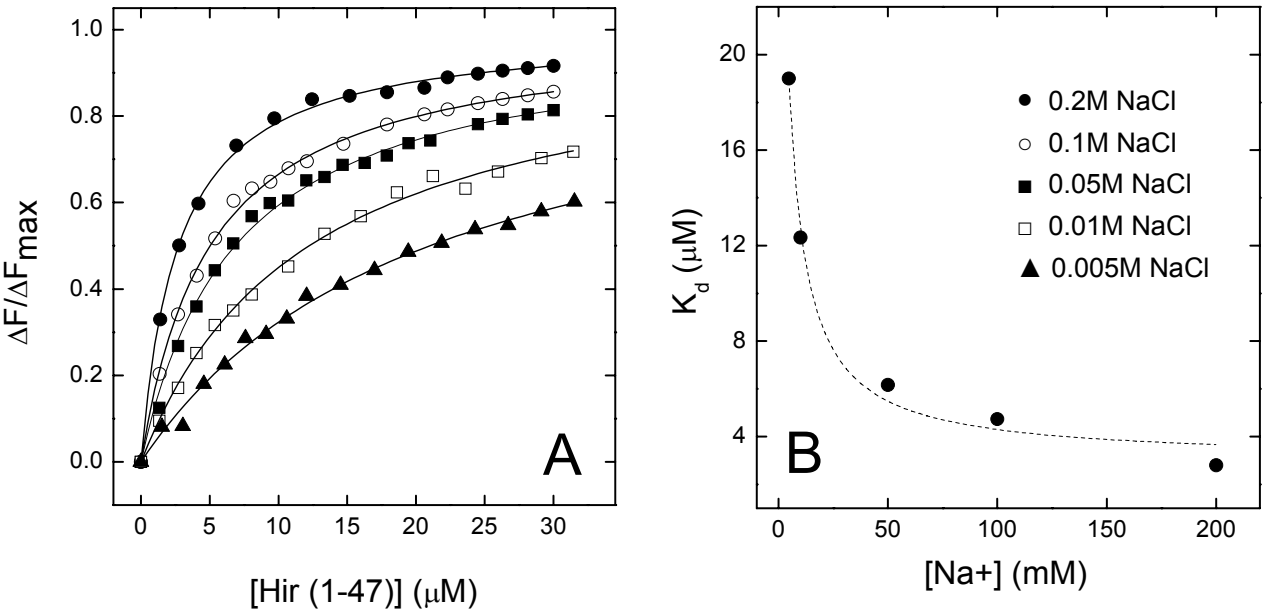

Figure 8. Binding of Hir(1-47) to thrombin mutant D102N under saturing concentration of Hir(48-64), as a function of [Na+]. (A) Fluorescence data were taken at 25 ± 0.1 °C in 5 mM Tris-HCl buffer, pH 8.0, 0.1% PEG-8000, containing increasing concentrations of NaCl, as indicated. To a solution of D102N (40 nM) and Hir(48-64) (100 μM) was added aliquots (1-10 μl) of Hir(1-47) to a final concentration of 30 μM. Spectra were taken at 25 ± 0.1 °C in a 1-cm pathlength quartz cuvette (3 ml internal volume) by exciting the protein samples at 280 nm. (**B**) The dissociation constants of Hir(1-47) for D102N were plotted as a function of Na+. The linkage equation used to fit the data permitted us to obtain the extrapolated value of K_d of Hir(1-47) at 0M NaCl (see table 2) and the dissociation constant of Na+ for mutant D102N under saturing concentrations of Hir(48-64) (i.e. = 10 mM).

Binding of Hir(1-47)S2R to the thrombin mutant D102N. Hir(1-47) covers the catalytic pocket and penetrates the S2 and S3 sites whereas analogue Hir(1-47)S2R makes an extra-interaction respect to Hir(1-47) with S1 site. The effects of the replacement of Ser2 with Arg, whose long charged side-chain is expected to facilitate penetration of the inhibitor into thrombin recognition sites, act with a greater extent in the case of the more closed Na+-free form than in the case of the Na+-bound form of the enzyme, which is already accessible for binding. As expected the K_d value for the fast form diminished of 25 times, from 40 to 1.6 nM, and the K_d value for the slow form dropped down of 120 times, from 1440 to 12 nM (Table 3) both respect to Hir(1-47). In the case of D102N, that resembles a compact and inaccessible sphere, both Na+-free and Na+-bound conditions were very sensitive to the analogue Hir(1-47)S2R thanks to the presence of that arginin-hook that could penetrate into the active site. Consequently the K_d values for the interaction of Hir(1-47)S2R fall down of 600 times passing from the micromolar range to the nanomolar range. Opposite to Hir(1-47), the presence of saturing concentrations of Hir(48-64) further increased the affinity of the analogue Hir(1-47)S2R up to 4 times only in the absence of Na+ whereas an insignificant effect was observed in the presence of Na+.

Apparently this situation could sound contradictory and without sense, but it perfectly reflects the behaviour of an allosteric enzyme. In the case of Hir(1-47), to maximize the interaction with the mutant, both Na+ and Hir(48-64) are needed. They, in fact, force D102N to assume a more open and accessible conformation that is fundamental for the interaction with Hir(1-47). Such inhibitor, in fact, uses a lock and key mechanism to interact with the active site of thrombin. Conversely, the extra positive side chain of Hir(1-47)S2R functions as an hook that penetrates deep into the active site, anchors the S1 site and once bounded, forces the structure to open throughout an induced fit mechanism. So in this scenario, the presence of an allosteric modulator permits to increase the affinity of our probe only moving and reorienting the region next to the S1 site.

Table 3. Binding of Hir(1-47)S2R to Wild-Type Thrombin and Mutant D102N

	Wild-Type Thrombin			
	0.2 M NaCl	**0.2 M ChCl**	**$\Delta G_{b}c$ (kcal/mol)**	**r**
S2R	1.6 ± 0.02[a] nM	12 ± 0.2[a] nM	-1.2	7.5
	Mutant D102N			
	0.2 M NaCl	**0.2 M ChCl**	**$\Delta G_{b}c$ (kcal/mol)**	**r**
S2R	40 ± 2 nM	270 ± 4 nM	-1.1	6.7
S2R +Hir(48-64)	30 ± 2 nM	77 ± 3 nM	-0.6	2.6

[a] K_d values for S2R to wild-type thrombin were determined from the analysis of the competitive inhibition of the hydrolysis of the substrate D-Phe-Pro-Arg-*p*-nitroanilide (20 μM), and calculated according to the slow tight-binding model of thrombin inhibition (Ayala & Di Cera, 1994). All measurements were carried out at 25°C in 5 mM Tris, pH 8.0 containing 0.1% PEG-8,000 in the presence of 200 mM NaCl for the fast form or 200 mM ChCl when the slow form was being studied.

[b] ΔGc is the coupling free energy, measured as $\Delta Gc = \Delta Gb$,fast - ΔGb,slow (Ayala & Di Cera, 1994). The value of ΔGc is negative if the inhibitor binds preferentially to the fast form.

DISCUSSION

Serine proteases play a pivotal role in many different, important biological processes, including digestion, inflammation, cell differentiation and blood coagulation. The results of protein engineering studies accumulated so far indicate that mutations of the amino acids at the active site of some of these enzymes dramatically decrease or even abolish their catalytic function, while the 3D structure of the resulting mutants remains essentially unchanged. Relevant examples in this field are the mutation of the catalytic Asp102 with Asn in trypsin (24) and that of the catalytic Ser195 with Ala in human alpha-thrombin (25). Recently, the Asp102Asn mutant (D102N) of human alpha-thrombin has been produced and its crystallographic structure solved at high resolution (4). As expected, the hydrolytic activity is

decreased by $16x10^3$ fold, compared to that of the wild-type enzyme. Quite surprisingly, the 3D structure is significantly compromised, especially in the Na+-binding site and in the primary specificity site, adopting a self-inhibited conformation, with the active site occluded. Very recently the Na+-binding mechanism to thrombin has been unravelled by solution rapid kinetic studies (2). The mechanism seems to obey the following biphasic scheme: S* ⇔ S ⇔ F. In this mechanism it is claimed that S* is a very low populated form of thrombin(< 5%) that totally lacks of any ligand and Na+ binding properties. Considering the crystallographic evidences on thrombin mutant D102N, it has been proposed that this mutant could genuine represent the inactive S* thrombin form.

To determine if the crystallographic structure of D102N might represent S* in solution phase or it is an unpredictable picture generating by the isosteric mutation Asp→Asn, we performed systematic solution studies in order to investigate the behaviour of the mutant in solution. In this study, a thorough conformational characterization of the mutant protein was conducted by circular dichroism, fluorescence spectroscopy and stability measurements, and using several different ligands/inhibitors that map selectively different regions of the enzyme.

Our results show that D102N mutant binds Na+ with six-fold lower affinity (K_d 120 mM) than wild type thrombin (18.5 mM). In the absence of Na+ (0.2 M ChCl), the affinity of full-length hirudin for D102N mutant is reduced by about 300-fold, whereas that of the C-terminal tail Hir(48-64) is only two-fold lower. Under salt conditions stabilizing the fast form of the wild type enzyme (0.2 M NaCl), Hir(1-47) binds D102N with a 600-fold lower affinity compared to the wild type enzyme. The affinity of Hir(1-47) for the D102N mutant increases by five-fold upon increasing NaCl concentration from 0.2 to 0.8 M. Even the binding of PABA, a low-molecular weight inhibitor binding in the primary specificity site S1 of thrombin, was enhanced in the presence of 0.8 M NaCl. Additional effects on the binding of Hir(1-47) to D102N were observed in the presence of saturating concentrations of the C-terminal hirudin tail Hir(48-64), since the dissociation constant for Hir(1-47) dropped down of ten times. Most notably the analogue Hir(1-47)S2R binds D102N in the nanomolar range, only 20 times lower respect to the wild-type, suggesting an induce-fit mechanism that definitely opens the enzyme.

These findings are fully consistent with the high-resolution structure of D102N, showing that the recognition sites are not accessible for ligand binding. However, the D102N mutant is not a dead enzyme and at higher Na+ concentration and/or in the presence of exosite-1 binders it can assume a more open conformation, likely resembling that of the wild-type enzyme, in agreement with data reported very recently (26). Our findings also highlight the extraordinary structural plasticity of thrombin molecule and demonstrate that even a single isosteric amino acid replacement, like the D102N mutation, can cause dramatic and unpredictable changes in the resulting mutant structure. The structural rearrangement observed with D102N can be rationalized considering the unique surface electrostatic potential of thrombin, characterized by two positive patches (i.e., exosites 1 and 2) flanking the negative catalytic pocket, which, in turn, is surrounded by a negative ring formed by Glu39, Asp60e, Glu61,

Asp63, Glu97a, Asp189, Glu192, Asp193, Glu217, Asp221, and Asp222. Replacement of the negative D102 with the neutral N102 is likely to dramatically perturb the surface electrostatic potential of thrombin, thus stabilizing the enzyme into a more closed conformation (Fig. 9). In the near future, further protein engineering and molecular dynamics studies will contribute to clarify this point, that may be of general relevance to all chymotrypsin-like serine proteases.

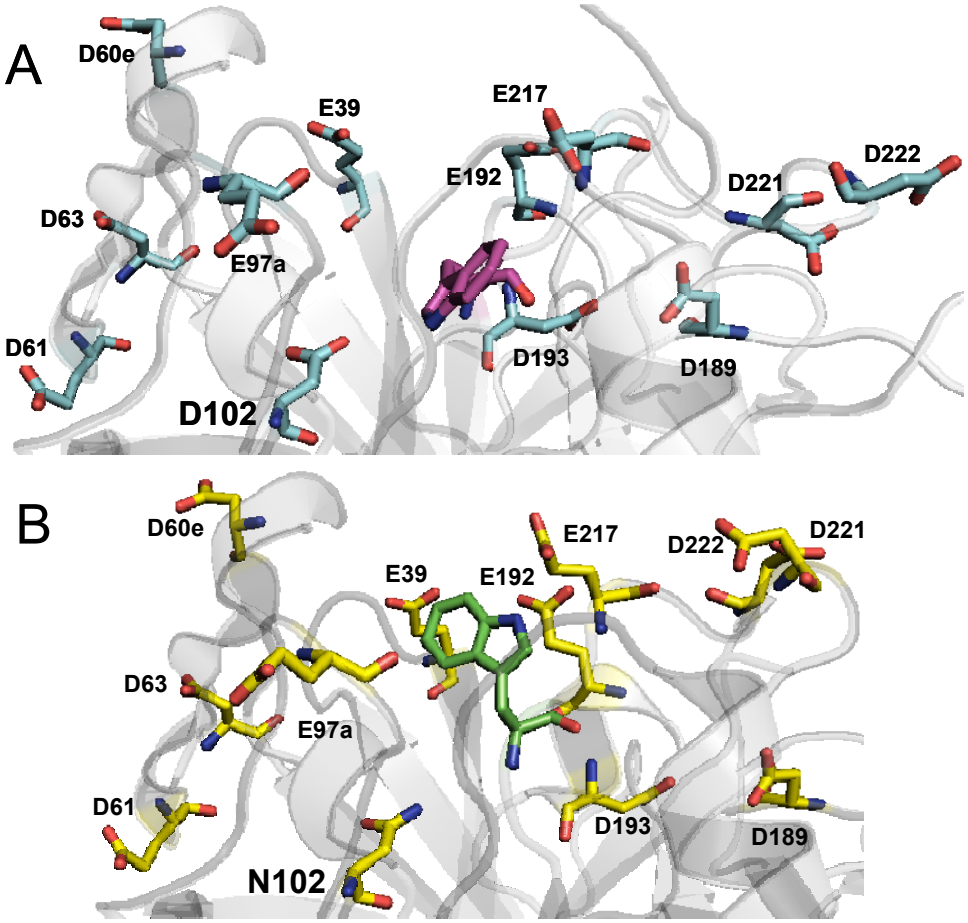

Figure 9. Stereo view structures of the PPACK inhibited Na_-bound form (A) and D102N (CPK, with C in yellow) (B) reveals the molecular basis of the 215-219 strand collapse into the active site. For clarity in the wild-type structure PPACK has been removed.

The results obtained with D102N mutant also pose serious problems in the interpretation of protein engineering data, where changes in the chemical composition of the protein chain are related in straightforward way to changes in the function, without careful structural characterization of the resulting mutant protein.

REFERENCES

1. Di Cera, E., Page, M. J., Bah, A., Bush-Pelec, L. A., and Garvey L. (2006). Thrombin Allostery. *Phys. Chem. Chem Phys.* 9, 1292-1306.

2. Bah, A., Carvey, L. C., Ge, J. and Di Cera E. (2006). Rapid Kinetics of Na+ Binding to Thrombin. *J. Biol. Chem.* 281, 40049-40056.
3. Guinto, E.R., Vindigni, A., Ayala, Y.M., Dang, Q.D., and Di Cera, E. (1995). Identification of Residues Linked to the slow-->fast transition of Thrombin. *Proc Natl Acad. Sci. USA* 92, 11185-11189.
4. Pineda, A. O., Chen, Z., Bah, A., Carvey, L. C., Mathews, S. F., and Di Cera E. (2006). Crystal structure of thrombin in a self-inhibited conformation. *J. Biol. Chem.* 281, 32922-39928.
5. De Filippis, V., Colombo, G., Russo, I., Spadari, B., and Fontana, A. (2002) Probing hirudin-thrombin interaction by incorporation of noncoded amino acids and molecular dynamics simulation. *Biochemistry*. 43, 1537-1550.
6. Vindigni, A., De Filippis, V., Zanotti, G., Visco, C., Orsini, G., and Fontana, A. (1994) Probing the structure of hirudin from Hirudinaria manillensis by limited proteolysis: Isolation, characterization and thrombin-inhibitory properties of N-terminal fragments. Eur. J. Biochem. 226, 323-333.
7. Albericio, F. (2004) Developments in peptides and amide synthesis. *Curr. Opin. Chem. Biol.* 8, 211-221.
8. De Filippis, V., Vindigni, A., Altichieri, L., and Fontana A. (1995) Core domain of hirudin from leech. *Hirudinaria manillensis.* Chemical synthesis, purification and characterization of a Trp3-analogue of fragment 1-47. *Biochemistry.* 34, 9552-9564.
9. De Filippis, V., Qiarzago, D., Vindigni, A., Di Cera, E. and Fontana, A. (1998). Synthesis and Characterization of more Potent Analogues of Hirudin fragment 1-47 Containing non-Natural Amino Acids *Biochemistry*, 37, 13507-13515.
10. Stoll, V.S., and Blanchard, J. (1990) Buffers: principles and practice. *Methods Enzymol.* 182, 24-38.
11. Gill, S.G. and von Hippel, P.H. (1989) Calculation of protein extinction coefficients from amino acid sequence data. *Anal. Biochem.* 182, 319-326.
12. Dang, Q.D., Vindigni, A., and Di Cera, E. (1995) An allosteric switch controls the procoagulant and anticoagulant activities of thrombin. *Proc. Natl. Acad. Sci*. USA 92, 5977-5981.
13. Evans, S. A., Olson, S. T., and Shore J. D. (1982). p-Aminobenzamidine as a Fluorescence Probe for the Active Site of Serine Proteases. *J. Biol. Chem.* 257, 3014-3017.
14. Eftink, M. R. (1994) The use of fluorescence methods to monitor unfolding transitions in proteins. *Biophys. J.* 66, 482-501
15. De Filippis, V., De Dea, E., Lucatello, F., and Frasson, R. (2005). Effect of Na+ Binding on the Conformation, Stability and Molecular Recognition Properties of Thrombin. *Biochem. J.,* 390, 485-492.
16. Di Stasio, E., Bizzarri, P., Misiti, F., Pavoni, E., and Brancaccio, A. (2004) A fast, accurate procedure to collect and analyse unfolding fluorescence signal: the case of dystroglycan. *Biophys. Chem.* 107, 197-211.

17. Lakowicz, J.R. (1999) Principles of Fluorescence Spectroscopy 2nd ed., Kluwer Academic/Plenum, New York.
18. Copeland, R. A. (2000) Kinetics of Single-Substrate Enzyme Reactions. In Enzymes, pp. 109-145, Wiley-VHC Inc., New York
19. Krem, M.M., and Di Cera, E. (2003) Dissecting substrate recognition by thrombin using the inactive mutant S195A. *Biophys Chem.* 100, 315-323.
20. Di Cera, E., Dang, Q.D. and Ayala, Y.M. (1997). Molecular Mechanisms of Thrombin *Function. Cell. Mol. Life Sciences* 53, 701-730.
21. Bode, W., Turk, D. and Karshikov, A. (1992) The Refined 1.9-Å X-ray Crystal Structure of D-Phe-Pro-Arg-chloromethylketone-inhibited Human α-Thrombin: Structure Analysis, overall Structure, Electrostatic Properties, Detailed Active-Site Geometry, and Structure-Function Relationships. *Protein Sci.* 1, 426-471.
22. Ayala, Y., and Di Cera, E. (1994). Molecular Recognition by Thrombin. Role of the Slow-Fast Transition, Site-Specific Ion Binding Energetics and Termodynamic Mapping of Structural Components. *J. Mol. Bio.* 235, 733-746.
23. Jackman, M. P., Parry, M. A. A., Hofsteenge, J. and Stone S. R. (1992). Intrinsic Fluorescence Change and Rapid Kinetics of the Reaction of Thrombin with Hirudin. *J. Biol. Chem.* 267, 15375-15383
24. Craik, C.S., Roczniak, S., Largman, C., Rutter, W.J. (1987). The catalytic role of the active site aspartic acid in serine protease. *Science.* 237, 909- 913.
25. Huntington, J.A., and Esmon, C. (2003) The molecular basis of thrombin allostery revealed by a 1.8-Å structure of the "slow" form. *Structure* 11, 469-479.
26. Gandhi PS, Chen Z, Mathews FS, Di Cera E. Structural identification of the pathway of long-range communication in an allosteric enzyme. *Proc Natl Acad Sci U S A.* 2008 12;105:1832-7.

CHAPTER 2.3.

Thrombin Allostery: Effect of Exosite 1 and 2 Binders on the Molecular Recognition Properties and Catalysis of Thrombin

Nicola Pozzi [1], Roberta Frasson[1], Davide Zaramella[1] and Vincenzo De Filippis [1]

[1] *Department of Pharmaceutical Sciences, University of Padua, via F. Marzolo 5, I-35131 Padua, Italy*

INTRODUCTION

Thrombin is an allosteric enzyme that plays a pivotal role in maintaining haemostasis. Once generated at the end of the coagulation cascade, thrombin is engaged in procoagulant, anticoagulant and fibrinolytic processes. These seemingly contrasting roles are carefully regulated by thrombin's interaction with factors and co-factors that are located either in blood or vasculature. The binding of ligands to thrombin is promoted by exosites 1 and 2, which are positively charged domains that flank the active site. These exosites facilitate the binding of substrates or cofactors and align them for optimal interaction with the active site.

Exosite 1 is predominantly used by substrates such as fibrinogen, factors V and VIII, and the protease activated receptors (PARs) on platelets. Effectors that modulate thrombin activity, including thrombomodulin, hirudin, and heparin cofactor II, also utilize exosite 1. Fewer processes are mediated by exosite 2, which serves largely as a tether that anchors thrombin for participation in other reactions. Thus, heparin binds exosite 2 and catalyzes thrombin inhibition by antithrombin and heparin cofactor II. Exosite 2 also is used by glycoprotein 1bα (GP1bα) on platelets to localize thrombin for activation of PARs. Although the prevailing role of the exosites is to bring substrates and cofactors into proximity with thrombin, there is evidence that the exosites also serve as allosteric regulators of thrombin activity. For instance the binding of a thrombomodulin fragment (EGF 4-5-6) to exosite 1 was shown to alter the environment of an active site fluorescent probe (1) and accelerates the rate of protein C and TAFI activation in an allosteric fashion. In contrast, exosite 1-binding peptides from heparin cofactor II or fibrinogen decrease the rate of protein C activation (2). Additionally, the binding of ligands to exosite 1 alters the rates of chromogenic substrate hydrolysis (2,3,4). Allosteric effects are not limited to exosite 1 because prothrombin fragment 2 (F2), a cleavage product of prothrombin, binds exosite 2 and decreases the rate at which thrombin converts fibrinogen to fibrin and is inhibited by antithrombin. Also the fibrinogen elongated γ-chain, recently pointed out as an exosite 2 binder, inhibits thrombin-induced platelet aggregation towards allosterically modulate PAR-1 hydrolysis (5). Moreover a monoclonal antibody that binds to exosite 2 affects the rate at which thrombin cleaves various p-nitroanilide

substrates having arginine in the P1 position, generally increasing the k_{cat} for substrates having glycine in P2 and decreasing the k_{cat} for substrates having proline in P2 (6). In support of the concept that these alterations are allosteric in origin, fluorescent probes bound to the active site of thrombin undergo a change in fluorescence intensity when exosite 2 is occupied (7,8). Even if there is good evidence for allosteric regulation of the active site by the exosites, it remains unclear how the long-range communication is transferred from the exosites to the active site and which are the specificity sites of thrombin major involved along the process.

In order to unravel some features of this system, we composed a library of well-established exosite 1 (hirudin$^{54-65}$, haemadin$^{45-57}$, PAR-1$^{50-60}$, and HD1) and exosite 2 (γ'-peptide$^{408-427}$, GpIbα$^{268-282}$, HD22, heparin) binders. The effect of these allosteric modulators on the catalytic cycle of thrombin (i.e. E+S↔ES→E+P) was studied. Initially we analyzed changes of the catalytic process as a whole, exploiting the specific activity of thrombin towards two model chromogenic substrates, such as S2238 ((D)-Phe-Pipecoyl-Arg-pNA) and S2366 (PyroGlu-Pro-Arg-pNA). We then exclusively investigated the Michaelis-complex (ES) formation, focusing our attention on the thrombin active site. For this purpose we used two highly specific inhibitors such as p-aminobenzamidine (PABA) and the N-terminal domain of hirudin (Hir(1-47)). Finally we proposed two different binding models for exosite 1 and 2 that might reasonably explain structural and biochemical effects observed in thrombin so far.

MATERIALS AND METHODS

Materials. N^{α}-Fmoc protected amino acids, solvents and reagents for peptide synthesis were purchased from Applied Biosystems (Foster City, CA) or Bachem AG (Bubendorf, Switzerland). PABA, deuterated water, and trypsin were from Sigma. Buffers, urea and organic solvents were of analytical grade and purcahsed from or Fluka. S2238 and S2366 were purchased was purchased from Chromogenix (Milan, Italy). HD1 and HD22 were purchased from Primm (Milan, Italy).

Expression and Purification of Recombinant Thrombin. Human recombinant α-thrombin was expressed and refolded as previously described. Briefly, after transformation of pET23(+)-Pre2 vector into E. coli strain BL21Star(DE3)pLysS, cells were cultured at 37°C in LB broth with 50 ug/ml ampicillin and 34 ug/ml chloramphenicol to a OD_{595} of 0.8, followed by induction with 1 mM isopropyl β-D-thiogalactoside (IPTG) for 6 h. Harvested cells were stored at –80°C. Thawed cell pellets (typically from 0.8 liter of cell culture) were lysed in 20 mM Tris-HCl, 1% (v/v) Triton-X, 20 mM EDTA and 20 mM dithiothreitol (DTT), pH 7.4, and sonicated on ice in 15-s bursts for a total of 3 min. After centrifugation at 4500 rpm for 15 min, inclusion body pellets were sequentially washed, then centrifugated, with 20 mM Tris-HCl, 20 mM EDTA, first containing 20 mM (DTT) and 1% (v/v)

Triton-X, then containing 1 M NaCl, and finally with 20 mM Tris-HCl, 20 mM EDTA alone. The washed pellets were resuspended in 1 ml of H_2O-TFA 0.1%, subdivided in aliquots of 100 µl each and stored at -20°C until use. Each aliquot was then solubilized in 1 ml 6 M guanidinium-chloride, 30 mM L-cysteine, and incubated at 25°C for three hours. Refolding was initiated by dilution of the solubilized protein to 5 ml of Gnd-HCl 6 M, 50 mM NH_4+AC-, 0.6 M L-arginine, 0.5 M NaCl, 1 mM EDTA, 10% Glycerol, 0.2% Brij 58, 1 mM L-cysteine, then by a dropwise dilution with 250 ml of 50 mM NH_4+AC-, 0.6 M L-arginine, 0.5 M NaCl, 1 mM EDTA, 10% glycerol, 0.2% brij 58, 1 mM L-cysteine, pH 8.5. The refolded protein was dyalised against 10 litres of 25 mM tris-HCl, 2 mM EDTA, 0.1% PEG 6000 and 0.12 M NaCl at 25°C, overnight. The precipitate was removed by centrifugation and filtration before purification of the correctly folded prethrombin-2 on a 5 ml heparin-Sepharose column (GE Lifescience) eluting with a gradient of 0.12-0.95 M NaCl. The inactive protein eluted from heparin-sepharose column was collected and incubated for 1 h at 37° with snake venom from E. carinatus (1:10, enzyme:substrate ratio) that had been pre-treated with PMSF to inhibit serine protease activity. After 3-fold dilution with 50 mM Tris-HCl, pH 7.4, thrombin was purified on a heparin-Sepharose column as described above. The concentration of thrombin was estimated by measuring the absorbance at 280 nm and the samples were immediately frozen until use.

The purity of thrombin preparations (~98%) was established by SDS/PAGE (12% acrylamide gel) and RP-HPLC on a C4 analytical column (4.6 x 150 mm, 5 µm particle size, 300 Å porosity) from Grace-Vydac (Hesperia, CA, U.S.A.). The column was equilibrated with 0.1% (v/v) aqueous TFA and eluted with a linear 0.1% (w/w)-TFA-acetonitrile gradient at a flow rate of 0.8 ml/min. The absorbance of the effluent was recorded at 226 nm. The chemical identity of the purified proteins was established by ESI-TOF mass spectrometry on a Mariner instrument from Perseptive Biosystems (Stafford, TX, U.S.A.). The nozzle temperature was set at 140°C and the electrostatic potential at 4.4 kV. The instrument was calibrated using the standard protein kit from Sigma.

Synthesis and Chemical Characterization of Hir(1-47) and exosite binders. Recombinant hirudin variant HM2 (9) was a generous gift of Dr. Gaetano Orsini (Farmitalia Carlo-Erba, Milan, Italy). The peptide Hir(1-47) was obtained by limited proteolysis of hirudin HM2 with trypsin, as detailed elsewhere (10). The other peptides were obtained by solid-phase synthesis, using standard Fmoc-chemistry (11) on a model PS3 automated synthesizer from Protein Technologies (Tucson, AZ) (12). The peptides were purified by RP-HPLC and their chemical identity was carefully established by high-resolution mass spectrometry on a Mariner ESI-TOF instrument from Perseptive Biosystems (Stafford, TX).

Spectroscopic measurements. Protein and peptide concentration was determined by UV absorption at 280 nm (13) on a Lambda-2 spectrophotometer from Perkin-Elmer (Norwalk, CT) using a molar

absorptivity value of 66390 M^{-1} cm^{-1} for rThb, 2920 $M^{-1}\cdot cm^{-1}$ for fragment Hir(1-47) and 6970 $M^{-1}\cdot cm^{-1}$ for PAR-1^{50-60}. The concentration of haemadin$^{45-57}$, having only Phe as aromatic chromophore in the sequence was taken as 400 $M^{-1}\cdot cm^{-1}$ at 257 nm, respectively. Finally the concentration of hirudin$^{54-65}$ (HV1), γ'-peptide$^{408-427}$ and GpIbα$^{268-282}$, containing phosphotyrosine residues, was taken as 548, 696 and 1044 $M^{-1}\cdot cm^{-1}$ at 257 nm, respectively. The active-site concentration of thrombin solutions was determined by titration with hirudin HM2 in the presence of FPR as chromogenic substrate, using a procedure similar to that reported elsewhere (14), and found identical (within 5% error) to that determined by UV absorption. The concentration of PABA stock solutions was determined using a molar absorptivity value of 15000 at 293 nm (15)

Interaction of the exosite-binder peptides to thrombin studied by tryptophan fluorescence The interaction of the exosite-binder peptides to thrombin was studied by recording the increase of thrombin's tryptophan fluorescence at the λ_{max} (i.e., 334 nm) as a function of peptide concentration. The interaction was monitored by adding, under gentle magnetic stirring, to a solution of thrombin (1.4 ml, 50 nM) in 10 mM Hepes buffer pH 7.5, 150 mM NaCl, 0.1% PEG at 37°C, aliquots (2-10 µl) of a suitable stock solution of ligand. Fluorescence spectra were recorded on a Jasco (Tokyo, Japan) model FP-6500 spectrofluorometer, equipped with a Peltier model ETC-273T temperature control system from Jasco. Excitation and emission wavelengths were 295 and 334 nm, respectively, using an excitation/emission slit of 3/10 nm, respectively. For all measurements, the Long-Time-Measurement software (Jasco) was used. Under these conditions, at the end of the titration, a Trp-photobleaching lower than 2% was observed. The optical density of the solution at both 295 and 334 nm was always lower than 0.05 units and therefore no inner filter effect occurred during titration experiments. Fluorescence intensities were corrected for dilution (< 5-8 % at the end of the titration) and subtracted for the contribution of the ligand, if any, at the indicated concentration. The fluorescence values, measured in duplicate, were analyzed as a function of the peptide concentration by a hyperbole equation to obtain the value of the F_{max} (corresponding to the fluorescence at peptide concentration=∞). This parameter was used to calculate $\Delta F_{max} = F_{max}-F°$ (where F° is the fluorescence value in the absence of the peptide). The fluorescence changes expressed as $(F_{obs}-F°)/\Delta F_{max}$ were analyzed as a function of the total peptide concentration according to a single site binding isotherm. Nonlinear least squares fitting was performed using the program Origin 7.5 (MicroCal Inc.), that allowed to obtain the best-fitting parameter values along with their standard errors.

Influence of exosite-directed ligands on thrombin chromogenic activity. The influence of exosite-directed ligands on the chromogenic activity of alpha-thrombin was determined by monitoring the hydrolysis of 200 µM S2238 or 500 µM S2366 by 0.2 or 2 nM thrombin in the absence or presence of 15 µM hirudin$^{54-65}$, 100 µM haemadin$^{45-57}$, 400 µM PAR-1^{50-60}, 3 µM HD1, 300 µM γ'-peptide$^{408-427}$, 80

μM GpIbα$^{268-282}$, 1.5 μM HD22 or 30 μM Heparin. Experiments were performed in polystyrene cuvettes using 10 mM Hepes, 150 mM NaCl, PEG8000 0.1%, pH 7.4 at 37°C. Use of polyethylene glycol 8000 prevents adsorbance of the enzyme to the cuvette walls and greatly increases the stability of the sample (16).

Steady state hydrolysis of the chromogenic substrate S2238 (from 40 to 0.625 μM) was studied in the absence and presence of 6 different exosite concentrations (i.e. hirudin$^{54-65}$, haemadin$^{45-57}$, γ'-peptide$^{408-427}$, GpIbα$^{268-282}$) ranging from 0.5 to 8 fold the K_d. Thrombin was used at 50 pM. Experiments were performed in 96-well plates (final volume 220 μl) using 10 mM Tris-HCl, 0.15 M NaCl, 0.1% PEG 8000, pH 7.50 at 25 °C. Assays were performed by following the release of p-nitroaniline resulting from the hydrolysis of the substrate at 405 nm. The concentration of released p-nitroanilide was measured using the extinction coefficient of 9920 M-1cm-1 at 405 nm (17). K_m and k_{cat}, were determined by nonlinear regression analysis of the Michaelis-Menten equation.

Probing the accessibility of S1 site by PABA binding. The interaction of PABA with thrombin was monitored by adding, under gentle magnetic stirring in a 1 cm pathlength cuvette, aliquots (2-10 μl) of PABA stock solution (12.5-50 mM) to a solution of thrombin (1.4 ml, 376 nM). At each PABA concentration, thrombin sample was equilibrated for 2 min at 37 ± 0.2 °C and excited at 335 nm, using an excitation/emission slit of 5 and 10 nm, respectively. The increase in fluorescence intensity of PABA in the presence of the enzyme was recorded at the 376 nm as a function of PABA concentration. Fluorescence data were corrected for IFE, since fluorescence intensity is only proportional to the absorbance of the sample up to an optical density of 0.05 units, both at λ_{ex} and λ_{em} (18,19)The following equation was used:

$$F_{corr} = F_{obs} \cdot 10^{[(\Delta Aex + \Delta Aem)/2]} \qquad \text{(eq. 1)}$$

where ΔA_{ex} and ΔA_{em} are the observed additional absorbance at the excitation (λ_{ex} = 335 nm) and emission (λem = 376 nm) wavelengths. Fluorescence data were then corrected for sample dilution (< 10% of the final volume) and finally expressed as $\Delta F = F-F°$, where F° and F is the fluorescence of PABA in the presence and absence of thrombin, respectively.

For a simple one-site binding mechanism R + L ↔RL (also see below) data were interpolated with equation 2, using the program Origin 7.5 (MicroCal Inc., Northampton, MA) to obtain the fitting parameters ΔF_{max} and K_d:

$$\Delta F = F-F° = (\Delta F_{max} \cdot [L])/(K_d + [L]) \qquad \text{(eq. 2)}$$

where K_d is the dissociation constant of the complex, RL, and ΔFmax is the maximum fluorescence change at infinite concentration of ligand, $[L]\infty$. Equation 2 assumes that at equilibrium $[L]_{free} \approx [L]_{tot}$ and thus it is valid only when $K_d >> [R]$, as usually observed for PABA complexes.

Probing the accessibility of S2, S3 and S4 site by Hir(1-47) binding. The interaction of Hir(1-47) with thrombin, in the absence or in the presence of exosite binders, was monitored by adding, under gentle magnetic stirring, to a solution of thrombin (1.4 mL, 50 nM) in Hepes 10 mM, pH 7.4, 150 mM NaCl and 37°C aliquots (2-10 μL) of inhibitor stock solutions (2-250 μM) in the same buffer. At each inhibitor concentration, protein samples were equilibrated for 2 min at 37°C and excited at 295 nm, using an excitation/emission slit of 3 and 10 nm, respectively. Fluorescence spectra were recorded on a Jasco (Tokyo, Japan) spectrofluorometer equipped with a Peltier model ETC-273T temperature control system from Jasco. The increase in fluorescence intensity at the λ_{max} (334 nm) of thrombin was recorded as a function of inhibitor concentration. Fluorescence data were corrected for sample dilution (< 5% of the final volume) and expressed as $(F-F°)/\Delta F_{max}$, where F° and F is the fluorescence of thrombin in the absence and presence of the inhibitor, respectively, and ΔF_{max} is the maximum fluorescence change at saturating concentrations of inhibitor. For a simple one-site binding mechanism R + L ↔ RL, the fluorescence intensity (F) of the receptor (R) at a given concentration of ligand (L) is linearly related to the concentration of the complex [RL], $F = [RL]\cdot F_{bound} + [R]_{free}\cdot F_{free}$. Since $[R]_{free} = [R] – [RL]$, then $(F°-F)/\Delta F_{max} = [RL]/[R]$ (20).The data were fitted to equation 3 (21), using the program Origin 7.5 (MicroCal Inc.):

$$[RL]/[R] = \{([R] + [L] + K_d) - \{([R] + [L] + K_d)^2 - 4\cdot[R][L]\}^{1/2}\}/2\cdot[R] \qquad \text{(eq. 3)}$$

where K_d is the dissociation constant of complex and [R] is the total concentration of the receptor.

RESULTS

Properties of exosite 1 and 2 binders. Among all factors, cofactors, inhibitors and substrates that are supposed to interact with thrombin exosite 1 or 2, we selected some well established exosite 1 and exosite 2 binders for composing our library. In particular for studying exosite 1 we selected hirudin$^{54-65}$, haemadin$^{45-57}$, PAR-1$^{50-60}$, and the aptamer HD1 whereas for investigating exosite 2 we selected γ'-peptide$^{408-427}$, GpIbα$^{268-282}$, the aptamer HD22 and the glycosaminoglycan heparin (Table 1). Although all ligands are negatively charged into an ordinary physiological environment (pH 7.4), exosite 1 binders result less acidic than exosite 2 binders, considering the number of charged aminoacids with respect to the total number of residues (22). Moreover exosite 1 have at least one hydrophobic/aromatic

residue suggesting a binding mechanism that occurs throughout a primary steering interaction further stabilized by aromatic/hydrophobic contacts. In support of this concept a single Phe residue is located just in the middle of the sequence of hirudin$^{54-65}$ and haemadin$^{45-57}$ whereas the presence of a small -Phe-Trp- sequence in PAR-1$^{50-60}$ generates a hot hydrophobic spot suitable for exosite 1 interaction. By contrary, the acidic features of the exosite 2 binders are dramatically increased by the substitution of multiple tyrosine residues with the post-traductional phosphotyrosine derivatives (Y-PO_3H_2). Natural peptides involved in coagulation have indeed sulphotyrosine moieties (Y-SO_3H) that, during SPPS, are replaced by the equivalent but more stable phosphotyrosine residues (23).

Determination of the dissociation constants (K_d). Whenever possible dissociation constants for the exosite binder peptides were determined by exploiting the increasing of the intrinsic fluorescence (λ_{ex} 295 nm, λ_{em} 334 nm) of thrombin that gave rise during complex formation (Fig. 1A). Notably, as reported in Table 1, the fluorescence intensity of the enzyme increased up from 15% to 30% in the case of hirudin$^{54-65}$ and γ'-peptide$^{408-427}$, respectively. All tested peptide demonstrated a saturable dose-dependent behaviour with a calculated stochiometry of 1:1. Exceptionally the glycosaminoglycan heparin, at concentration higher 8 times than the calculated K_d, presented a non saturable behaviour, in agreement with its well known binding mode. In this study, in fact, heparin is not fractionated and therefore could recruit more molecules of the enzyme along the same polymer strand. At high concentration of heparin, when the high affinity site is almost saturated, this effect is more pronounced and leads to this typical non-specific binding effect. Differently PAR-1$^{50-60}$ peptide was not tested by fluorescence because the signal generated by its single tryptophan residue, at the peptide concentration required for the titration, hid the enzyme fluorescence. Hence its K_d value was obtained by exploiting the increased catalytic activity towards S2238, as it will be discuss below. Finally, K_d values for HD1 and HD22 were obtained by previous works, as indicated (5,24). In general the K_d values obtained for exosite 2 binders were higher with respect to those observed for exosite 1 ligands, probably due to a more efficient stabilization of the complex realized by hydrophbic/aromatic interactions. In support of this the increase of the ionic strength slightly modified the affinity of the exosite 1 binders for thrombin but dramatically decreased the affinity of the exosite 2 binders which contract more crucial ionic interactions (data not shown).

Altogether the fluorescence data suggested an overall conformational change of thrombin in which the chemical environment of tryptophan residues became more rigid and hydrophobic (19). Most notably our results are fully consistent with preceding data reported in literature where the binding of an allosteric modulators, either Na^+, exosite 1 or exosite 2 binder, induces long-range effects on the structure of the enzyme as a whole (5,25,26,27,28).

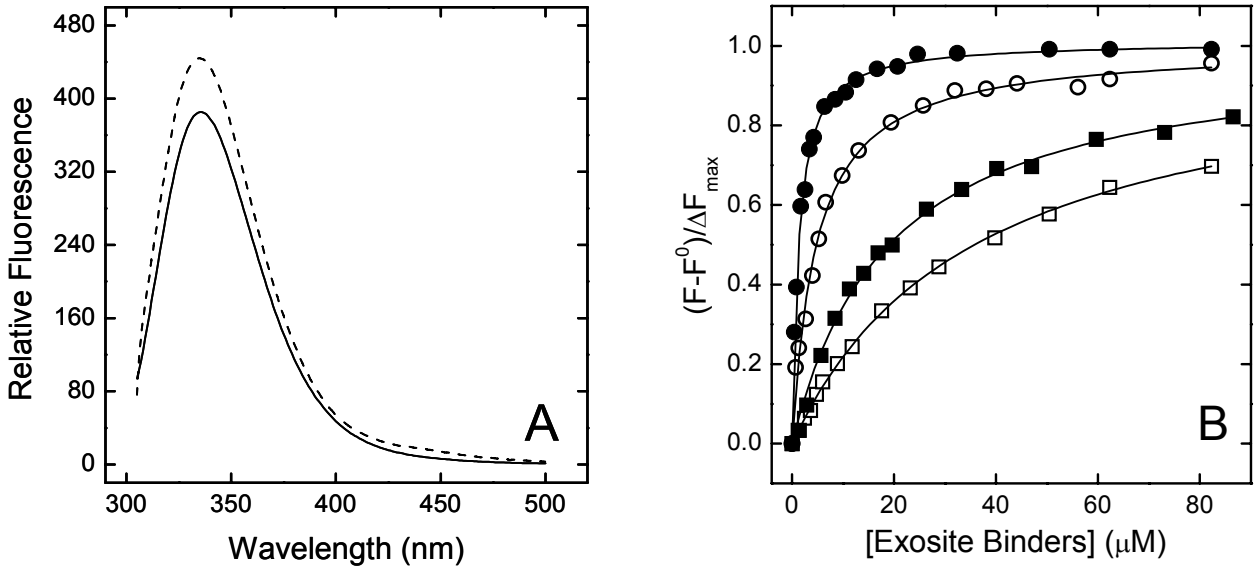

Figure 1. Interaction of the exosite-binder peptides to thrombin studied by tryptophan fluorescence. A) The intrinsic fluorescence of thrombin (—) gave rise up to 15% after the addiction of an exosite binder (i.e. hirudin$^{54-65}$, 15 μM). Fluorescence spectra were recorded by exciting the sample at 295 nm, using a scan speed of 220 nm/min. **B)** The interaction of the peptides with thrombin was monitored by adding, under gentle magnetic stirring, to a solution of thrombin (1.4 ml, 50 nM) in 10 mM Hepes buffer (pH 7.5), 0.15 M NaCl containing 0.1% PEG at 37°C, aliquots of a stock solution of the studying peptide (i.e., hirudin$^{54-65}$ (●), haemadin$^{45-57}$ (○), γ'-peptide$^{408-427}$(□) and GpIbα$^{268-282}$ (■)). For simplicity, data were normalized as $\Delta F/\Delta F_{max}$ (see Materials and Methods). The solid lines represent the least square fit with K_d value reported in Table 1.

Table 1. Exosite 1 and Exosite 2 binders properties

Peptide	Sequence	Ex	K_d (μM) [a]	Fluorescence [b]
Hirudin$^{54-65}$	^{54}GD**F**EEIPEEYpLQ^{65}	1	1.2 ± 0.2	+ 15%
Haemadin$^{45-57}$	^{45}SEFEE**F**EIDEEEK^{57}	1	8.1 ± 1.0	+ 22%
PAR-1$^{50-60}$	G-^{50}DKYEP**FW**EDEE^{60}	1	35± 2	n.d.
γ'-peptide$^{408-427}$	^{408}VRPEHPAETEYpDSLYpPEDDL^{427}	2	35 ± 3	+ 30%
GpIbα$^{262-282}$	^{262}GDEGDTDLYpD YpYpPEE^{282}	2	18 ± 2	+ 20%
HD1	5'-GGTTGGTGTGGTTGG-3'	1	250 ± 3 nM	-
HD22	5'-AGTCCGTGGTAGGGCAGGTTGGGGTGACT-3'	2	78 ± 3 nM	-
Heparin	----------	2	5 ± 0.3	+ 15% (not saturable)

[a] K_d values were obtained in 10 mM Hepes pH 7.4 PEG_{8000} 0.1% 0.15 M NaCl at 37°C. [b] Fluorescence increase refers to λ_{ex} 295 nm and λ_{em} 334 nm. Yp stands for phosphotyrosine. n.d. stands for not detectable in the experimental condition herein reported.

Effect of the exosite binders on the catalysis of thrombin. To test the catalytic activity of thrombin in the presence of exosite binders, we selected two chromogenic substrates such as S2238 (D-Phe-Pip-Arg-pNA) and S2366 (Pyro-Glu-Pro-pNA). S2238 is a fibrinogen-like substrate and therefore it represents the procoagulant pathway whereas S2366 is a protein C-like substrate and hence it represents the

anticoagulant pathway. Although the prevailing role of the exosites is to bring substrates and cofactors into proximity with thrombin, it has been reported in literature that the exosite binders are able to positively or negatively modulate the catalytic activity of thrombin toward different substrates (29,30,31). To date, however, a general behaviour model or classification is still missing.

The effect of allosteric modulators on thrombin activity was studied first in a qualitatively assay in which thrombin, peptides and substrates were held constant. In such a way we obtained information about changing of the initial rate velocity for substrate hydrolysis. In particular we observed that exosite 1 binders, increased catalysis with a mean of 30% (from 15% to 48%) toward S2238 whereas decreased catalysis with a mean of 20% (from 4% to -50%) toward S2366 (Fig. 2A). By contrary exosite 2 binders decreased catalysis either toward S2238 and S2366 with a mean of 10% for both (Fig. 2B). Even from these preliminary data, it appears clear how exosite 1 and exosite 2 binders exerts an allosteric control directly on thrombin catalysis cycle generating opposite effects depending on the nature of the substrate. Notably A) the perturbation of exosite 1 allosterically activates thrombin for procoagulant substrates but inactivates thrombin for anticoagulant substrates and B) the perturbation of exosite 2 produces a medium-small inhibition effect on thrombin activity.

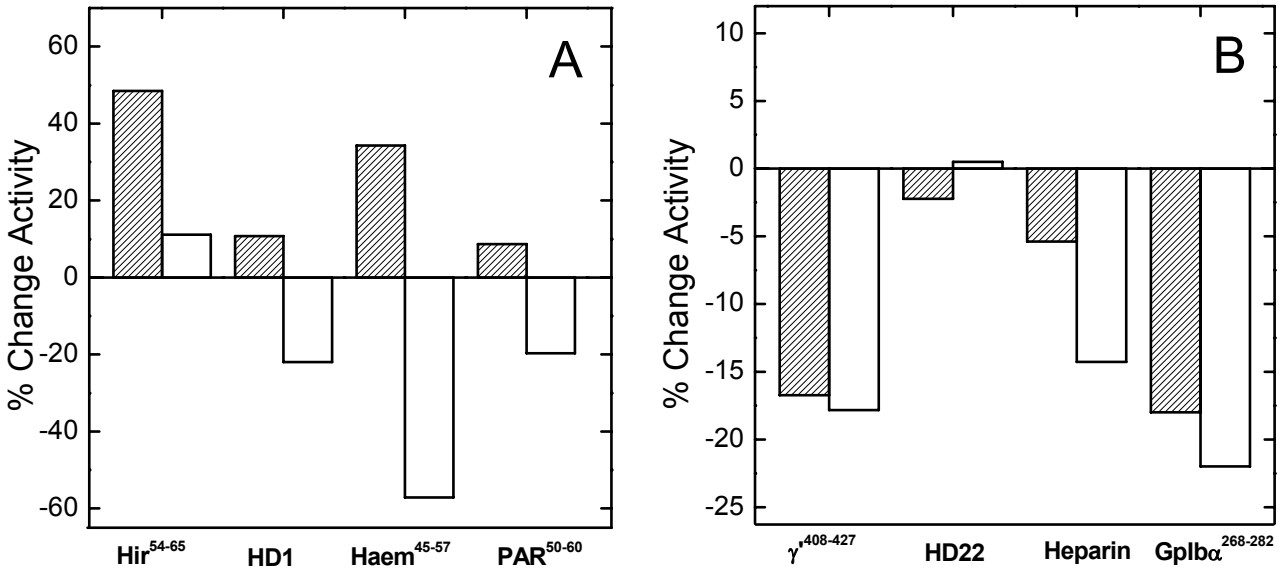

Figure 2. Influence of exosite-directed ligands on thrombin chromogenic activity. The effect of the exosite 1 **(A)** or exosite 2 **(B)** binders on thrombin activity towards either S2238 (gray bar) or S2366 (white bar) is reported. A solution of thrombin (0.2 nM or 2 nM) was incubated for 30 min at 37°C with different saturing concentrations of ligands (see Materials and Methods) before adding the substrate solution. The per cent change of activity has been calculated considering as the reference the initial velocity obtained from a solution of thrombin in the presence of the substrate alone. All data refer to Hepes 10 mM, 0.15 M NaCl pH 7.5, PEG_{8000}0.1% (w/w) at 37°C.

Effect of the exosite-binder on the molecular recognition properties of thrombin. The catalytic machinery of an enzyme is almost biphasic and therefore can be represented by the following scheme: E+S↔ES→E+P. The first step is characterized by a reversible equilibrium binding process in which the substrate and the enzyme get in contact and generate the Michaelis-complex, ES (21). Therefore

competitive inhibitors that limit to this step efficiently describe the primary binding event. The second step of the catalytic machinery consists in the irreversible processing of the substrate to generate the final product(s) and to regenerate the enzyme, ES→E+P (Fig.5A).

Relevant outstanding of allosteric mechanisms in enzymes should be provide by separating the initial binding event from the overall catalytic process. The experiments performed with S2238 and S2366 gave us indications about the overall catalytic process but lack to produce detailed information on the very first changes that the enzyme experiences in the presence of an allosteric modulator. Hence with the aim to better investigate, into a relevant physiological environment (Hepes 10 mM, pH 7.4, 150 mM NaCl and 37°C), how exosite 1 or 2 binders could affect the molecular recognition properties of thrombin, we performed equilibrium binding experiment using suitable inhibitors that selectively map the specificity sites of thrombin.

Thrombin is a trypsin-like protease belonging to the chymotrypsin family. Its primary specificity site, indicated as S1, is formed by the acidic moiety of D189. Conversely S2 site is quite hydrophobic in nature and it is centred around the W60 loop with residues Y60, W60 and L99 mainly involved. Some features of the S2 site continue into the adjacent S3 site that is called aryl binding site and is composed principally by the indole ring of W215 (Fig. 3A) (32).

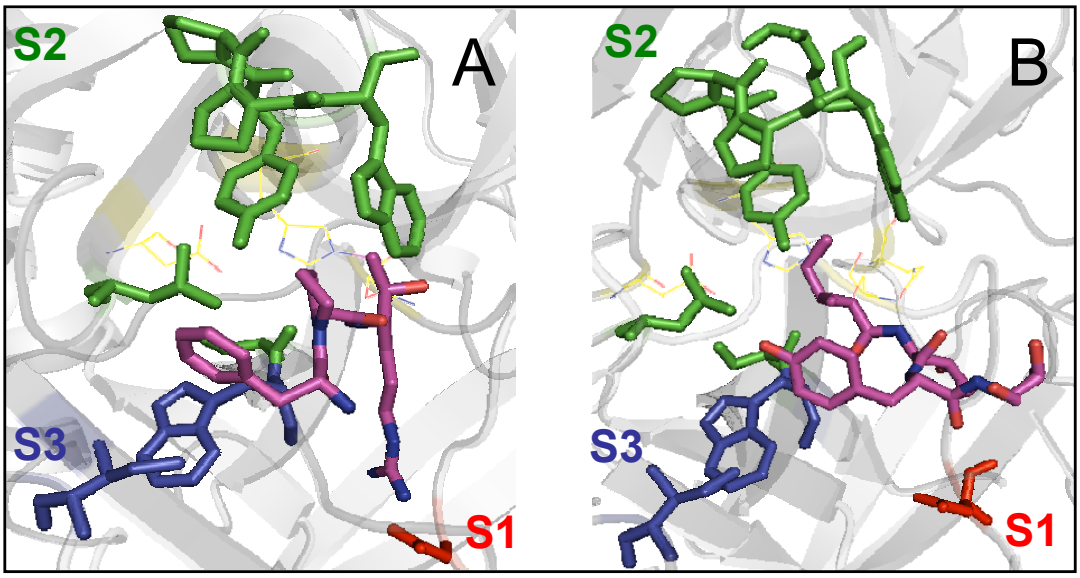

Figure 3. Insight of the active site of thrombin. (A) To better understand some features of the active site of thrombin, we divided the catalytic pocket into its inner specificity sites. S1 (red) is formed by Asp189 and it's located at the bottom of the hole. S2 (green) is mainly centred around the W60d loop and finally indole moiety of W215 (blue) composes part of the aryl binding site. In this scenario, PABA binds to D189 through forming a stable salt-bridge whereas **(B)** Hir(1-47), basing on the crystal structure of the hirudin-thrombin complex (33) cover the main part of the active site. Thus Ile1' of hirudin contacts the S2 site of thrombin, shaped by Tyr60a and Trp60d; Thr2' covers, but does not penetrate, the S1 site, containing Asp189 at the bottom; Tyr3' fills the apolar S3 site, formed by Trp215, Leu99, and Ile174.

Considering the structure of the active site of thrombin, our equilibrium binding experiments were performed using p-aminobenzamidine (PABA) as a probe to map the orientation and accessibility of S1 site whereas the N-terminal domain of hirudin - Hir(1-47) - was used to evaluate the overall accessibility of the active site, and in particular of the specificity sites S2, S3 and S4 (Fig. 3B). The binding of PABA was monitored by fluorescence, taking into account the correction for the inner filter effect (IFE) observed at high concentrations of the probe (see Materials and Methods). In fact the fluorescence of PABA changes as a function of the environment following this simple law: the more hydrophobic the more fluorescence (15) (Fig. 4A). Because the active site of thrombin offers a more hydrophobic environment respect to the solvent, PABA fluorescence gives rise. Although using a different strategy, also in the case of Hir(1-47) we exploited fluorescence spectroscopy to follow the complex formation. In fact the intrinsic fluorescence of thrombin, in the presence of saturing concentrations of Hir(1-47), increased up to 20-30% (Fig.4B) (34). Changes in the affinity of these probes for thrombin, in the presence of saturing concentrations of exosite binders, are expected to reflect alteration of the accessibility of the active site.

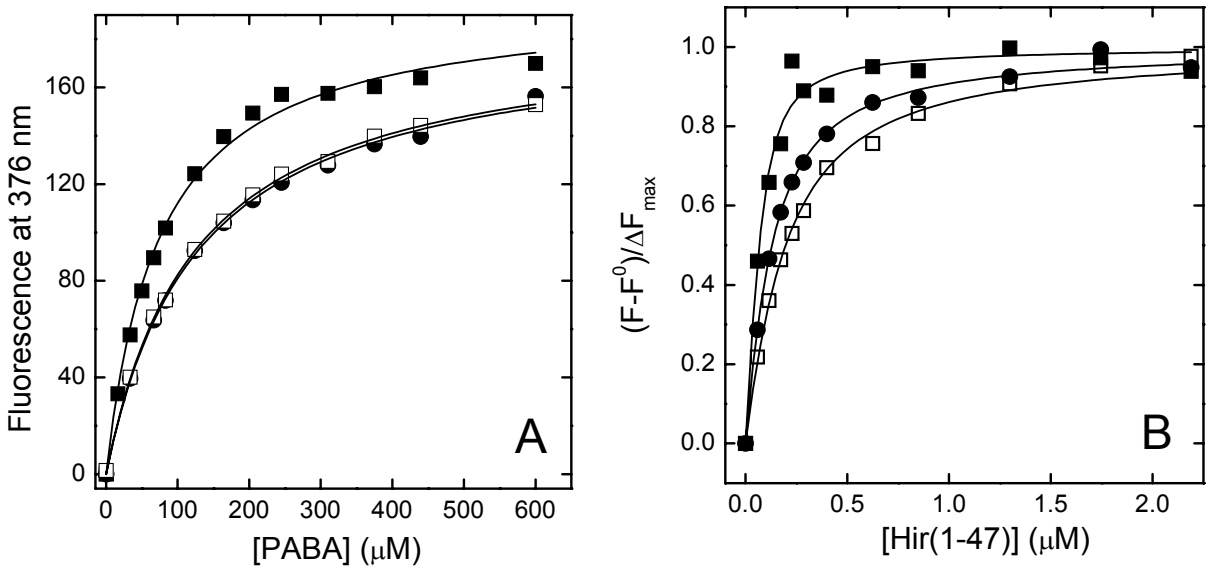

Figure 4. (A) PABA binding as a probe to investigate the accessibility of S1 site. The interaction of thrombin with PABA in the absence (●) or in the presence of saturing concentrations of hirudin$^{54\text{-}65}$ (■) or γ'-peptide$^{408\text{-}427}$ (□) was monitored by adding to a thrombin solution (1.5 ml, 376 nM) aliquots of a stock solution of PABA. Samples were exciting at 335 nm and the fluorescence signal was recorded at 376 nm. Raw data were corrected for the IFE and subtracted for the corresponding base line due to the PABA solution only (see Materials and Methods). Experiments were performed in Hepes 10 mM, 0.15 M NaCl pH 7.5, PEG_{8000}0.1% (w/w) at 37°C. **(B) Binding of Hir(1-47) as a probe for S2, S3 and S4 subsites.** The interaction of Hir(1-47) with thrombin in the absence (●) or in the presence of saturing concentrations of hirudin$^{54\text{-}65}$ (■) or γ'-peptide$^{408\text{-}427}$ (□) was monitored by adding to a thrombin solution (1.5 ml, 50 nM) aliquots of a stock solution of Hir(1-47). Samples were exciting at 295 nm and the fluorescence signal was recorded at 334 nm. Dissociation constant values (K_d) were calculated with eq. 2 or 3 (see Materials and Methods) and are reported in table 2 and 3 for PABA and Hir(1-47), respectively.

Our results propose a clear-cut evidence that exosite 1 binders open the active site (S1-S2-S3) and generate a more accessible enzyme. In particular in the presence of saturing concentrations of exosite 1 binders, the equilibrium dissociation constants (K_d) for PABA decreased of 30-40% (from 126 μM to 90 μM) respect to the free enzyme. A stronger effect was observed when Hir(1-47) was used as a probe: the equilibrium dissociation constants (K_d) for Hir(1-47) decreased up to 3 times, exactly from 120 nM to 40 nM (Table 2 and Table 3). Notably the effect observed for exosite 1 binders is almost the same produced by saturing concentration of Na^+, the main allosteric modulator of thrombin (35). Binding of peptides to exosite 1 in fact either acts directly on the active site but also promotes allosterically the binding of Na^+, switching the enzyme from the slow to the fast form. Thus exosite 1, Na^+ binding site and active site are thermodynamically related. Another key aspect emerging from these data refers to the structural plasticity of thrombin, since perturbation at different sites can evoke very similar changes in the enzyme conformation. Remarkably interaction of hirudin$^{54-65}$ to exosite 1 enhances the affinity of thrombin for substrates and inhibitors, but also induces very similar changes in the far-UV CD (36) and fluorescence spectra (37), and even increases the resistance of the 148-loop to proteolysis, as observed for Na^+ binding (38).

By contrast exosite 2 binders did not affect the accessibility of the S1 site and slightly decreased the accessibility of S2, S3 and S4 sites. In fact, in the presence of saturing concentrations of exosite 2 binders, the binding of PABA remained unchanged but the K_ds for Hir(1-47) increased up to 20-30%, exactly from 120 nM to 150 nM. (Table 2 and Table 3). These data seem to argue for the lack of a direct communication between exosite 2 and active site and suggest that the enzyme assumes a more rigid and locked conformation, unable to adapt to substrates and/or inhibitors.

Table 2: Effect of Exosite Binders on PABA binding to thrombin

	K_d*	$r_{wt/ex}$
rTHB	126 ± 5	-
	Exosite 1	
+ Hirudin$^{54-65}$	91 ± 2	1.38
+ HD1	84 ± 3	1.50
+ Haemadin$^{45-57}$	94 ± 3	1.34
+ GPAR1$^{50-60}$	95 ± 5	1.34
	Exosite 2	
γ' peptide	127 ± 6	1
+ HD22	113 ± 4	1.11
+ Heparin	124 ± 4	1.01
+ GpIbα	126 ± 3	1

* K_d values were calculated in HEPES 10 mM 150 mM NaCl pH 7.4 PEG_{6000} 0.1% at 37°C. Concentration of peptides were hirudin$^{54-65}$ 15 μM, haemadin$^{45-57}$ 100 μM, PAR-1$^{50-60}$, 300 μM, HD1 1.5 μM, γ'-peptide$^{408-427}$ 200 μM, GpIbα$^{268-282}$ 110 μM, HD22 1.5 μM heparin 30 μM.

Table 3: Effect of Exosite Binders on Hir(1-47) binding to thrombin		
	K_d*	$r_{wt/ex}$
rTHB	120 ± 5	-
Exosite 1		
+ Hirudin$^{54-65}$	33 ± 2	3.6
+ HD1	62 ± 3	1.9
+ Haemadin$^{45-57}$	36 ± 3	3.3
+ GPAR1$^{50-60}$	n.d.	n.d.
Exosite 2		
γ' peptide	165 ± 6	0.7
+ HD22	150 ± 5	0.8
+ Heparin	145 ± 10	0.8
+ GpIbα	160 ± 3	0.7

* K_d values were calculated in HEPES 10 mM 150 mM NaCl pH 7.4 PEG_{6000} 0.1% at 37°C. Concentration of peptides were hirudin$^{54-65}$ 15 μM, haemadin$^{45-57}$ 100 μM, PAR-1$^{50-60}$, 300 μM, HD1 1.5 μM, γ'-peptide$^{408-427}$ 200 μM, GpIbα$^{268-282}$ 110 μM, HD22 1.5 μM heparin 30 μM.

Effect of the exosite binders on the transformation of the bound substrate. Once the initial encounter complex is formed (ES), the bound substrate must be acted upon by the chemical reactive components of the enzyme active site to transform the substrate to product(s). This typically occurs via the formation of intermediate species in which the active site components interact with specific portion of the substrates to distort bond length and angles in a way that directs the substrate structure toward the transition state of the chemical reaction and form there on to the product state (Fig. 5A).

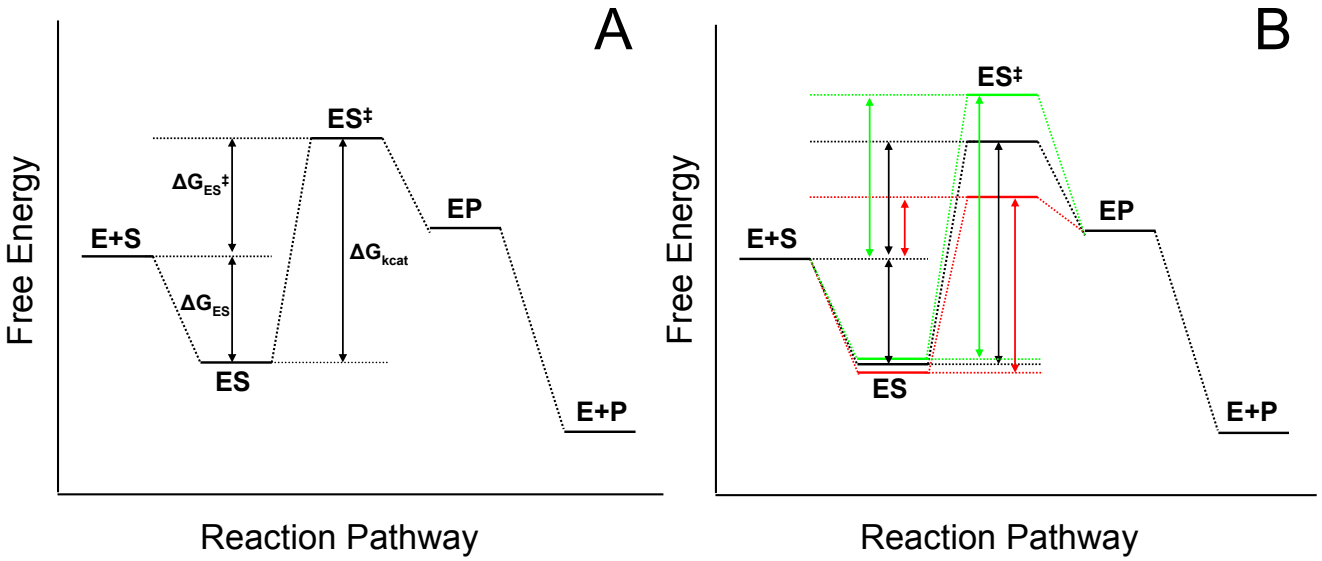

Figure 5. (A) Free energy diagram for the reaction pathway of a chemical reaction catalyzed by an enzyme. **(B)** The effect of exosite 1 (red) or 2 (green) binder on the reaction pathway is shown.

Until now we have found that exosite 1 ligands open the active site and generate a more accessible enzyme that better interacts with procoagulant substrates. Supporting this, K_d values for PABA and Hir(1-47) significantly decreased as well as the activity of thrombin toward S2238 increased. Conversely exosite 2 binders did not alter the binding recognition properties of thrombin for PABA and Hir(1-47), but significantly decreased the activity of thrombin toward S2238 and S2366. However, in both cases information obtained are not sufficient to complete the analysis of the system. Remarkably A) only the decrease of K_d in the presence of exosite 1 binders can't justified such a great increment of activity toward S2238 and B) the lack of effect on binding properties in the presence of exosite 2 binders can't absolutely explain the decreased catalytic efficiency of thrombin.

So with the aim of better understand the origin of these effects, we performed steady state analysis towards S2238. Searching for the peptide able to generate the maximum effect on S2238 hydrolysis, we selected hirudin$^{54-65}$ and haemadin$^{45-57}$ for exosite 1 whereas γ'-peptide$^{408-427}$ and GpIbα$^{268-282}$ for exosite 2. To rule out any consideration about Na+ allostery and therefore to be sure that the effect we were observing was due to exosite occupancy, we worked in Tris 5 mM pH 7.5 150 mM NaCl PEG_{6000} 0.1% at 25°C. Within this experimental setting thrombin is almost present in the fast form or Na+-bound form. Hirudin$^{54-65}$ and haemadin$^{45-57}$ slightly decreased K_m but singnificantly increased k_{cat} of thrombin for the substrate, suggesting that binding at exosite 1 acts on thrombin throughout a synergic mechanism. Decreasing of K_m, which describes the initial Michaelis-complex formation (ES), and increasing of k_{cat} that represents the Gibbs free energy for the transition from ES to $ES^{‡}$ (representing the bound transition state of the substrate) generate an overall activated enzyme more catalytically competent (Table 4A). Differently γ'-peptide$^{408-427}$ and GpIbα$^{268-282}$ had a little, if any, effect on K_m value for S2238 but dramatically decreased k_{cat} values (Table 4B). And this is exactly what we expected by an allosteric modulator. In fact as with any chemical reaction, it is the formation of the transition state that represents the most rate-limiting chemical step in the reaction pathway. Rationalizing this effect by considering the enzyme as a whole, we speculated that exosite 2 binders rigidify the structure of the enzyme increasing the energy barrier for the attainment of the reaction transition state (Fig. 5B).

Table 4A: Michaelis-Menten parameters of S-2238 hydrolysis by thrombin in the presence of different concentration of hirudin$^{54-65}$ and haemadin$^{45-57}$

Hirudin$^{54-65}$ (μM)	k_{cat} (sec^{-1})	K_m (μM)	k_{cat}/K_m ($x10^7\ M^{-1}\ sec^{-1}$)
0	97.5	2.2	44.3
0.3125	102.3	2.2	46.5
0.625	109.3	2.1	52.0
1.25	114.3	1.9	60.1
2.5	117.6	2	58.8
5	119.6	1.8	66.4
10	119.9	1.8	66.6
Haemadin$^{45-57}$ (μM)	**k_{cat} (sec^{-1})**	**K_m (μM)**	**k_{cat}/K_m ($x10^7\ M^{-1}\ sec^{-1}$)**
0	93.8	2.1	44.6
1.25	95.3	2	47.6
2.5	97.3	2	48.6
5	99.4	2	49.7
10	101.7	2	50.8
20	103.6	1.8	57.5
40	105.2	1.9	55.3

*Experimental conditions were Tris 5 mM pH 7.5 150 mM NaCl PEG_{6000} 0.1% at 25°C

Table 4B: Michaelis-Menten parameters of S-2238 hydrolysis by thrombin in the presence of different concentration of γ′ peptide$^{408-427}$ and GpIbα$^{268-282}$

γ′ peptide$^{408-427}$ (μM)	k_{cat} (sec^{-1})	K_m (μM)	k_{cat}/K_m ($x10^7\ M^{-1}\ sec^{-1}$)
0	98.3	2.2	44.6
3.125	93.8	2.3	40.8
6.25	84.4	2.8	30.1
12.5	80.5	2.5	32.2
25	76.1	2.5	30.4
50	70.5	2.6	27.1
100	61.1	2.4	25.4
GpIbα$^{268-282}$ (μM)	**k_{cat} (sec^{-1})**	**K_m (μM)**	**k_{cat}/K_m ($x10^7\ M^{-1}\ sec^{-1}$)**
0	96.1	2.5	38.4
1.9	86.1	2.3	37.4
3.75	83.8	2.3	36.4
7.5	80.1	2.1	38.1
15	76.1	2.2	34.5
30	68.9	2.2	31.3
60	59.4	2.5	23.7

*Experimental conditions were Tris 5 mM pH 7.5 150 mM NaCl PEG_{6000} 0.1% at 25°C

DISCUSSION

Thrombin is an allosteric enzyme that plays a pivotal role in maintaining haemostasis. The binding of ligands to thrombin is promoted by exosites 1 and 2, which are positively charged domains that flank

the active site. These exosites facilitate the binding of substrates or cofactors and align them for optimal interaction with the active site. Even if there is good evidence for allosteric regulation of the active site by the exosites, it remains unclear how the long-range communication is transferred from the exosites to the active site and which are the specificity sites of thrombin major involved along the process.

In this study we investigated the effect of a small library of exosite 1 and 2 binders to finally propose a reasonable model that tries to explain biochemical data accumulated so far. Thus, altogether our results can be rationalised investigating the different binding mode between exosite 1 and 2 binders. Thrombin is a serine protease that is composed by 2 orthogonal β-barrel (namely β1 and β2) and in the middle of them it is conserved the active site (H57, D102, S195). In particular H57 and D102 are contained in β1-barrel whereas the catalytic S195 is located in β2-barrel. Exosite 1 is fully contained in β1-barrel and its shape follows a more vertical direction, indicated as polar, considering the Bode standard orientation of thrombin (Fig.6A). Conversely exosite 2 is major located in β2-barrel but it has some relevant extension into β1-barrel (i.e., Arg 97, Arg101). Moreover exosite 2 it is wider than exosite 1 and its shape follows a more horizontal direction, indicated as equatorial (Fig 6B).

Starting from these structural observations, we propose that exosite 1 binders dock into a polar direction and therefore trigger a more open and accessible conformation of the active site. Accordingly exosite 1 binders generally increase either the affinity for substrates/inhibitors and the catalytic efficiency of the enzyme. Nevertheless the final observed result depends on the nature of the substrate/inhibitors, too. In fact this putative open form of the enzyme is suitable to host procoagulant substrates that are bulky and hydrophobic in nature whereas is moderately less efficient towards small and/or hydrophilic P3 substrates such as S2366 and anticoagulant protein C (2). When an exosite 1 binder interacts with thrombin and opens the catalytic pocket, the interaction of a bulky hydrophobic amino acid becomes more efficient and therefore the complex results energetically favourable. By contrast a smaller and hydrophilic substrate looses some stabilizing interactions (polar or van der Waals contacts) into the open cavity, interactions that could have been contracted in the closer form of the enzyme. That is what we observe in our study in which S2238 orients a bulky aromatic aminoacid, D-Phe (Vol: 135 A^3), into the aryl binding site (S3) whereas S2366 possess a smaller and polar aminoacid (Pyro-Glu) in P3. The polar binding mode herein proposed find structural evidences investigating the crystal structures of thrombin in complex with hirudin$^{55\text{-}64}$ (1HAH.pdb) (39) or with HCII (1JMO.pdb) (40). Moreover some structural features proposed here are supported by a very recent work based on dynamic simulation of thrombin (41) in which passing from a bounded form to a free form of the enzyme researchers observed a (A) distortion of the 220- and 186-loops that constitute the Na^+-binding site; (B) folding back of the Trp148 loop towards the body of the protein, (C) a 180 degrees rotation of the Asp189 side-chain, and (D) projection of the Trp60D loop toward the solvent accompanied by the rearrangement of the Trp215 side chain toward the 95-100 loop.

Opposite respect to exosite 1, exosite 2 binders dock into an equatorial direction. This putative binding mode links the two β-barrels of the enzyme and hence functions as a wire that latches the enzyme structure, hindering catalysis. Supporting this observation, exosite 2 binders mainly affect the processing of the substrate without perturbing the molecular recognition properties of the enzyme. The model herein proposed is confirmed analysing the crystal structure of thrombin in complex with GpIbα (1P8V.pdb) (42). Notably the platelet receptor disposes its C-terminal region all along exosite 2 and in particular the C-terminal carboxyl group of the Tyr-SO_3H279 makes a salt-bridge with the positively charged guanido-group of Arg101 of the enzyme and its sulphate group contracts stabilizing electrostatic interactions either with Arg93 and Lys240, localized on the β-strand 86-107 and on the α-helix 234-245 of thrombin, respectively. Continuing from the C-terminal to the N-terminal, the Asp277 of GpIbα is in contact either with Arg101 and with Arg233. TyrSO_3H278 interacts with Lys236 and finally TyrSO_3H276 helps to stabilize an electropositive cluster formed by Lys235 and Lys236 belonging to the α-helix 234-245 and by Arg126 belonging to the α-helix 125-130. The binding mode is further confirmed in the γ'-peptide-thrombin complex, too (2HWL.pdb) (43). Tyr$PO_3H_2$422 of the peptide interacts with Lys240 of the enzyme whereas Asp419 contacts Arg93 and Arg101. Similarly to the TyrSO_3H278 of GpIbα, Tyr$PO_3H_2$418 of the γ'-peptide stabilizes the electropositive cluster formed by Lys235 and Lys236 belonging to the α-helix 234-245 and by Arg126 belonging to the α-helix 125-130. Finally two acidic residues, Glu415 and Glu417, interacts with Arg233 contained in the α-helix234-245.

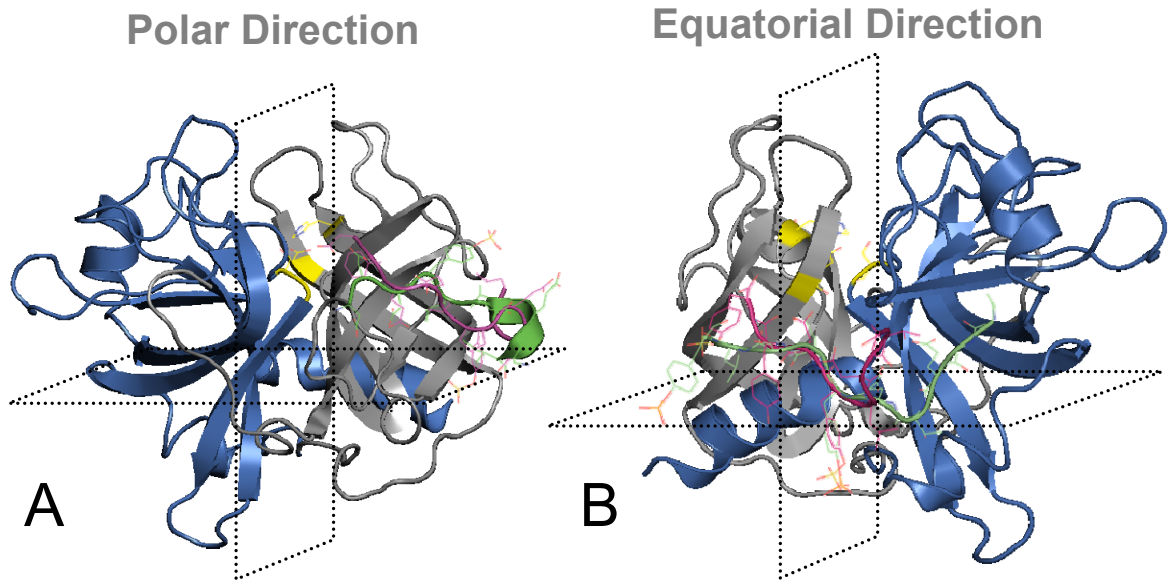

Figure 6. Models of thrombin's interaction with exosite 1 binder s or exosite 2 binders. Thrombin is composed by 2 orthogonal β-barrel (namely β1 gray and β2 blue) and in the middle of them it is conserved the active site (H57, D102, S195, yellow) (see text). Here thrombin is divided in two orthogonal flats called polar and equatorial flat, respectively. **(A)** Overlapping of two typical exosite 1 binders such as hirugen$^{55\text{-}65}$ (1HAH.pdb) and the N-terminal of HCII (1JMO.pdb). They dock into a polar direction. **(B)** Overlapping of two typical exosite 1 binders such as γ'-peptide$^{408\text{-}427}$ (2HWL.pdb) and GpIbα$^{268\text{-}282}$ (1P8V.pdb). They dock into a equatorial direction. Pictures were generated using either Pymol or MOE software.

In summary, the results herein reported offer a reasonable explanation of most of the exosite-mediated allosteric effects observed in thrombin so far and propose a model to easy catalogue and predict if a new ligand will interact with exosite 1 or exosite 2. Remarkably the perturbation of exosite 1 allosterically activates thrombin for procoagulant substrates but inactivates thrombin for anticoagulant substrates whereas the perturbation of exosite 2 produces an inhibition effect on thrombin activity. Consequently binders of exosite 2 could be conceivably used to further design new allosteric inhibitors of the enzyme.

REFERNCES

1. Ye, J., Liu, L.W., Esmon, C.T., and Johnson, A.E. (1992) The fifth and sixth growth factor-like domains of thrombomodulin bind to the anion-binding exosite of thrombin and alter its specificity. *J. Biol. Chem.* 267, 11023-11028.
2. Hortin GL, Trimpe BL. Allosteric changes in thrombin's activity produced by peptides corresponding to segments of natural inhibitors and substrates. *J Biol Chem*. 1991 15; 266:6866-71.
3. Liu, L.W., Vu, T.K., Esmon, C.T., and Coughlin, S.R. (1991) The region of thrombin receptor resembling hirudin binds to thrombin and alters enzyme specificity. *J. Biol. Chem.* 266, 16977–16980.
4. Petrera NS, Stafford AR, Leslie BA, Kretz CA, Fredenburgh JC, Weitz JI. Long range communication between exosites 1 and 2 modulates thrombin function. *J Biol Chem*. 2009 18; 284:25620-9.
5. Lancellotti, S., Rutella, S., De Filippis, V., Pozzi, N., and Rocca, B. (2008) Fibrinogen-elongated γ chain inhibits thrombin-induced platelet response, hindering the interaction with different receptors. *J. Biol. Chem.* 283, 30193-30204.
6. Colwell, N.S., Blinder, M.A., Tsiang, M., Gibbs, C.S., Bock, P.E., Tollefsen D.M. (1998) Allosteric effects of a monoclonal antibody against thrombin exosite II. *Biochemistry.* 37, 15057-65.
7. Bock PE. Active-site-selective labeling of blood coagulation proteinases with fluorescence probes by the use of thioester peptide chloromethyl ketones. II.Properties of thrombin derivatives as reporters of prothrombin fragment 2 bindingand specificity of the labeling approach for other proteinases. J Biol Chem. 1992Jul 25;267(21):14974-81. PubMed PMID: 1634536.
8. Liaw PC, Fredenburgh JC, Stafford AR, Tulinsky A, Austin RC, Weitz JI. Localization of the thrombin-binding domain on prothrombin fragment 2. *J Biol Chem*. 1998 10;273:8932-9.
9. Scacheri, E., Nitti, G., Valsasina, B., Orsini, G., Visco, C., Ferreia, M., Sawyer, R.T., and Sarmientos, P. (1993) Novel hirudin variants from the leech. *Hirudinaria manillensis*. Amino acid sequence, cDNA cloning and genomic organization. *Eur J Biochem.* 214, 295-304.

10. Vindigni, A., De Filippis, V., Zanotti, G., Visco, C., Orsini, G., and Fontana, A. (1994) Probing the structure of hirudin from *Hirudinaria manillensis* by limited proteolysis: Isolation, characterization and thrombin-inhibitory properties of N-terminal fragments. *Eur. J. Biochem.* 226, 323-333.
11. Atherton E, Sheppard RC (1989) In *Solid phase peptide synthesis*. IRL Press. Oxford, UK
12. Lancellotti S, De Filippis V, Pozzi N, Peyvandi F, Palla R, Rocca B, Rutella S, Pitocco D, Mannucci PM, De Cristofaro R. Formation of methionine sulfoxide by peroxynitrite at position 1606 of von Willebrand factor inhibits its cleavage by ADAMTS-13: A new prothrombotic mechanism in diseases associated with oxidative stress. *Free Radic Biol Med.* 2009. *[Epub ahead of print]*
13. Gill, S.G. and von Hippel, P.H. (1989) Calculation of protein extinction coefficients from amino acid sequence data. *Anal. Biochem.* 182, 319-326.
14. Dang, Q.D., Vindigni, A., and Di Cera, E. (1995) An allosteric switch controls the procoagulant and anticoagulant activities of thrombin. *Proc. Natl. Acad. Sci*. USA 92, 5977-5981.
15. Evans SA, Olson ST, Shore JD. p-Aminobenzamidine as a fluorescent probe for the active site of serine proteases. *J Biol Chem*. 1982 25; 257:3014-7.
16. De Cristofaro R, Di Cera E. Effect of protons on the amidase activity of human alpha-thrombin. Analysis in terms of a general linkage scheme. *J Mol Biol.* 1990;216:1077-85.
17. Workman, E.F., and Lundblad, R.L. (1978) The effect of monovalent cations on the catalytic activity of thrombin. *Arch. Biochem. Biophys*. 185, 544-548.
18. Puchalski, M.M., Morra, M.J., and von Wandruszka, R. (1991) Assessment of inner filter effect corrections in fluorimetry. *Fresenius J. Anal. Chem.* 340, 341-344.
19. Lakowicz, J.R. (1999) *Principles of Fluorescence Spectroscopy* 2nd ed., Kluwer Academic/Plenum, New York.
20. Eftink, M.R. (1997) Fluorescence methods for studying equilibrium macromolecule-ligand interactions. *Methods Enzymol*. 278, 221-257.
21. Copeland, R.A. (2000). *Enzymes: a Practical Introduction to Structure, Mechanism, and Data Analysis.* 2nd ed., J. Wiley & Sons, New York.
22. Huntington, J.A. (2008) How Na^+ activates thrombin – A review of the functional and structural data. *Biol. Chem.* 389, 1025-1035.
23. De Filippis, V., Colombo, G., Russo, I., Spadari, B., and Fontana, A. (2002) Probing hirudin-thrombin interaction by incorporation of noncoded amino acids and molecular dynamics simulation. *Biochemistry.* 43, 1537-1550.
24. Kretz CA, Stafford AR, Fredenburgh JC, Weitz JI. HD1, a thrombin-directed aptamer, binds exosite 1 on prothrombin with high affinity and inhibits its activation by prothrombinase. *J Biol Chem.* 2006 8;281:37477-85.

25. Jackman MP, Parry MA, Hofsteenge J, Stone SR. Intrinsic fluorescence changes and rapid kinetics of the reaction of thrombin with hirudin. *J Biol Chem*. 1992 5;267:15375-83.

26. Bah A, Garvey LC, Ge J, Di Cera E. Rapid kinetics of Na+ binding to thrombin. *J Biol Chem*. 2006 29;281:40049-56.

27. Sabo TM, Maurer MC. Biophysical investigation of GpIbalpha binding to thrombin anion binding exosite II. *Biochemistry.* 2009 4;48:7110-22.

28. Sabo TM, Farrell DH, Maurer MC. Conformational analysis of gamma' peptide (410-427) interactions with thrombin anion binding exosite II. *Biochemistry.* 2006 20;45:7434-45.

29. De Cristofaro R, Rocca B, Bizzi B, Landolfi R. The linkage between binding of the C-terminal domain of hirudin and amidase activity in human alpha-thrombin. *Biochem J.* 1993 15;289:475-80.

30. Fredenburgh JC, Stafford AR, Weitz JI. Evidence for allosteric linkage between exosites 1 and 2 of thrombin. *J Biol Chem*. 1997 10;272:25493-9.

31. Liu LW, Vu TK, Esmon CT, Coughlin SR. The region of the thrombin receptor resembling hirudin binds to thrombin and alters enzyme specificity. *J Biol Chem.* 1991 15;266:16977-80.

32. Bode, W., Turk, D., and Karshikov, A. (1992) The refined 1.9-Å X-ray crystal structure of D-Phe-Pro-Arg-chloromethylketone-inhibited human α-thrombin: Structure analysis, overall structure, electrostatic properties, detailed active-site geometry, and structure-function relationships. *Protein Sci*. 1, 426-471.

33. Rydel, T.J., Tulinski, A., Bode, W., and Huber, R. (1991) Refined structure of the hirudin-thrombin complex. *J. Mol. Biol.* 221, 583-601.

34. De Filippis, V., Frasson, R., and Fontana, A. (2006) 3-Nitrotyrosine as a Spectroscopic Probe for Investigating Protein-Protein Interactions. *Protein Sci.* 15, 976-986.

35. Di Cera E, Dang QD, Ayala YM. Molecular mechanisms of thrombin function. *Cell Mol Life Sci.* 1997;53:701-30. Review.

36. 1: He GX, Williams JP, Postich MJ, Swaminathan S, Shea RG, Terhorst T, Law VS, Mao CT, Sueoka C, Coutré S, Bischofberger N. In vitro and in vivo activities of oligodeoxynucleotide-based thrombin inhibitors containing neutral formacetal linkages. *J Med Chem*. 1998 22;41:4224-31.

37. Parry MA, Stone SR, Hofsteenge J, Jackman MP. Evidence for common structural changes in thrombin induced by active-site or exosite binding. *Biochem J.* 1993 Mar 15;290: 665-70.

38. De Filippis, V., De Dea, E., Lucatello, F., and Frasson, R. (2005) Effect of Na^+ binding on the conformation, stability, and molecular recognition properties of thrombin. *Biochem. J.* 390, 485-492.

39. De Filippis, V., De Dea, E., Lucatello, F., and Frasson, R. (2005) Effect of Na^+ binding on the conformation, stability, and molecular recognition properties of thrombin. *Biochem. J.* 390, 485-492.

40. Carter, W.J., Cama, E., Huntington, J.A. (2005) Crystal structure of thrombin bound to heparin. *J. Biol. Chem.* 280, 2745-2749.
41. De Amorim HL, Netz PA, Guimarães JA. Thrombin allosteric modulation revisited: a molecular dynamics study. *J Mol Model*. 2009. [Epub ahead of print]
42. Dumas JJ, Kumar R, Seehra J, Somers WS, Mosyak L. Crystal structure of the GpIbalpha-thrombin complex essential for platelet aggregation. *Science*. 2003 11;301:222-6.
43. Pineda AO, Chen ZW, Marino F, Mathews FS, Mosesson MW, Di Cera E. Crystal structure of thrombin in complex with fibrinogen gamma' peptide. *Biophys Chem*. 2007;125:556-9.

CHAPTER 2.4.

The Fibrinogen Elongated γ-Chain Inhibits Thrombin-Induced Platelet Response, Hindering the Interaction with Different Receptors

Stefano Lancellotti[1], Sergio Rutella[2], Vincenzo De Filippis[3], **Nicola Pozzi**[3], Bianca Rocca[4] and Raimondo De Cristofaro[1]

[1]Institute of Internal Medicine and Geriatrics, and Haemostasis Research Centre, Catholic University School of Medicine, Rome, Italy;
[2]Department of Hematology, Laboratory of Immunology, Catholic University School of Medicine, Rome, Italy;
[3]Department of Pharmaceutical Sciences, University of Padua, Italy;
[4]Institute of Pharmacology, Catholic University School of Medicine, Rome, Italy

Published in J Biol Chem. (JBC) 2008 31;283 (44):30193-204

INTRODUCTION

Fibrinogen is a key molecule in both primary and secondary hemostasis, due to its role in forming the platelet plug by connecting activated platelets and in forming plasma fibrin clot upon thrombin cleavage. Fibrinogen consists of two symmetric half molecules, each containing a set of 3 different polypeptide chains termed Aα, Bβ, and γ. The latter contains several sites that interact with different ligands such as other fibrin(ogen) molecules, coagulation enzymes, growth factors, and integrins (1). The product of thrombin digestion of fibrinogen, that is fibrin, binds with a considerable specificity thrombin, so that in the early studies fibrin was termed antithrombin I (2). Thrombin has a divalent interaction with two classes of binding sites on fibrin, one of low affinity in the E domain and the other of high affinity in the D domain of fibrin(ogen) molecules (3). Binding of thrombin to fibrinogen involves sequences of both Aα and Bβ chain, which contain recognition sites in the fibrinogen E domain. This recognition sites are still able to interact with thrombin after cleavage of fibrinopeptide A and B and form the low affinity binding site for the enzyme. The D domains contain a γ chain variant, termed γ′, arising from an alternative mRNA splicing (4), resulting in an elongated chain composed of 427 instead of 411 residues. The inserted region at the C-terminus is composed of 20 amino acids (^{408}VRPEHPAETEYDSLYPEDDL^{427}), rich of acidic side chains and two sulphate anions linked to Tyr418 and Tyr422 (5). The elongated γ chain, termed γ′, mainly hetero-dimerizes in the fibrinogen molecule with the more abundant γA chain, thus generating the γA/γ′ dimers (6). This fibrinogen, also called γA/γ′ fibrinogen, shows a high inter-individual variability in the ratio to the total fibrinogen γ

chain (7). The different expression of γ′ chain has been variably associated with thrombotic disorders both in venous and arterial circulation.

Previous genetic studies showed, for instance, that the fibrinogen γ-H2 haplotype is characterized by a reduced fibrinogen γ′ levels and reduced fibrinogen γ′ to total fibrinogen ratio. This haplotype is associated with a significantly increased risk for venous thrombosis (6). Biochemical studies showed that γ′ chains binds to α-thrombin with high affinity (8) and that the 408-427 region of γ′ chain binds to the anion binding exosite (ABE)-II of thrombin (1,9). Moreover, fibrinopeptide B cleavage by thrombin from γ′/γA fibrinogen is slower than in γA/γA fibrinogen (10). This effect was also associated with a reduced lateral aggregation of fibrin fibrils. All these findings may contribute to explain the reported enhanced risk for venous thromboembolism associated with a reduced expression of γ′ chain. However, at variance with these findings, other studies showed that fibrin fibers containing γ′ chains are more resistant than γ chains to proteolysis by fibrinolytic enzymes (11), so that fibrin clots containing a more abundant amount of γ′ chains could be associated with higher thrombotic risk. Notwithstanding the decreased sensitivity to fibrinolytic enzymes, the influence of a reduced expression of γ′/γA on enhanced risk for venous thromboembolism was prevalently demonstrated in clinical studies, although the detailed mechanism is only partially unraveled.

At variance with venous thromboembolism, the significance of altered expression of γ′ chain on arterial thrombosis remains largely elusive (6,7,12,13). Platelets are major players of arterial thrombus formation, as also demonstrated by the clinical efficacy of anti-platelet agents in cardiovascular prevention. The fibrinogen γ′ chain, through its ability to bind to thrombin, might enhance the amount of clot-bound thrombin, known to be active in the presence of the heparin-antithrombin complex, and thus scarcely inactivated by traditional anticoagulants (heparins, indirect Factor Xa inhibitors) (3). Thus, clot-bound, active thrombin may represent a storage pool of the enzyme, facilitating arterial thrombus formation and growth.

In this study, we investigated the effect of the fibrinogen γ′ and also of its 20-amino acid-insertion peptide, on the thrombin interaction with the platelet receptors glycoprotein (Gp) Ibα, protease-activated receptor 1 and 4 (PAR-1 and PAR-4), responsible for the thrombin-induced platelet activation. Fragment D was used as the best surrogate to selectively study the high affinity binding site for thrombin in γ chain in a conformation similar to that present in the native fibrinogen molecule and suitable for thrombin binding studies. This experimental approach was aimed at assessing whether γ′ chain can affect platelet activation by inhibiting competitively the interaction between the enzyme and GpIbα and by acting as an allosteric effector on PARs hydrolysis by thrombin. The obtained results may shed light on the possible role of fibrinogen γ′ chain onthe thrombin-induced platelet activation and thus on possible implications on both anti-thrombotic and pro-thrombotic properties of fibrinogen in arterial circulation, where platelets play a central role in thrombo-haemorrhagic syndromes.

My contribution to this study was principally focused on the investigation of the long-range effect caused by the binding of γ' peptide$^{408-427}$ either on the overall enzyme structure and then specifically on the exosite 1 (ABE-I). In particular, after synthesizing fluorescent probes and peptides, I planned and performed all fluorescence experiments.

MATERIALS AND METHODS

Synthesis of fibrinogen γ′ peptide. The fibrinogen γ′ 408-427 peptide (^{408}VRPEHPAETEYD SLYPEDDL^{427}) N-acetylated and amidated at the C-terminal toghether with the scrambled sequence (PTAHDYVDEERPYLPEELSD) as a control, were synthesized by the peptide synthesis facility of the Brain Research Center at the University of British Columbia (Vancouver, Canada). The tyrosine residues 418 and 422 were phosphorylated, being these residues sulphated in natural γ chains (5). The RP-HPLC analysis showed that these peptides were 95% pure, with a molecular mass of 2580.3 ±0.2 a.m.u., as determined by mass spectrometry.

Purification of fibrinogen γA/γA and γA/γ′ D fragments. Both γA/γA (D) and γA/γ′ (D*) D fragment of fibrinogen were purified by a modified procedure, as previously reported (14). Human fibrinogen, free of plasminogen was purchased from Calbiochem (Inalco, s.r.l., Milano Italy). This preparation was chromatographed on a DEAE-sepharose fast flow XK column connected to a FPLC apparatus (GE Healthcare, Milan, Italy) to separate the fibrinogen fraction rich of γ′ chains. The column was equilibrated with 5 mM Na-phosphate-40 mM Tris, pH 8.50 at a flow rate of 1 ml/min. One gram of fibrinogen was adsorbed on the column. After the elimination of non-adsorbed proteins, fibrinogen fractions were eluted using a stepwise gradient and three different eluting buffer solutions: 1) 30 mM Na-phosphate-60 mM Tris pH 7.60; 2) 50 mM Na-phosphate-80 mM Tris, pH 6.80; 3) 500 mM Na-phosphate-0.5 M Tris, pH 4.40. All these buffers contained 1 mg/ml aprotinin as protease inhibitor. Three major peaks were obtained and the fibrinogen fraction containing one γA and one γ′ chain was eluted with the third buffer solution, while the fraction containing two γA chains was obtained with the first buffer. D-fragments were prepared from plasmin digests of the first and the third peak obtained in the DEAE chromatography, and gel-filtered on DG-10 columns (Bio-Rad Lab., Milan, Italy) equilibrated with 50 mM Tris-HCl, 0.15 M NaCl, 10 mM CaCl2, pH 8.50. Human plasmin (specific activity: 5 U/mg, Calbiochem, Milan, Italy) was added at a final concentration of 0.05 U/ml (0.01 mg/mg fibrinogen), and incubated with the pooled and concentrated fibrinogen peak 1 and 3 of the DEAE chromatography in the above buffer at 25°C for 120 min. The fibrinogen was pre-treated for 15 min with 5 mM iodoacetamide to inhibit any minimal trace of contaminating Factor XIII, before the addition of plasmin. The reaction was stopped by the addition of aprotinin (10 mg/ml final concentration). Fragment D (containing γA chains only) and D* (containing γ′ chain only) were purified

from peak 1 and 3, respectively, using a second DEAE column (Supelco, Sigma-Aldrich, St. Louis, MO, USA) 4.6x25 mm and a two-pumps HPLC apparatus (Jasco Easton, USA), equipped with a spectrophotometric device (model 2075), and a spectrofluorometric detector (FP-2020, Jasco). The spectrophotometric detection of the eluted peaks was accomplished at 280 nm, whereas the fluorescence of the proteins was monitored by using λ_{exc} = 280 nm and λ_{em} = 340 nm. The developed gradient was 0-0.5 M NaCl in 20 mM Tris-HCl, pH 8.0 in 60 min. The flow rate was 1 ml/min. Fragment D was eluted at about 0.2 M NaCl, whereas fragment D* was obtained at 0.45 M NaCl. The concentration of fragment D and D* was calculated spectrophotometrically at 280 nm using an extinction coefficient E0.1% = 2.0 $cm^2 \cdot mg^{-1}$, using the primary sequence of fragment D and the spectrophotometric method by Pace et al. (15). The fractions containing the fragment D and D* were pooled, concentrated and their purity checked by SDS-PAGE using 4-12% gradient gels under both not reducing and reducing conditions. The identity of the γ′ chain was checked by immunoblotting of the bands obtained in SDS-PAGE of reduced fragment D*, using a mouse anti-human monoclonal antibody (clone 2.G2.H9) from Millipore S.p.A. (Milano, Italy), a secondary anti-mouse HRP-conjugated antibody and an ECL™ Western Blotting Detection System (GE Healthcare Life Sciences, Milano, Italy). The γA chains obtained from reduced fragment D did not react with the monoclonal antibody 2.G2.H9 (data not shown).

Thrombin-fragment D* interaction. Human α-thrombin was purified and characterized as previously reported (16). Binding of thrombin to purified fibrinogen fragment D* was studied by a solid-phase binding assay, immobilizing Fragment D* (5 μg/ml) on microtiter plates (96-well; Nunc-Immuno Maxisorp Nunc), overnight at 4 °C in 50 mM bicarbonate buffer, pH 9.60. The plate surface was blocked at 37 °C for 4 h with 250 μl/well of a buffer solution containing 1 mg/ml BSA, 50 mM Tris-HCl, pH 7.5. After aspiration of the blocking solution, plates were dried at room temperature and stored over desiccant at 4 °C. Use of the anti γ′ chain monoclonal antibody 2.G2.H9 conjugated to Alexa Fluor 488 (Invitrogen, Milano, Italy) allowed to obtain a quantitative estimate of the amount of immobilized fragment D*. Under the above conditions, the amount of immobilized fragment D* was equal to about 10 ng/well (about 0.12 pmoles/well). This estimate was based on the use of serial dilutions of a reference solution of the 2.G2.H9 monoclonal antibody, whose Alexa 488 fluorescence was measured using λ_{exc}= 494 nm and λ_{em}= 520 nm. Thus, at maximum saturation using 100 μl of the buffer solution, about 1 nM thrombin could be bound by immobilized fragment D*. Control experiments were also performed using fragment D instead of fragment D* at the same concentration.

Thrombin (78 nM - 5 μM) was incubated for 30 min in the absence and presence of the γ′ peptide. The γ′ peptide was used at fixed concentration spanning from 22.5-180 μM. The binding buffer was 10 mM Tris-HCl, 0.15 M NaCl, 0.1% PEG 6000, pH 7.50 at 25 °C (TBSP). After incubation at 25 °C for 30 min, and aspiration with three washing cycles with TBSP, a sheep anti-thrombin polyclonal antibody

(~10 mg/ml, from US Biological, DBA, Milan, Italy) was added at an optimal dilution of 1:500 in TBSP and incubated for 120 min. After aspiration of the solutions and three washing cycles, 100 µl of rabbit anti-sheep HRP-conjugated polyclonal antibody (~2 mg/ml, dilution 1:250) from US Biological (DBA, Milan, Italy) were added and incubated for 60 min at 25 °C. After aspiration and three washing cycles, 100 µl of 5 mM 3,5,3′,5′-tetramethylbenzidine (TMB) in the presence of 5 mM H_2O_2 were added and the reaction was stopped after 15 min. using 1 M H_2SO_4. This end point was chosen based on preliminary experiments showing a linear increase of the absorbance (15 points, R>0.95) over that time interval even at the highest concentration of thrombin. This finding ruled out that the absorbance measured after 15 min. incubation did not reflect the real amount of thrombin bound to fragment D* and was not due to substrate depletion. An entire data set of thrombin binding to fragment D* (35 points) was simultaneously fitted to the following equation:

$$Abs = Abs_{max} (T/[T+K_d^*]) \quad \text{(eq. 1)}$$

where Abs is the value of the absorbance measured at 450 nm, Abs_{max} is the asymptotic value of the absorbance, T is the thrombin concentration and K_d^* is the apparent equilibrium dissociation constant of thrombin binding to fragment D*, equal to $K_d^\circ(I/K_i)$, being K_d° the real equilibrium binding constant, I is the concentration of either fragment D* or γ′ peptide and K_i the equilibrium dissociation constant of binding of these ligands to thrombin.

Binding of fibrinogen γ′ peptide to thrombin studied by tryptophan fluorescence. Binding of γ′ peptide to thrombin was studied by recording the increase of thrombin's tryptophan fluorescence at the λ_{max} (i.e., 334 nm) as a function of fibrinogen γ′ peptide. The interaction of the latter with thrombin was monitored by adding, under gentle magnetic stirring, to a solution of thrombin (1.4 ml, 50 nM) in 5 mM Tris-HCl buffer (pH 7.5), 0.1% PEG, in the presence of 0.15 M NaCl, aliquots (2-5 µl) of γ'-peptide (2.33 mM). Fluorescence spectra were recorded on a Jasco (Tokyo, Japan) model FP-6500 spectrofluorometer, equipped with a Peltier model ETC-273T temperature control system from Jasco. Excitation and emission wavelengths were 295 and 334 nm, respectively, using an excitation/emission slit of 10 nm. For all measurements, the Long-Time-Measurement software (Jasco) was used. Control experiments were also performed to ruled out not specific effects, using the γ'-peptide scrambled peptide at a concentration of 100 µM. Under these conditions, at the end of the titration, a Trp-photobleaching lower than 2% was observed. The optical density of the solution at both 295 and 334 nm was always lower than 0.05 units and therefore no inner filter effect occurred during titration experiments. Fluorescence intensities were corrected for dilution (2-3% at the end of the titration) and subtracted for the contribution of the ligand at the indicated concentration. The fluorescence values, measured in duplicate, were analyzed as a function of the γ′ peptide concentration by a hyperbole

equation to obtain the value of the F_{max} (corresponding to the fluorescence at γ′ peptide concentration=∞). This parameter was used to calculate $\Delta F_{max} = F_{max}-F°$ (where F° is the fluorescence value in the absence of the peptide). The fluorescence changes expressed as $(F_{obs}-F°)/\Delta Fmax$ were analyzed as a function of the total γ′ peptide concentration according to a single site binding isotherm. Nonlinear least squares fitting was performed using the program Origin 7.5 (MicroCal Inc.), that allowed to obtain the best-fitting parameter values along with their standard errors.

Effect of γ′ peptide and fragment D* on thrombin-GpIbα interaction. Solid phase binding experiments to evaluate the effect of fibrinogen γ′ peptide on thrombin- GpIbα (1-282) interaction were performed as detailed in the previous paragraph, by immobilizing purified GpIbα (1-282) fragment (10 μg/ml) on polystyrene plates. Purification of platelet GpIbα (1-282) fragment was performed as previously detailed (20). Thrombin (20 nM-1.28 μM) was incubated in the presence of both 408-427 γ′ peptide and fragment D* at fixed concentrations spanning from 10 to 320 μM and from 0.2 and 3.2 μM, respectively. The binding buffer was TBSP. Both the experimental procedure of the binding assay and the analysis of the experimental data sets were the same of those used to study the thrombin-fragment D* interaction, detailed in the previous paragraph. Control experiments in which different concentrations of GpIbα(1-282) fragment from 0.31 μg/ml to 10 μg/ml were immobilized on the microplate wells for binding to 10 nM thrombin, showed that in the time scale of the HRP reaction with TMB (15 min), the signal at 450 nm was always linear for all tested GpIb fragment concentrations. These results validated the assumption that in this solid phase binding assay the absorbance measured at 450 nm after 15 min reflected the amount of thrombin bound to GpIb. Additional control experiments were also carried out with the synthetic peptide analog GpIbα (268-282), as a competitive inhibitor of thrombin binding to immobilized GpIb(1-282) fragment. This peptide, encompassing the C-terminal tail 268-282 of GpIbα, was synthesized and characterized as previously detailed (19). The three sulphated tyrosines, present in the natural peptide sequence (residue 276, 278-279), were replaced by phosphotyrosine.

Effect of HD1 and HD22 aptamers on thrombin- fragment D* interaction. The ssDNA-aptamers 5'-GGTTGGTGTGGTTGG-3' (HD1) and 5'- AGTCCGTGGTAGGGCAGGTTGGGGTGACT-3' (HD22) were synthesized by Primm s.r.l. (Milano, Italy). HD1 and HD2 are ss-DNA aptamers, that specifically bind to ABE-I and ABE-II, respectively, (21). In these experiments 500 nM α-thrombin was added to fragment D*, immobilized on microplates as detailed in the previous paragraph, in the presence of different concentrations of HD22 (20-1280 nM) and HD1 (87.5-5600 nM) and incubated for 60 min. The detection of bound thrombin was performed by an immunoassay, as previously described.

Hydrolysis of chromogenic substrate D-Phe-Pip-Arg-pNA by thrombin in the presence of γ′ peptide and fibrinogen fragment D*.Steady state hydrolysis of the chromogenic substrate D-Phe-Pip-Arg-pNA (S-2238) was studied in the absence and presence of 6 different γ′ peptide concentrations ranging from 2.5 to 320 μM and fragment D* concentrations spanning from 0.2 to 3.2 μM. Thrombin was used at 1 nM in 10 mM Tris-HCl, 0.15 M NaCl, 0.1% PEG 6000, pH 7.50 at 25 °C.

Hydrolysis of PAR-1(38-60) and PAR-4(44-66) peptide by thrombin. PAR-1(38-60) (^{38}LDPRSFLLRNPNDKYEPFWEDEE^{60}) and PAR-4(44-66) (^{44}PAPRGYPGQVCANDSDTLE LPDS^{66}) peptides were synthesized by PRIMM (Milan, Italy). Cleavage of these peptides by 0.1-1 nM thrombin was monitored by RP-HPLC as previously detailed (22). The Michaelis-Menten parameters k_{cat} and K_m were calculated in the absence and presence of fixed concentrations of the γ′ peptide ranging from about 2.5 to 320 μM. The k_{cat}/K_m of PAR-1 peptide hydrolysis in the presence of fragment D* (from 0.2 to 6.4 μM) was calculated at peptide concentration of 1 μM, that is a concentration lower than the Km value of the thrombin-PAR interaction. Under these conditions, the first order rate constant of the peptide hydrolysis was proportional to the k_{cat}/K_m value, as experimentally verified. The hydrolysis reaction was performed in 10 mM Tris-HCl, 0.15 M NaCl, 0.1% PEG 6000, pH 7.50 at 25 °C. The k_{cat}/K_m values were analyzed as a function of both γ′ peptide and fibrinogen fragment D* using the following linkage equation (23):

$$(k_{cat}/K_m)^{app} = [k_{cat}/K_m^{\circ} + k_{cat}/K_m^{1}\,(I/K_i)]/Z \qquad \text{(eq. 2)}$$

where Z = 1+I/Ki, Ki is the equilibrium dissociation constant of either γ′ peptide or fragment D* binding to thrombin, I is the inhibitor concentration; and the super-script 0 and 1 refer to the k_{cat}/K_m value pertaining to free and γ′ peptide- or D*-bound thrombin form, respectively. Control experiments were also carried out using 320 μM scrambled γ′ peptide to exclude spurious effects generated by ionic strength phenomena.

Binding of [Fluorescein]-Hirudin54-65(PO_3H_2) to human α-thrombin in the absence and presence of γ′ peptide. Fluorescein-conjugated and phosphorylated C-terminal hirudin 54-65 peptide, [F]-Hirudin54-65(PO_3H_2), having the sequence GDFEEIPEEY(PO_3H_2)LQ was synthesized as previously described (24) . Binding of this peptide to ABE-I of thrombin was studied by monitoring the decrease of the peptide fluorescence occurring upon interaction with thrombin, as previously reported (25). Fluorescence spectra were recorded on a Jasco (Tokyo, Japan) spectrofluorometer, as detailed above. Excitation and emission wavelengths were 492 and 516 nm, respectively, using an excitation/emission slit of 3/5 nm. During titration experiments, the decrease of fluorescence intensity at 516 nm was recorded as a function of thrombin concentration. For all measurements, the Long-Time-Measurement

software (Jasco) was used. Fluorescence intensities were corrected for dilution (i.e. 8-10%) at the end of the titration. Data were analyzed by the following binding isotherm equation (26), using the program Origin 7.5 (MicroCal Inc.):

$$\left(\frac{F_0}{F}\right)=\left(\frac{\alpha}{2}\right)\times\left(1+\frac{K_d+L}{P_0}-\sqrt{\left(\left(1+\frac{K_d+L}{P_0}\right)^2-\frac{4\times L}{P_0}\right)}\right)+1 \qquad \text{(eq. 3)}$$

where α is the maximum fluorescence change, K_d is the dissociation constant, L is the total concentration of thrombin, and P0 is the concentration of [F]-Hir54-65(PO_3H_2).

Thrombin-induced aggregation of gel-filtered platelets. Platelets from healthy volunteers were gel-filtered on Sepharose 2B columns (GE Healthcare, Milan, Italy) as previously reported (22). Born's aggregation of gel-filtered platelets, performed on a 4-channel PACKS-4 aggregometer (Helena Laboratories, Sunderland, UK) as previously detailed (22), was induced by 1 nM thrombin in the absence or presence of different concentrations of γ′ peptide and fibrinogen fragment D*. Control experiments were performed with both 50 μM PAR1 and 1 mM PAR4 activating peptides (PAR1-AP [SFLLRN–NH2] and PAR4-AP [AYPGKF-NH2], respectively, from PRIMM), 10 μM ADP and 10 μg/ml collagen from Helena Laboratories. The specific effect of fragment D* was also evaluated by using fragment D at the same concentrations.

Monitoring of full length PAR-1 hydrolysis by thrombin on intact platelets by flow cytometry. Gel-filtered platelets from healthy controls were mixed with 1 nM thrombin at 25 °C in the absence and presence of the γ′ peptide ranging from 27 to 310 μM and of fibrinogen fragment D* from 0.1 to 32 μM. After 120 sec the hydrolysis of PAR-1 molecules on platelet membrane was stopped with 1 μM PPACK and the uncleaved PAR-1 molecules were detected by flow cytometry, as previously described (22). Briefly, after cleavage reaction was stopped, platelets were labelled for 30 minutes at 4°C with saturating amounts of PE-conjugated anti-thrombin receptor monoclonal antibodies (SPAN-12 clone; Beckman Coulter, Milan, Italy), as detailed elsewhere (22). Isotype-matched, PE-conjugated irrelevant antibodies were used to measure background fluorescence. Samples were run through a FACSCanto® flow cytometer (Becton Dickinson, Mountain View, CA, USA) with standard equipment. Uncleaved PAR-1 expression levels were reported in terms of mean fluorescence intensity (MFI) ratio of the SPAN-12+ platelet population.

RESULTS

Purification of fragment D and D*.The purifications of both fibrinogen fragment D*, containing one γA and one γ′ chain, and of normal fragment D were successfully accomplished by DEAE-chromatography. Fragment D in SDS-PAGE showed a m.w. of about 85 kDa, whereas fragment D* had a slightly higher m.w. as compared with fragment D, in agreement with the presence of the elongated γ′ chain (Figure 1A). SDS-PAGE under reducing conditions and immunoblotting of the reduced sample with an anti-γ' monoclonal antibody allowed us to identify the genuine presence of fibrinogen fragment D*, as shown in Fig. 1B-C. Purified fragment D* was then used in the functional and solid-phase binding experiments, where the nominal concentration of the γ′ chain was assumed the same as that of the entire fragment D*.

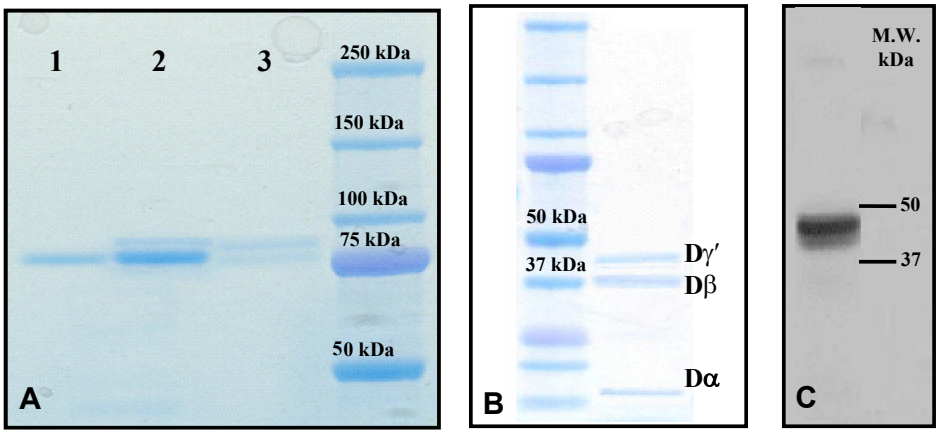

Figure 1. SDS-PAGE of purified fibrinogen fragments D. (A) The gel was 4-12% polyacrylamide under non-reducing conditions. Lane 1: purified fibrinogen fragment D; lane 2: total fibrinogen fraction eluted by 50 mM Na-phosphate-80 mM Tris, pH 6.80 in the first chromatographic step using DEAE-sepharose (see text); lane 3: fraction eluted by 0.5 M NaCl in 20 mM Tris-HCl, pH 8.0 in the second chromatographic step using DEAE-sepharose (see text). The molecular weight markers are indicated on the right. **(B)** The gel was 4-12% polyacrylamide under reducing conditions. The sample was fragment D* obtained from the DEAE-chromatography. The component with a m.w. of ≈41000 kDa is the elongated gamma chain fragment contained in fragment D*. The other bands pertain to the β-chain region of fragment D* (m.w. 37.6 kDa) and the α-chain fragment (m.w. 12 kDa). The faint band below the Dγ* may be a minor fragment produced by plasmin digestion, possibly generated by cleavage at Ser86 of the γ chain (61). The molecular weight markers are indicated on the left. **C)** Western blot of the fragment D* sample shown on the left. Detection of the γ′ chain was obtained using the mouse monoclonal antibody 2.G2.H9, raised against the peptide sequence VRPEHPAETEYDSLYPEDDL of human fibrinogen elongated γ′ chain.

Characterization of the fibrinogen fragment D* interaction with thrombin. The interaction of purified fragment D* with thrombin was studied by a solid phase binding assay, that showed a specific interaction with a K_d value of 0.4±0.03 μM (Fig. 2). The sequence of 20 amino acids of the γ′ peptide present in the fragment D* drives this interaction, as the purified γ′ peptide competitively inhibited with a K_i value of about 47 μM the thrombin-fragment D* interaction, as shown by Figure 2A. This interaction involved the ABE-II of thrombin, as its binding was competitively inhibited by specific

ligands of this thrombin exosite whereas no significant interaction was observed with fragment D (data not shown). The involvement of the ABE-II of thrombin was also confirmed by the inhibition of the binding of 500 nM thrombin to immobilized fragment D* by the ss-DNA aptamer HD22 (IC_{50}=81±6 nM; see Fig. 2B), while no effect was observed using the ssDNA aptamer HD1, which binds to ABE-I of the enzyme, (data not shown).

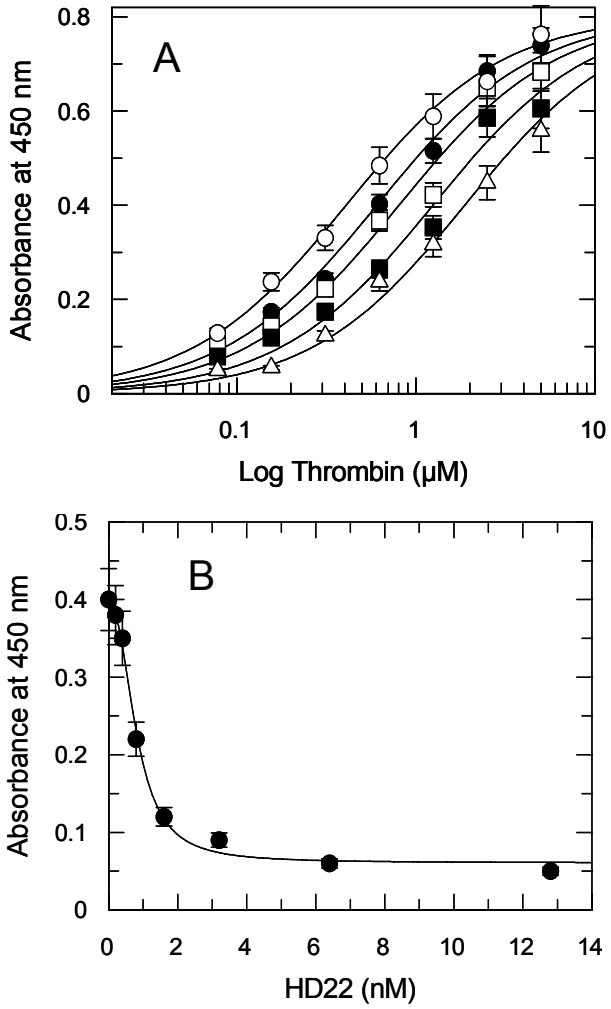

Figure 2. (A) Binding of thrombin to immobilized fragment D* in the presence of varying concentrations of purified γ′ peptide used at the following concentrations (O) 0, (•) 22.5 μM, (□) 45 μM, (■) 90 μM, and (Δ) 180 μM. The continuous lines were drawn according to the best fit parameter values of a simultaneous fit to single site binding isotherm and a competitive inhibition scheme: K_d of thrombin binding to fragment D*= 0.41±0.04μM, K_i of the γ′ peptide = 47.5±6 μM. **(B) Binding of 500 nM thrombin to immobilized fibrinogen fragment D* as a function of the aptamer HD22 concentration.** The continuous line was drawn according to the best-fit IC_{50} value equal to 81±6 nM.

Binding of γ′ peptide to thrombin monitored by tryptophan fluorescence . The binding of γ′ peptide to thrombin causes a significant increase of tryptophan fluorescence, without appreciable change in the λ_{max} value (Fig. 3A). Hence, we exploited this change for estimating the affinity of the γ′ peptide for thrombin, as shown in Figure 3. The corresponding K_d value for γ′ peptide binding was calculated as 30±5 μM, in good agreement with the value determined by the solid-phase binding experiments reported

above. The increase in the fluorescence quantum yield suggests that the chemical environment of Trp-residues in thrombin becomes, on average, more rigid and apolar than in the ligand-free enzyme (28).

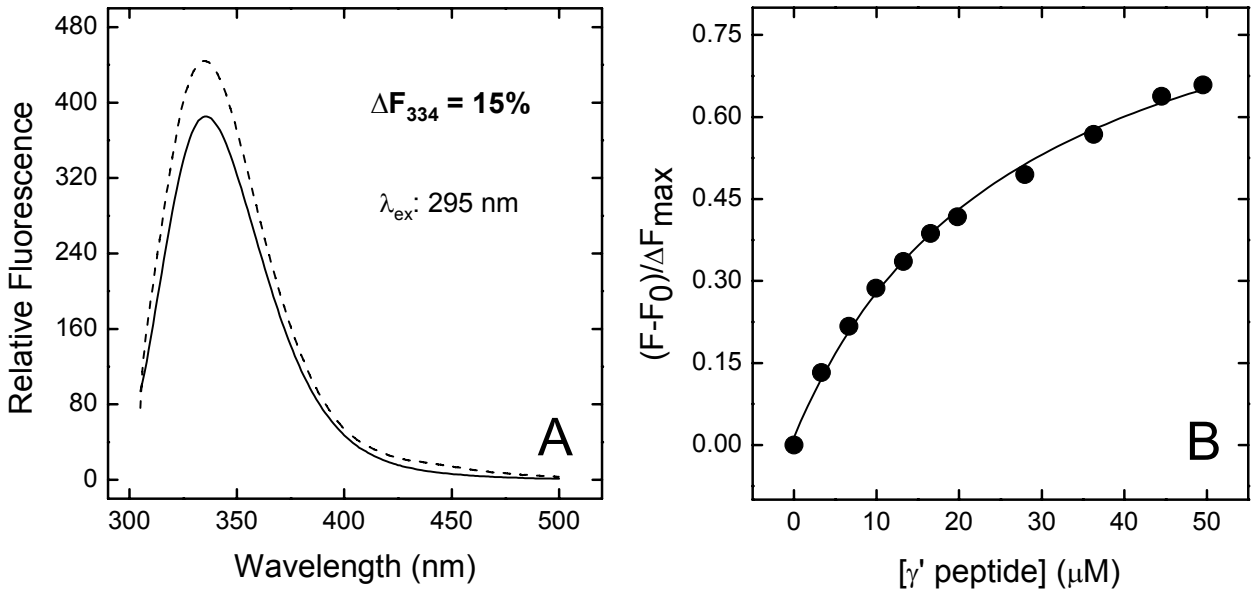

Figure 3. The interaction of γ'-peptide with thrombin was monitored by adding, under gentle magnetic stirring, to a solution of thrombin (1.4 ml, 50 nM) in 5 mM Tris-HCl buffer (pH 7.5), containing 0.1% PEG, and 0.15 M NaCl, aliquots (2-5 μl) of γ'-peptide (2.33 mM). The solid lines represent the least square fit with K_d value of 30 ± 5 μM.

Effect of γ′ peptide and fibrinogen fragment D* on platelet aggregation. The fibrinogen γ′ peptide inhibited dose-dependently the thrombin-induced aggregation of gel-filtered platelets, up to about 70%, in a specific manner, as demonstrated by the lack of effect by the scrambled γ′ peptide (see Fig. 4A-B). Likewise, purified fibrinogen fragment D* inhibited platelet aggregation up to about 70%, although it was impossible to reach full inhibition, even at higher fragment concentration (Figure 4B). At variance with these findings, no significant effect was observed with fragment D (Figure 4B). The analysis of these data provided IC_{50} values of 42±3.5 μM for the γ′ peptide and 0.47±0.03 μM for the D* fragment. Aggregation induced by saturating concentrations of ADP (10 μM), collagen (10 μg/ml), PAR-1-AP (50 μM) or PAR-4-AP (1 mM) was not affected by the γ′ peptide or fragment D* (data not shown), indicating a specific interaction with thrombin.

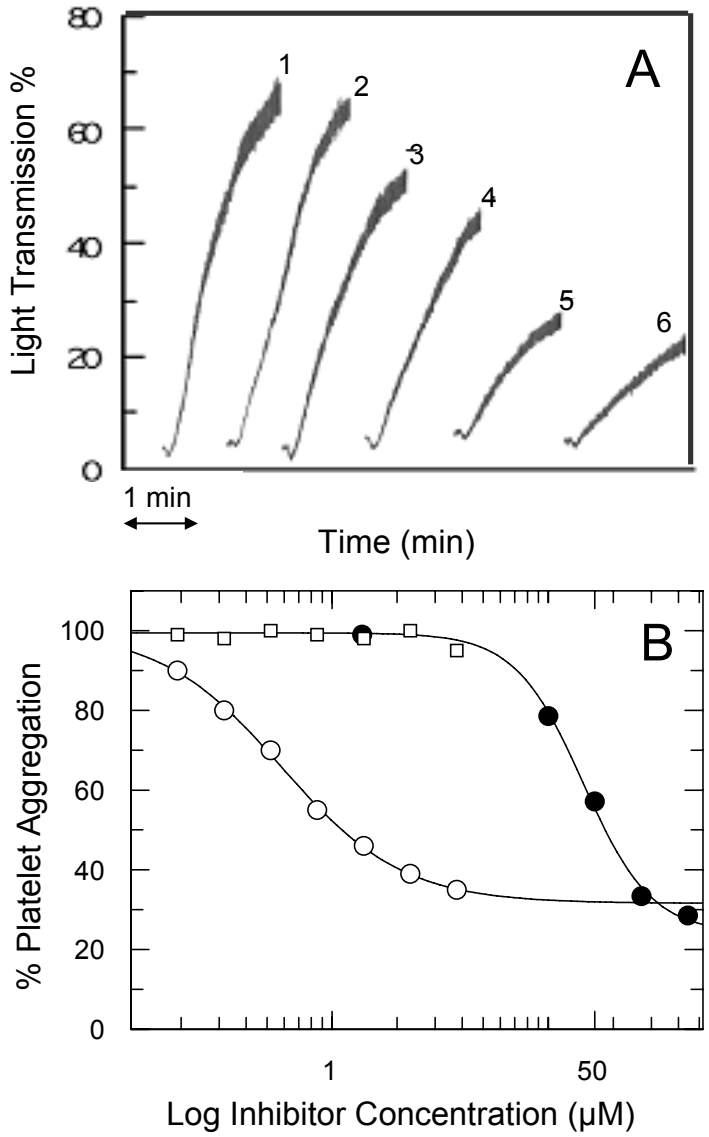

Figure 4. (A) Aggregation of gel-filtered platelets by 1 nM thrombin in the absence (1) and presence of 25 (3), 50 (4), 100 (5) and 200 μM (6) fibrinogen γ′ peptide. The trace 2 was obtained in the presence of 200 μM scrambled γ′ peptide, whose sequence was generated by the RandSeq program, available at www.expasy.org web site. **(B) Inhibition analysis of thrombin-induced platelet aggregation** in the presence of γ* peptide (■), fibrinogen fragment D* (○) and D (□). The continuous lines were drawn according to the best-fit IC50 values of 42±3.5 μM for the γ′ peptide and 0.47±0.03 μM for the D* fragment

Effects of γ′ peptide and fibrinogen fragment D* on thrombin-GpIbα interaction. Both γ′ peptide and fibrinogen fragment D* inhibited competitively the binding of thrombin to immobilized GpIbα (1-282) with a Ki of about 40 μM and 0.5 μM, respectively, (Figures 5A-B). Instead, no effect was observed with fragment D (data not shown). The competitive nature of the observed inhibition by both γ′ peptide and fragment D* was confirmed by control experiments performed with the synthetic peptide analog GpIbα (268-282), which binds to thrombin with a K_i value of 9 μM (19). These findings can explain in part the inhibitory effect of the γ′ peptide and fragment D* on thrombin-induced platelet aggregation, due to the activating role of thrombin-GpIb interaction on platelet aggregation (22,29).

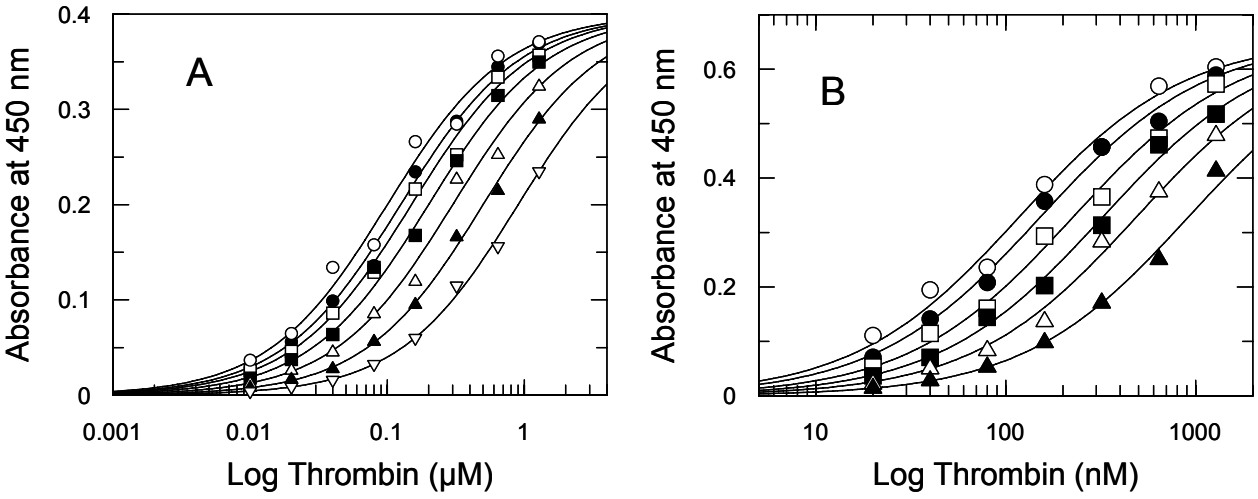

Figure 5. Binding of purified human α-thrombin to immobilized platelet GpIbα(1-282) fragment. (A) Binding of thrombin in the presence of different concentrations of γ′ peptide. The continuous lines were drawn according to the best fit parameter values of a single site binding isotherm: Kd of thrombin binding = 86±7 nM, Ki of γ′ peptide inhibition = 40±6 μM. The concentrations of γ′ peptide were: (○) 0, (•) 10 μM, (□) 20 μM, (■) 40 μM, (Δ) 80 μM, (▲) 160 μM, and (□) 320 μM. **(B)** Binding of thrombin in the presence of varying concentrations of fragment D* 0 (○), (•) 0.2 μM, (□) 0.4 μM, (■) 0.8 μM, (Δ) 1.6 μM, (▲) 3.2 μM. The continuous lines were drawn according to the best fit parameter values of a single site binding isotherm: K_d of thrombin binding = 115±7 nM, Ki of fragment D* = 0.48±0.37 μM. Each point represents the mean of two different measurements. Each experimental data set was analyzed by simultaneous fitting.

Effect of γ′ peptide and fibrinogen fragment D* on thrombin-catalyzed PAR-1 and PAR-4 cleavage. Fibrinogen γ′ peptide inhibited the cleavage of the PAR-1 substrate, as shown in Figures 6A. The inhibitory effect was allosteric in nature, as PAR-1 (38-60) substrate interacts with the ABE-I and the active site of thrombin and not with ABE-II (30), where γ′ peptide binds (9). Moreover, the inhibitory effect concerned mostly the k_{cat} value, as shown in Table 1. When the k_{cat}/K_m values were analyzed by a linkage equation (Eq. 2) as a function of γ′ peptide concentration, a best-fit K_i value of about 40 μM was obtained, in good agreement with the value derived from the GpIb solid-phase binding and fluorescence titration experiments (Figure 6B). No significant effect was observed using 320 μM scrambled γ′ peptide, thus ruling out spurious ionic strength effects. Likewise, the k_{cat}/K_m values of PAR-1 hydrolysis as a function of fragment D* concentration decreased, reaching an asymptotic value (Figure 6C). In this case, the value of the equilibrium dissociation constant was about 0.5 μM, about 80-fold lower than that measured for γ′ peptide, in analogy to the results obtained in solid-phase binding experiments with GpIbα. No significant effect was instead observed using the fragment D (Figure 6C).At variance with PAR-1, the hydrolysis of PAR-4 was not affected by γ′ peptide, as the k_{cat}/K_m values measured as a function of the γ′ peptide concentration were scattered around a mean of about $4x10^5$ M^{-1} sec^{-1} (data not shown). In addition, experiments were carried out using the synthetic peptide substrate D-Phe-Pip-Arg-pNA (S-2238). Both γ′ peptide and fragment D* reduced the catalytic competence of thrombin toward S-2238, being this effect linked mostly to a reduction of the k_{cat} values, as listed in Table 2.

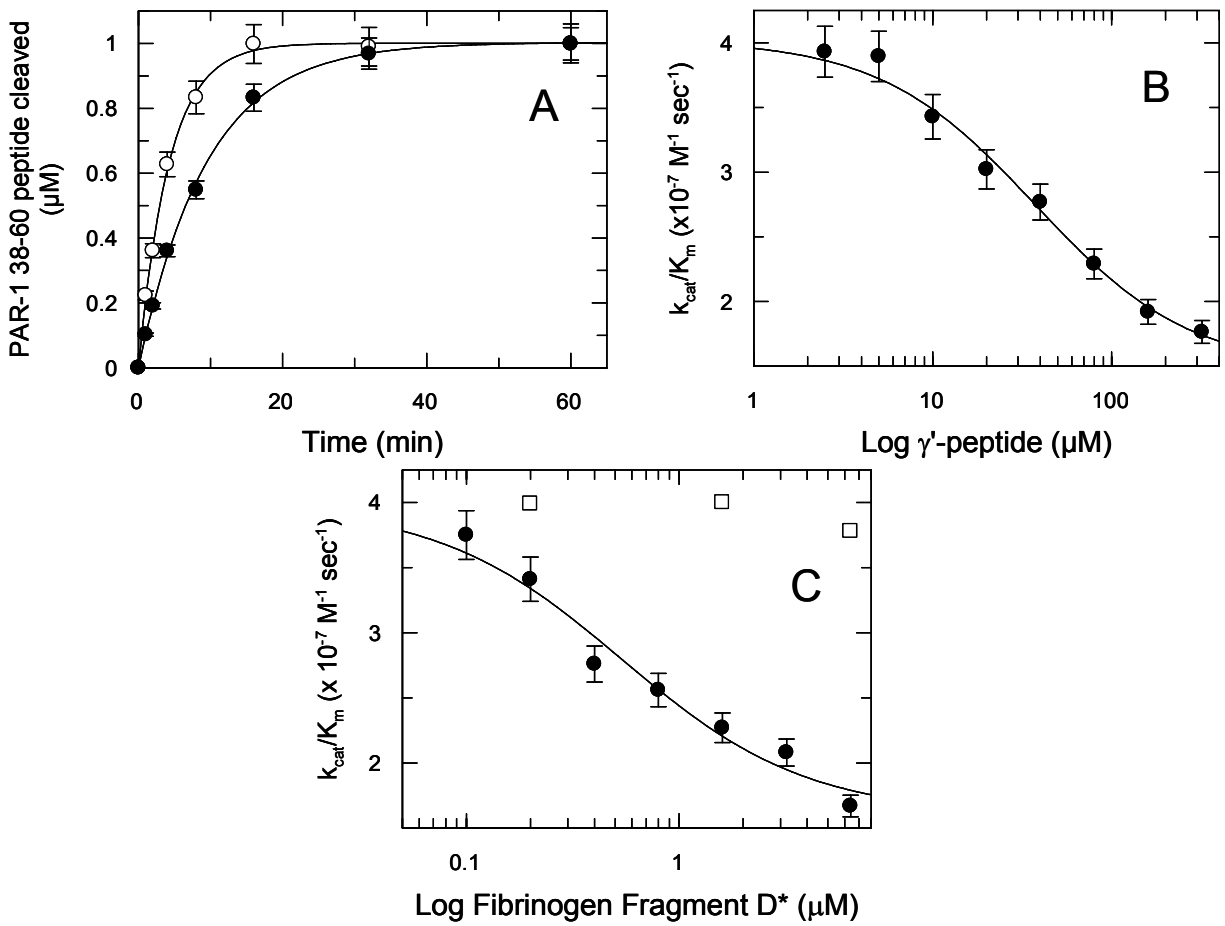

Figure 6. (A) Cleavage of 1 μM PAR-1(38-60) by 0.1 nM thrombin in the absence (○) and presence (•) of saturating concentration (320 μM) of the γ′ peptide. The concentration of the cleaved PAR-1 peptide over time, [Cleaved PAR-1]t, were fitted to the first order equation: [Cleaved PAR-1]t = 1 μM x [1-exp(-k t)]. Under these pseudo-first order conditions, k = e° (k_{cat}/K_m) where e° is the thrombin concentration. The continuous lines were drawn according to the best fit values of the k_{cat}/K_m values equal to 3.83±0.1 $x10^7$ M^{-1} sec^{-1} and 1.76±0.1 $x10^7$ M^{-1} sec^{-1} in the absence and presence of γ′ peptide, respectively. **(B)** Values of k_{cat}/K_m of PAR-1(38-60) hydrolysis by thrombin as a function of γ′ peptide. The continuous line was drawn according to eq. 2 with the best fit values were: $(k_{cat}/K_m)° = 4±0.1x10^7$ M^{-1} sec^{-1}, $(k_{cat}/K_m)^1 = 1.47±0.1x10^7$ M^{-1} sec^{-1}, K_i =37.4±6 μM. **(C)** Values of k_{cat}/K_m of PAR-1(38-60) hydrolysis by thrombin as a function of fragment D*(•) and fragment D (□) concentration. The continuous line was drawn according to eq. 2 with the best fit values were: $(k_{cat}/K_m)° = 3.97±0.13x10^7$ M^{-1} sec^{-1}, $(k_{cat}/K_m)^1 = 1.60±0.15x10^7$ M^{-1} sec^{-1}, K_i = 0.54±0.15 μM. The vertical bars are the standard deviations from two determinations.

Table 1: Michaelis-Menten parameters of PAR-1(38-60) hydrolysis by human α-thrombin in the presence of different concentration of γ′ peptide

γ′ peptide concentration (μM)	k_{cat} § (sec^{-1})	K_m (μM)	k_{cat}/K_m ($x10^7$ M^{-1} sec^{-1})
0	78	2	3.9
2.5	79	2.02	3.9
5	74	1.99	3.71
10	72	2.1	3.43
20	68	2.3	2.96
40	59	2.13	2.77
80	55	2.4	2.29
160	48	2.5	1.92
320	45	2.55	1.76

*Experimental conditions were Tris 5 mM pH 7.5 150 mM NaCl PEG_{6000} 0.1% at 25°C

Table 2 Michaelis-Menten parameters of S-2238 hydrolysis by human α-thrombin in the presence of different concentration of γ′ peptide and fibrinogen fragment D*

γ′ peptide concentration (μM)	k_{cat} (sec^{-1})	K_m (μM)	k_{cat}/K_m ($x10^7 M^{-1} sec^{-1}$)
0	85.0	2.00	4.30
2.5	84.5	2.20	3.84
5	79.6	2.10	3.79
10	79.8	2.30	3.47
20	72.4	2.30	3.18
40	64.7	2.40	2.70
80	63.6	2.80	2.27
160	56.6	2.90	1.95
320	52.2	2.98	1.75
Fibrinogen fragment D* (μM)	**k_{cat} (sec^{-1})**	**K_m (μM)**	**k_{cat}/K_m ($x10^7 M^{-1} sec^{-1}$)**
0.2	74	2.10	3.50
0.4	60	2.06	2.91
0.8	55	1.95	2.82
1.6	50	1.88	2.66
3.2	47	1.94	2.42

*Experimental conditions were Tris 5 mM pH 7.5 150 mM NaCl PEG_{6000} 0.1% at 25°C

A dose-dependent inhibition of the hydrolysis of full length PAR-1 molecules on intact platelets was also observed as a function of increasing concentrations of γ′ peptide, as shown in Figure 7A. At high peptide concentrations the inhibition reached an asymptotic value, in agreement with the results obtained with the synthetic PAR-1 peptide. Similar effects were observed with the fragment D* (Figure 7B). Thus, γ′ peptide can exert its inhibitory effect on platelet activation by inhibiting competitively the interaction between the enzyme and GpIbα and by causing an allosteric inhibition of PAR-1 hydrolysis.

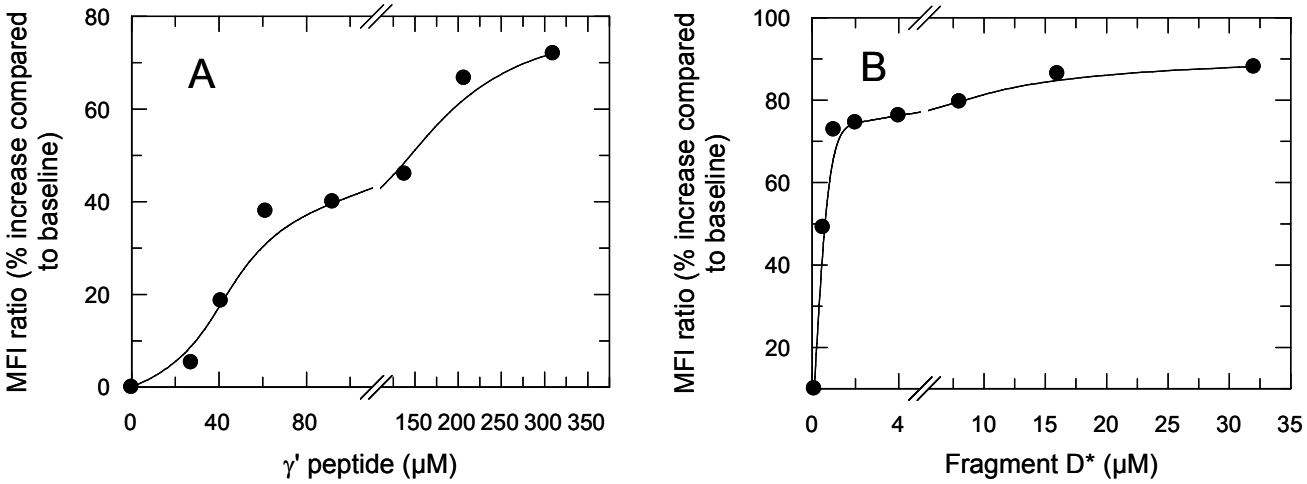

Figure 7. Effect of γ′ peptide (A) and fibrinogen fragment D* (B) on thrombin cleavage of PAR-1 molecules on gel-filtered platelets. The MFI ratio was defined as MFI of test histograms/MFI of control histograms (background fluorescence without γ′ peptide). Data are representative of mean ± SD recorded in 3 independent experiments run in duplicate.

The effect of γ′ peptide on the interaction of thrombin with [F]-Hirudin54-65(PO3H2) was also investigated to assess whether or not the negative influence of the γ′ peptide on PAR-1 but not PAR-4 hydrolysis arose from a conformational change induced in the ABE-I, where PAR-1 but not PAR-4 binds. These experiments showed that the Kd value of [F]-Hirudin54-65(PO3H2) was not significantly changed in the presence of high concentration of the γ′ peptide (i.e. 74 μM) , as shown in Figure 8. The equilibrium dissociation constants of the hirudin peptide was in fact equal to 19.7 ± 1.2 and 14.3 ± 1.5 nM, in the absence and presence of the γ′ peptide, respectively. Altogether, these findings suggest that the inhibiting effect of the γ′ peptide on the cleavage of both PAR-1 and the synthetic substrate S2238 stems mainly from conformational changes induced in the catalytic site of thrombin.

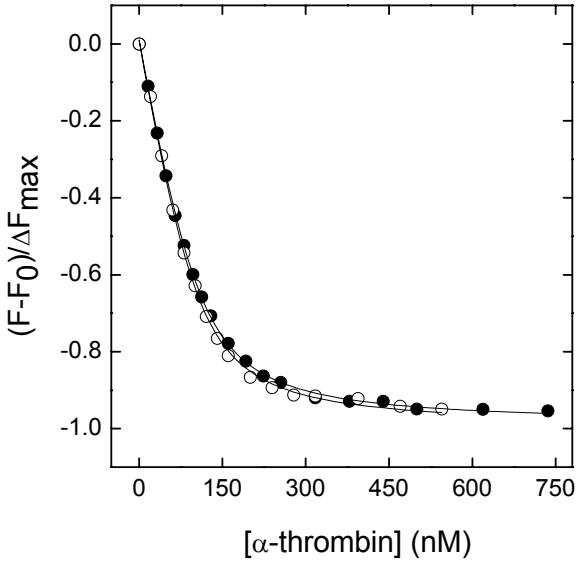

Figure 8. The γ' peptide did not influence allosterically exosite 1. Plot of the normalized fluorescence fractional change (F-F0/ΔFmax) of [F]-Hir54-65(PO3H2) (110 nM) as a function of human α-thrombin concentration in the absence (●) or in the presence (○) of 74 μM of γ' peptide. The continuous lines were drawn according to eq. 3, with best fit parameters Kd = 19.7 ± 1.2 nM (●) and 14.3 ± 1.5 nM (○).

DISCUSSION

The present study showed for the first time that the fibrinogen sequence 408-427 in the elongated γ′ chain inhibits the thrombin-induced aggregation of platelets through a combined mechanism, impairing both GpIbα and PAR-1 interactions. Since it has been previously shown that binding of thrombin to GpIbα could enhance the efficiency of thrombin cleavage of PAR-1 (22), the double effect of γ′ peptide on both GpIbα interaction and PAR-1 cleavage may cooperatively determine a strong inhibition on platelet activation/aggregation, as indeed observed. These results are unprecedented, as they show how the same ligand may hinder at the same time the thrombin interaction with the two thrombin-elicited receptors involved in platelet activation, i.e. GpIb and PAR-1.

The interaction of fragment D* is energetically driven by the insertion γ′ sequence 408-427, which specifically binds to ABE-II, as demonstrated by various experimental strategies. In fact, both γ′ peptide and fragment D* are able to displace from ABE-II ligands, which are known to interact with this site, such as GpIbα and the ssDNA aptamer HD22. However, the synthetic γ′ peptide and the fragment D* showed a different affinity for thrombin. The K_d value of fragment D* was about 80-fold lower than that of the synthetic peptide. These results parallel previous findings on the binding of fibrinogen γ-chain to platelet GpIIb-IIIa, where a 70-fold difference in affinity between the synthetic peptide 400-411 of the fibrinogen γ chain and the native fibrinogen fragment D was found (31). Similar results were obtained for the binding of the N-terminal domain 1-282 of GpIbα to thrombin, where the affinity of the properly sulphated C-terminal peptide 268-282 is about 50 times lower than that of the full-length GpIbα (1-282) fragment (19,20). These observations can be reasonably explained by assuming that the protein core may orient the C-terminal tail of the γ-chain in a conformation productive for binding or that the main body of the protein, beyond the C-terminal extension, enhances affinity by directly interacting with thrombin. The latter situation is documented by the crystal structure of GpIbα-thrombin complex (32), where numerous hydrophobic and electrostatic interactions, not involving the C-terminal tail, further stabilize the complex. Although the isolated C-terminal segment of the γ-chain displays some nascent secondary structure element, NMR data indicate that it is highly flexible and intrinsically disordered in solution (33). This conformational flexibility is also confirmed by the poor electron density observed for the C-terminal γ-segment in the crystallographic structures of fibrinogen D fragment (PDB code: 1LT9, 1FZC, 1FIC) (34-36). On the other hand, the structure of a smaller γ-chain fragment (PDB code: 1FIC) reveals that the segment Leu392-Gly403 extends along the protein surface making numerous hydrogen bonds with the rest of the γ-chain (36). Hence, these contacts may facilitate interaction with thrombin by orienting the elongated γ'-segment in a conformation productive for binding.

It is known that approximately 10% of circulating fibrinogen molecules contain the elongated γ′ chain. If we refer to a normal plasma fibrinogen concentration (200-400 mg/dl corresponding to ≈6-12 μM), this would correspond to a concentration of elongated γ′ chain of about 0.6-1.2 μM, nicely overlapping the K_d value of the fragment D* interaction with the enzyme (Kd ~ 0.5 μM). Thus, variations in the ratio between normal and elongated γ′ chain can significantly affect thrombin's ligation in vivo, in keeping with the notion that the maximum change of the fractional saturation of a macromolecule as a function of its ligand concentration occurs when the latter is present at levels similar to the K_d value (37).

Moreover, it has to be outlined that in this study a surrogate for γ′ fibrin was used. The latter actually interacts with thrombin engaging both exosite 2 and 1 (3), although exosite 1 binds to fibrinogen fragment E with low affinity (3). Thus, we can speculate that γ′ fibrin can inhibit thrombin-induced platelet activation more extensively than fragment D*, as it competitively blocks both PAR-1

cleavage, via engagement of exosite 1, and GpIb ligation, via binding to exosite 2, that allosterically down-regulates also PAR-1 cleavage, as demonstrated in the present study.

The allosteric effect linked to binding of the elongated γ′ chain to thrombin's ABE-II resulted in a decrease of the catalytic specificity of the enzyme for good substrates such as PAR-1 and the synthetic tripeptide S-2238, whereas no significant effect was observed with the PAR-4 peptide (44-66). Thus, platelet activation induced by PAR-4 hydrolysis, that occurs mainly at high thrombin concentrations and signals independently from PAR-1 (38), is not affected by either γ′ peptide or fragment D*. This may also contribute to explain the lack of complete inhibition of the thrombin-induced platelet aggregation observed even at high γ′ peptide and fragment D* concentrations (see Figure 4B). The extracellular region of PAR-1 interacts with thrombin active site through the sequence ^{38}Leu-Asp-Pro-Arg^{41} and with ABE-I using a hirudin-like sequence (24,30). This is not the case for PAR-4, that orients Pro44 and Pro46 of the sequence 44Pro-Ala-Pro-Arg47 in the catalytic pocket but does not interact with ABE-I residues, using the C-terminal segment (39,40). Recently, the crystal structure of murine thrombin in complex with the extracellular fragment of murine PAR-4 confirmed this mode of binding (41). Perturbation of ABE-I by hirugen or PAR-1 exodomain (42-60) allosterically induces significant structural changes in the free catalytic pocket of thrombin, mainly at and around Ser195 (16,30,42), that result into altered reactivity of the enzyme toward synthetic and natural substrates (24-26,43) and for binding of inhibitors (44-46). Notably, ligand binding to ABE-I can either enhance or inhibit the cleavage of small chromogenic substrates carrying an Arg-residue at P1 position, according to their chemical structure at P2 and P3 positions (24,26). Similar conclusions can be drawn for the perturbation of ABE-II, where binding of some ligands such as prothrombin fragment F2 or GpIbα causes negligible or even opposite effects on thrombin-mediated cleavage of chromogenic substrates (26,47). For instance, hydrolysis of S-2238 (D-Phe-Pro-Arg-pNA) is inhibited in the presence of F2, whereas cleavage of tosyl-Gly-Pro-Arg-pNA is enhanced at a similar extent (26). These findings confirm the extreme molecular plasticity of thrombin. Unfortunately, crystal structures of thrombin bound to several different ligands, including the prothrombin F2 fragment (48) (PDB code 1HPQ), heparin (49) (PDB code: 1XMN), and GpIbα(1-282) (32,50) (PDB code 1P8V and 1OOK), indicate that thrombin accommodates ABE-II ligands with little, if any, change in its folded structure and thus do not explain the observed variations in thrombin function upon ligand binding. These discrepancies likely arise from crystal packing effects (49), or from the presence of the PPACK inhibitor (32,48), that locks the active site and the specificity exosites of the enzyme into a fixed conformation, thus abrogating the structural changes that may be induced by ligand binding in solution. Very recently, the crystal structure of thrombin complex with the fibrinogen γ′-peptide (408-427) has been solved at 2.4 Å resolution. No significant change in the structure of the enzyme-peptide complex could be detected when compared to that of free thrombin (9) (pdb code: 2HWL). Conversely, solution studies involving hydrogen-deuterium exchange (HDX) coupled with MALDI-TOF mass spectrometry showed that the gamma' peptide

interacts at or near the thrombin ABE-II residues R93, R97, R173, and R175. Moreover, the binding of the γ′ peptide induces a conformational perturbation to the enzyme as a whole, by significantly protecting from deuterium exchange other regions of thrombin, such as the autolysis loop, the edge of the active site region, some portion of ABE-I and the A-chain (51). Most of Trp-residues in thrombin (i.e., Trp96, Trp141, Trp148, Trp207, and Trp215) are embedded in segments whose HDX efficiency is reduced upon γ′ peptide binding, while other tryptophans (i.e., Trp29 and Trp237) are in direct contact with the perturbed segments (51) (Fig 9).

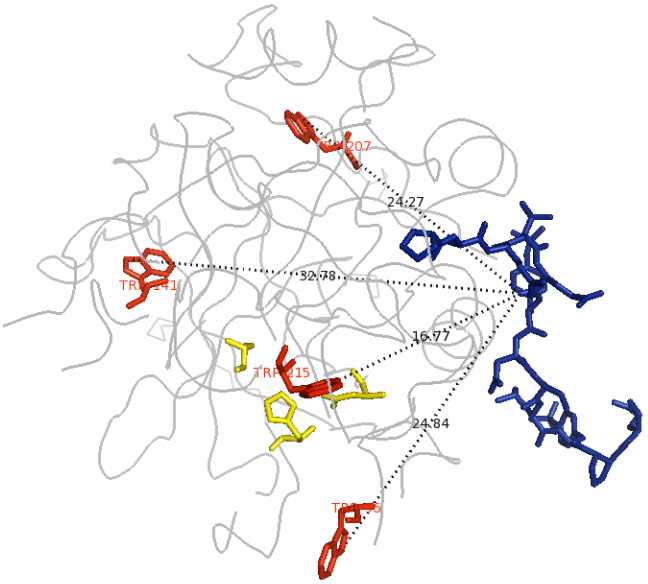

Table 3. HDX Exchange

		γ'- IIa	
Residues	**D_{max}**	**1 min**	**10 min**
85-94	8.8	-5.6	-17.7
85-96	10.9	-12.3	-25.9
85-99	15.2	-16.4	-21.8
135-149D	19.4	-4.6	-0.5
202-207	6.8	-13.2	-6.1
212-217	15.9	-6.3	-1.5

Figure 9. (A) Representation of thrombin in complex with γ' peptide (2HWL.pdb)**.** In red are highlighted the tryptophan residues that are major involved in the H-D exchange process. Notable they are located 15-32 Å away from the ABE-II. **(B) Solution studies involving hydrogen-deuterium exchange (HDX) coupled with MALDI-TOF mass spectrometry** showed how in the presence of γ'-peptide, several fragments of thrombin reduce the exchange velocity with respect to the control composed by thrombin alone.

Hence, it is not surprising that the formation of γ′ peptide-thrombin complex results into a higher fluorescence intensity of the enzyme, as shown in Fig. 3, compatible with a conformational change of thrombin in which the chemical environment of Trp-residues becomes more rigid and hydrophobic (28). Thus, it is conceivable that the structural perturbations caused by γ′-peptide binding propagates from the ABE-II residues toward the S2-S4 subsites of the catalytic cleft of the enzyme and that these changes are sensed differently by the various P3 residues present in S-2238, PAR-1, and PAR-4. In agreement with this allosteric hypothesis, the k_{cat}/K_m of S-2288 (D-Ile-Pro-Arg-pNA) by thrombin was increased by 40% at high concentration of the synthetic γ′ peptide (160 μM, data not shown), demonstrating that even subtle changes in the side-chain volume (Ile = 124 Å3; Phe = 135 Å3) and electronic properties at the P3 site can significantly change the allosteric linkage between binding to ABE-II and hydrolytic activity of thrombin.

In principle, the inhibition of PAR-1 cleavage by thrombin might also arise from conformational transitions in ABE-I induced long-range by γ′ peptide binding to ABE-II, leading to a lower affinity of the C-terminal PAR-1 segment for ABE-I. The effect of γ′ peptide on PAR-4 cleavage would be negligible because this latter substrate does not bind to ABE-I. This working hypothesis is worth of attention in the light of the proposed, but still debated, allosteric linkage existing between ABE-I and ABE-II (25,26). To test this hypothesis, we investigated the effect of γ′ on the binding of the fluorescein-conjugated C-terminal 54-65 peptide of hirudin, [F]-Hirudin54-65(PO_3H_2), a well known ligand for ABE-I (52). The fluorescence experiments showed that the binding of [F]-Hirudin54-65(PO_3H_2) was not significantly affected by the γ′ peptide, as shown by Fig. 8. Thus, it is likely that binding of the elongated γ chain to thrombin induces a conformational change mainly occurring at the catalytic site of the enzyme.

The influence of γ′ chain on venous thrombosis has been largely recognized (6). In particular, a decrease of this chain was associated with a net increase of the risk factor for venous thromboembolism (6). In contrast, as anticipated above, the role of this fibrinogen chain for arterial thrombosis is still debated (6,7,13). Clinical studies were conducted in the attempt to demonstrate whether altered levels of γ′ chain are inversely or directly correlated with increased risk for arterial thrombosis. These studies showed that the association of γ′ chain expression with arterial thrombotic diseases is paradoxically different from that shown in venous thrombosis. In particular, the reduced γ′/γA ratio occurring in certain fibrinogen polymorphisms, such as FGG-H2, was not associated with either acute myocardial infarction (53) or ischemic stroke (IS). Instead, increased γ′ levels were shown to be positively associated with an increased risk for both AMI and IS (54,55). However, this association was shown to be strengthened by the presence of increased levels of plasma fibrinogen concentration (54,55) and by FGG 9340T and FGA 2224G polymorphisms (54,55). Other factors, such as total fibrinogenemia (56), the γ′ chain's ability to protect thrombin by the heparin-AT inhibition (3) and to confer to fibrin clots resistance to fibrinolytic degradation may represent confounding factors in these studies. Thus, whether or not the thrombin interaction with γ′ chain of fibrinogen plays any patho-physiological role in particular clinical settings remains controversial. In a recent study on IS (55), both γ′ chain and total fibrinogen level were elevated in the acute phase of the disease and subsequently decreased in the convalescent phase. The increased γ′ chain in the acute phase stems from the elevation of IL 6, which can promote the synthesis of the γA and γ′ chains (57,58). Thus, further studies aimed at investigating the γ'/γA ratio rather than the absolute content of γ' are needed, especially in clinical situations, like acute thrombosis, where plasma fibrinogen is usually increased, and thus investigating the absolute γ' content alone might be misleading.

Based on our data, indicating a net platelet inhibitory effect of fibrinogen γ′ chain upon thrombin stimulation, we can infer that elevation of γ′ chain level, as a possible result of acute phase response, might exert a beneficial effect on the acute phase of thrombotic syndromes. A recent study in a baboon

thrombosis model showed indeed that the 410–427 γ′ peptide is able not only to inhibit fibrin-rich thrombus formation, because of the inhibition of the intrinsic coagulation pathway (related to inhibition of FVIII activation by thrombin), but also platelet-rich thrombus formation in the arterial circulation (59). These findings may be also relevant for clinical applications of ssDNA aptamers, like HD22, whose specific target is ABE-II of thrombin (60). On the contrary, the anti-thrombin and anti-platelet effect of the γ′ chain may be deleterious in hemorrhagic sequelae of vascular accidents, such as hemorrhagic stroke. In the latter condition, the expansion of the hematoma's volume causes the post-stroke complications often responsible for the high mortality from the disease. The findings reported in this study predict that the presence of enhanced expression of γ′ chain, could exert deleterious effects on the thrombin-induced platelet activation, and thus on either the arrest or onset of the hemorrhage.

In conclusion, the role of different expression of γ′ chain in circulating fibrinogen may variably influence the thrombotic and hemorrhagic manifestations in different clinical settings or different phases of a vascular disease

REFERENCES

1. Mosesson, M. W. (2003) *J Thromb Haemost* 1(2), 231-238
2. Seegers, W. H., Nieft, M., and Loomis, E. C. (1945) *Science* 101(2629), 520-521
3. Fredenburgh, J. C., Stafford, A. R., Leslie, B. A., and Weitz, J. I. (2008) *J Biol Chem* 283(5), 2470-2477
4. Chung, D. W., and Fujikawa, K. (2002) *Biochemistry* 41(37), 11065-11070
5. Farrell, D. H., Mulvihill, E. R., Huang, S. M., Chung, D. W., and Davie, E. W. (1991) *Biochemistry* 30(39), 9414-9420
6. Uitte de Willige, S., de Visser, M. C., Houwing-Duistermaat, J. J., Rosendaal, F. R., Vos, H. L., and Bertina, R. M. (2005) *Blood* 106(13), 4176-4183
7. Lovely, R. S., Falls, L. A., Al-Mondhiry, H. A., Chambers, C. E., Sexton, G. J., Ni, H., and Farrell, D. H. (2002) *Thromb Haemost* 88(1), 26-31
8. Meh, D. A., Siebenlist, K. R., and Mosesson, M. W. (1996) *J Biol Chem* 271(38), 23121-23125
9. Pineda, A. O., Chen, Z. W., Marino, F., Mathews, F. S., Mosesson, M. W., and Di Cera, E. (2007) *Biophys Chem* 125(2-3), 556-559
10. Cooper, A. V., Standeven, K. F., and Ariens, R. A. (2003) *Blood* 102(2), 535-540
11. Falls, L. A., and Farrell, D. H. (1997) *J Biol Chem* 272(22), 14251-14256
12. Mannila, M. N., Eriksson, P., Lundman, P., Samnegard, A., Boquist, S., Ericsson, C. G., Tornvall, P., Hamsten, A., and Silveira, A. (2005) *Thromb Haemost* 93(3), 570-577

13. Drouet, L., Paolucci, F., Pasqualini, N., Laprade, M., Ripoll, L., Mazoyer, E., Bal dit Sollier, C., and Vanhove, N. (1999) *Blood Coagul Fibrinolysis* 10 Suppl 1, S35-39
14. Kuyas, C., Haeberli, A., and Straub, P. W. (1982) *J Biol Chem* 257(3), 1107-1109
15. Pace, C. N., Vajdos, F., Fee, L., Grimsley, G., and Gray, T. (1995) *Protein Sci* 4(11), 2411-2423
16. De Cristofaro, R., Rocca, B., Bizzi, B., and Landolfi, R. (1993) *Biochem J* 289 (Pt 2), 475-480
17. Richardson, J. L., Kroger, B., Hoeffken, W., Sadler, J. E., Pereira, P., Huber, R., Bode, W., and Fuentes-Prior, P. (2000) *Embo J* 19(21), 5650-5660
18. Atherton, E., and Sheppard, R. C. (1989) Solid phase peptide synthesis : a practical approach, IRL Press, Oxford, England ; New York
19. De Cristofaro, R., and De Filippis, V. (2003) *Biochem J* 373(Pt 2), 593-601
20. De Cristofaro, R., De Candia, E., Rutella, S., and Weitz, J. I. (2000) *J Biol Chem* 275(6), 3887-3895
21. Tasset, D. M., Kubik, M. F., and Steiner, W. (1997) *J Mol Biol* 272(5), 688-698
22. De Candia, E., Hall, S. W., Rutella, S., Landolfi, R., Andrews, R. K., and De Cristofaro, R. (2001) *J Biol Chem* 276(7), 4692-4698
23. De Cristofaro, R., Peyvandi, F., Palla, R., Lavoretano, S., Lombardi, R., Merati, G., Romitelli, F., Di Stasio, E., and Mannucci, P. M. (2005) *J Biol Chem* 280(24), 23295-23302
24. Liu, L. W., Vu, T. K., Esmon, C. T., and Coughlin, S. R. (1991) *J Biol Chem* 266(26), 16977-16980
25. Verhamme, I. M., Olson, S. T., Tollefsen, D. M., and Bock, P. E. (2002) *J Biol Chem* 277(9), 6788-6798
26. Fredenburgh, J. C., Stafford, A. R., and Weitz, J. I. (1997) *J Biol Chem* 272(41), 25493-25499
27. Richardson, J. L., Fuentes-Prior, P., Sadler, J. E., Huber, R., and Bode, W. (2002) *Biochemistry* 41(8), 2535-2542
28. Lakowicz, J. R. (1999) Principles of fluorescence spectroscopy, Kluwer Academic/Plenum, New York, USA
29. Soslau, G., Class, R., Morgan, D. A., Foster, C., Lord, S. T., Marchese, P., and Ruggeri, Z. M. (2001) *J Biol Chem* 276(24), 21173-21183
30. Mathews, II, Padmanabhan, K. P., Ganesh, V., Tulinsky, A., Ishii, M., Chen, J., Turck, C. W., Coughlin, S. R., and Fenton, J. W., 2nd. (1994) *Biochemistry* 33(11), 3266-3279
31. Kirschbaum, N. E., Mosesson, M. W., and Amrani, D. L. (1992) *Blood* 79(10), 2643-2648
32. Dumas, J. J., Kumar, R., Seehra, J., Somers, W. S., and Mosyak, L. (2003) *Science* 301(5630), 222-226
33. Mayo, K. H., Burke, C., Lindon, J. N., and Kloczewiak, M. (1990) *Biochemistry* 29(13), 3277-3286
34. Kostelansky, M. S., Betts, L., Gorkun, O. V., and Lord, S. T. (2002) *Biochemistry* 41(40), 12124-12132
35. Spraggon, G., Everse, S. J., and Doolittle, R. F. (1997) *Nature* 389(6650), 455-462

36. Yee, V. C., Pratt, K. P., Cote, H. C., Trong, I. L., Chung, D. W., Davie, E. W., Stenkamp, R. E., and Teller, D. C. (1997) *Structure* 5(1), 125-138
37. Wyman, J., and Gill, S. J. (1990) Binding and linkage: functional chemistry of biological macromolecules, University Science Books, Mill Valley, Cali
38. Faruqi, T. R., Weiss, E. J., Shapiro, M. J., Huang, W., and Coughlin, S. R. (2000) *J Biol Chem* 275(26), 19728-19734
39. Cleary, D. B., Trumbo, T. A., and Maurer, M. C. (2002) *Arch Biochem Biophys* 403(2), 179-188
40. Jacques, S. L., and Kuliopulos, A. (2003) *Biochem J* 376(Pt 3), 733-740
41. Bah, A., Chen, Z., Bush-Pelc, L. A., Mathews, F. S., and Di Cera, E. (2007) *Proc Natl Acad Sci U S A* 104(28), 11603-11608
42. Vijayalakshmi, J., Padmanabhan, K. P., Mann, K. G., and Tulinsky, A. (1994) *Protein Sci* 3(12), 2254-2271
43. Jacques, S. L., LeMasurier, M., Sheridan, P. J., Seeley, S. K., and Kuliopulos, A. (2000) *J Biol Chem* 275(52), 40671-40678
44. Bock, P. E. (1992) *J Biol Chem* 267(21), 14974-14981
45. Bock, P. E. (1992) *J Biol Chem* 267(21), 14963-14973
46. Henry, B. L., Monien, B. H., Bock, P. E., and Desai, U. R. (2007) *J Biol Chem* 282(44), 31891-31899
47. Jandrot-Perrus, M., Clemetson, K. J., Huisse, M. G., and Guillin, M. C. (1992) *Blood* 80(11), 2781-2786
48. Arni, R. K., Padmanabhan, K., Padmanabhan, K. P., Wu, T. P., and Tulinsky, A. (1993) *Biochemistry* 32(18), 4727-4737
49. Carter, W. J., Cama, E., and Huntington, J. A. (2005) *J Biol Chem* 280(4), 2745-2749
50. Celikel, R., McClintock, R. A., Roberts, J. R., Mendolicchio, G. L., Ware, J., Varughese, K. I., and Ruggeri, Z. M. (2003) *Science* 301(5630), 218-221
51. Sabo, T. M., Farrell, D. H., and Maurer, M. C. (2006) *Biochemistry* 45(24), 7434-7445
52. Rydel, T. J., Tulinsky, A., Bode, W., and Huber, R. (1991) *J Mol Biol* 221(2), 583-601
53. Furlan, M., Robles, R., and Lamie, B. (1996) *Blood* 87(10), 4223-4234
54. Mannila, M. N., Lovely, R. S., Kazmierczak, S. C., Eriksson, P., Samnegard, A., Farrell, D. H., Hamsten, A., and Silveira, A. (2007) *J Thromb Haemost* 5(4), 766-773
55. Cheung, E. Y., de Willige, S. U., Vos, H. L., Leebeek, F. W., Dippel, D. W., Bertina, R. M., and de Maat, M. P. (2008) *Stroke* 39(3), 1033-1035
56. Thomas, D. P., and Roberts, H. R. (1997) *Ann Intern Med* 126(8), 638-644
57. Mannila, M. N., Eriksson, P., Leander, K., Wiman, B., de Faire, U., Hamsten, A., and Silveira, A. (2007) *J Intern Med* 261(2), 138-147
58. Duan, H. O., and Simpson-Haidaris, P. J. (2003) *J Biol Chem* 278(42), 41270-41281

59. Lovely, R. S., Boshkov, L. K., Marzec, U. M., Hanson, S. R., and Farrell, D. H. (2007) *Br J Haematol* 139(3), 494-503
60. Lancellotti, S., De Cristofaro, R. (2008) Cardiovascular and Haematological Agents in Medicinal Chemistry *In Press*
61. Everse, S. J., Pelletier, H., and Doolittle, R. F. (1995) *Protein Sci* 4(5), 1013-1016

CHAPTER 2.5.

Conformational and biochemical characterization of a biologically active rat recombinant Protease Nexin-1 expressed in E. coli

Rosaria Arcone [1], Alberto Chinali [2], **Nicola Pozzi** [3], Maddalena Parafati [1], Fabio Maset [3], Concetta Pietropaolo [2] and Vincenzo De Filippis [3]

[a]*Dipartimento di Scienze Farmacobiologiche, Università di Catanzaro "Magna Graecia", Italy*
[b]*Dipartimento di Biochimica e Biotecnologie Mediche, Università di Napoli "Federico II", Italy*
[c]*Dipartimento di Scienze Farmaceutiche, Università di Padova, Italy*

Published in Biochim. Biophys. Acta. (BBA) 2009; 1794(4):602-14.

INTRODUCTION

Glia-derived nexin or Protease nexin-1 (PN-1) is a 44 kDa glycoprotein expressed and secreted by a variety of cells, including fibroblasts (1), myoblasts (2), vascular smooth muscle cells (3), astrocytes (4), and neuronal cells (5). PN-1 belongs to the serpin super-family (6) and inhibits several serine proteases, including thrombin, urokinase, tissue plasiminogen activator and plasmin (7**,** 8) with a mechanism of suicide substrate mediated by the formation of a covalent complex with the target protease (9). Once formed, the serpin-protease complex binds back to the cells and is internalized and degraded, thus providing a localized mechanism for inhibiting and clearing the protease from the extracellular environment (8). Through the production of inhibitors such as PN-1, glial cells would be able to modulate the extent of neuronal migration and cause modifications compatible with the early, target independent outgrowth of neurite. A fine localized balance between neuronal proteolytic activity and PN-1 inhibition would sustain neurite elongation (8).

Although the molecular nature of the PN-1 inhibitory complex in native conditions remains controversial, in vitro it consists of a 1:1 covalent protease-PN-1 complex and it appears to be stable both in in reducing SDS-electrophoresis (7) and physiological conditions (10). Studies on the distribution of PN-1 in various tissues have shown that it is a major serpin found in physiologic amounts in the brain (5**,** 11), primarily secreted by glial cells (12) and differentially expressed during neuronal differentiation (13). PN-1 has been found to inhibit thrombin-mediated neurite outgrowth retraction (14) and in the protects neuronal cells from proteolytic damage and thrombin-induced apoptosis in brain

injury (15, 16). Recent data (17) suggest that PN-1 exerts biological functions not mediated by its inhibitory activity on proteases.

During our studies aimed to dissect the structure-function relationships of PN-1, we approached the task of devising an efficient system to produce large amounts of recombinant protein, either in native or mutated form. To this aim, a cDNA coding for rat PN-1 was isolated by RT-PCR and cloned in vectors exploiting an inducible T7 RNA polymerase and able to express PN-1 either as a His-tag fusion protein (pE15.b plasmid) or as a mature protein (pT7.7 plasmid). The recombinant protein (rPN-1) was expressed in E. coli BL21(DE3)pLysE strain, purified to homogeneity, characterized for its chemical identity, as well as for its conformational and biochemical properties and tested for its biological activity in numerous functional assays. rPN-1 was also expressed in an inducible eukaryotic expression system, using HeLa Tet-off cells.

Our results show that *E. coli* is a convenient expression system for obtaining fully active rPN-1 in sufficiently high yields for structural and functional studies.

My contribution to this work was focused on the investigation of the structural and conformational properties of the rPN-1 togheter with the homology model. Relevant information was also obtained from the inhibition activity assays towars thrombin, in the presence or in the absence of heparin.

MATERIALS AND METHODS

Construction of rat PN-1 vector. Total RNA was purified from rat cortical astrocytes according to (18), dissolved in water (1 μg/μl) and stored at -20°C. Ten pmol of random hexamers were mixed with 1 μg of total RNA in a final volume of 10 μl. The mixture was heated for 5 minutes at 70 °C, then kept at room temperature. Subsequently, 4 μl of first-strand buffer (5x concentrated; Gibco BRL), 2 μl of 100 mM dithiothreitol, 1 μl of dNTPs solution (10 mM each), 2 μl water and 1 μl (2.5 U) of Mo-MuLV reverse transcriptase (Gibco, BRL) were added and incubated 10 minutes at room temperature and 45 minutes at 37 °C. The reaction was terminated by adding 80 μl of water and heating at 94 °C for 5 minutes. Two μl of this mixture were used for PCR amplification of cDNA encoding PN-1. PCR primers were synthesized utilizing the published sequence of cDNA encoding rat glia-derived nexin (19). The sense primer, 5' CTC GTC **TGA ATT C**AT GAA TTG GCA TTT TCC C3' includes 11 nucleotides adjacent to the sequence encoding the first amino acid of the signal peptide (-11 to +18, numbering starts from the adenine of the ATG triplet corresponding to the translation initiation site) and containing EcoRI restriction site; the antisense primer, 5' CTC ACT A**TC TAG A**GG CTT GTT CAC CTG CCC C3', complementary to the 3'-untraslated region (UTR), position +1423 and containing a XbaI restriction site. The reaction was carried out in a total volume of 50 μl containing 20 pmol of each PCR primer, 5 μl of Taq polymerase buffer (10x, Perkin Elmer Cetus), 2 μl of 2.5 mM of each dNTP

and 2 U of Taq polymerase (Perkin Elmer Cetus). The PCR amplification was carried out through 5 cycles of denaturing (94°C, 1 minute), annealing (57°C, 1.5 minute) and extension (72°C, 2 minutes), followed by further 35 cycles using a different annealing temperature (60°C, 1.5 minute). The final extension was at 72°C for 10 minutes. The 1451-bp PCR product containing the cDNA encoding PN-1 was recovered by agarose gel electrophoresis purified and ligated into pGEM-T vector (Promega). The resulting plasmid pGEM-T-PN-1 was controlled by restriction mapping and the cloned cDNA was verified by nucleotide sequence analysis (20). A NdeI restriction site was introduced at the serine-20 codon (numbering start at the methionine-1 of PN-1 leader peptide), in frame with the remaining coding sequence, by site-specific mutagenesis directed by a synthetic oligonucleotide carrying the appropriate nucleotide substitutions, used as a primer in a PCR on pGEM-T-PN-1 DNA.

For production of polyclonal antibodies against PN-1, the PCR fragment was excised by NdeI-XbaI restriction endonucleases and cloned in the pET-15b vector (Novagen, UK), which allows the expression of a Hexa-His-tagged protein easily purified by affinity chromatography on a nickel-agarose column. The resulting vector was named pET-15b-PN-1. Polyclonal antiserum was raised in rabbit against affinity purified His-tagged PN-1 (21).

To produce a large amount of mature PN-1, a NdeI-SalI fragment (1170 bp) was excised from pET-15b-PN-1 DNA and inserted in a pT7.7 plasmid (22). The resulting vector was named pT7.7-PN1. For in vitro transcription and translation of PN-1 cDNA, a SalI restriction site was introduced in the polylinker region of pGEM-T-PN-1 plasmid by PCR mutagenesis and the SalI-XbaI fragment containing the PN-1 cDNA region was excised and cloned in the pGEM-4Z vector, resulting in a pGEM-4Z-rPN-1 vector.

To obtain an inducible expression system of PN-1 in eukaryotic cells, a 1212 bp EcoRI-XbaI fragment, including the sequence coding for the signal peptide, was cloned in the pTRE vector (Clontech, Cambridge, UK). The resulting plasmid, pTRE-PN-1, was further modified by inserting a Kozak consensus sequence (23) to optimize the translation in eukaryotic cells. The final vector was indicated as pTRE-Kozak-rbs-PN-1. All the constructs were controlled by restriction mapping and DNA sequence analysis.

Expression in E. coli, renaturation and purification of rPN-1. The pET-15b-PN-1 or pT7.7-PN-1 expression vectors were introduced in E. coli BL21(DE3)pLysE strain which expresses the T7 RNA polymerase under the inducible lac UV5 promoter. Bacterial growth, isolation of inclusion bodies and extraction of proteins were performed as previously reported (24). The in vitro refolding of rPN-1 was obtained through a two-step dialysis; first step against a low concentration of the denaturing agent (2 M GdnHCl, 50 mM Tris-HCl pH 8.0) containing 2 mM DTT. The second dialysis step was performed against 50 mM Tris-HCl pH 8.0, 0.15 M NaCl, 1 mM DTT, 10% glycerol. The refolded extract was centrifuged at 15000 g for 45 min to remove insoluble material and loaded at 1 ml/min onto a HiTrap

Heparin HP column (5 ml, GE Healthcare Life Science) connected to a FPLC system (GE Healthcare Life Science). The column was equilibrated in the dialysis buffer and after 10 volumes washing, the elution was performed at 4 ml/min by applying 10 volumes of a linear gradient to 1.5 M NaCl and collecting 0.5 ml fractions. Protein analysis was performed by SDS-PAGE and Western blotting and fractions containing rPN-1 were pooled, aliquoted and stored at -20°C.

The Hexa-His-PN-1 protein was purified from bacterial lysate using nickel agarose (Ni-NTA) resin (Qiagen, Germany) according to the manufacturer's instructions. The concentration of total protein was determined by a Bio-Rad protein assay (25) using bovine serum albumin as a standard. Twelve percent polyacrilamide SDS-PAGE was performed as described by Laemmli (26). After electrophoresis, proteins were stained by Coomassie brilliant blue R-250 or electrophoretically transferred to nitrocellulose filters (BA85; Schleicher & Schull). Blots were probed with rabbit antisera against PN-1 followed by incubation with a peroxidase-conjugated anti-rabbit IgG in PBS, containing 5% dry milk and developed according to the Enhanced Chemioluminescence (ECL) technique.

Analytical techniques

RP-HPLC. The purity of rPN-1 preparations was checked by loading an aliquot (100 µl) of rPN-1 solution (0.12 mg/ml) onto a Vydac (The Separation Group, Hesperia, CA) C4 column (4.6 x 150 mm, 5µm particle size), eluted with a linear acetonitrile-0.078% TFA gradient at flow rate of 0.8 ml/min. The absorbance of the effluent was recorded at 226 nm.

Mass spectrometry. Accurate molecular weight determination of rPN-1 was obtained with a Mariner ESI-TOF high-resolution mass spectrometer (Perseptive Biosystems, Stafford, TX). Tipically, RP-HPLC purified rPN-1 (5 µg) was lyophilized, dissolved in 1:1 water:acetonitrile mixture (20 µl), containing 1% (by vol.) formic acid, and then analyzed by mass spectrometry, obtaining mass values in agreement with the expected amino acid composition within 0.01% mass accuracy.

Two-Dimensional Electrophoresis. 2D electrophoresis was conducted on a BioRad Protean IEF-Cell apparatus, using essentially the procedure provided by the manufacturer (27). For the first dimension, an immobilized pH-gradient (IPG) strip (pH 3-10) (Biorad-1632009) was incubated with 300 µl of rehydration buffer (i.e., 0.1% (w/v) CHAPS, 0.1% (w/v) Bio-Lyte 3-10, 8M urea, 0.1 M DTT, and 0.001% (w/v) Bromophenol Blue) containing the lyophilised rPN-1 sample (5 µg) and 5 µl of protein standard (BioRad, 161-0320). Rehydration was carried out at 20±0.5 °C for 15 hours and applying a constant potential of 50 V. Prior to isoelectrofocusing (IEF), desalting of the strip was achieved by applying a potential of 250 V for 15 min. IEF was conducted at 10 kV·h for 3 hours and then at 10 kV·h, up to 60 kV. Finally, the strip was frozen at –80°C. To reduce protein disulfide bonds eventually present, the strip was then incubated under gentle stirring for 10 min with 6 ml of 0.375 M Trs-HCl buffer, pH 8.8, 6 M urea, 2% SDS, 20% glycerol (buffer A), containing 2% DTT. The reducing buffer was discarded and the strip incubated for 10 min with buffer A containing 2.5% iodoacetamide, for

blocking unreacted DTT. The second dimension was carried out by loading the strip on a (20 x 20 cm) SDS-PAGE vertical slab (26) (stacking gel: 4% acrylamide; running gel: 12% acrylamide) run overnight at a constant current of 10 mA. The gel was stained using a modified silver staining protocol (28).

Spectroscopic Measurements

Determination of protein concentration. The concentration of PN-1 was determined by ultraviolet (UV) absorption at 280 nm on a double beam model Lambda-2 spectrophotometer from Perkin-Elmer. The extinction coefficient at 280 nm was calculated using a molar absorption coefficient of 1,280 $M^{-1}\cdot cm^{-1}$ for tyrosine, 5,690 $M^{-1}\cdot cm^{-1}$ for tryptophan, 120 $M^{-1}\cdot cm^{-1}$ for disulfides (29), and taken as 0.83 mg $^{-1}\cdot cm^{2}$. The concentration of thrombin was determined either by UV absorbance at 280 nm, using a molar absorption coefficient of 65770 $M^{-1}\cdot cm^{-1}$ (30) or, alternatively, by titration of thrombin active-site with hirudin (31).

Circular dichroism. CD spectra were recorded on a Jasco model J-810 spectropolarimeter equipped with a thermostated cell-holder connected to a NesLab (Newington, NH) model RTE-111 water-circulating bath. Far- and near-UV CD spectra were recorded at 20±0.5 °C in 50 mM Tris-HCl buffer, pH 8.8, containing 0.6 M NaCl and 10% (v/v) glycerol, using a 1- or 10-mm path length quartz cells in the far- and near-UV region, respectively.

Fluorescence. Emission spectra were recorded at 20±0.5 °C on a Perkin-Elmer spectrofluorimeter model LS-50B, equipped with a thermostated cell-holder connected to a Haake F3-C water-circulating bath. Protein samples in 50 mM Tris-HCl buffer, pH 8.8, containing 0.6 M NaCl and 10% (v/v) glycerol were excited at 280 or 295 nm, using an excitation/emission slit of 5/10 nm.

Heparin binding to rPN-1. For measuring heparin binding to rNP-1, a Jasco model FP-6500 spectrofluorimeter, equipped with a Peltier model ETC-273T temperature control system, was used. Excitation and emission wavelengths were at 280 and 341 nm, respectively, using an excitation/emission slit of 10/10 nm. During titration experiments, the increase of fluorescence intensity at 341 nm was recorded as a function of heparin concentration. For all measurements, the Long-Time-Measurement software (Jasco) was used. Under these conditions, photobleaching of Trp-residues was essentially absent. To a solution of rPN-1 (2 ml, 130 nM) in 5 mM Tris-HCl buffer pH 7.5, 0.15 M NaCl, 0.1% PEG-8000, were added under gentle magnetic stirring aliquots (2-8 µl) of a stock solution (146 U/ml) of unfractionated porcine heparin (Calbiochem). Of note, 1 U of heparin is an amount equivalent to 2 µg of pure heparin, having an average molecular weight of 14.500 Da (32). Fluorescence intensities were corrected for dilution (2-3% at the end of the titration) and subtracted for the signal of the ligand (i.e., heparin) at the indicated concentration.

Molecular Modelling and Computational Methods. The structure of rPN-1 in the active and latent form was modeled on the corresponding crystallographic structures of PAI-1 (PDB codes: 1dvmA, for the active form, and 1dvnA, for the latent form) (33), that displays high sequence similarity with PN-1 (19). The three-dimensional model of rPN1 was obtained using the Swiss-Model automated comparative protein modeling server (http://swissmodel.expasy.org/SWISS-MODEL.html) (34). Accessible surface area (ASA) calculations were carried out by using a computer program available on-line at the site http://molbio.info.nih.gov/structbio/basic.html (35). Alignment of the rat PN-1 sequence (SwissProt code: P07092) with that of the human PAI-1 (SwissProt code: P05121) was carried out using the computer program Clustal W (vs. 1.83) available on-line at the site http://www.ebi.ac.uk/clustalw (36). The theroretical pI value of rPN-1 was calculated using the software ProtParam, available on-line at the site http://www.expasy.ch/cgi-bin/protparam. N-Glycosylation sites were predicted using the program NetNGlyc, available on-line at the site http://www.cbs.dtu.dk/services/NetNGlyc/.

Thrombin-rPN-1 complex formation monitored by SDS-PAGE. rPN-1 was mixed with natural thrombin (Calbiochem) (2:1 molar ratio) at room temperature (22±1°C) in in 5 mM Tris-HCl buffer pH 7.5, 0.15 M NaCl, 0.1% PEG-8000. Samples were taken at time intervals, mixed immediately with reducing SDS-loading buffer, and heated for a further 3 min at 100°C. SDS-gel electrophoresis was performed in a 12% acrylamide SDS-gel (26) and proteins were stained with Coomassie Brilliant Blue R-250.

Thrombin inhibition assays. In the absence of heparin, the inhibition of natural thrombin by rPN-1 was determined at 25±0.5°C by a discontinuous assay procedure similar to that described for thrombin inhibition by antithrombin-III (32). Briefly, the protease (1 nM) was incubated in the presence of rPN-1 (40 nM) in 300 µl (final volume) of 5 mM Tris-HCl, 0.15 M NaCl, 0.1% PEG 8000, pH 7.5. The residual protease activity was determined at time intervals by diluting 50 µl of the reaction mixture into 950 µl of the same buffer containing the chromogenic substrate (D)-Phe-L-pipecolyl-L-Arg-*p*-nitroanilide (Sigma) (S-2238, 93 µM). The inhibition of *p*-nitroaniline release from S-2238 was monitored by measuring the absorbance at 405 nm, using a molar absorption coefficient for p-nitroaniline of 9920 $M^{-1}\cdot cm^{-1}$. The concentration of S-2238 was determined by measuring the absorbance at 342 nm, using a molar absorption coefficient of 8270 $M^{-1}\cdot cm^{-1}$ (37). The per cent residual thrombin concentration was determined as the ratio of v_i/v_0, where v_i and v_0 are the initial velocities of thrombin-catalyzed substrate hydrolysis in the presence or absence of rPN-1. The % active thrombin was plotted as a function of time and the data fitted to equation 1, from which pseudo a first-order association constant, k_a, could be estimated (see Data Analysis).

In the presence of heparin, thrombin inhibition assays were carried out at 25±0.5°C by a continuous assay procedure. rPN-1 (2.0 nM) was incubated for 15 min at the same temperature with S-2238 (85.7

μM) and increasing concentrations (from 100 pM to 100 μM) of unfractionated porcine heparin (Calbiochem) in 950 μl of 5 mM Tris-HCl, 0.15 M NaCl, 0.1% PEG 8000, pH 7.5. The reaction was started by addition of 50 μl thrombin, up to a final concentration of 50 pM. After rapid mixing (5 s), substrate hydrolysis was immediately recorded by measuring the increase of the absorbance at 405 nm. Progress curves were fitted to equation 2 and analyzed as detailed below.

Data analysis. Either in the absence or presence of heparin, the inhibition of thrombin by PN-1 has been previously shown to conform to the mechanism reported in Scheme 1 (32, 38):

$$E + I \underset{k_{-1}}{\overset{k_1}{\leftrightarrow}} EI^* \xrightarrow{k_2} EI \qquad \text{(Scheme 1)}$$

where the protease, E, reversibly binds the inhibitor, I, to form the encounter complex, EI*, that irreversibly converts into the stable protease-serpin complex, EI, with a rate constant k_2. K_{EI} is the equilibrium constant for the noncovalent complex formation, $K_{EI} = k_{-1}/k_1$, where k_1 and k_{-1} are the association and dissociation rate constants, respectively. If the equilibrium E + I ↔ EI* is rapid compared with the rate of formation of EI (i.e., $k_2 << k_{-1}$) and if (I) << K_{EI} (i.e., when (EI*) is negligible), then the reaction follows simple second-order kinetics and appears to be a one-step irreversible process:

$$E + I \xrightarrow{k_a} EI \qquad \text{(Scheme 2)}$$

where k_a is the second-order rate constant for the formation of nondissociating complex EI. From Scheme 2 it follows that $dE/dt = -k_a (E)\cdot(I)$. Integration of equation 1 under pseudo first-order conditions (i.e., (I) > 10·(E)), yields equation 1:

$$(E)_t = (E)_0 \cdot \exp(-k_{obs} \cdot t) \qquad (1)$$

where $(E)_0$ and $(E)_t$ are the enzyme concentrations at time zero and t, respectively, and k_{obs} is the pseudo first-order rate constant given by $k_{obs} = k_a \cdot (I)_0$, where $(I)_0$ is the serpin concentration. The values of $(E)_t$ were determined by the discontinuous assay method (32) (see above), plotted as a function of reaction time and fitted to equation 1, yielding k_{obs} as a fitting parameter. In the discontinuous method, thrombin was incubated with PN-1 and samples of the reaction mixture were taken at various times. Measurements of residual enzyme activity were conducted by monitoring the initial rate of chromogenic substrate hydrolysis, S (i.e., S-2238), that yields the product P (i.e., p-nitroaniline). Finally, from the

knowledge of serpin concetration, $(I)_0$, the value of k_a could be easily calculated. Here we used this procedure to analyze thrombin inhibition data by rPN-1 in the absence of heparin.

In the presence of heparin, the affinity of PN-1 for thrombin increases by about 1000-fold, thereby preventing an accurate estimation of k_a using the discontinuous method (32). To overcome this limitation, we used a continuous assay method (see above) in which continuous monitoring of thrombin-PN-1 reaction was conducted in the presence of S-2238. It has been previously shown (38-40) that thrombin inhibition by PN-1 follows a reversible slow binding process according to the mechanism depicted in Scheme 3:

$$EI^* \underset{k_{-1}}{\overset{k_1}{\leftrightarrow}} I + E + S \overset{K_m \quad k_{cat}}{\leftrightarrow} ES \rightarrow E + P \qquad \text{(Scheme 3)}$$

Under pseudo first-order conditions, and with negligible consumption of substrate (<10%), the amount of product, P, as a function of time, t, is given by the exponential equation (39, 40):

$$(P)_t = v_s \cdot t + ((v_0 - v_s)/k_{obs}) \cdot (1 - \exp(-k_{obs} \cdot t)) \qquad (2)$$

where k_{obs} is the pseudo first-order rate constant for product formation and v_0 and v_s are the initial and steady-state velocities, respectively. Estimates of k_{obs}, v_0, and v_s were obtained by fitting to equation 2 the data of product generation obtained at different heparin concentrations, from 100 pM to 100 μM. At each heparin concentration, the second-order rate constant, k_1, can be related to k_{obs}, v_0, v_s, and K_m by equation 3:

$$k_1 = (k_{obs} \cdot (1 - v_s/v_0))/(I) \cdot (1 + (S)/K_m) \qquad (3)$$

where K_m is the Michaelis constant for thrombin-catalyzed hydrolysis of S-2238 at 25°C, previously estimated as 3.0±0.3 μM (41). When the value of k_1 was plotted against the concentration of heparin, a bell-shaped curve is obtained. Such a curve is empirically described by equation 4:

$$k_1 = k_1^\circ/(1 + (H)/K_1 + K_2/(H)) \qquad (4)$$

where k_1° is the maximum value of k_1 obtained at an optimal heparin concentration, and K_1 and K_2 are empirical constants that represent the concentrations of heparin at which the half-maximal value of k_1 is observed. Estimates of k_1°, K_1 and K_2 were obtained by fitting the data of k_1 vs. (H) to equation 4.

Cell Cultures, DNA transfections and immunocytochemistry. NB2A mouse neuroblastoma cells (kindly provided by Dr V. De Franciscis, CNR, Italy) and human HeLa Tet-Off cells (Clontech) were

cultured in Dulbecco's modified Eagle's medium (DMEM) supplemented with 10% fetal bovine serum (FBS), or 10% Tet system approved fetal bovine serum (Clontech) for the HeLa Tet-off cells. All culture media were also supplemented with 1.5 mM L-glutamine, 50 IU/ml penicillin and 50 μg/ml streptomycin. The cells were maintained at 37°C in a 5% CO_2 atmosphere and were subcultured twice a week by 3-5-fold dilution with culture medium.

For DNA transfection, cells were seeded subconfluent on cover slips and in 60-mm plates; 24 hr after plating, transfection was carried out using 1-7 μg of pTRE-Kozak-rbs-PN-1 DNA using the Lipofectamin 2000 reagent technique (Invitrogen, Life Technologies) according to the manufacturer's instructions; 18 hours after transfection, cells were washed with culture media and maintained in the presence (10 ng/ml) or absence of doxycycline hydrochloride (Sigma-Aldrich, Italy). At 24, 48 and 72 h following depletion of the antibiotic, cells were harvested and culture media collected for western blotting analysis and the cover slip cultures processed for indirect immunofluorescence staining.

Subconfluent cells on glass cover slips, were fixed with cold 3.7% formaldehyde (Fluka, France) in PBS with Ca^{2+} (0.1g/lt) and Mg^{2+} (0.1g/lt) for 20 min, permeabilized with 0.1% Triton X-100 in PBS for 5 min. The cover slips were incubated for 2 h at room temperature with polyclonal PN-1 antibodies (21) at a 1:20 dilution in a PBS-0.2% gelatin solution, washed three times for 5 min with 0.5 NaCl, 0.02 M NaPO4 pH 7.4 and finally, with PBS. An anti-rabbit IgG (Fc-specific) fluorescein-isothiocyanate (FITC)-conjugated (Jackson Immunoresearch Laboratories) was used as secondary antibody, at 1:200 dilutions in PBS-0.2% gelatin, for 1 h at room temperature.

Cover slips were washed and mounted with Mowiol (Hoechst, FRG) on microscope slides and observed with a Zeiss Axiovert 10 photomicroscope using a 63xPlan-Apochromat lens and fluorescein (450-490 nm, FT515-LP565) filters. After several washings, nuclear staining was performed. Cover slips were incubated for 20 min with 385 nM 4',6-diaminide-2-phenylindole (DAPI, Sigma) (42), then washed and mounted with Mowiol (Hoechst, FRG) on microscope slides. Cells were observed by a Zeiss Axiovert 10 photomicroscope using a 100x oil immersion objective Plan-Apochromat lens and DAPI (379-401 nm, 435-485 nm) filters.

For F-actin staining, cells were fixed, permeabilized, washed with PBS (with Ca^{2+} and Mg^{2+}) and then incubated in the dark for 20 min at room temperature with 0.768 μM rhodamine phalloidin (Molecular Probes) in PBS. Cells were rapidly washed for three times with buffer, mounted with Mowiol and observed with a Zeiss Axiovert 10M photomicroscope using a 63xPlan-Apochromat lens and rhodamine (546 nm, 590 nm) filters.

Induction of neurite outgrowth in NB2A neuroblastoma cells. NB2A cells were grown subconfluent on cover slips and cultured for 24 h in DMEM supplemented with 10% FBS. Cells were then differentiated to a neuronal morphology by serum deprivation (0% FBS), or kept undifferentiated in

0.8% FBS, for 4 hr. Cells were exposed to 50 nM rPN-1 alone or in combination with 2 nM thrombin, and after 3hr incubation were fixed and processed for immunocytochemistry.

RESULTS

Expression, purification, and chemical characterization. A cDNA fragment coding for rat PN-1 was isolated by RT-PCR using specific synthetic oligonucleotides on total RNA from rat cortical astrocytes (18). The PCR DNA product was inserted in pGEM-T vector. The resulting vector, pGEM-T-PN-1, was sequenced and found to contain the rat PN-1 cDNA, as reported in the NCBI/Gene Bank (accession number M17784).

Site specific mutagenesis was performed to introduce a NdeI restriction site which would allow us to excise a NdeI-XbaI DNA fragment coding for the mature PN-1. Thereafter, the mature PN-1 cDNA was cloned in pET-15b and in pT7.7 vectors, resulting in pET-15b-PN-1 and pT7.7-PN-.1 vectors, respectively. E. coli cells, strain BL21(DE3)pLysE, were transformed with pET-15b-PN-1 DNA and produced the His-tagged PN-1. Bacterial culture was processed as detailed in Materials and Methods and the fused rPN-1 protein was purified by IMAC on a nickel-loaded column (see below). The purified protein was used to produce polyclonal anti-PN-1 antibodies in rabbit, that were able to recognize PN-1 expressed in rat oligodendrocytes (21).

The recombinant protein was efficiently expressed in E. coli following IPTG induction (Fig. 1A, + IPTG). As also observed for the His-tagged form, mature rPN-1 was delivered to the inclusion bodies. After solubilization of inclusion bodies (24), rPN-1 was refolded in vitro by dialysing against Tris buffer, pH 8.8, containing moderate concentrations of denaturants and reducing agents (i.e., 2 M Gnd-HCl and 2 mM DTT) and then against the same buffer, without denaturant, containing 0.15 M NaCl, 1 mM DTT, and 10% glycerol. Addition of DTT prevented oxidation of the three free Cys-residues in the PN-1 structure during refolding (43), while glycerol was added to increase protein solubility. The refolding mixture was purified by affinity chromatography on a heparin-Sepharose column, whereby rPN-1 eluted as a single peak at 0.8 M NaCl. Expression, refolding and purification of rPN-1 was monitored by SDS-PAGE (Fig. 1A) and Western blot (Fig. 1B) analyses, showing the presence of a single intense band, at the molecular weight expected for rPN-1 (i.e., 42 kDa) and immunoreactive against PN-1 antibodies. Strikingly, the expression and purification procedure herein reported allowed us to recover about 3 mg of homogeneous (see below) rPN-1 per liter of cell culture.

The homogeneity of rPN-1 was also checked by reversed phase (RP) HPLC, demonstrating that the protein elutes as a single peak on a C4 analytical column (Fig. 1C). Accurate molecular weight determination of rPN-1, carried out by ESI-TOF mass spectrometry (Inset to Fig. 1C), yielded a mass value of 41774.4 ± 5 a.m.u. in close agreement with that expected from the amino acid composition of

rPN-1 (average mass: 41777.6 u.m.a.) (19). The isoelectric point, pI, of rPN-1 was estimated by two-dimensional electrophoresis (Fig. 1D), yielding a pI value of 9.7, consistent with the theoretical value deduced form the amino acid composition, pI 9.72. The minor spot at pI 9.6 likely originates from the artefactual cyanylation of some Lys-residues that sometimes occurs during long-time incubation (i.e., 15 h) of the IEF strip with protein samples in the presence 8 M urea (see Methods). Within the limits of the analytical methods used, these results provide strong evidence for the homogeneity and chemical identity of our recombinant rPN-1 preparation, that was subsequently used for conformational and functional characterization.

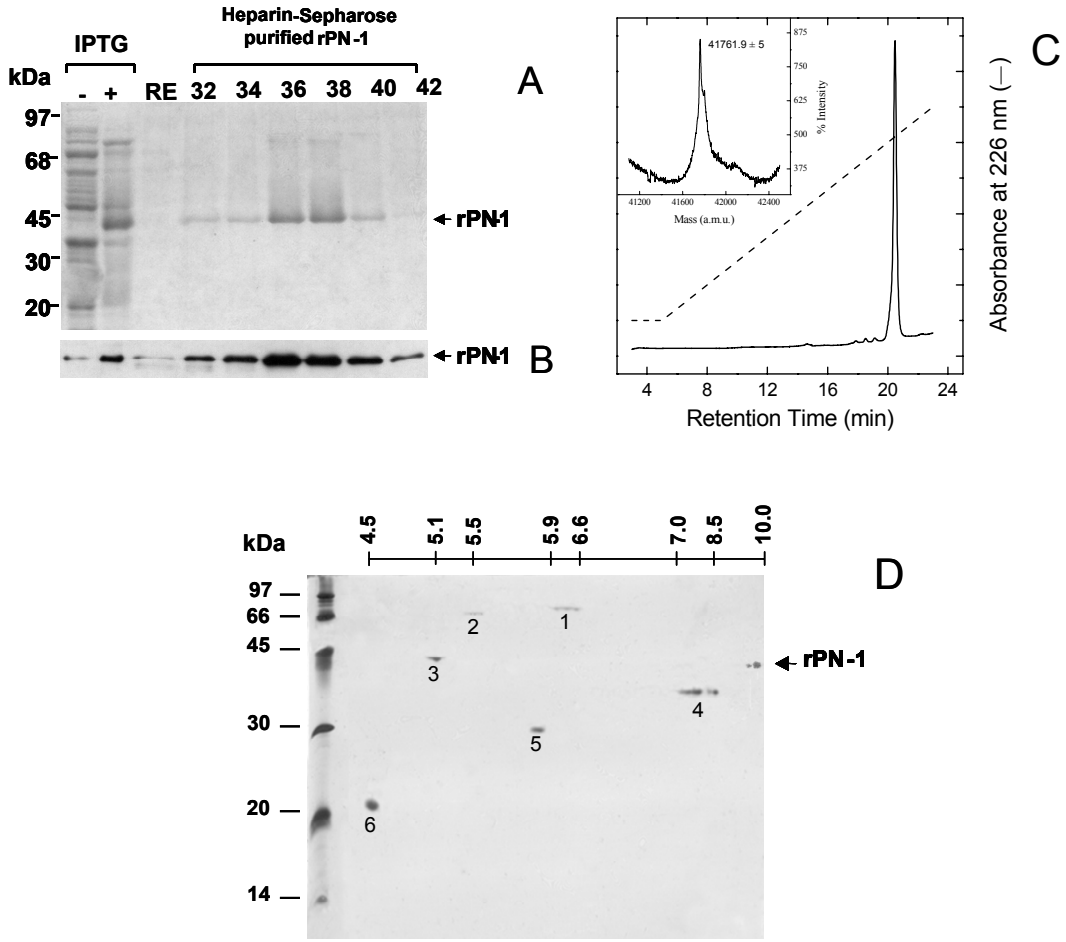

Figure 1. **Expression in *E. coli* and purification of rPN-1** monitored by SDS-PAGE and Western blotting**. (A)** SDS-gel elecrophoresis was conducted in a 12% acrylamide gel and proteins were visualized by Coomassie blue staining. From the left to the right: 20 µl of bacterial cell lysate from BL21(DE3) cells transformed with the pT7.7/PN1 vector DNA in the absence (-) and in the presence (+) of 0.4 mM IPTG; 100-ng aliquot of the renaturation mixture (RM) of rPN-1; 10-µl aliquots of the chromatographic fractions (32-42) eluted from the heparin-Sepharose column; molecular weight protein markers are indicated on the left-hand side. **(B)** Western blot analysis of the same samples run in the SDS-gel, as in panel **A**. rPN-1 was revealed by immunostaining and enhanced chemioluminescence. **(C)** RP-HPLC analysis of heparin-Sepharose purified rPN-1. An aliquot (10 □g) of rPN-1 was loaded onto a C4 column (4.6 x 150 mm) eluted with an acetonitrile-0.1% TFA gradient (---) from 10 to 60 % in 15 min. (**Inset**) Deconvoluted ESI-TOF mass spectrum of RP-HPLC purified rPN-1. (**D**) 2D-gel electrophoresis of purified rPN-1. The first dimension was run on an immobilized pH-gradient strip, from 3 to 10, while the second dimension on a 12% acrylamide SDS-gel, as detailed in the Methods. Proteins were visualized by silver staining. The pI value of rPN-1 was estimated as high as 9.6-9.7, using the BioRad pI protein standard for 2D electrophoresis, that contains (**1**) hen egg white conalbumin (pI 6.0, 6.3, 6.6); (**2**) BSA (pI 5.4, 5.5, 5.6); (**3**) bovine muscle actin (pI 5.0, 5.1); (**4**) rabbit muscle GAPDH (pI 8.3, 8.5); (**5**) bovine carbonic anhydrase (pI 5.9, 6.0); (**6**) soybean trypsin inhibitor (pI 4.5).

Model building. The molecular model of rPN-1 was built by homology modelling technique on the crystallographic structures of PAI-1 in the active form (PDB code: 1dvmA) (33), with which PN-1 shares 42% sequence identity and 65% similarity (see Fig. 2A) (19). The resulting model structure (Fig. 2B) resembles that typical of the serpin fold comprised of a bundle of 9 α-helices (A-I) and a β-sandwich composed of three β-sheets (A-C). The reactive center loop (RCL), i.e., the loop which is cleaved by the target protease, extends at the top of the molecule, spans from Asp330 at the C-terminal end of strand 5A to Arg355, and contains the scissible bond Arg345-Ser346.

In our model, four lysines (i.e., Lys71, Lys74, Lys75 and Lys78) are gathered on the exposed surface of helix D, which is followed by a surface loop containing three extra lysines (Lys83, Lys84 and Lys86), well positioned with helix D to form a large positively charged cluster, corresponding to the proposed heparin-binding site on PN-1 structure (44). Notably, PN-1 contains seven positive charges in the 71-86 segment; in the corresponding region, antithrombin III (AT-III) and heparin cofactor II (HC-II) contain five positive charges and PAI-1 only three positive charges and one negative charge. Likely, this stronger electrostatic potential may explain the higher affinity of PN-1 for heparin (K_d = 0.8±0.6 nM) (39, 40) compared to that of other serpins, like AT-III for instance (K_d = 8.8±1.3 nM) (32).

```
P05121      VHHPPSYVAHLASDFGVRVFQQVAQASKDRNVVFSPYGVASVLAMLQLTTGGETQQQIQA 60
P07092      SQLNSLSLEELGSDTGIQVFNQIIKSQPHENVVISPHGIASILGMLQLGADGRTKKQLST 60
            :  .  : .*.** *::**:*: ::. ..***:**:*:**:*.**** :.*.*::*:.:

P05121      AMGFKIDDKGMAPALRHLYKELMGPWNKDEISTTDAIFVQRDLKLVQGFMPHFFRLFRST 120
P07092      VMRYNVN--GVGKVLKKINKAIVSKKNKDIVTVANAVFVRNGFKVEVPFAARNKEVFQCE 118
            .* ::::  *:. .*::: * ::.  *** ::.::*:**:..:*:   * .:  .:*:.

P05121      VKQVDFSEVERARFIINDWVKTHTKGMISNLLGKGAVD-QLTRLVLVNALYFNGQWKTPF 179
P07092      VQSVNFQDPASACDAINFWVKNETRGMIDNLLSPNLIDSALTKLVLVNAVYFKGLWKSRF 178
            *:.*:*.:   *   ** ***..*:***.***. . :*  **:******:**:* **: *

P05121      PDSSTHRRLFHKSDGSTVSVPMMAQTNKFNYTEFTTPDGHYYDILELPYHGDTLSMFIAA 239
P07092      QPENTKKRTFVAGDGKSYQVPMLAQLSVFRSGSTKTPNGLWYNFIELPYHGESISMLIAL 238
            ..*::* *  .**.: .***:** . *.  . .**:* :*:::******:::**:**

P05121      PYEKEVPLSALTNILSAQLISHWKGNMTRLPRLLVLPKFSLETEVDLRKPLENLGMTDMF 299
P07092      PTESSTPLSAIIPHISTKTINSWMNTMVPKRMQLVLPKFTALAQTDLKEPLKALGITEMF 298
            * *...****:   :*:: *. * ..*.     ******:  ::.**::**: **:*:**

P05121      RQFQADFTSLSDQEPLHVAQALQKVKIEVNESGTVASSSTAVIVSARMAPEEIIMDRPFL 359
P07092      EPSKANFAKITRSESLHVSHILQKAKIEVSEDGTKAAVVTTAILIARSSPPWFIVDRPFL 358
            .  :*:*:.:: .*.***:: ***.****.*.** *:  *:.*: ** :*  :*:*****

P05121      FVVRHNPTGTVLFMGQVMEP 379
P07092      FCIRHNPTGAILFLGQVNKP 378
            * :******::**:*** :*
```

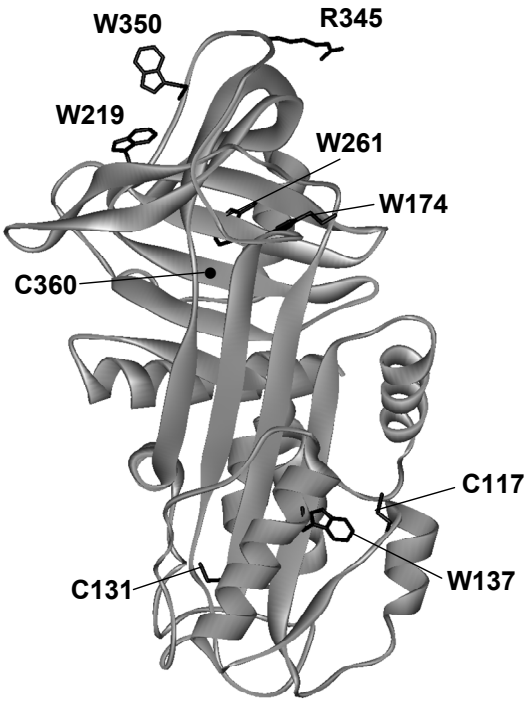

Figure 2. Structural model of rPN-1. (**A**) Clustal-W alignment of the rat PN-1 (SwissProt code: P07092) and human PAI-1 (SwissProt code: P05121). (**B**) Schematic representation (solid ribbon, light gray) of the three-dimensional structure of rPN-1, as obtained form molecular modelling studies. The model was generated on the crystallographic coordinates of PAI-1 in the native/active form (1dvm_A.pdb), as detailed in the Methods. The side-chains of the Trp- and Cys-residues are indicated.

PN-1 sequence contains three cysteines (i.e., Cys117, Cys131, and Cys360), that are not conserved in the template PAI-1 structure (33). In the model presented here, all cysteines are too far in the three-dimensional structure to form any disulfide bridge. Moreover, ASA calculations suggest that only one Cys is buried in the protein core (i.e., Cys360), whereas the remaining two are highly (i.e., Cys117) or moderately (i.e., Cys 131) solvent exposed. These conclusions are fully consistent with earlier chemical modification studies with 5,5'-dithiobis-nitrobenzoic acid (43), conducted on the human recombinant PN-1 (SwissProt entry code: P07093) and showing that under native conditions all Cys-residues are in the reduced, free thiol state and accessible to solvent. Human PN-1 shows 84% sequence homology with the rat protein (SwissProt entry code: P02092) (19) and both proteins contain three cysteines in their sequence. Of these, the solvent exposed Cys117 and Cys131 are conserved, whereas the buried Cys360 of rat PN-1 is replaced by Phe in the human protein. On the other hand, Cys209 of human PN-1 is substituted by Ser at the corresponding position, which is rather exposed on the rat PN-1 structure. The presence of at least one sulphydryl group freely accessible on the protein surface is consistent with the observation that disulfide-mediated dimerization may occur on standing (43).

Conformational characterization. The conformational properties of rPN-1 were investigated by CD in the far- and near-UV region and by steady state fluorescence spectroscopy. The far-UV CD spectrum of rPN-1 (Fig. 3A) is typical of a protein containing a mixed α/β secondary structure, with two shallow minima centered at 220 and 210 nm (45), and is similar in both shape and intensity to those of AT-III (46) and plasminogen activator inhibitor-1 (PAI-1) (47), both proteins displaying remarkable sequence similarity to PN-1 (19). The CD spectrum of rPN-1 in the near-UV region shows a broad positive band in the 255-300 nm range (Fig. 3B). The contribution of the 19 Phe-residues appears as a typical 6-nm spaced band system between 260 and 272 nm, while the positive band at 292 nm is diagnostic of Trp-residue(s) embedded in a rigid protein environment (48). Moreover, the near-UV CD spectrum of rPN-1 shows similar spectral features when compared with that of AT-III (46), reflecting again the sequence and structural similarities existing between these two proteins.

The fluorescence spectra of rPN-1 obtained after exciting the sample at 280 and 295 nm show a red-shifted λ_{max} value at ~345 nm (Fig. 3C), indicating that the majority of the five Trp-residues in the PN-1 structure are located in polar and, likely, solvent exposed environment (49). Moreover, the absence of the contribution of Tyr-residues in the 280-nm spectrum indicates that there is an efficient Tyr-Trp energy transfer, reflecting the compact structure of rPN-1 in the folded state. Under strong denaturing conditions (5 M Gdn-HCl), the value of λ_{max} is further shifted to 351 nm, typical of polypeptide chains in the fully unfolded state, while the contribution of Tyr appears as a weak, shallow band at ~303 nm. Comparison of The fluorescence spectra reveal that rPN-1 has a λ_{max} value red-shifted by ~10 nm,

compared to that of the homologous serpins AT-III (46) and PAI-1 (47), suggesting that the five Trp-residues in rPN-1 are located, on average, in a more polar environment.

This conclusion is supported by the model structure of rPN-1 and by accessible surface area calculations, showing that the majority of Trp-residues are solvent exposed (Fig. 2B). In particular, the side-chains of Trp137, Trp219 and Trp350 are much more accessible than those of Trp174 and Trp261, buried in the protein core. For comparison, mature PAI-1 contains four Trp-residues, at positions 86, 139, 175, and 262 (the numbering follows the rPN-1 sequence). Of these, three (namely, Trp139, Trp175, and Trp262) are conserved in rPN-1 sequence (namely, Trp137, Trp174, and Trp261). Analysis of the crystallographic structure of PAI-1 (45) indicates that Trp175 and Trp262 are shielded from the solvent, whereas Trp86 and Trp139 are only moderately accessible to water, in keeping with the lower λ_{max} value determined in the fluorescence spectrum of PAI-1 (39).

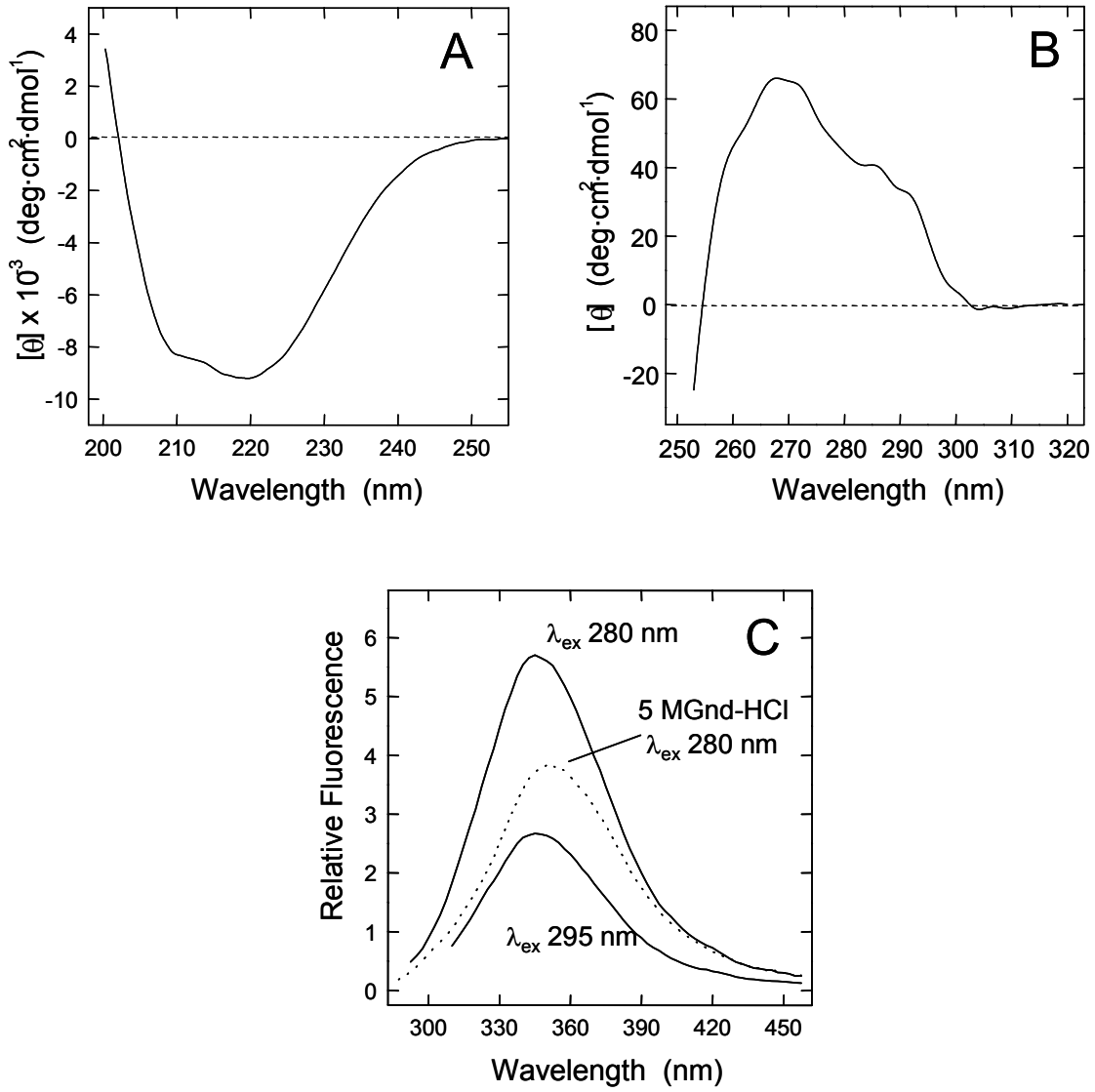

Figure 3. Conformational characterization of rPN-1. Far- **(A)** and near-UV**(B)** CD spectra were taken at a protein concentration of 78 μg/ml. (**C**) Fluorescence spectra were recorded after exciting the rPN-1 samples (7 μg/ml) at 280 and 295 nm, or in the presence of 5 M Gnd-HCl, as indicated. All spectra were recorded at 20±0.5 °C in 50 mM Tris-HCl buffer, pH 8.8, containing 0.6 M NaCl and 10% (v/v) glycerol.

Functional studies

Heparin binding. In the presence of 1.7 μM unfractionated porcine heparin, the fluorescence intensity of rPN-1 is increased by 25% (Fig. 4A), as already observed with AT-III (32), without changes in the λ_{max} value (i.e., the wavelength at which the intensity of fluorescence is highest). Fluorescence titration of rPN-1 with heparin (Fig. 4B) displays saturation behaviour both at 30 and 130 nM serpin. In these conditions, the K_d value for the heparin-rPN-1 complex could not be determined, likely because the concentration of rPN-1 used in these measurements largely exceeds the K_d of heparin-rPN-1 complex, previously determined (i.e., 0.8±0.6 nM) (40). On the other hand, rPN-1 concentrations in the K_d range would result into a fluorescence change too small to be accurately measured. From the data reported in Fig. 4B, however, a 1:1 stoichiometry for the binding of heparin to rPN-1 could be easily determined.

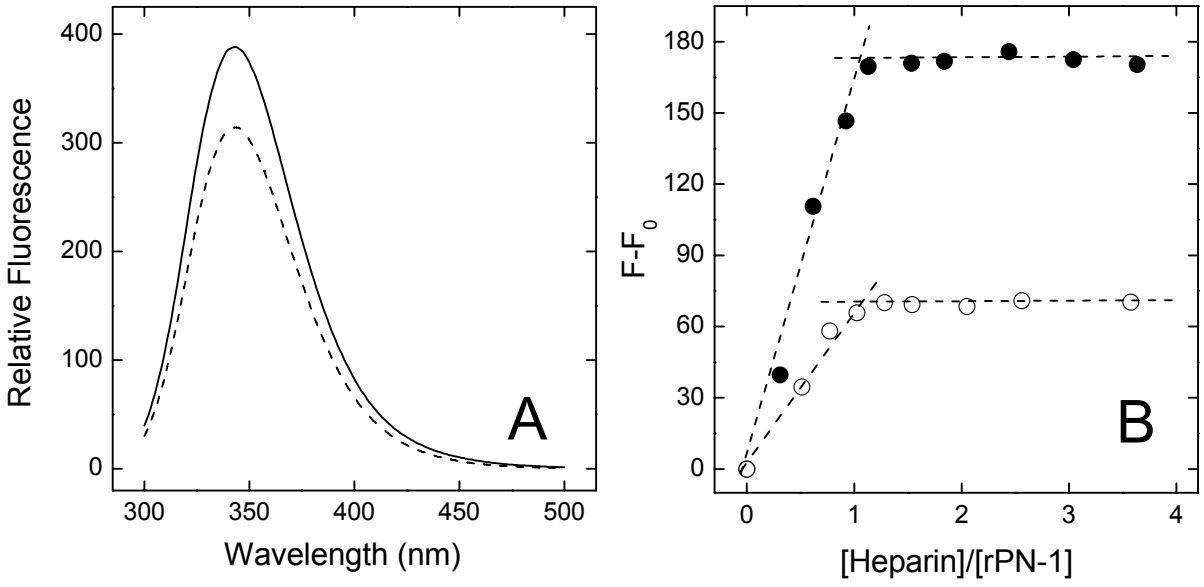

Figure 4. Binging of heparin to rPN-1 monitored by fluorescence change. (**A**) Fluorescence spectra of rPN-1 in the absence (---) and presence (—) of unfractionated porcine heparin (1.7 μM). Spectra were taken after exciting rPN-1 samples (80 nM) at 280 nm. (**B**) Titration of rPN-1 with heparin. The binding of heparin (0-7 □M) to rPN-1 at 30 nM (o) and 130 nM (●) was monitored after exciting the samples at 280 nm and recording the increase of fluorescence at λ_{max} (i.e., 341 nm) as a function of (heparin)/(rPN-1) ratio. Fluorescence change is expressed as (F_0-F), where F_0 and F are the fluorescence values of rPN-1 in the absence and presence of heparin, respectively. The stoichiometry of heparin binding to rPN-1 was obtained as the (heparin)/(rPN-1) ratio where the regression line (---) of the initial linear increase in fluorescence intersects the regression line (---) of maximum fluorescence change corresponding to saturation of the inhibitor (**Olson et al., 1993**). All measurements were carried out at 25±0.1 °C in 5 mM Tris-HCl buffer pH 7.5, 0.15 M NaCl, 0.1% PEG.

Formation of thrombin-rPN-1 complex monitored by SDS-PAGE. The time-course kinetics of rPN-1 binding to thrombin (molar ratio of 2:1) without heparin was monitored by SDS-gel electrophoresis in the time range 5 s - 1 h (Fig. 5). Even after 5-s reaction, thrombin is almost quantitatively sequestered to form a stable thrombin-rPN-1 complex (i.e., the acyl-enzyme intermediate) migrating in the gel with an apparent molecular weight of 65 kDa, roughly given by the sum of the molecular weight of rPN-1 (~42

kDa) and that of thrombin heavy chain (~32 kDa). As the reaction time increases, the intensity of the 65-kDa band (cpx) further increases and concomitantly that corresponding to the protease (thb) is barely detectable after 1-h reaction. Interestingly, the intensity of the rPN-1 band (native) remains constant over time and no cleaved serpin form even after 1-h reaction could be detected, with Coumassie Blue staining at least. The cleaved form is generated after formation of the acyl-enzyme intermediate and subsequent conformational change. When loop insertion in the β-sheet is not rapid enough to compete with deacylation, then the reaction proceeds directly to the cleaved product (10, 50). The absence of the cleaved form is usually taken as a good indication for 1:1 stoichiometry in complex formation (6). With respect to this, the stoichiometry of the reaction is defined as the number of moles of serpin needed to inhibit one mole of proteinase as a kinetically trapped complex. As shown in Fig. 5, a weak band appears at a molecular weight slightly lower than that of the thrombin-rPN-1 acyl-intermediate. This band likely corresponds to a thrombin cleaved form of the serpin-protease complex (cpx*). Serpins, indeed, have been demonstrated to remarkably increase the conformational flexibility of the protease bound to the serpin (51), with a resulting increased susceptibility of the inhibited protease towards proteolysis by the active protease molecules in equilibrium with the serpin-bound protease (50, 52).

Recombinant PN-1 expressed in E. coli failed to form a stable complex with the functionally inactive thrombin mutant (Ser195Ala) produced earlier (53), in which the catalytic Ser195 was replaced by Ala (unpublished Results). This finding is in keeping with the notion that Ser195 is involved in the inhibitory mechanism of serpins (6, 51, 54).

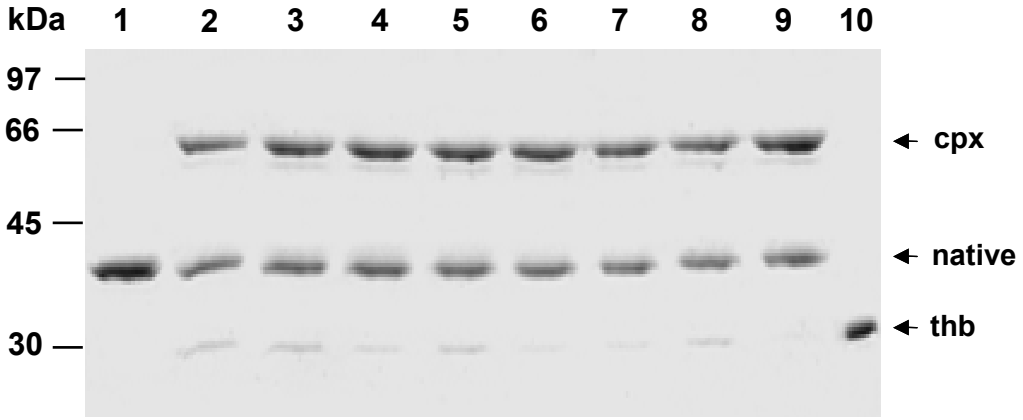

Figure 5. SDS-PAGE analysis of the reaction mixture of rPN-1 with thrombin. At each time-point, to 22 µll of the reaction mixture, containing 2.4 µg of rPN-1 and 0.9 µg of α-thrombin (2:1 molar ratio), incubated at room temperature (22±1°C) in 5 mM Tris-HCl buffer pH 7.5, 0.15 M NaCl, 0.1% PEG-8000, were added 6 µl of pre-heated reducing SDS-loading buffer. After rapid mixing, samples were heated for a further 3 min at 100°C. The gel was stained with Coumassie Blue. *Lane 1* is rPN-1 alone; *lanes 2-9* correspond to 5-, 15-, 30-, 60-, 120-, 600-, 1200-, and 3600-s time points of the reaction; *lane 10* is thrombin alone. Molecular-weight markers were loaded in the left-handed well. Reactants and products are labelled as follows: *native*, intact rPN-1; *thb*, thrombin (heavy chain); *cpx*, stable thrombin-rPN-1 complex; *cpx**, cleaved complex.

Thrombin inhibition by rPN-1 in the absence and presence of heparin. Thrombin inactivation by rPN-1 in the absence of heparin was determined by the discontinuous assay method, according to which the protease and the serpin were incubated at 25±0.5°C under pseudo-first order conditions (i.e., (rPN-1) >> (trombin)) in Tris-HCl buffer, pH 7.5. The residual protease activity was determined at time intervals by measuring the initial velocity of S-2238 substrate hydrolysis at 405 nm in the absence (v_0) and presence (v_i) of rPN-1. The per cent active thrombin was plotted as a function of time (Fig. 6A) and the data fitted to equation 1, from which a figure of the pseudo first-order association rate constant, k_a, could be estimated as 1.1±0.1 x 10^6 $M^{-1}\cdot s^{-1}$ (see Methods for details). This value is fully consistent with those reported for natural, k_a = 1.4 x 10^6 $M^{-1}\cdot s^{-1}$ (39), and recombinant PN-1 expressed in chinese hamster ovary cells, k_a = 0.8 x 10^6 $M^{-1}\cdot s^{-1}$ (43), or in yeast, k_a =1.4 x 10^6 $M^{-1}\cdot s^{-1}$ (40).

In the presence of heparin, the affinity of rPN-1 for thrombin increases by 10^3-fold (39, 40) and therefore the discontinuous method would not yield reliable k_a values. To overcome this limitation, inhibition assays were carried out at 25±0.5°C by continuously measuring over time inactivation of thrombin by rPN-1 in the presence of S-2238 and increasing concentrations of heparin (100 pM–100 μM) (32). The reaction was started by addition of thrombin (50 pM) and the progress curves of the release of p-nitroanilide as a function of time were fitted to equation 2 (Fig. 6B). From these data, the second-order association rate constant, k_1, could be estimated at each heparin concentration. Plotting k_1 values as a function of heparin concentration (Fig. 6C) yielded a typical bell-shaped curve, similar to previous data reported with natural (39) or recombinant (40) PN-1. The data were fitted to equation 4, yielding an optimal heparin concentration, $(H)_{opt}$, at which the k_1 value is maximal, $k_1° = 0.45\pm0.02$ x 10^9 $M^{-1}\cdot s^{-1}$. Notably, this value is very similar to that reported for natural PN-1, $k_1° = 0.46\pm0.04$ x 10^9 $M^{-1}\cdot s^{-1}$ (39). For further increase of heparin concentration, the cofactor seems to have an inhibitory effect on serpin-thrombin interaction, consistent with the template model of heparin-accelerated inhibition of thrombin by serpins (32. The affinity of heparin for PN-1 (K_d = 0.8±0.6 nM) (40) is much higher than that for thrombin (K_d = 0.69±0.06 μM) (55). This large difference in affinities implies that the assembly of the ternary serpin-heparin-protease complex, I·H·P, occurs predominantly as a bimolecular association between the serpin-heparin binary complex, I·H, and the free protease, P, according to the template model reported in Scheme 4:

$$I\cdot H + P \underset{}{\overset{K_{IHP}}{\leftrightarrow}} I\cdot H\cdot P \overset{k_{IH}}{\rightarrow} I\cdot P + H \qquad \text{(Scheme 4)}$$

where K_{IHP} is the equilibrium dissociation constant of the encounter I·H·P complex and k_{IH} is the first-order rate constant for the conversion of the I·H·P complex to the stable I·P complex and release of heparin (32). According to this model, at heparin concentrations higher than $(H)_{opt}$, the free heparin not bound to rPN-1 can compete with the inhibitor-heparin complex, I·H, for the binding to thrombin thereby reducing the reaction rate for the formation of thrombin-rPN-1 complex.

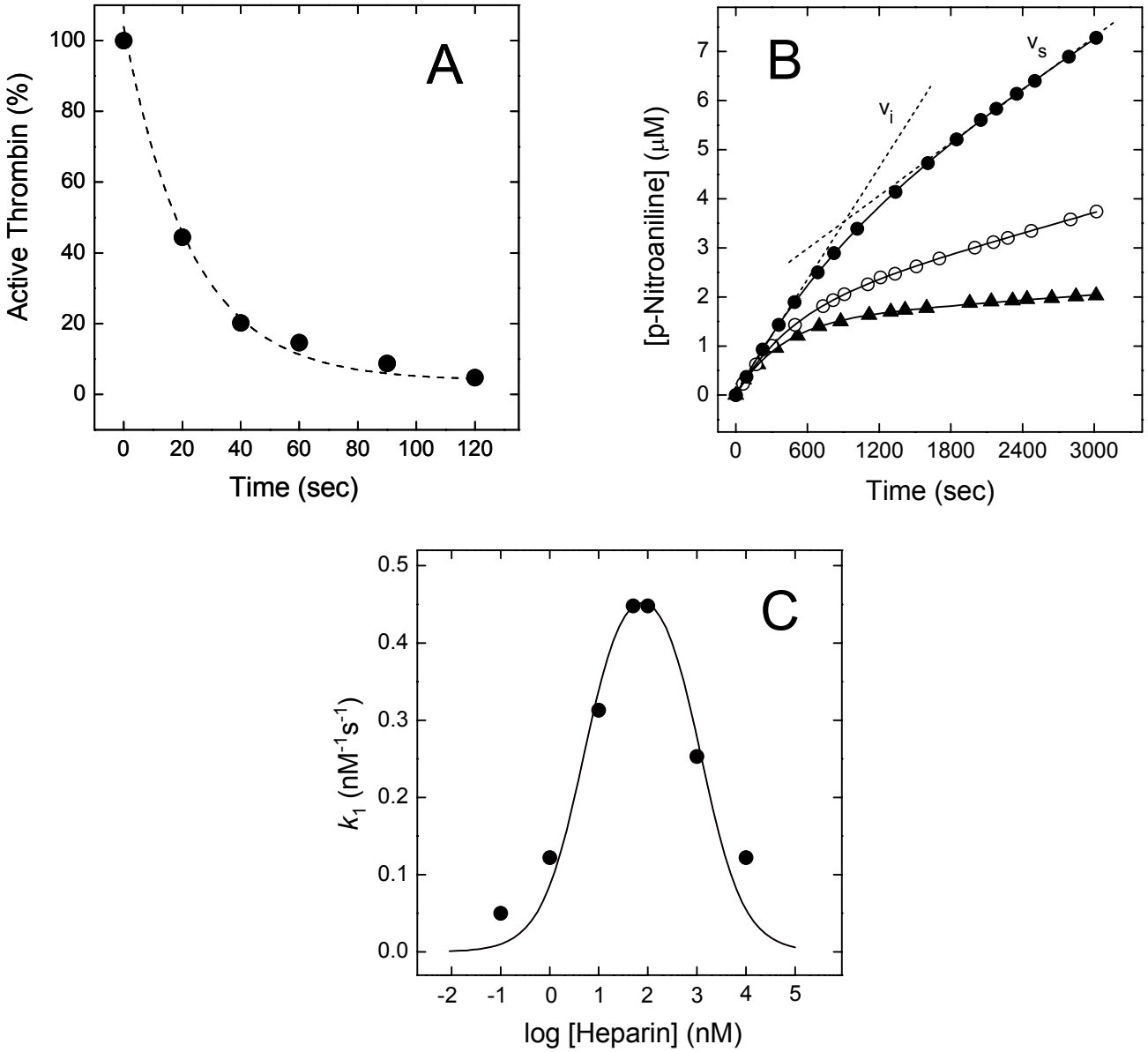

Figure 6. Thrombin inactivation by rPN-1 in the absence (A) and presence (B, C) of heparin. In the absence of heparin (**A**), the inhibition of α-thrombin by rPN-1 was determined by the discontinuous assay method, according to which the protease (1 nM) was incubated with rPN-1 (40 nM) in 5 mM Tris-HCl, 0.15 M NaCl, 0.1% PEG 8000, pH 7.5. The residual protease activity was determined at time intervals by measuring at 405 nm the inhibition of p-nitroanilide release from S-2238 (93 μM). The % active thrombin was plotted as a function of time and the data fitted to equation 1, from which a k_{obs} value of $4.3\pm0.4\cdot10^{-2}$ s^{-1} was obtained. If $k_{obs} = k_a\cdot(rPN\text{-}1)$, then the pseudo first-order association rate constant, k_a, could be estimated as $1.1\pm0.1 \times 10^6$ $M^{-1}\cdot s^{-1}$ (see Data Analysis for details). (**B**) In the presence of heparin, thrombin inhibition assays were carried out at 25 ± 0.5°C by continuously measuring over time inactivation of thrombin (50 pM) by rPN-1 (2.0 nM) in the presence of S-2238 (85.7 □M) and 1 (●), 10 (o), and 100 nM (▲) heparin. The release of p-nitroanilide as a function of time was fitted to equation 2, from which the values of k_{obs}, v_0 and v_s were obtained as fitting parameters. From these values, the second-order association rate constant, k_1, can be estimated at each heparin concentration, using equation 3. (**C**) Plot of k_1 as a function of heparin. The data were fitted to equation 4, yielding the optimal (heparin) at which k_1 value is maximal, $k_1°$.

Induction of neurite outgrowth by rPN-1 in neuroblastoma cells. Previous studies have shown the relevance of protease-inhibitor balance in brain plasticity (56), and, more specifically, the role of PN-1 and thrombin (14, 57). In particular, it has been demonstrated that thrombin regulates process outgrowth from neurons and astrocytes and that this effect is mediated via a thrombin receptor which is activated by proteolytic cleavage (56). PN-1 can block or reverse this cellular effect of thrombin by inhibiting its proteolytic activity and preventing receptor activation (14, 57).

Here, we explored the ability of rPN-1 to modulate neuronal differentiation and the effects of thrombin-PN1 interaction on neuronal morphology. To this aim, we chose the mouse NB2A neuroblastoma cell line, which has been extensively used as a model system for studying the effects of PN-1 and thrombin on neurite (44). NB2A cells show an undifferentiated phenotype when grown in presence of serum. However, accumulating evidences have demonstrated that mouse NB2A cells elaborate axonal neurites in response to various agents such as dibutyryl cyclic AMP, or culture conditions, e.g., serum deprivation (58). Hence, neurite outgrowth and cell rounding were monitored as indicators of morphological differentiation following exposure of NB2A cells to rPN-1. We also investigated whether rPN-1 effects could be reversed by thrombin. In these experiments we used a wild-type, fully active recombinant thrombin, produced as described earlier (53).

Fig. 7 shows the results of experiments in which cells were exposed to different treatments and visualized by using immunocitochemistry and photomicrography. When cultured in presence of low amount of serum (0.8% FBS), NB2A cells showed an undifferentiated phenotype (Fig. 7A); the addition of 50 nM rPN-1 induced after 3 h neuronal differentiation, with formation of neurite processes (Fig. 7C). The differentiated phenotype was also observed following concomitant treatment with 50 nM rPN-1 and 2 nM thrombin for 3 h (Fig. 7E), although the simultaneous addition of rPN-1 and thrombin to NB2A cells resulted in a decreased neurite length and a lower number of primary branches (Fig. 7E) when compared with cells treated with rPN-1 alone (Fig. 7C). Withdrawal of serum from culture media for 4 h caused neurite outgrowth (Fig. 7B) and this effect was reversed by treatment with 2 nM thrombin for 3 h (Fig. 7D); notably, serum-deprived cells exposed simultaneously to 2 nM thrombin and 50 nM rPN-1 showed a differentiated phenotype (Fig. 7F).

Taken together, these results demonstrate that recombinant PN-1 has neurite promoting activity in NB2A cells similar to that of endogenous PN-1 (4), and that likely this effect is mediated by inhibition of thrombin amidolytic activity caused by irreversible binding PN-1 to thrombin active site.

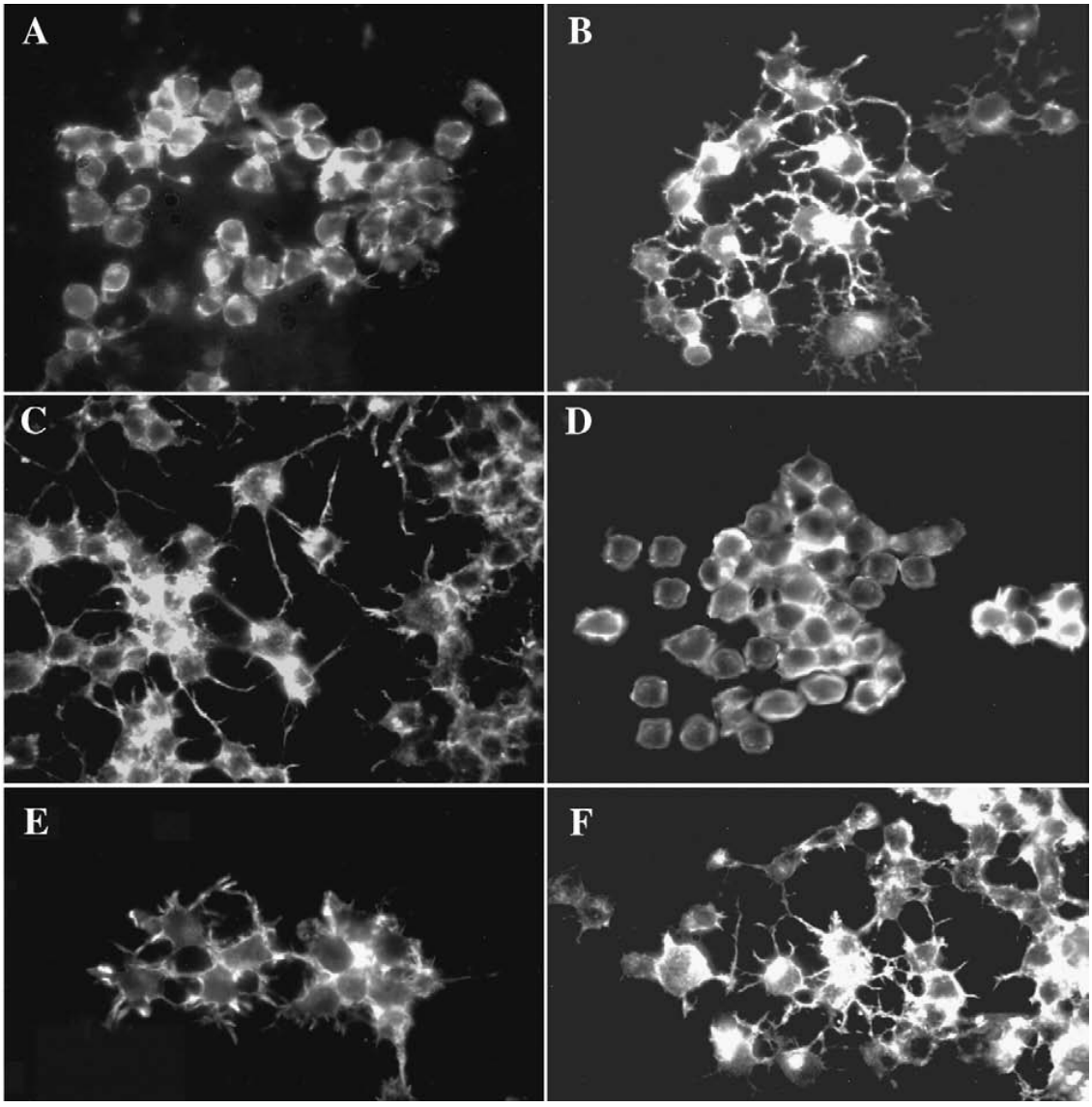

Figure 7. rPN-1 induces neurite outgrowth in NB2A cells by inhibition of thrombin. Cells were grown subconfluent on cover slips, kept in DMEM containing 10% serum for 24 hr, then differentiated to a neuronal morphology by serum deprivation, or kept undifferentiated in 0.8 % FBS for 4 hr. (**A**) Cells maintained in DMEM supplemented with 0.8% FCS; (**B**) cells in DMEM without FCS; (**C**) cells in DMEM supplemented with 0.8% FCS exposed to 50 nM rPN1 for 3 hr; (**D**) cells in DMEM without FCS exposed to 2 nM thrombin for 3 hr; (**E**) cells in DMEM supplemented with 0.8% FCS exposed to 50 nM rPN1 and 2 nM thrombin for 3 hr: (**F**) cells in DMEM without FCS exposed to 50 nM rPN1 and 2 nM thrombin for 3 hr. After the treatment, the cells were fixed, incubated with rhodamine phalloidin and processed for immunofluorescence microscopy.

Inducible expression of PN-1 in HeLa Tet-Off system. Recombinant PN-1 has been also expressed in the Tet-Off system (59) which allows repression of a single gene by tetracycline or doxycycline. After transfection of HeLa Tet-off cells with pTRE-Kozak-rbs-PN-1 plasmid, we analyzed PN-1 expression in the presence and absence of doxycycline at different time points.

Fig. 8 shows the results of the immunofluorescence analysis of PN-1 expression. After removal of doxycyline, PN-1 appeared in the cell cytoplasm of transfected HeLa cells (Fig. 8B; 24, 48 and 72 h),

and no signal was observed in the presence of the antibiotic (Fig. 6D; 24, 48 and 72 h). At 24 h, a strong perinuclear fluorescence was observed in the putatively Golgi region, as expected for a secreted protein. At 48 and 72 h, cell cytoplasm was strongly stained, thus indicating a high level of protein synthesis. As a control, the same fields were stained with DAPI (Fig. 8C, 24, 48 and 72 h).

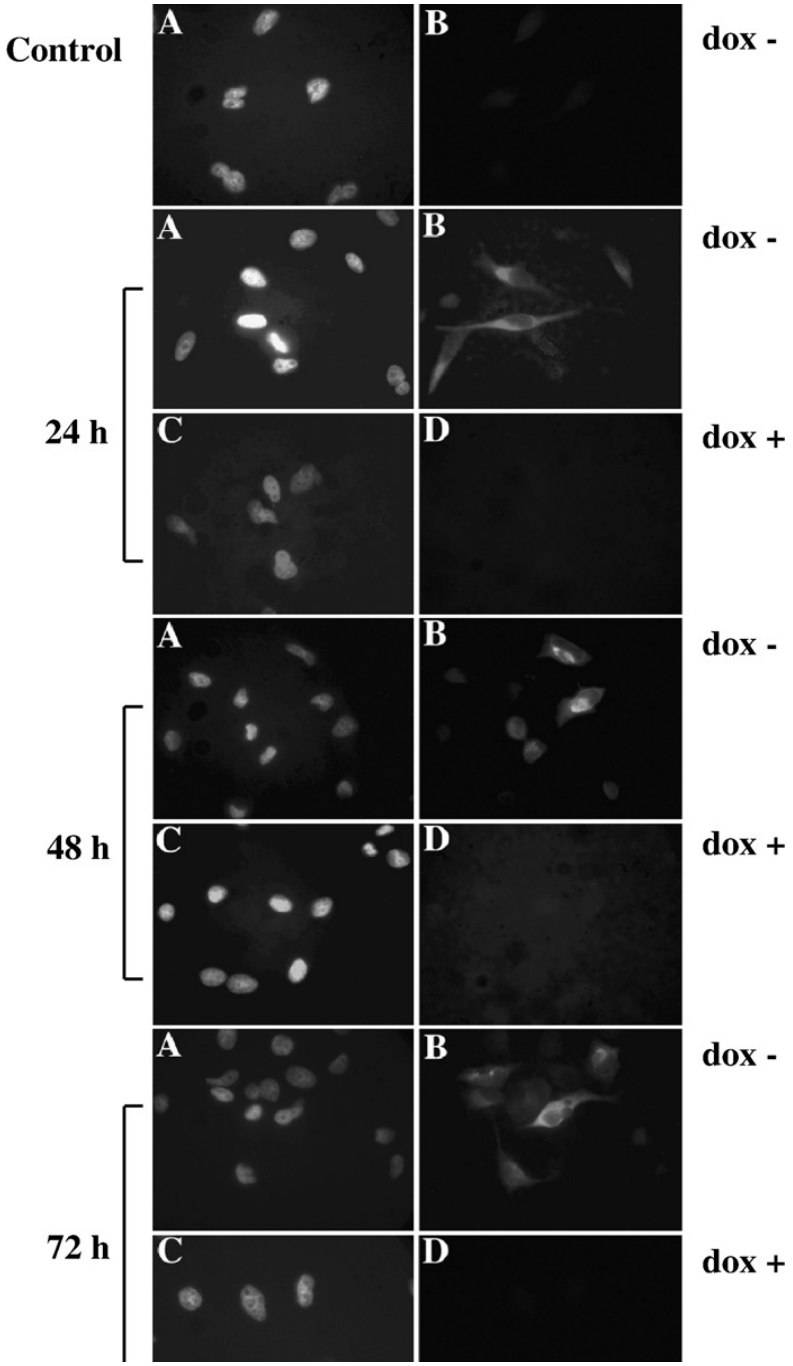

Figure 8. Inducible expression of rPN-1 in pTRE-PN-1 transfected HeLa Tet-off cells. Immunofluorescence microscopy in the presence of doxycycline or following doxycycline removal from the culture media, at the indicated time. Nuclei were stained with DAPI. Cells were grown to 80% confluence on glass cover slips, transiently transfected with the pTRE-Kozak-rbs-PN-1 plasmid. At the indicated times after removal of doxycycline, cells were fixed with formaldehyde and processed for immunofluorescence staining, using anti-PN-1 polyclonal serum, followed by fluorescein isothiocyanate antirabbit IgG, and DAPI stained.

These results were confirmed by Western blot analysis of secreted PN-1: briefly, after transfection, the culture media were collected and the secreted proteins concentrated by ultrafiltration (Amicon, cut-off 30 kDa) and subjected to Western blotting with an anti-PN-1 polyclonal antiserum. To obtain a semiquantitative estimation of rPN-1 secretion following doxycycline removal, we loaded on SDS-PAGE aliquots of culture media corresponding to 100 □g of total proteins extracted from the cells. As shown in Fig. 9A, the removal of the antibiotic led to a high-level secretion of PN-1 at about 43 kDa. From the time course analysis of the secretion yields, we estimated a maximal secretion at 48 h, which remained stable at 72 h. PN-1 signal appeared as a doublet, presumably because of some heterogeneity in the glycosylation of the protein (60). No signal was detected in non-transfected HeLa Tet-Off cells (NT) as well as in transfected cells cultured in the presence of doxycycline, thus indicating a tight control of the pTRE promoter.

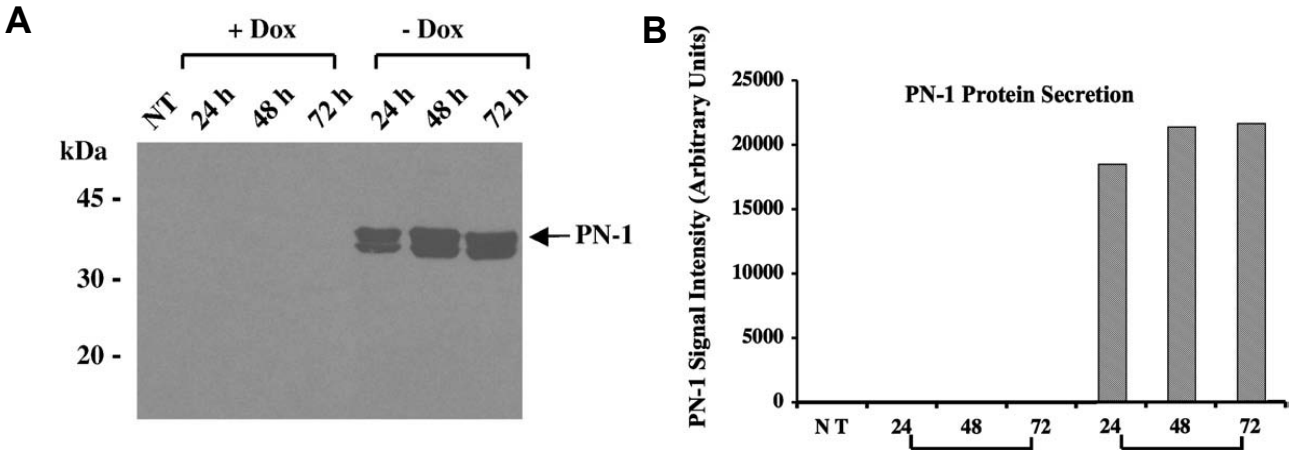

Figure 9. Inducible secretion of PN-1 in HeLa Tet-off cells. (**A**) Time course of rPN-1 secretion, following removal of doxycycline from the culture media of HeLa Tet-off cells transfected with pTRE-Kozak-PN-1 plasmid. Cells were grown to 80% confluence in 100-mm dishes in the presence of doxycycline (10 ng/ml). Plates were prepared in duplicate and 18 h after transfection; cells were washed with DMEM supplemented with 10% FBS and incubated in the presence or absence of the antibiotic. At the indicated times, culture media were collected and the cells were harvested, resuspended in a lysis buffer and the total protein content measured by Bradford assay. The culture media were concentrated by microfiltration and volumes corresponding to equal amounts of cellular proteins were loaded on 12% SDS-PAGE followed by Western blotting; signal was revealed by enhanced chemioluminescence (ECL). NT, culture media from non transfected HeLa Tet-off cells; the arrow indicates rPN1 (Mr 42 kDa). Numbers on the left represent $M_r \times 10^{-3}$ of molecular size standards. (**B**) Bar graphs represent the quantification of PN-1 secretion from Western-blotting analysis. The amount of rPN-1 is expressed in arbitrary units. (+) addition of doxycycline; (-) removal of doxycycline.

DISCUSSION

Rat glia-derived PN-1 has an apparent molecular weight of 43 kDa (60), about 2 kDa higher than that deduced form its cDNA sequence (i.e., 41.7 kDa) (19), assigned to glycosylation reactions. Scanning of rat PN-1 amino acid sequence for possible N-glycosylation sites identifies Asn364 as a

likely candidate, in the loop region connecting strand 358-364 and strand 369-376 in the B8 sheet. Notably, natural PN-1 was sensitive to periodic acid staining (60) and treatment of glioma cells with tunicamycin, a well known inhibitor of glycosylation in eukaryots, resulted in a decrease of about 3 kDa in the apparent molecular weight of PN-1 isolated from these cells (44). Being a glycoprotein, PN-1 has been expressed using several eukaryotic systems, including yeast (44), chinese hamster ovary cells (43), and baculovirus (44). In all cases, the recombinant PN-1 proteins were found to be functionally identical to the natural species (40). Nevertheless, the exceedingly low levels of expression and the poor yields of purification of rPN-1 from cell cultures were sufficient only for conducting functional studies whilst impairing structural investigation, for which larger amounts of protein are required. More recently, during studies aimed at identifying in rat seminal vesicles the protein responsible of the inhibition of prostasin, an invasion suppressor in prostate cancer cells, rat PN-1 was also expressed in *E. coli* (61).

The aim of our study was to develop an expression system suitable for producing large amounts of pure and biologically active rPN-1 to be used in crystallization studies aimed at elucidating the threedimesional structure of this physiologically important serpin at the atomic level. Hence, we explored the possibility of expressing the protein in an inducible manner either in an eukaryotic expression system, using the HeLa Tet-Off cells, and in a simple prokaryotic system like *E. coli*. Notably, in the former case we observed a tight doxycycline-regulated synthesis and secretion of PN-1, as demonstrated by immunocychemical and protein analysis of HeLa Tet-off cells transfected with pTRE-Kozak-PN-1 plasmid (Figg. 8 and 9). Notwithstanding, this system still suffered of poor expression yields. At variance, high-level expression of either His-Tagged fusion protein and mature form was obtained in *E. coli* under control of the T7 RNA polymerase promoter. The purified His-tagged PN-1 was used to obtain an anti-PN-1 antiserum that specifically recognized the endogenous protein expressed in rat oligodendrocytes, as previously shown (21).

Hence, we decided to express mature rPN-1 on a larger scale in *E. coli* cell cultures. After solubilization of inclusion bodies and *in vitro* refolding, the mature rPN-1 was purified to homogeneity by heparin-sepharose affinity chromatography, allowing us to recover about 3 mg of highly homogenous protein *per liter* of bacterial culture, as demonstrated by the appearance of a single, immunoreactive band in reducing SDS-electrophoresis (Fig. 1 A, B) and of a single, sharp peak eluting from a C4 RP-HPLC column (Fig. 1C). Notably, the molecular mass of rPN-1 agrees well with the theoretical value of the mature rat PN-1 (Inset to Fig. 1C). Finally, a pI value of 9.7 was determined for rPN-1 by 2D-gel electrophoresis (Fig. 1D), consistent with the theoretical value deduced form the amino acid composition of rat PN-1 (i.e., pI 9.72). The protein was stable when kept at -20° C as eluted from the heparin-sepharose column and no significant loss of activity was observed even for samples stored for six months.

The amount of purified rPN-1 obtained in this work was at least 10-50 fold higher than that attainable with eukaryotic systems (44) and this allowed us to carry out for the first time a detailed

conformational characterization of rPN-1 in solution by means of steady state fluorescence spectroscopy and circular dichroism in the far- and near-UV region (Fig. 3). These spectroscopic data compared favourably with those obtained with other serpins, such as AT-III (46) and PAI-1 (47), and validated the theoretical model of PN-1 structure reported in Fig. 2. Next, the native-like structure of rPN-1 and the resulting biochemical properties were probed with respect to the ability of the recombinant protein to (1) bind heparin, (2) form a SDS-stable complex with thrombin, and (3) inhibit thrombin amidolytic activity in the absence and presence of heparin.

The data shown in Fig. 4 demonstrate that rPN-1 binds heparin tightly and in a normal manner, with a 1:1 serpin-cofactor stoichiometric ratio. As already observed with AT-III (32, 46), heparin binding remarkably enhances the fluorescence intensity of rPN-1, without changing the λ_{max} value. These data are unprecedented and compatible with a rigidification of the chemical environment of some Trp-residues (e.g., Trp174) nearby the heparin-binding site (49). However, further studies are required to clarify whether this conformational change simply reflects a structural adaptation of PN-1 in response to cofactor binding or, alternatively, if it plays an effective role in promoting PN-1 binding to the target proteases, according to the allosteric activation mechanism previously highlighted for AT-III function (32).

Although PN-1 exhibits broad protease inhibitory specificity, α-thrombin has been recognized as its primary physiological target (7, 8). With respect to this, the formation of a SDS-stable complex with thrombin (see Fig. 5), occurring with a 1:1 stoichiometry, is a clear-cut proof of the native-like structure of our recombinant PN-1 (9). In fact, upon complex formation both the serpin and protease undergo massive conformational changes (51) involving the formation of a tetrahedral covalent intermediate between the Ser195 Oγ of the enzyme and the carbonyl carbon of the amino acid at P1 position of the scissible P1-P1' bond in the reactive centre loop (RCL) of the inhibitor. In a second step, the Ser195-acyl-intermediate is formed while the peptide bond between P1 ad P1' has been broken (6, 54). Once formed, the serpin-protease complex rapidly adopts its lowest energy conformation through the incorporation of the N-terminal portion of the RCL into □-sheet A and translocation of the tethered protease for the top to the bottom of the serpin, with a resulting distortion of the protease conformation (51). At this stage, deacylation of the acyl-enzyme trapped intermediate, to form the active protease and the cleaved serpin, is prevented largely by destruction of the oxyanion hole in the protease (51). For these complex and concerted reactions to occur, it is necessary that strict stereochemical and dynamical requirements are fulfilled in both serpin and protease structure. Therefore, the quantitative formation of a stable thrombin-rPN-1 complex (Fig. 5) can be taken as a signature of the native-like conformation of recombinant PN-1 expressed in *E. coli*.

Similar conclusions can be drawn from thrombin inhibition experiments yielding a value of 1.1±0.1 x 10^6 $M^{-1}\cdot s^{-1}$ for the association rate constant, k_a, of thrombin-rPN-1 interaction (Fig. 6A). Strikingly, this value agrees well with those reported earlier for natural (39), and recombinant PN-1 expressed in

different systems (40, 43). In the presence of unfractionated porcine heparin (Fig. 6B, C), the k_a value increases by about three orders of magnitude ($k_1° = 0.45±0.02 \times 10^9$ $M^{-1}·cm^{-1}$) at the optimal heparin concentration ($(H)_{opt} \sim 60$ nM). These values are fully consistent with those reported for natural PN-1 (39) and suggest that the rate of association of thrombin and PN-1 in the presence of heparin is essentially at the diffusion-controlled limit.

Finally, the cellular effects of rPN-1 were investigated by measuring the ability of the recombinant serpin to promote neurite outgrowth in neuroblastoma NB2A cells. The results shown in Fig. 7 provide evidence that recombinant PN-1 has neurite promoting activity in NB2A cells similar to that of natural PN-1 (4), and that this effect is mediated by inhibition of thrombin amidolytic activity, in agreement with previous studies showing that PN-1 can block or reverse the cellular effects of thrombin by inhibiting its proteolytic activity, thus preventing proteolytic activation of thrombin receptor(s) on neuronal cells (14, 57).

Altogether, our results demonstrate that E. coli is a suitable expression system for obtaining milligram quantities of pure and fully active recombinnat PN-1 to be used in future structural and functional studies.

REFERENCES

1. D.L. Eaton, J.B. Baker, Phorbol ester and mitogens stimulate human fibroblast secretions of plasmin-activatable plasminogen activator and protease nexin, and antiactivator/antiplasmin, *J. Cell Biol.* 97 (1983) 323–328.
2. D.C. Guttridge, A. Lau, L. Tran, D.D. Cunningham, Thrombin causes a marked delay in skeletal myogenesis that correlates with the delayed expression of myogenin and p21CIP1/WAF1, *J. Biol. Chem.* 272 (1997) 24117–24120.
3. M.C. Bouton, B. Richard, P. Rossignol, M. Philippe, M.C. Guillin, J.B. Michel, M. Jandrot-Perrus, The serpin protease-nexin 1 is present in rat aortic smooth muscle cells and is upregulated in L-NAME hypertensive rats, *Arterioscler. Thromb. Vasc. Biol.* 23 (2003) 142–147.
4. M.C. Hoffmann, C. Nitsch, A.L. Scotti, E. Reinhard, D.Monard, The prolonged presence of glia-derived nexin, an endogenous protease inhibitor, in the hippocampus after ischemia-induced delayed neuronal death, *Neuroscience* 49 (1992) 397–408.
5. E. Reinhard, H.S. Suidan, A. Pavlik, D. Monard, Glia-derived nexin/protease nexin-1 is expressed by a subset of neurons in the rat brain, *J. Neurosci. Res*. 37 (1994) 256–270.
6. G.A. Silverman, P.I. Bird, R.W. Carrell, F.C. Church, P.B. Coughlin, P.G. Gettins, J.A. Irving, D.A. Lomas, C.J. Luke, R.W. Moyer, P.A. Pemberton, E. Remold-O'Donnell, G.S. Salvesen, J. Travis, J.C. Whisstock, The serpins are an expanding superfamily of structurally similar but functionally

diverse proteins. Evolution, mechanism of inhibition, novel functions, and a revised nomenclature, *J. Biol. Chem.* 276 (2001) 33293–33296.

7. J.B. Baker, D.A. Low, R.L. Simmer, D.D. Cunningham, Protease-nexin: a cellular component that links thrombin and plasminogen activator and mediates their binding to cells, *Cell* 21 (1980) 37–45.
8. R.J. Crisp, D.J. Knauer, M.F. Knauer, Roles of the heparin and low density lipid receptor-related protein-binding sites of protease nexin 1 (PN1) in urokinase-PN1 complex catabolism. The PN1 heparin-binding site mediates complex retention and degradation but not cell surface binding or internalization, *J. Biol. Chem.* 275 (2000) 19628–19637.
9. B.F. Le Bonniec, E.R. Guinto, S.R. Stone, Identification of thrombin residues that modulate its interactions with antithrombin III and alpha 1-antitrypsin, *Biochemistry* 34 (1995) 12241–12248.
10. D.A. Lawrence, S.T. Olson, S. Muhammad, D.E. Day, J.O. Kvassman, D. Ginsburg, J.D. Shore, Partitioning of serpin–proteinase reactions between stable inhibition and substrate cleavage is regulated by the rate of serpin reactive center loop insertion into beta-sheet A, *J. Biol. Chem.* 275 (2000) 5839–5844.
11. I.M. Mansuy, H. van der Putten, P. Schmid, M. Meins, F.M. Botteri, D. Monard, Variable and multiple expression of Protease Nexin-1 during mouse organogenesis and nervous system development, Development 119 (1993) 1119–1134.
12. R. Giau, J. Carrette, J. Bockaert, V. Homburger, Constitutive secretion of protease nexin-1 by glial cells and its regulation by G-protein-coupled receptors*, J. Neurosci.* 25 (2005) 8995–9004.
13. O. Beilin, D.M. Karussis, A.D. Korczyn, D. Gurwitz, R. Aronovich, D. Hantai, N. Grigoriadis, R. Mizrachi-Kol, J. Chapman, Increased thrombin inhibition in experimental autoimmune encephalomyelitis*, J. Neurosci. Res.* 79 (2005) 351–359.
14. K.P. Cavanaugh, D. Gurwitz, D.D. Cunningham, R.A. Bradshaw, Reciprocal modulation of astrocyte stellation by thrombin and protease nexin-1, *J. Neurochem*. 54 (1990) 1735–1743.
15. C. Nitsch, A.L. Scotti, D. Monard, C. Heim, K.H. Sontag, The glia-derived protease nexin 1 persists for over 1 year in rat brain areas selectively lesioned by transient global ischaemia, *Eur. J. Neurosci*. 5 (1993) 292–297.
16. D.D. Cunningham, L. Pulliam, P.J. Vaughan, Protease nexin-1 and thrombin: injuryrelated processes in the brain, *Thromb. Haemost*. 70 (1993) 168–171.
17. Y. Onuma, M. Asashima, M. Whitman, A Serpin family gene, protease nexin-1 has an activity distinct from protease inhibition in early Xenopus embryos, *Mech. Dev.* 123 (2006) 463–471.
18. M. Grimaldi, R. Arcone, G. Ciliberto, G. Schettini, Synergistic stimulation of interleukin 6 release and gene expression by phorbol esters and interleukin 1 beta in rat cortical astrocytes: role of protein kinase C activation and blockade, *J. Neurochem.* 64 (1995) 1945–1953.

19. J. Sommer, S.M. Gloor, G.F. Rovelli, J. Hofsteenge, H. Nick, R. Meier, D. Monard, cDNA sequence coding for a rat glia-derived nexin and its homology to members of the serpin superfamily, *Biochemistry* 26 (1987) 6407–6410.
20. F. Sanger, S. Nicklen, A.R. Coulson, DNA sequencing with chain-terminating inhibitors, *Proc. Natl. Acad. Sci. U. S. A.* 74 (1977) 5463–5467.
21. F. Blasi, A. Ciarrocchi, A. Luddi, M. Strazza, M. Riccio, S. Santi, R. Arcone, C. Pietropaolo, R. D'Angelo, E. Costantino-Ceccarini, M. Melli, Stage-specific gene expression in early differentiating oligodendrocytes, *Glia* 39 (2002) 114–123.
22. F.W. Studier, A.H. Rosenberg, J.J. Dunn, J.W. Dubendorff, Use of T7 RNA polymerase to direct expression of cloned genes, *Methods Enzymol*. 185 (1990) 60–89.
23. M. Kozak, At least six nucleotides preceding the AUG initiator codon enhance translation in mammalian cells, *J. Mol. Biol.* 196 (1987) 947–950.
24. R. Arcone, P. Pucci, F. Zappacosta, V. Fontaine, A. Malorni, G. Marino, G. Ciliberto, Single-step purification and structural characterization of human interleukin-6 produced in Escherichia coli from a T7 RNA polymerase expression vector*, Eur. J. Biochem*. 198 (1991) 541–547.
25. M.M. Bradford, A rapid and sensitive method for the quantitation of microgram quantities of protein utilizing the principle of protein-dye binding, *Anal. Biochem*. 72 (1976) 248–254.
26. U.K. Laemmli, Cleavage of structural proteins during the assembly of the head of bacteriophage T4, *Nature* 227 (1970) 680–685.
27. P.R. Jungblut, R. Seifert, Analysis by high-resolution two-dimensional electrophoresis of differentiation-dependent alterations in cytosolic protein pattern of HL-60 leukemic cells*, J. Biochem. Biophys. Methods* 21 (1990) 47–58.
28. J. Heukeshoven, R. Dernick, Simplified method for silver staining of proteins in polyacrylamide gels and the mechanism of silver staining, *Electrophoresis* 6 (1985) 103–112.
29. S.C. Gill, P.H. von Hippel, Calculation of protein extinction coefficients from amino acid sequence data, *Anal. Biochem*. 182 (1989) 319–326.
30. J.W. Fenton II, M. Fasco, A.B. Stackrow, Human thrombins: production, evaluation, and properties of α-thrombin, *J. Biol. Chem*. 252 (1977) 3587–3598.
31. Q.D. Dang, E. Di Cera, A simple activity assay for thrombin and hirudin, *J. Protein. Chem*. 13 (1994) 367–373.
32. S.T. Olson, I. Björk, J.D. Shore, Kinetic characterization of heparin-catalyzed and uncatalyzed inhibition of blood coagulation proteinases by antithrombin, *Methods Enzymol*. 222 (1993) 525–559.
33. T.J. Stout, H. Graham, D.I. Buckley, D.J.Matthews, Structures of active and latent PAI-1: a possible stabilizing role for chloride ions, *Biochemistry* 39 (2000) 8460–8469.

34. J. Kopp, T. Schwede, The SWISS-MODEL repository of annotated threedimensional protein structure homology models, *Nucleic Acids Res*. 32 (2004) D230–234.
35. M. Gerstein, A resolution-sensitive procedure for comparing protein surface and its application to the comparison of antigen-combining sites, *Acta Cryst*. A48 (1992) 271–276.
36. J.D. Thompson, D.G. Higgins, T.J. Gibson, CLUSTALW: improving the sensitivity of progressive multiple sequence alignment through sequence weighting, positionspecific gap penalties and weight matrix choice, *Nucleic Acids Res*. 22 (1994) 4673–4680.
37. R. Lottenberg, C.M. Jackson, Solution composition dependent variation in extinction coefficients for p-nitroaniline, *Biochim. Biophys. Acta* 742 (1983) 558–564.
38. S.R. Stone, H. Nick, J. Hofsteenge, D. Monard, Glial-derived neurite-promoting factor is a slow-binding inhibitor of trypsin, thrombin, and urokinase, Arch. Biochem. Biophys. 252 (1987) 237–244.
39. A. Wallace, G. Rovelli, J. Hofsteenge, S.R. Stone, Effect of heparin on the gliaderived- nexin–thrombin interaction, *Biochem. J.* 257 (1989) 191–196.
40. G. Rovelli, S.R. Stone, A. Guidolin, J. Sommer, D. Monard, Characterization of the heparin-binding site of glia-derived nexin/protease nexin-1, *Biochemistry* 31 (1992) 3542–3549.
41. C.M. Wells, E. Di Cera, Thrombin is a Na(+)-activated enzyme, *Biochemistry* 31 (1992) 11721–11730.
42. B.I. Tarnowski, F.G. Spinale, J.H. Nicholson, DAPI as a useful stain for nuclear quantitation, *Biotech. Histochem*. 66 (1991) 297–302.
43. D.L. Evans, M. McGrogan, R.W. Scott, R.W. Carrell, Protease specificity and heparin binding and activation of recombinant protease nexin I, *J. Biol. Chem*. 266 (1991) 22307–22312.
44. S.R. Stone, M.L. Brown-Luedi, G. Rovelli, A. Guidolin, E. McGlynn, D. Monard, Localization of the heparin-binding site of glia-derived nexin/protease nexin-1 by site-directed mutagenesis, *Biochemistry* 33 (1994) 7731–7735.
45. S. Brahms, J. Brahms, Determination of protein secondary structure in solution by vacuum ultraviolet circular dichroism, *J. Mol. Biol*. 138 (1980) 149–178.
46. M. Bruch, V. Weiss, J. Engel, Plasma serine proteinase inhibitors (serpins) exhibit major conformational changes and a large increase in conformational stability upon cleavage at their reactive sites, *J. Biol. Chem*. 263 (1988) 16626–16630.
47. A.M. Dwivedi, R.W.Woodeshick, H.L. Walton, T.M. Reilly, A spectroscopic study of the conformations of active and latent forms of recombinant plasminogen activator inhibitor-1, *Biochem. Biophys. Res. Commun*. 175 (1991) 437–443.
48. E.H. Strickland, Aromatic contributions to circular dichroism spectra of proteins, CRC *Crit. Rev. Biochem*. 2 (1974) 113–175.

49. J.R. Lakowicz, Fluorescence studies of structural fluctuations in macromolecules as observed by fluorescence spectroscopy in the time, lifetime, and frequency domains, *Methods Enzymol*. 131 (1986) 518–567.
50. A. Zhou, R.W. Carrell, J.A. Huntington, The serpin inhibitory mechanism is critically dependent on the length of the reactive center loop, *J. Biol. Chem*. 276 (2001) 27541–27547.
51. J.A. Huntington, R.J. Read, R.W. Carrell, Structure of a serpin–protease complex shows inhibition by deformation, *Nature* 407 (2000) 923–926.
52. E.S. Stavridi, K. O'Malley, C.M. Lukacs,W.T. Moore, J.D. Lambris, D.W. Christianson, H. Rubin, B.S. Cooperman, Structural change in alpha-chymotrypsin induced by complexation with alpha 1-antichymotrypsin as seen by enhanced sensitivity to proteolysis, *Biochemistry* 35 (1996) 10608–10615.
53. R. Arcone, M.G. Pagliuca, A. Chinali, M. Grimaldi, G. Schettini, A. Gast, C. Pietropaolo, Thrombin mutants with altered enzymatic activity have an impaired mitogenic effect on mouse fibroblasts and are inefficient modulators of stellation of rat cortical astrocytes, *Biochim. Biophys. Acta* 1451 (1999) 173–186.
54. D.A. Lawrence, D. Ginsburg, D.E. Day, M.B. Berkenpas, I.M. Verhamme, J.O. Kvassman, J.D. Shore, Serpin–protease complexes are trapped as stable acylenzyme intermediates, *J. Biol. Chem*. 270 (1995) 25309–25312.
55. S.T. Olson, Transient kinetics of heparin-catalyzed protease inactivation by antithrombin III. Linkage of protease-inhibitor–heparin interactions in the reaction with thrombin, *J. Biol. Chem*. 263 (1988) 1698–1708.
56. V.L. Turgeon, L.J. Houenou, The role of thrombin-like (serine) proteases in the development, plasticity and pathology of the nervous system, *Brain Res. Brain Res. Rev*. 25 (1997) 85–95.
57. D.D. Cunningham, Regulation of neuronal cells and astrocytes by protease nexin-1 and thrombin, *Ann. N.Y. Acad. Sci.* 674 (1992) 228–236.
58. E. Klann, K.R. Shelton, A lead-associated nuclear protein which increases in maturing brain and in differentiating neuroblastoma 2A cells exposed to cyclic AMP-elevating agents, *Brain Res. Dev. Brain Res*. 57 (1990) 71–75.
59. M. Gossen, H. Bujard, Tight control of gene expression in mammalian cells by tetracycline-responsive promoters, *Proc.Natl.Acad. Sci.U. S. A*. 89 (1992) 5547–5551.
60. J. Guenther, H. Nick, D. Monard, A glia-derived neurite-promoting factor with protease inhibitory activity, *EMBO J.* 4 (1985) 1963–1966.
61. L.M. Chen, X. Zhang, K.X. Chai, Regulation of prostasin expression and function in the prostate, *Prostate* 59 (2004) 1–12.

3. BETA2-GLYCOPROTEIN I

CHAPTER 3.1

The Antiphospholipid Syndrome (APS)

The antiphospholipid syndrome (APS) is an autoimmune disease that is characterized clinically by vascular thrombosis and pregnancy morbidity, and serologically by the presence of antiphospholipid antibodies in the plasma of patients.(1) APS is highly related to other autoimmune diseases, especially systemic lupus erythematosus (SLE). Approximately 20–35% of patients with SLE fulfill the criteria for APS. Although the clinical criteria that characterize the disease occur frequently, the incidence of APS is low. The importance of the presence of antiphospholipid antibodies for the confirmation of the syndrome highlights the need for highly specific diagnostic assays to detect these antibodies. At present, several assays, such as phospholipid-dependent coagulation assays, anti-β2-glycoprotein I (β2GPI)-enzyme-linked immunosorbent assay (ELISA)-based assays and anticardiolipin ELISA-based assays, show a variable, but mediocre, correlation with thrombosis when studied in prospective cohort studies. The consequence of the low specificity of the assays is the suboptimal treatment of patients (2,3)

History of APS

Over the years, APS has developed from an incomprehensible correlation between a prothrombotic phenotype and an in vitro assay for the detection of a bleeding tendency (lupus anticoagulant [LA]) to a well-recognized syndrome (Fig. 1). A commonly used assay to detect the presence of antiphospholipid antibodies has its origin in 1906, when Wasserman described a method to detect syphilis (4). Pangborn found that the antigen that was recognized by reagin (antibodies produced by syphilis patients) was a phospholipid that could be extracted from beef heart, which is now known to be cardiolipin (5). During that time it became evident that some patients who tested positive for reagin did not suffer from syphilis but occasionally displayed a prothrombotic phenotype (6,7). This observation was the basis for the development of the anticardiolipin antibody ELISA that is still used to detect patients with APS. Almost 50 years after the introduction of the reagin assay, the existence of what was subsequently called LA was observed by Conley and Hartman (8) They described two patients with SLE whose plasma contained a unique coagulation inhibitor; this inhibitor prolonged whole-blood clotting time and prothrombin time, even when the plasma was diluted with normal pool plasma. As this inhibitor was predominantly found in patients with SLE, the in vitro anticoagulant phenomenon was called lupus anticoagulant. Despite the fact that APS is mainly known for its correlation between antiphospholipid antibodies and thrombosis, pregnancy morbidity was the first clinical manifestation that was reported to be associated with LA (9). The correlation between vascular thrombosis and LA was first described

in 1963 by Bowie et al. and was followed by many others (10). However, it took until the early 1990s to discover that antiphospholipid antibodies did not recognize phospholipids directly but indirectly via phospholipid-binding plasma proteins (11–14) Although many plasma proteins have been found to be involved in APS, antibodies against β2GPI are thought to be the antibodies with most clinical significance (15).

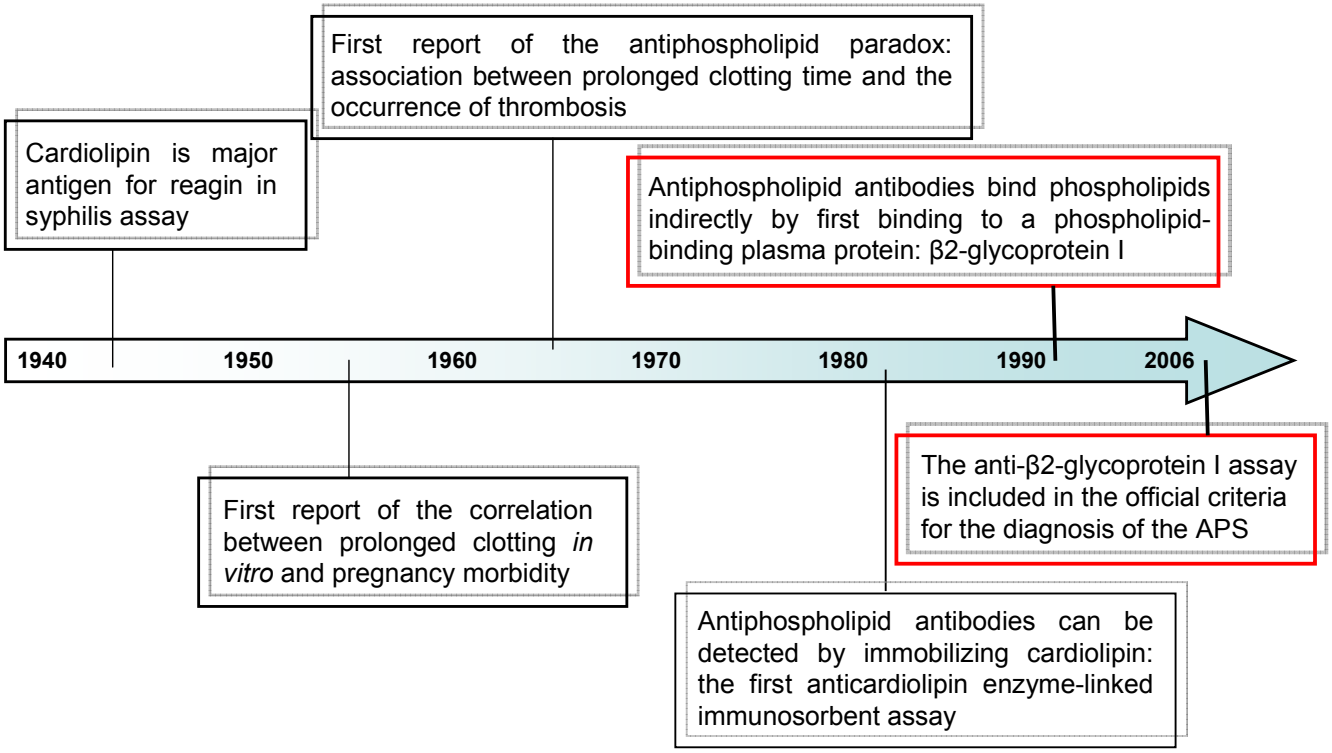

Figure 1. Line time of crucial discoveries in antiphospholipid syndrome (APS)

Diagnosing Patients with APS

The clinical criteria for diagnosing a patient with APS are clear and can be established objectively. By contrast, the laboratory criteria initially seem to be clear, but in practice the assays that are defined to measure the presence of antiphospholipid antibodies in plasma are controversial, and their outcome depends on the laboratory in which the assay is performed. Despite the many attempts to increase the specificity of the laboratory criteria and the establishment of consensus criteria for the serology, a high number of patients are still inaccurately diagnosed when the revised Sapporo classification criteria for APS are followed (16,17). According to these criteria for APS, fulfillment of at least one clinical and one laboratory criterion are required. The anticardiolipin ELISA is generally considered to have high sensitivity but low specificity. The aspecificity of this assay can be explained by the fact that infections and drugs sometimes coincide with the presence of anticardiolipin antibodies (18–20). These infection-related anticardiolipin antibodies bind to cardiolipin directly, independently of plasma proteins, and

their presence is not correlated with a prothrombotic phenotype. The high sensitivity of the anticardiolipin antibody ELISA for infection-related antibodies generates significant numbers of false-positive results, which makes the assay unsuitable for the detection of patients at risk of thrombosis. This unsuitability was recently confirmed by a meta-analysis by Galli et al., (3) who showed that antiphospholipid antibodies detected with an anticardiolipin ELISA did not correlate significantly with thrombosis in general. These authors also reported that the LA assay correlates best with thrombosis. Surprisingly, the latest addition to the diagnostic criteria, the anti-β2GPI ELISA, failed to show a significant correlation with thrombosis (2). This finding was unexpected, because β2GPI is thought to be the most clinically important antigen in APS. The major reason for the poor correlation of anti-β2GPI antibodies with clinical symptoms is probably the lack of standardization of the anti-β2GPI antibody ELISA. Despite numerous attempts to standardize the anticardiolipin antibody ELISA and the anti-β2GPI antibody ELISA, large differences are still found when assays from different manufacturers are used. Different types of plate, different sources of β2GPI and the lack of an international calibrator are thought to be the main causes of the discrepancies. However, the lack of correlation with thrombosis could also be explained by the observation that not all antibodies against β2GPI are pathologic; only antibodies that target a specific domain of the protein correlate with thrombosis (21). The anti-β2GPI antibody ELISA detects all antibodies that are reactive against β2GPI, which makes it less specific, and probably not very suitable as a general diagnostic test. Although anti-β2GPI antibodies seem to be important in the correlation with thrombosis, this is not the case for antiphospholipid-related pregnancy morbidity. A meta-analysis by Opatrny et al. reports that LA best correlated with recurrent fetal loss, as it does with thrombosis, but that there was no correlation between pregnancy morbidity and anti-β2GPI antibodies (22). Anticardiolipin antibodies did show a significant correlation with recurrent fetal loss, but not with thrombosis. This finding might indicate a different pathogenetic mechanism for thrombosis and pregnancy morbidity.

Mechanisms Predisposing to Thrombosis

In the last few years the role of several biochemical mechanisms have been investigated to explain the pathogenesis of the antiphospholipid syndrome, but unclear and sometimes contrast results have been proposed. Very recently many researchers have been focus their attention on the immunocomplex composed by the anti-β2GpI Ab/β2GpI. In particular it has been demonstrated that this complex interacts with several proteins belonging to the complement system or to the coagulation cascade altering their function and consequently leading to thrombosis. Herein it is reported a brief review of the immunocomplex effects on some relevant biological systems. For a in-depth review on the pathogenesis of the APS see Giannakopoulos et al., 2007.

Complement System. The possible role of complement activation in APS pathogenesis is suggested by the demonstration of increased complement activation products in the plasma of patients with APS who have had cerebral ischemic event, compared with patients suffering from non-PAS-related cerebral ischemia (23). In patients with APS, aPL Abs tend to be the IgG isotype, though the IgM and IgA isotypes can be present concurrently. The IgG2 subclass is more prevalent in APS but has a reletively weak ability to fix complement via the classical pathway in humans. This argues for the necessity to consider additional mechanisms to the classical complement pathway.

Platelets. A possible role of dysregulated platelet activation contributing to the thrombotic manifestation of APS has been suggested by the demonstration of elevated levels of platelet-derived thomboxane metabolic breakdown products in the urine of patients diagnosed with APS compared to the controls (24). In vitro, submaximal prestimulation of platelets by agonists such as thrombin or collagen appears to be a prerequisite for β2GpI-reactive Abs in the presence of β2GpI to able to potentiate activation. (25). Prestimulation with an agonist leads to the exposure of PS on the cell outer membrane. It is hypothesized that the anti-β2GpI Ab/β2GpI complex has to initially form on the exposed PS before interacting with specific platelet receptors. In particular ApoER2' receptor (26) and the GpIbα subunit (27) of the GpIb/IX/V receptors has been shown to bind more efficiently with dimerized β2GpI. Both these interactions leads to platelet activation and aggregation through the thromboxane A2 and the phosphoinositde-3 kinase/Akt pathways (28,29,30)

Endothelial Cell Receptors. Zhang et al. (31)demonstrated that β2GpI binding to annexin A2 enabled anti-β2GpI Abs to activate endothelium inducing the expression of a procoagulant phenotype. Meroni et al. (32)have noted that anti-β2GpI Abs, in the presence of β2GpI, are able to activate the nuclear factor-kB (NF-kB) pathway in endothelial cells, leading to the expression of a procoagulant and proinfiammatory phenotype. TLRs may mediate a role, through direct binding between β2GpI and TLRs but it has not been demonstrated yet.

Activated Protein C (aPC). A number of murine monoclonal anti-β2GpI Abs in the presence of β2GpI have been shown to be ale to inhibit aPC anticoagulant activity in vitro. It is hypothesized that the anti-β2GpI Ab/β2GpI complex may either compete with components of the aPC complex for limited phospholipid binding sites or disrupt an interaction with the aPC complex (33)

Annexin A5. The proposition made by this theory is that annexin A5, a protein that binds anionic phospholipids with high affinity, may form a protective anticoagulant shield on vascular cells and that anti-β2GpI Abs in complex with β2GpI may disrupt its function by competition (34).

Factor XI and Plasminogen. β2GpI is able to directly bind FXI and inhibits its activation by thrombin and FXIIa. β2GpI clipped by plasmin at Lys317-Thr318 is able to bind FXI but looses the ability to inhibit FXI activation. Yasuda et al (35) have been demonstrated that clipped β2GpI binds plasminogen and inhibits its conversion into plasmin by tPA, suggesting that β2GpI may potentially provide a regulatory link between the fibrinolysis and the FXI/thrombin activation.

Thrombin. It has been demonstrated that β2GpI is able to interact with thrombin using both exosites (36). Notwithstanding the physiological meaning and the mechanism of this interaction, if any, has to be totally clarify.

REFERENCES

1. Levine JS et al. (2002) The antiphospholipid syndrome. *N Engl J Med* 346: 752–763
2. Galli M et al. (2003) Anti-β2-glycoprotein I and antiprothrombin antibodies and the risk of thrombosis in the antiphospholipid syndrome. *Blood* 102: 2717–2723
3. Galli M et al. (2003) Lupus anticoagulants are stronger risk factors for thrombosis than anticardiolipin antibodies in the antiphospholipid syndrome: a systematic review of the literature. *Blood* 101: 1827–1832
4. Wasserman A et al. (1906) Eine serodiagnostiche reaction bei syphilis [German]. *Dtsch Med Wochenschr* 32: 745
5. Pangborn MC (1941) A new serologically active phospholipid from beef heart. *Proc Soc Exp Biol Med* 48: 484–486
6. Moore JE and Mohr GF (1952) Biologically false positive tests for syphilis: type, incidence, and cause. *J Am Med Association* 150: 467–473
7. Moore JE and Lutz WB (1955) Natural history of systemic lupus erythematosus: approach to its study through chromic biological false positive reactors. *J Chronic Dis* 1: 297–316
8. Conley CL and Hartman RCA (1952) A hemorrhagic disorder caused by circulating anticoagulant in patients with disseminated lupus erythematosus. *J Clin Invest* 31: 621–622
9. Beaumont JL (1954) Syndrome hemorrhagic acquis du a un anticoagulant [French]. Sang 25: 1–5
10. Bowie EJW et al. (1963) Thrombosis in systemic lupus erythematosus despite circulating anticoagulants. *J Lab Clin Med* 62: 416–430
11. Galli M et al. (1990) Anticardiolipin antibodies (ACA) directed not to cardiolipin but to a plasma protein cofactor. *Lancet* 335: 1544–1547
12. Matsuura H et al. (1990) Anticardiolipin cofactor(s) and differential diagnosis of autoimmune disease. Lancet 336: 117–118
13. McNeil HD et al. (1990) Antiphospholipid antibodies are directed against a complex antigen that includes a lipid-binding inhibitor of coagulation: β2-glycoprotein I (apolipoprotein H). *Proc Natl Acad Sci USA* 87: 4120–4124
14. Bevers EM et al. (1991) Lupus anticoagulant IgG's (LA) are not directed to phospholipids only, but to a complex of lipid-bound human prothrombin. *Thromb Haemost* 66: 629–632
15. De Laat B et al. (2004) β2-glycoprotein I, playmaker in the antiphospholipid syndrome. *Clin Immunol* 112: 161–168

16. Wilson WA et al. (1999) International consensus statement on preliminary classification criteria for definite antiphospholipid syndrome: report of an international workshop. *Arthritis Rheum* 42: 1309–1311
17. Miyakis S et al. (2006) International consensus statement on an update of the classification criteria for definite antiphospholipid syndrome (APS). *J Thromb Haemost* 4: 295–306
18. Consigny PH et al. (2002) High prevalence of co-factor independent anticardiolipin antibodies in malaria exposed individuals. *Clin Exp Immunol* 127: 158–164
19. Abuaf N et al. (1997) Autoantibodies to phospholipids and to the coagulation proteins in AIDS. *Thromb Haemost* 77: 856–861
20. Uhtman IW et al. (2002) Viral infections and antiphospholipid antibodies. *Semin Arthritis Rheum* 31: 256–263
21. De Laat B et al. (2005) IgG antibodies that recognize epitope Gly40-Arg43 in domain I of β2-glycoprotein I cause LAC and their presence correlates strongly with thrombosis. *Blood* 105: 1540–1545
22. Opatrny L et al. (2006) Association between antiphospholipid antibodies and recurrent fetal loss in women without autoimmune disease: a metaanalysis. *J Rheumatol* 33: 2214–2221
23. Davis WD, Brey RL. Antiphospholipid antibodies and complement activation in patients with cerebral ischemia. *Clin Exp Rheumatol* 1992; 10: 455-460
24. Forastiero R, Martinuzzo M, Carreras LO, Maclouf J. Anti-beta2 glycoprotein I antibodies and platelets activation in patients with antiphospholipid antibodies: association with increased excretion of platelet-derived thromboxane urinary metabolites. *Thromb Haemost*. 1998; 79: 42-45.
25. Giannakopoulos B., Passam F., Rahgozar S., Krilis S.A. (2007) Current concepts on the pathogenesis of the antiphospholipid syndrome. *Blood* 109: 422-430.
26. Lutters BC, Derksen RH, Tekelengurg WL, Lenting PJ, de Groot PJ. Dimers of β2-glycoprotein I increase platelet deposition to collagen via interactio with phospholipids and tha apolipoprotein E receptor 2'. *J Biol Chem* 2003; 278: 33831-33838.
27. Shi T, Giannakopulos, B, Yan, X et al. Antiβ2-Glycoprotein I antibodies in complex with β2-Glycoprotein I activate platelets in a dysregulated manner via glycoprotein Ib-IX-V. *Arthrisis Rheum* 2006; 54: 2558-2567
28. Karporaal, SJ, IA, van Eck, M, et al. Binding of low density lipoprotein to platelet apolipoprotein E receptor 2' results in phosphorilation of p38MAPK, *J Biol Chem* 2004; **279**: 52526-5253429
29. Canobbio, I, Reineri, S, Sinigaglia, F, Balduini, C, Torti, M. A role for p38 MAP kinase in platelet activation by von Willebrand factor. *Thromb Hamost* 2004; **91**: 102-110
30. Yap, CL;Anderson, KE, Hughan,SC, Dopheide, Sm, Salem, HHJackson, SP. Essential role for phosphoinositede 3 kinase in shear-dependent segnaling between platelet glycoprotein Ib/V/IX and integrin alpha(IIb)beta(3). *Blood* 2002; 99: 151-158

31. Zhang J, McCrae KR. Annexin A2 mediathes endothelial cell activation by antiphospholipidds/antiβ2 glycoprotein I antobodies. *Blood* 2005; 105: 1964-1969.
32. Meroni PL, Del Papa N, Raschi E, Panzeri P, Borghi MO, Tincani A, et al. Beta2-glycoprotein I as a 'cofactor' for anti-phospholipid reactivity with endothelial cells. *Lupus* 1998; 7: S44-7
33. Safa O, Esmon CT, Esmon NL. Inhibition of APC anticoagulant activity on oxidized phospholipid by anti-beta2-glycoprotein I monoclonal antibodies. *Blood*.2005; 106: 1629-1635.
34. Rahgozar S, Giannakopoulos B, Yan X, Wei J, Cheng Qi J, Gemmell R, Krilis SA. Beta2-glycoprotein I protects thrombin from inhibition by heparin cofactor II: potentiation of this effect in the presence of anti-beta2-glycoprotein I autoantibodies. *Arthritis Rheum*. 2008 58(4):1146-55.
35. Schousboe I. beta 2-Glycoprotein I: a plasma inhibitor of the contact activation of the intrinsic blood coagulation pathway. *Blood.* 1985;66:1086-91.
36. Rahgozar S, Yang Q, Giannakopoulos B, Yan X, Miyakis S, Krilis SA. β2Glycoprotein I binds thrombin via exosite I and exosite II. Anti-b2-glycoprotein I antibodies potentiate the inhibitory effect of b2-glycoprotein I on thrombin mediated factor XIa generation. *Arthritis and Rheumatism*. 2007. 56:605-613.

CHAPTER 3.2

Chemical Synthesis and Characterization of Wild-Type and Biotinylated N-Terminal Domain 1-64 of β2-Glycoprotein I

Nicola Pozzi [1], Alessandra Banzato [2], Samuele Bettin [1], Elisa Bison [2], Vittorio Pengo [2] and Vincenzo De Filippis [1,]

[1] *Department of Pharmaceutical Sciences, University of Padova, Via F. Marzolo 5, 35131 Padova, Italy*

[2] *Cardiology Unit, Department of Cardiologic, Thoracic and Vascular Sciences, University of Padova, Italy*

Submitted to Protein Science PRO-09-0488 23/12/2009

INTRODUCTION

The antiphospholipid syndrome (APS) is a severe autoimmune disease associated with a variety of clinical manifestations, including arterial and venous thrombosis, and recurrent fetal loss (1-3). APS is characterized serologically by high levels of autoantibodies (aAbs) mainly directed against β_2-Glycoprotein I (β2GpI) (3,4), a 54-kDa plasma glycoprotein synthesized in the liver and abundantly present in normal plasma (~0.2 mg/ml) (5). β2GpI is now recognized as the major autoantigen involved in APS (3,6) and the presence of anti-β2GpI Abs strongly correlates with the occurrence of thrombotic events in APS patients (4,7).

The mature sequence of human β2GpI consists of 326 amino acids with four N-linked carbohydrate chains,(8,9) localized in the third and fourth domain (see below) and accounting for about 19% of the protein mass (Fig. 1). The crystallographic structure reveals that human β2GpI is composed of four repeating units (domains I-IV), that belong to the complement control protein family (CCP) (10), and a distinctly folded C-terminal domain (domain V), arranged like beads on a string to form an elongated J-shaped molecule (11,12). Conversely, small-angle X-ray scattering studies indicate that β2GpI in solution assumes a predominantly S-shaped conformation, resulting from a tilt between domain II and III (13). β2GpI displays internal sequence and structural homology (8,11,12) and indeed domains I-IV are homologous units of about 60 amino acids sharing a common elliptically β-sandwich structure, stabilized by two conserved disulfide bridges. These domains are also characterized by the presence of high proline content (i.e., 8-15%), a conserved Cys-Pro peptide bond in the N-terminal region of each

domain and a single Trp-residue stacked against the disulfide bond connecting the first and third cysteine. Conversely, domain V is aberrant because it contains 82 amino acids that fold into a central β-spiral structure flanked by two small helices. In addition, it contains three (instead of two) disulfides, has a relatively low proline content (i.e., 3.5%), and the single Trp-residue is not structurally conserved. It is widely accepted that β2GpI binds to anionic phospholipd membranes using positively charged patches in domain V (Fig. 1A)(14), while it interacts with pathogenic aAbs by the N-terminal domain (DmI) (4,15). Of note, high plasma levels of anti-β2GpI Abs recognizing DmI strongly correlate with thrombosis, whereas aAbs recognizing other different regions of β2GpI do not seem to be pathogenic (4,7). Mutagenesis studies indicate that the antigenic epitope of β2GpI in DmI is discontinuous in nature and comprises amino acid residues Asp8 and Asp9, the Arg39-Arg43 segment, and the domain I-II interlinker region (7,16,17). Whether anti-β2GpI aAbs directly bind to a constitutively expressed epitope of β2GpI in DmI or to a cryptic epitope that becomes exposed in DmI only after β2GpI binds to negatively charged surfaces has been the subject of a lengthy debate (18).

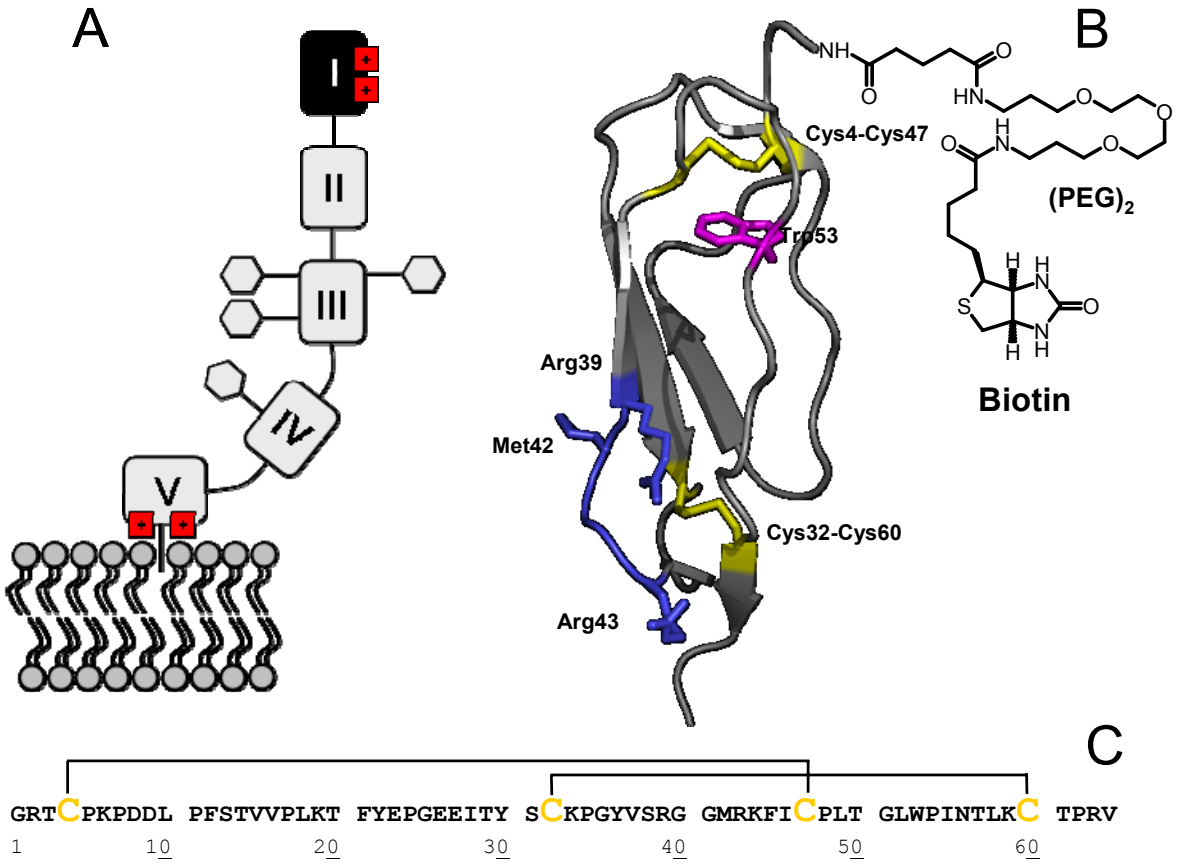

Figure 1. Structure and membrane binding of β2GpI. A: Schematic representation of full-length β2GpI interacting with phospholipid membranes. The four glycosylation sites in domain III and IV (i.e., Asn143, Asn164, Asn174, Asn243) are indicated by hexagons (adapted from ref. 3). **B**: Schematic representation of the threedimensional structure of N-DmI in the crystallographic structure of β2GpI (1qub).[11] Disulphide bonds Cys4-Cys47 and Cys32-Cys60 and Trp53 are shown in stick together with key amino acids (i.e., Arg39, Met42 and Arg43) in the putatively primary antigenic epitope. Ribbon drawing of DmI was generated on the crystal structure of β2GpI using the software program ViewerPro 4.2 (Accelrys Inc.). **C**: Primary structure of the synthetic peptide DmI(1-64), as deduced from the amino acid sequence of full-length β2GpI.[8] Cysteine residues are in grey and disulfide bonds are indicated by plain lines.

Multiple mechanisms have been proposed for explaining the clinical manifestations of APS, including 1) complement activation, 2) dysregulated activation of platelets, endothelial cells and monocytes, 3) disruption of the interactions of anticoagulant factors (i.e., activated protein C and annexin A5), 4) inhibition of fibrinolysis, 5) inhibition of thrombin-mediated activation of factor XI.[19-21] Even though it is still unclear which of these mechanisms is actually predominant *in vivo*, it is widely accepted that they are all affected by the presence of anti-β2GpI aAbs (19,22,23). Hence, the possibility to find out a molecule which is able to effectively compete with β2GpI for the binding to anti-β2GpI aAbs, without eliciting the cellular effects mediated by anti-β2GpI Abs, would be a promising approach for developing safer therapeutic strategies in APS (19). On the other hand, the presence in the plasma of APS patients of pathogenic and non-pathogenic aAbs recognizing several distinct regions of β2GpI (18), form domain I do domain V, has impaired so far the development of reliable immunochemical tools for the diagnosis of APS (3).

In this work we produced in high yields by total chemical synthesis the entire domain I, encompassing residues 1-64 of β2GpI (Fig. 1B, C). The synthetic polypeptide was able to efficiently fold into a native-like structure, with the correct disulfide topology, and remarkably stable to chemical and thermal denaturation. By ELISA competition assays, we demonstrated that synthetic D-I dose-dependently inhibited binding of full-length β2GpI to anti-β2GpI-Abs from APS patients, with IC_{50} values comparable to those of full-length β2GpI. The versatility of chemical synthesis was also exploited to produce an N-terminally biotin-$(PEG)_2$-derivative of N-DmI (Biotin-N-DmI). When loaded onto a streptavidin-coated plate, Biotin-N-DmI was selectively recognized by pathogenic autoantibodies form APS patients. Overall, our results demonstrate that large quantities of correctly folded DmI can be conveniently produced by chemical methods for potential therapeutic and diagnostic applications in APS.

MATERIALS AND METHODS

Purification and chemical characterization of β2GpI.

Natural β_2GpI was purified from normal human plasma by means of perchloric acid precipitation, followed by affinity chromatography on a HiTrap (1 x 2.5 cm) heparin-Sepharose column (GE-Healthcare) and cation exchange chromatography on a Mono-S (0.6 x 5 cm) column (GE-Healthcare), as previously detailed (6). The homogeneity of β_2GpI preparations was established by Coomassie–stained polyacrylamide gel electrophoresis in the presence of SDS (4-12% acrylamide) (SDS-PAGE), under reducing and non-reducing conditions, and by RP-HPLC on a Zorbax (Agilent Technologies, Santa Clara, CA) C4 analytical column (4.6 x 150 mm), eluted with a linear acetonitrile-0.1% TFA

gradient. The protein material eluted from the column was lyophilized and analyzed by mass spectrometry. Typically, samples (10 μl, 1-10 μM) in water:acetonitrile solution (1:1 v/v), containing 1 % formic acid, were loaded at a flow rate of 10 μl/min on a Mariner ESI-TOF instrument from PerSeptive Biosystems (Stafford, TX). Spray tip potential was set at 3.0 kV, while the nozzle potential and temperature were set at 200 Volts and 140°C, respectively.

Analytical size-exclusion chromatography and dynamic light scattering. Analytical size-exclusion chromatography (SEC) was carried out by loading β_2GpI (50 μg) onto a Superose-12 (1 x 30 cm) column (GE-Healthcare) eluted at a flow rate of 0.5 ml/min with 20 mM Tris-HCl buffer, pH 7.5, containing 0.15 M NaCl and the apparent molecular weight was estimated according to (24). Dynamic light scattering measurements on β_2GpI solution (0.82 mg/ml) were carried out at 25°C in 20 mM Tris-HCl, pH 7.5, containing 0.15 NaCl, using a Zetasizer system from Malvern Instruments (Malvern, UK). The hydrodynamic radius, R_H, was calculated from the Stokes-Einstein equation: $R_H = K \cdot T/6\pi\eta D$, where K and T are the Botzman's constant and the absolute temperature, η is the solvent viscosity and D is the diffusion coefficient of the protein measured experimentally.

Deglycosylation of β2GpI. Removal of *N*-Linked carbohydrate chains was carried out by incubating for 24 h at 37°C β_2GpI (0.5 mg/ml) with recombinant N-glycanase F from Roche (Mannheim, Germany) with an enzyme:protein ratio of 1:50 (by weight), in 50 mM phosphate buffer, pH 7.8, containing 10 mM EDTA, 0.1% SDS, 0.5% Triton-X and 1% β-mercaptoethanol (buffer A). Alternatively, the reaction was conducted for 24 h at 37°C in 20 mM Trs-HCl buffer, pH 7.5, containing 0.15 M NaCl (buffer B). The reaction mixture was analyzed by RP-HPLC, MS and SDS-PAGE (4-12% acrylamide) stained with Coomassie or with the GelCode Pierce staining kit for glycoproteins (Thermo Scientific, Rockford, IL).

Synthesis and chemical characterization.

Synthesis. The peptide sequence 1-64 of β_2GpI was synthesized by the solid-phase method using the 9-fluorenylmethyloxycarbonyl(Fmoc) strategy on a model PS3 automated synthesizer from Protein Technologies International (Tucson, AZ) (47). The peptide chain was assembled stepwise on a NovaSyn TGA resin (Novabiochem, Switzerland) derivatized with Fmoc-Val (0.24 mequiv/g). *tert*-Butiloxycarbonyl side-chain protecting group was used for Lys and Trp; *tert*-butyl for Ser, Thr, Asp, Glu and Tyr; triphenylmethyl for Asn and Cys; 2,2,4,6,7-pentamethyldihydrobenzofuran-5-sulfonyl group was used for Arg. Removal of N^{α}-Fmoc protecting groups was achieved by a 20-min treatment with 20% piperidine in N-methypirrolidone. Standard coupling reactions were performed with 2-(1*H*-benzotriazol-1-yl)-1,1,3,3-tetramethyluronium hexafluorophosphate (HBTU) and 1*H*-hydroxy-benzotriazole (HOBt) as activating agents, with a 4-fold molar excess of N^{α}-Fmoc-protected amino acids (Novabiochem) in the presence of diisopropylethylamine. For double couplings at peptide bonds

involving Val, Ile, Leu, and Phe, the stronger activator 2-(7-aza-1H-benzotriazol-1-yl)-1,1,3,3-tetramethyluronium hexafluorophosphate was used (HATU). After peptide assembly was completed, the side chain-protected peptidyl resin was treated for 120 min at room temperature with a mixture of TFA/H_2O/ethandithiol/triisopropylsilane (90:5:4:1 v/v/v/v). The resin was removed by filtration and the acidic solution, containing the unprotected peptide, was precipitated with ice-cold diethylether and then lyophilized. The crude peptide with Cys-residues in the reduced free thiol state, R-DmI, was fractionated by RP-HPLC on a Zorbax C18 analytical column. The peptide material eluted in correspondence of the major chromatographic peaks were collected, lyophilized and analyzed by MS. Disulfide-mediated oxidative renaturation of the crude R-DmI, to yield the correctly folded species, N-DmI, was carried out by dissolving the crude peptide (1.8 mg/ml) in 0.1 M Tris-HCl buffer, pH 8.4, and allowing the reaction to proceed for 24 h under air-oxidation conditions in the presence of 1 mM GSH and 4 mM GSSG. The folding reaction was monitored by RP-HPLC, using a Zorbax C18 analytical column. For preparative purposes, aliquots (~2 mg) of the crude N-DmI were injected onto a semipreparative Grace-Vydac (Hesperia, CA) C-18 column (1 x 25 cm, 5-μm particle size) eluted with a linear acetonitrile-0.1% TFA gradient from 30 to 42% in 30 min. The material corresponding to the major peak was collected, lyophilized, and used for subsequent studies.

Biotin-N-DmI was synthesized by reacting the peptidyl 1-64 resin with a two-fold molar excess of N-biotinyl-NH-$(PEG)_2$-COOH (Novabiochem; cat. 01-63-0133) in the presence of HBTU and HOBt. The resulting biotinylated DmI was purified and characterized as detailed above for the wild-type peptide.

Disulphide Bonds Assignment. The refolded peptide, N-DmI, (30 μg) was subjected to proteolysis with TPCK-treated bovine trypsin (Sigma) in 50 mM $NaHCO_3$ buffer, pH 8.4 (300 μl) or with bovine chymotrypsin (Sigma) in 50 mM Tris-HCl buffer, pH 7.8, containing 10 mM $CaCl_2$. Reactions were allowed to proceed for 3 hours at 37°C using a protease:substrate ratio of 1:25 (w/w). Thereafter, proteolysis reactions were stopped by acid quenching with 4% aqueous TFA and immediately analyzed by RP-HPLC. The chemical identity of the proteolytic fragments was established by MS analysis.

Refolding kinetics. To initiate folding, HPLC-purified R-DmI was dissolved (0.25 mg/ml) in 0.1 M Tris-HCl buffer, pH 8.4, in the absence or in the presence of 1 mM GSH and 4 mM GSSG. Prior to use, all buffers were extensively degassed under vacuum for at least 30 min. The folding intermediates were trapped in a time course manner by acidifying aliquots (50 μl) of the refolding mixture with an equal volume of 4% (v/v) aqueous TFA. Acid-trapped intermediates were added with 7 M Gnd-HCl solution (280 μl) and analyzed by RP-HPLC. The yield of the correctly folded species was estimated by integrating the area under the chromatographic peaks.

Reduction and carboxamidomethylation of cysteines. Purified N-DmI (150 μg) was reduced for 40 min at 37°C in 0.5 M Tris-HCl buffer (125 μl), pH 8.3, containing 1 mM EDTA, 6 M Gnd-HCl, and 0.1 M dithiotreitol. Carboxamidomethylation of Cys-residues was carried out for 1 h in the dark, in the

presence of 0.2 M iodoacetamide, maintaining the solution pH constant at 8.3. The reduced and carboxamidomethylated peptide, RC-DmI, was purified by RP-HPLC and its chemical identity established by MS analysis.

Spectroscopic measurements. Peptide concentration was determined by UV absorption at 280 nm on a double-beam V-630 spectrophotometer from Jasco (Tokyo, Japan). Molar absorptivity values were calculated according to Pace et al. (1995) (48) and taken as 10200 $M^{-1}\cdot cm^{-1}$, for N-DmI and Biotin-N-DmI, and 9970 $M^{-1}\cdot cm^{-1}$, for R-DmI and RC-DmI. Circular dichroism (CD) spectra were recorded on a Jasco J-810 spectropolarimeter equipped with a water-jacketed cell holder, connected to a NesLab RTE-111 (Newington, NH) water-circulating bath. The final spectra resulted from the average of four accumulations after base line subtraction. CD data were expressed as the mean residue ellipticity, $[\theta] = \theta_{obs}\cdot MRW/(10\cdot l\cdot c)$, where θ_{obs} is the observed signal in degrees, MRW is the mean residue weight, l is the cuvette pathlength in cm, and c is the protein concentration in g/ml. Fluorescence spectra were recorded on a Jasco model FP-6500 spectropolarimeter, equipped with a Peltier model ETC-273T temperature control system. Protein samples were excited at 280 or 295 nm, using excitation and emission slits of 10 nm. Fluorescence quenching experiments were performed by recording the decrease of fluorescence intensity of N-DmI or N^{α}-acetyl-tryptophanamide (NATA) as a function of acrylamide concentration. Fluorescence quenching data were fitted to the Stern-Volmer equation: $F_0/F = 1 + K_{sv}\cdot[Q]$, where F_0 and F are the fluorescence intensities in the absence and presence of quencher, Q, and K_{sv} is the Stern-Volmer quenching constant (28).

Stability measurements and data analysis

***Chemical denaturation*.** Gnd-HCl and urea-induced denaturation experiments were carried out by exciting protein samples at 280 nm (excitation slit 5 nm) and recording the fluorescence intensity at 350 nm (emission slit 10 nm). Prior to measurements, samples were incubated for 1 h at 25±0.1°C. At each denaturant concentration, the fluorescence signal was subtracted for that of the corresponding blank. Reversibility of denaturation was estimated by measuring the recovery of the fluorescence intensity upon 20-fold dilution of a protein stock solution (10 μM) in 6 M Gnd-HCl or 8 M urea with non-denaturing buffer.

Thermal denaturation. The decrease in the CD signal of N-DmI at 230 nm was recorded as a function of the sample temperature, T. Denaturation experiments were carried out in a 1-cm pathlength cuvette heated under gentle stirring at a linear heating rate of 40°C/hour. Reversibility of the thermal unfolding was determined by measuring the recovery of the CD signal upon cooling to the starting temperature.

Data analysis

Denaturant-induced unfolding data were analyzed within the framework of a two-state process, $N \Leftrightarrow D$, and the data points fitted to the equation (34):

$$F = \{(F_N + S_N[D] + (F_U + S_D[D]) \cdot exp(m[D] - \Delta G_D°)/RT\}/1 + exp(m[D \ \Delta G_D°)/RT \quad \text{(Eq. 1)}$$

where F is the observed fluorescence intensity, F_N and F_U the intensities of the native (N) and denatured (D) state in the absence of denaturant, s_N and s_U are the base line slopes for the native and denatured regions, $\Delta G_D°$ is the free energy change for the unfolding reaction in the absence of denaturant at 25°C, and m is the denaturation index ($m = -d\Delta G_U/d[D]$), that is the dependence of ΔG_D on denaturant concentration. Alternatively, $\Delta G_D°$ was estimated by linear extrapolation to [Gnd-HCl] = 0 of ΔG_D values calculated in the transition region, according to the equation (33):

$$\Delta G_D = \Delta G_D° - m \cdot [D] \quad \text{(Eq. 2)}$$

Thermal denaturation transition curves were analyzed according to a two-state model, as previously detailed (49). For each temperature in the transition region, it is possible to derive the equilibrium denaturation constant, K_D, and the free energy change of unfolding, $\Delta G_D = -RT \cdot lnK_D$, where R is the gas constant (1.987 cal·mol^{-1}·K^{-1}) and T is the absolute temperature. The melting temperature, T_m, defined as the temperature at which $\Delta G_D = 0$, was derived from the linear regression equation obtained by plotting ΔG_D as a function of T in the transition region. Entropy, ΔS_m, and enthalpy, ΔH_m, change of unfolding at T_m were calculated according to the equations $\Delta S_m = - d\Delta G/dT$ and $\Delta H_m = T_m \cdot \Delta S_m$, respectively. The enthalpy change, $\Delta H_D(T)$, at a given temperature in the transition region was calculated from the van't Hoff equation $\Delta H_D(T) = - [d(lnK_D)/d(1/T)] \cdot R$ and the heat capacity change of unfolding at constant pressure, $\Delta C_p = C_p(D) - C_p(N)$, was derived from the equation $\Delta C_p = d\Delta H(T)/dT$. The conformational stability of N-DmI at 25 or 37°C was determined according to the equation:

$$\Delta G_D(T) = \Delta H_m \cdot [1 - (T/T_m)] - \Delta C_p \cdot [(T_m - T) + T \cdot ln(T/T_m)] \quad \text{(Eq. 3)}$$

Fitting of data points was performed using the computer program Origin vs. 7.5 (Microcal Inc, CA).

Assays for antiphospholipid antibodies and ELISAs

Serological assays. Plasma samples from three patients (P1, P2 and P3) with primary APS, a history of thrombosis, and positive for anti-β2GpI IgG antibodies were included in this study. Ethical approval for the study was granted by the Research Ethics Committee of the University of Padova. Antibodies against β2GpI (anti-β2GpI Abs) were measured in an ELISA, as described earlier and were considered positive when the value (arbitrary units) exceeded the 99th percentile obtained using plasma from 40 healthy subjects (16 U) (50). To determine LAC activity, activated partial thromboplastin time and

dilute Russell Viper Venom Time (dRVVT) assays were performed as detailed elsewhere (4,51). Patients were considered LAC positive with a dRVVT mixing test ratio of more than 1.2 and a positive confirmatory test Anticardiolipin antibodies (anti-CL Abs) were measured in an ELISA as described andconsidered positive when GPL units were 40 units or more (4,50).

Competitive inhibition ELISA. Polyvinyl chloride 96-wells microtiter plates from Falcon (Franklin Lakes, NJ) were coated overnight at 4°C with a solution (10 μg/ml, 100 μl/well) of β_2GpI purified from human plasma in 0.1 M sodium bicarbonate buffer, pH 9.5. Thereafter, the plates were washed four times (x 4) with phosphate–buffered saline (PBS), containing 0.1% Tween-20, and the reactive sites blocked by treatment with 4% BSA (100 μl/well) in PBS for 2 hours. Samples were prepared by mixing a fixed volume (50 μl) of diluted plasma (1:50 v/v) from selected APS patients with an equal volume of solutions containing increasing concentrations (i.e., from 0 to 46 μM) of natural β_2GpI or synthetic N-DmI and RC-DmI. Each solution (100 μl) was incubated in the corresponding well for 1 hour at 37°C. Anti-β2GpI Abs titers of 218, 340 and 392 U/ml were determined in plasma samples of patient P1, P2, and P3, respectively, by an ELISA as described elsewhere (50). Briefly, the plates were washed (x 4) with PBS, containing 0.1% Tween-20, and 100 μl of alkaline phopshatase-conjugated anti-human IgG (Sigma), diluted 1:1000 (v/v) in PBS-2% BSA, were added *per* well and incubated at 37°C for 1 hour. Then the plates were washed (x 4) with PBS-0.1% Tween-20 and *p*-nitrophenylphosphate (pNPP) (Sigma) (100 μl *per* well) was added and incubated for 30 min. The release of *p*-nitrophenol was monitored by recording the absorbance at 405 nm using a microplate autoreader from Tecan (Männedorf, Switzerland). The data were corrected for the corresponding background values, plotted as a function of inhibitor concentration, *I*, (i.e., β_2GpI, N-DmI, and RC-DmI) and fitted to the equation:

$$A_{405} = [A_0 + (A_I \cdot [I]/IC_{50})/(1 + [I]/IC_{50})] \quad \text{(Eq. 4)}$$

where A_{405} is the absorbance at the specified inhibitor concentration, $[I]$, A_0 and A_I is the absorbance measured in the absence or presence of saturating $[I]$, and IC_{50} is the $[I]$ value at which 50% inhibition was observed.

Direct binding ELISA with Biotin-N-DmI. Streptavidin-coated microtiter plates (Sigma; cat. S-6940) were incubated with a solution of Biotin-N-DmI (25 μg/ml, 200 μl/well) in PBS, pH 7.4, for 2 h at room temperature (r.t.). After washing (x 3) with PBS-0.1% Tween-20, each well was added with a fixed volume (100 μl) of plasma from selected APS patients, diluted (1:100 v/v) with 4% BSA in PBS. After washing (x 3) with PBS-0.05% Tween-20, determination of anti- β_2GpI aAbs was carried out with an alkaline phopshatase-conjugated anti-human IgG, as detailed above.

RESULTS

Purification of β_2GpI

Natural β_2GpI was purified from normal human plasma by means of perchloric acid precipitation, followed by heparin-sepharose and cation exchange chromatography, as previously detailed (24). This procedure yields highly homogenous (>95%) β_2GpI preparations, as obtained from RP-HPLC and SDS-PAGE (Fig. 2-A). MS analysis of RP-HPLC purified β_2GpI yields an average molecular mass of 47290±10 a.m.u. (not shown). Under reducing conditions, β_2GpI migrates as a single band at ~53 kDa (Inset to Fig. 2-A), in agreement with the known lower electrophoretic mobility of glycosylated proteins. Of note, this band stained magenta with the glycoprotein specific GelCode staining (not shown). Extensive reaction (i.e., 24 h) of β_2GpI in nondenaturing conditions with N-glycanase F, an enzyme that cleaves carbohydrate chains at Asn-N-linked sites, produced four protein bands in the range 39-53 kDa, that likely correspond to the removal of a single carbohydrate chain at a time from the four N-glycosylation sites of β2GpI (Inset to Fig. 2-A). The same reaction conducted in denaturing buffer, containing detergents and reducing agents (see Methods), quantitatively yielded a single band at ~39 kDa in SDS-PAGE, in agreement with the molecular mass deduced from the amino acid sequence of β_2GpI 36255.7 a.m.u. Interestingly, the 39-kDa band that did not stain with the GelCode. These results concurrently indicate that our β2GpI preparation contains only N-glycosylation sites.

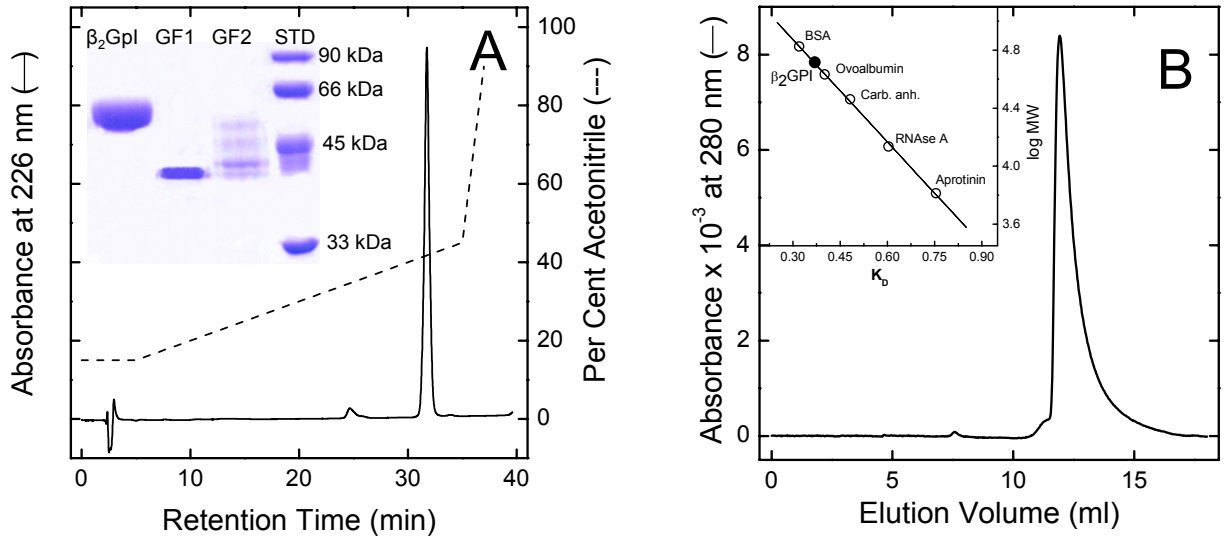

Figure 2. Analytical characterization of β2GpI. A: RP-HPLC analysis of β2GpI. An aliquot (30 μg) of purified β2GpI was applied to a Vydac C4 analytical column eluted with a linear acetonitrile-0.1% TFA gradient (---) at a flow rate of 0.8 ml/min. **Inset:** SDS-PAGE (4-12% acrylamide) analysis of β2GpI under reducing conditions. Lane 1, purified β2GpI (4 μg); lane 2 (GF1), an aliquot (10 μl) of the reaction mixture of β2GpI with N-glycanase F conducted under denaturing conditions in buffer A (see Methods); lane 3 (GF2), an aliquot (10 μl) of the reaction mixture of β2GpI with N-glycanase F under nondenaturing conditions in buffer B (see Methods); lane 4 (Std), molecular weight protein standards. **B:** Analytical size-exclusion chromatography of β2GpI. A sample of purified β2GpI (50 μg) was loaded onto a Superose-12 column eluted at a flow rate of 0.5 ml/min in 20 mM Tris-HCl buffer, pH 7.5, containing 0.15 M NaCl. **Inset:** estimation of the apparent molecular weight (MW) of β2GpI (•). The Superose-12 column was calibrated with molecular weight protein standards (O-O). LogMW values are plotted vs. the distribution constant, KD, of the protein standards.

When analysed by analytical size-exclusion chromatography, natural β_2GpI elutes as a monomer with an apparent molecular weight of 50.1±5 kDa (Fig. 2-B), compatible with the extensive glycosylation (~19%) of the protein and with the elongated structure it assumes in solution. The monomeric nature of β_2GpI in solution was also confirmed by dynamic light scattering, whereby a monodisperse protein population was observed, with a mean hydrodynamic radius of 5±0.5 nm (not shown), in good agreement with the radius of gyration determined by small-angle X-ray scattering (i.e., 4.3-4,5 nm) (13).

Synthesis and chemical characterization of N-DmI

After peptide chain assembly, resin cleavage, and diethylether precipitation, the crude peptide with the Cys-residues in the reduced form, R-DmI, was analyzed by RP-HPLC (Fig. 3A). The chromatogram shows two major peaks (i.e., p1 and p2) having a mass of 7163.4±0.5 a.m.u., identical to the average theoretical value deduced from the primary structure of R-DmI in β2GpI (i.e., 7163.4 a.m.u.) (8,9). These species are different *cis*↔*trans* proline isomers of the same polypeptide chain, that can be separated likely because they expose a slightly different apolar surface to the column stationary phase. Similar observations have been reported with other Pro-rich synthetic peptides (25). Oxidative disulfide folding of R-DmI to yield the native-like species, N-DmI, was achieved by dissolving the crude R-DmI in Tris-HCl buffer, pH 8.4 and allowing the reaction to proceed for 24 h in the presence of the red-ox couple GSH:GSSG (1 mM:4 mM). As shown in Fig. 3A, a single predominant peak at shorter retention time was obtained by RP-HPLC, compatible with the lower apolar surface that the folded N-DmI exposes to the RP-column. N-DmI was purified by semi-preparative RP-HPLC and its homogeneity and chemical identity established by analytical RP-HPLC (Fig. 3B) and mass spectrometry (Table 1), yielding a molecular mass (7159.4±0.7 a.m.u.) four units lower than that of R-DmI, consistent with the formation of two disulfide bonds upon oxidative folding.

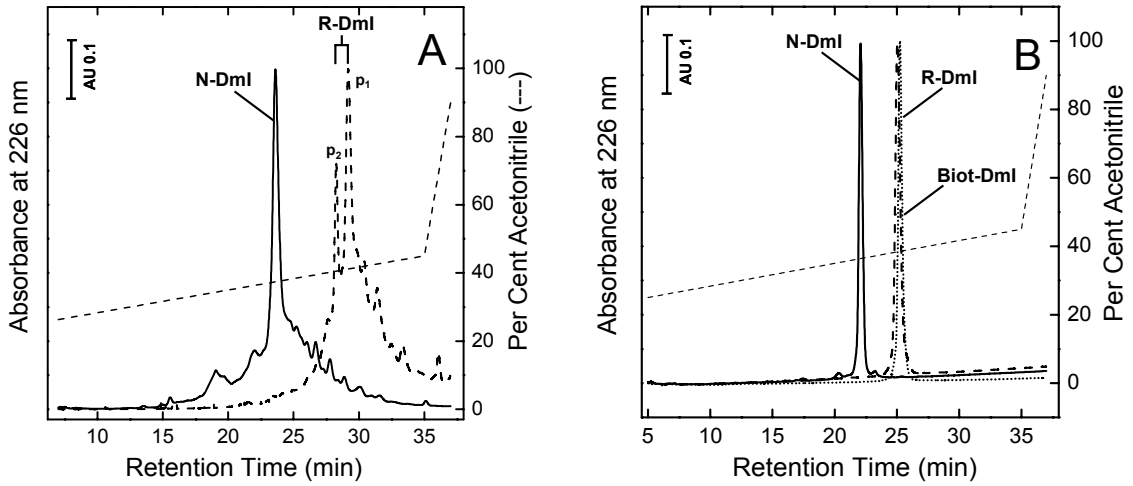

Figure 3. Purification of the synthetic N-DmI, R-DmI and Biotin-N-DmI. A: RP-HPLC analysis of crude peptides. **B**: purity check of HPLC-purified peptides. The column was eluted with a linear acetonitrile gradient (--) in 0.1% aqueous TFA at a flow rate of 0.8 ml/min and the peptide material corresponding to the major peaks in the chromatograms was collected and subjected to MS analysis (see also Table 1).

Table 1. Mass values of the synthetic peptides obtained by ESI-TOF analysis

	R	N	Δm
DmI	7163.4± 0.4	7159.4 ± 0.4	4
Biot-DmI	7705.9 ± 0.4	7701.9± 0.4	4

R and N are reported in a.m.u. and stand for reduced and native form, respectively

The correctness of disulfides pairing was established by peptide mass fingerprint analysis with trypsin (Fig. 4A) and chymotrypsin (Fig. 4B). MS data reported in Table 2 allowed us to cover the entire N-DmI sequence and to identify several proteolytic fragments each containing a single disulfide bond, Cys4-Cys47 or Cys32-Cys60 (Fig. 4C).

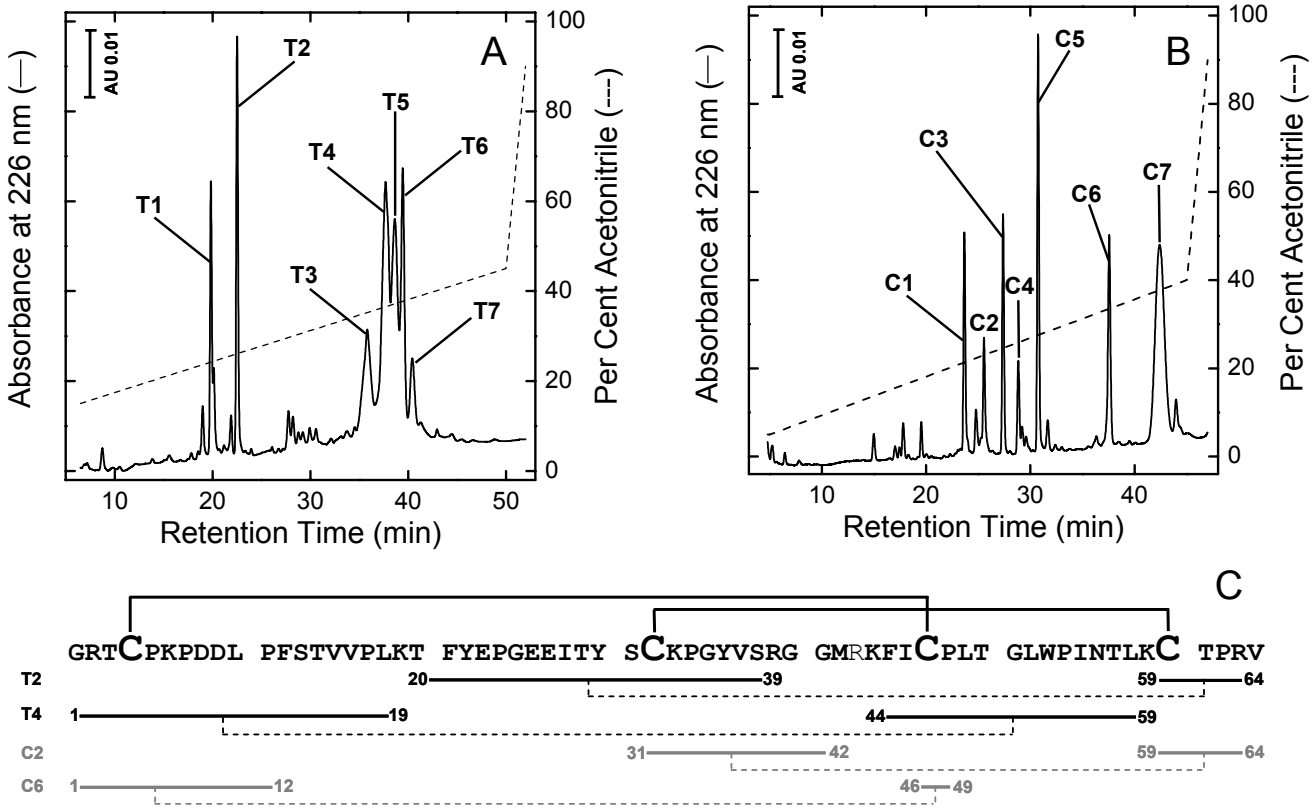

Figure 4. Assignment of disulphide bonds pairing of the synthetic N-DmI by enzymatic peptide mass fingerprint analysis. A: RP-HPLC of the proteolysis reaction with trypsin. **B**: RP-HPLC of the proteolysis reaction with chymotrypsin. N-DmI samples (30 μg) were incubated at 37°C for 3 h with the protease, using a protease:substrate ratio of 1:25 (w/w). After acid quenching, aliquots (20-50 μg) of the reaction mixtures were applied to a Zorbax C18 analytical column (4.6 x 150 mm). The chemical identity of tryptic (T) and chymotryptic (C) fragments was established by MS analysis, as reported in Table S1 of the Supplementary Materials. **C**: Amino acid sequence and disulphide bond topology of the synthetic N-DmI, as deduced from MS data reported in Table 2. Only the peptide fragments containing a single disulfide bond (---) are indicated.

Table 2. Peptide Mass Fingerprint Analysis of the Synthetic N-Domain I[a]

Peak Number	Fragment Sequence	Molecular Mass (a.m.u.)
T1	^{20}TFYEPGEEITYSCKPGYVSR^{39} | ^{60}CTPR^{63}	**2800.3 ± 0.1** *(2800.3)*
T2	^{20}TFYEPGEEITYSCKPGYVSR^{39} | ^{60}CTPRV^{64}	**2899.3 ± 0.1** *(2799.3)*
T3	^{20}TFYEPGEEITYSCK^{33} | ^{60}CTPRV^{64}	**2238.0 ± 0.2** *(2238.0)*
T4	^{1}GRTCPKPDDLPFSTVVPLK^{19} | ^{44}KFICPLTGLWPINTLK^{59}	**3912.2 ± 0.1** *(3912.1)*
T5	^{3}TCPKPDDLPFSTVVPLK^{19} | ^{44}KFICPLTGLWPINTLK^{59}	**3699.1 ± 0.3** *(3999.0)*
T6	N-DmI	**7159.4 ± 0.6** *(7159.4)*
T7	^{1}GRTCPKPDDLPFSTVVPLK^{19} | ^{45}FICPLTGLWPINTLK^{59}	**3570.2 ± 0.7** *(3570.9)*
C1	^{31}SCKPGY^{36} | ^{59}KCTPRV^{64}	**1353.6 ± 0.1** *(1353.6)*
C2	^{31}SCKPGYVSRGGM^{42} | ^{59}KCTPRV^{64}	**1941.0 ± 0.1** *(1940.9)*
C3	^{22}YEPGEEITY^{30}	**1100.5 ± 0.4** *(1100.1)*
C4	^{13}STVVPL^{18}	**615.0 ± 0.1** *(614.7)*
C5	^{19}KTFYEPGEEITY^{30}	**1475.7 ± 0.1** *(1475.6)*
C6	^{1}GRTCPKPDDLPF^{12} | ^{46}ICPL^{49}	**1786.9 ± 0.2** *(1786.8)*
C7	^{50}TGLWPINTL^{58}	**1014.6 ± 0.2** *(1014.1)*

[a]ESI-TOF MS analysis were performed on peptide samples derived from limited proteolysis reaction of the N-DmI with trypsin (T1-T7) or chymotrypsin (C1-C3) and fractionated by RP-HPLC

Folding kinetics of DmI.

To improve oxidative disulfide folding, several additives were tested, such as L-arginine, β-mercaptoethanol, GSH and GSSG, and trimethylamine N-oxide. Of these, the red-ox couple GSH-GSSG was proven to work best in DmI renaturation, allowing us to obtain almost exclusively the correctly folded species in yields higher than 60% (Fig. 5-B-C). Whereas, in the absence of glutathione or with other additives, the folding yields were always lower than 30% (5-A-C). At time intervals,

aliquots of the refolding mixture were blocked by adding aqueous TFA and 6M Gnd-HCl, to possibly solubilize all the intermediates generated during folding. Immediately after folding reaction was started, the solution turbidity increased (as also obtained by recording the absorbance at 350 nm), indicating the formation of some precipitate in the test tube (not shown). This was also confirmed by RP-HPLC analysis at short reaction times, showing the presence of only negligible amounts of DmI species in solution (Fig. 5-A-B). The protein pellet was centrifuged and analysed by SDS-PAGE.

Under reducing conditions, a single intense band migrating at ~7 kDa was present, whereas under non-reducing conditions any protein band could not be detected in the gel, suggesting that the precipitate remained undissolved in the sample loading buffer and did not even enter in the gel (Fig. 5-D). At longer reaction times, the solution became less turbid and the correctly folded disulfide species appeared in the RP-HPLC plots. Altogether, these results can be rationalized according to the following scheme:

$\underline{(DmI)_n} \Leftrightarrow n \cdot R\text{-}DmI \Leftrightarrow n \cdot N\text{-}DmI$ (Scheme 1)

whereby only a low amount of soluble monomeric R-DmI exists in equilibrium with disulfide cross-linked insoluble aggregates, $\underline{(DmI)_n}$, to yield almost exclusively the natively folded product, N-DmI.

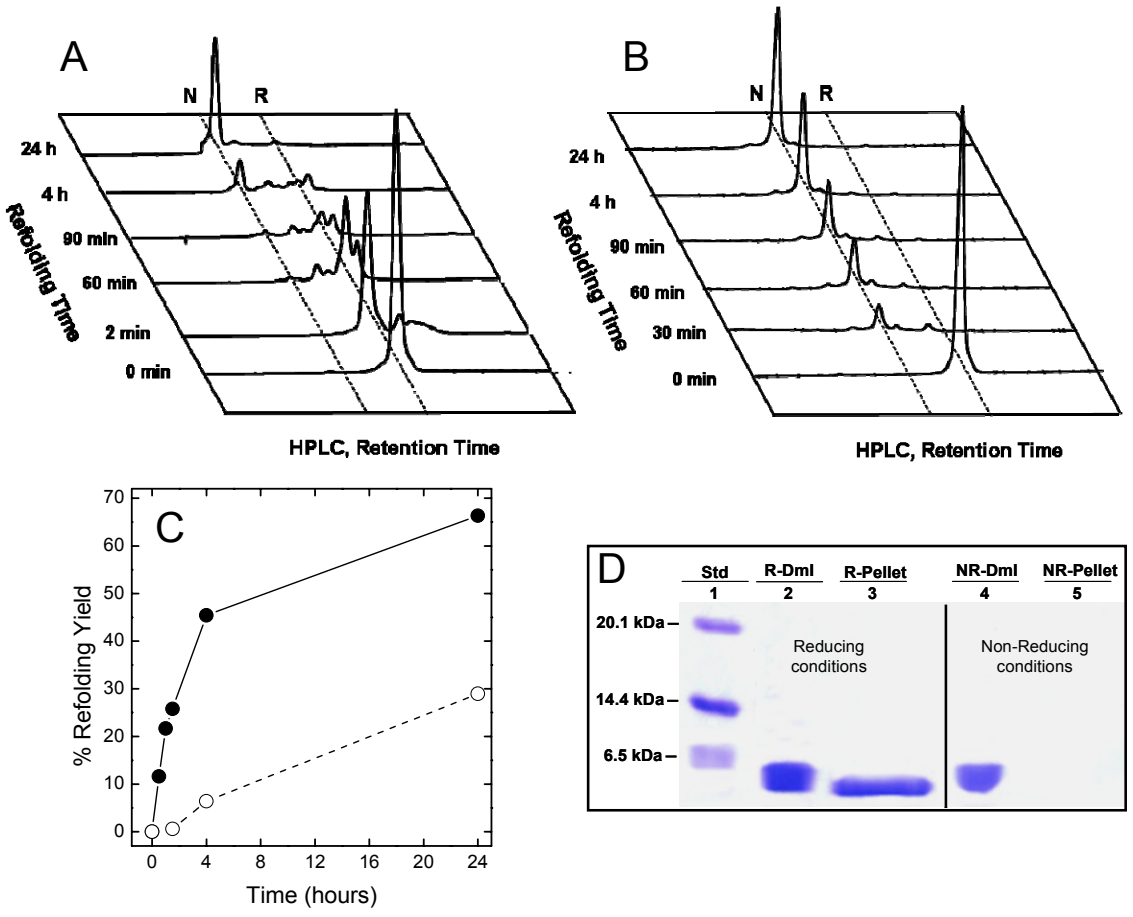

Figure 5. A-B-C: Time course RP-HPLC analysis of the oxidative disulfide folding of DmI. Fully reduced, HPLC-purified peptide R-DmI (0.25 mg) was allowed to fold at room temperature (20-22 °C) in 0.1 M Tris-HCl buffer, pH 8.4, (1 ml) in the absence (A) presence (B) of GSH (1 mM) and GSSG (4 mM). At time intervals,

aliquots (10 μg) of the refolding mixture were acid-quenched and analyzed by RP-HPLC (see Methods). R and N indicate the synthetic DmI with Cys-residues in the reduced and disulfide-bonded native state, respectively. **B: SDS-PAGE analysis of the refolding reaction of DmI under reducing and nonreducing conditions** Polyacrylamide gel electrophoresis (4-12% acrylamide) was carried out under reducing (R, lanes 2 and 3) and nonreducing (NR, lanes 4 and 5) conditions. Lane 1, molecular weight protein standards; lane 2, RP-HPLC purified N-DmI (5 μg); lane 3, an aliquot (4-6 μg) of the DmI pellet was dissolved in the sample loading buffer (15 μl), containing 0.1 M DTT; lane 4, RP-HPLC purified N-DmI (5 μg); lane 5, an aliquot (5-10 μg) of the DmI pellet, formed during folding reaction, was added with sample loading buffer (15 μl), without DTT.

Folding of DmI, in fact, is complicated by the presence of four cysteines and nine prolines. Cysteines, indeed, can combine in DmI to give seven different disulfide species, each containing one or two disulfide bonds. On the other hand, it is well known that in unfolded polypeptides proline exists either in the *cis* and *trans* conformation, with a *cis:trans* ratio of 30:70, and that *trans* ↔ *cis* isomerisation can remarkably slow down intramolecular protein folding (26), allowing the polypeptide chain to form intermolecular disulfide cross-linked aggregates. Of note, in native DmI eight of the nine prolines are in the more stable *trans* conformation, whereas the remaining Pro17 is in the *cis* conformation (11).

Conformational characterization of N-DmI

Fluorescence. The 280-nm emission spectrum of N-DmI displays a maximum centered at 347 nm (Fig. 6A), indicating that Trp53 is embedded in a polar environment. However, fluorescence quenching experiments with acrylamide (see Fig. 6B) indicate that Trp53 in N-DmI is not exposed to the solvent. These spectral features are fully consistent with the conformation that DmI assumes in the crystal structure of full-length β2GpI (11,12), where Trp53 is shielded from the solvent, with an accessible surface area of the indolyl moiety of only 5 $Å^2$, while the indole N-H group is hydrogen bonded to the carbonyl oxygen of Pro5 (11). Hydrogen bonding involving the indolyl N-H group is indeed the major cause of the red-shift in the λ_{max} emission of Trp (27). Reduction of disulfide bonds in R-DmI results in a 20% increase in fluorescence intensity, a small red shift in the λ_{max} value from 347 to 350 nm, and the appearance of tyrosine contribution as a shoulder at 303 nm (Fig. 6A). Very similar spectral features are observed by treating N-DmI with 8 M urea or 7 M Gnd-HCl (not shown). In the latter case, the fluorescence intensity was enhanced by more than six-fold (see Fig. 8A). The absence of Tyr-band in N-DmI can be explained considering that upon folding two of the three Tyr-residues (i.e., Tyr22 and Tyr30) are brought within Förster distance from Trp53 (~12 Å), with a resulting quenching of Tyr fluorescence (28). On the other hand, the remarkable reduction of fluorescence intensity observed in the folded N-DmI can be well explained in the light of the three-dimensional structure of DmI in β2GpI, whereby Trp53 is stacked against the disulfide bond Cys4-Cys47 (11,12). Notably, disulfides are known to dramatically quench Trp fluorescence by an electron transfer mechanism (29).

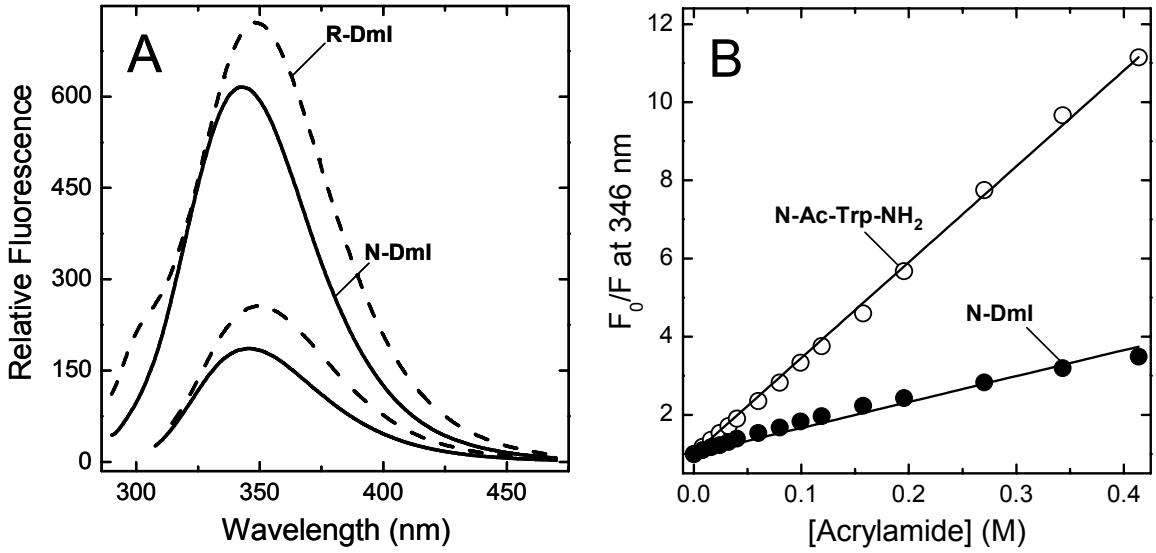

Figure 6. Fluorescence spectra and quenching experiments of DmI species. **A**: Fluorescence spectra. Protein samples (0.5 μM, 1.5 ml) were excited at 280 (upper curves) or 295 nm (lower curves). N-DmI (—), disulfide folded DmI; R-DmI (---), DmI with reduced disulfide bonds. For disulfide containing species (i.e., N-DmI) the spectra were recorded at a constant temperature (i.e., 25°C± 0.1°C) in sodium phosphate buffer, pH 7.4, containing 0.15 M NaCl. When the reduced species was being studied, spectra were taken in 50 mM ammonium acetate buffer, pH 4.5, to avoid disulfide scrambling. **B**: Acrylamide quenching of fluorescence of N-DmI (●-●) and N^{α}-acetyl-Trp-NH_2 (○-○). Fitting of data points to the Stern-Volmer equation (see Methods) yields K_{sv} values of 6.6±0.7 and 25±1.2 M^{-1} for N-DmI or N^{α}-acetyl-Trp-NH_2.

Circular dichroism. A figure of about 53% of β-sheet secondary structure can be deduced from the X-ray structure of DmI in β2GpI (11,12). Notwithstanding, the far-UV CD spectrum of N-DmI does not conform to the features typical of a β-sheet protein, usually displaying a negative band at 210-215 nm and a positive band at 195-198 nm (30). The spectrum of N-DmI, instead, resembles that of the model compound N^{α}-acetyl-Trp-NH_2 (Fig. 7A and Inset), with a negative absorption below 220 nm and a distinct positive band at 230 nm. Of note, this band disappears when the disulfide bonds are broken (Fig. 7A) and the spectrum of the reduced species, R-DmI, becomes that typical of an unfolded polypeptide chain (30). The unusual band at 230 nm can be assigned to the absorption of aromatic amino acids and in particular to Trp53 that in the β2GpI structure interacts with Cys4-Cys47 and Tyr22. The contribution of aromatics to the far-UV CD is indeed most prominent in proteins displaying low CD signal (i.e., like β-sheet proteins) and containing interacting aromatics (31). Of note, three aromatic pairs can be identified in the structure of DmI in β2GpI: Phe12-Tyr36, Tyr30-Phe45, and Tyr22-Trp53 (11,12). The near-UV CD spectrum of N-DmI (Fig. 7B) displays an extensive vibronic structure, demonstrating that, after *in vitro* folding, the synthetic peptide acquires a well defined and compact fold (32). In particular, the 6-nm spaced bands at 263 and 269 nm can be assigned to the contribution of the Phe-residues, while the absorption of the three tyrosines appears as a shallow band at 280 nm, superimposed to the dominant negative ^1L_b band of Trp53 occurring at 285 and 293 nm (32).

The presence of this band is consistent with the three-dimensional structure of β2GpI showing that the single Trp53 is embedded in a rigid and asymmetric environment (see Fig. 1B) (11).

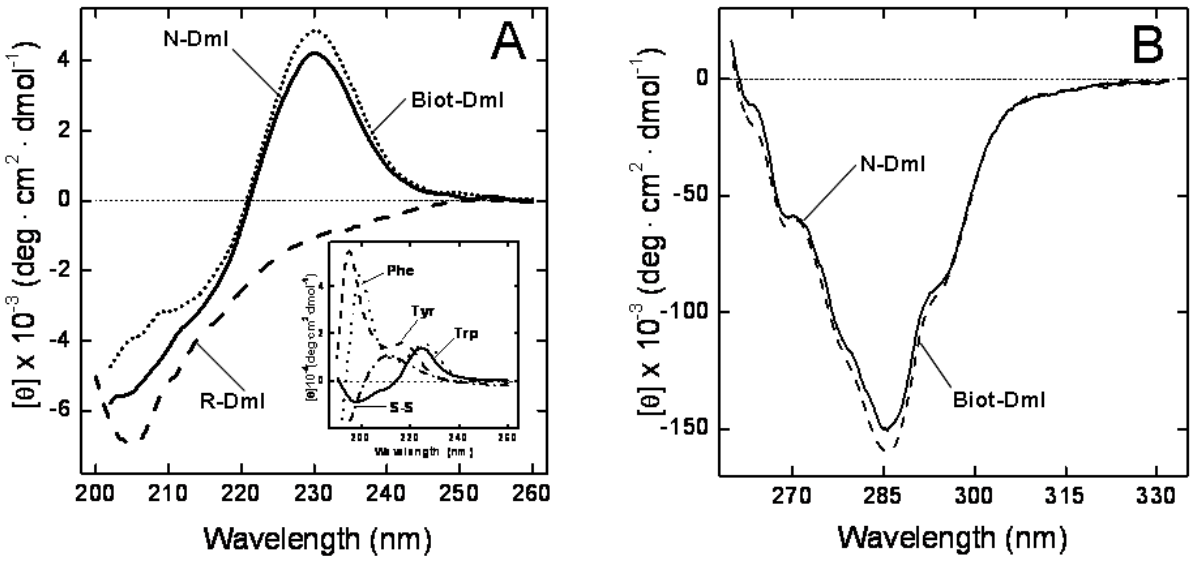

Figure 7. Circular dichroism spectra of N-DmI, R-DmI and Biotin-N-DmI. **A**: Far-UV CD spectra. **B**: Near-UV CD spectra. CD spectra were recorded at a protein concentration of 20 and 140 μM in the far- and near-UV region, respectively. **Inset**: Far-UV CD spectra of the model compounds cystine and N^{α}-acetyl-amide derivatives of Tyr, Phe, and Trp, as indicated. CD data for model compound solutions are expressed as molar ellipticity.

Thermodynamic stability

Taking advantage of the denaturant-dependent increase of fluorescence intensity, we monitored the denaturation of N-DmI as a function of urea or Gnd-HCl concentration (Fig. 8A). In both cases, the fluorescence change was fully reversible. In the presence of Gnd-HCl the denaturation curve displayed a sigmoidal shape, indicative of cooperative unfolding transition, whereas in the presence of urea the emission of N-DmI gradually increased without a distinct transition, in agreement with the well known lower denaturant potency of urea compared to that of Gnd-HCl. Analysis of the fluorescence data was carried out within the assumption of a two-state denaturation process (33,34) and allowed us to determine a $[\text{Gnd-HCl}]_{1/2}$ value of 2.8±0.1 M, with a denaturation index m = -1.5±0.1 kcal/(mol·M). Linear extrapolation of denaturation free energy change, ΔG_D, to [Gnd-HCl] = 0 yielded a $\Delta G_D°$ of 4.4±0.1 kcal·mol^{-1} at 25°C. Denaturation of N-DmI was also monitored by recording the decrease of the CD signal at 230 nm as a function of temperature increase (Fig. 8B). Even in this case, the unfolding process was highly cooperative and fully reversible, with a melting temperature, T_m, of 64.5±0.1°C. Classical van't Hoff analysis of the thermal denaturation curve yielded a ΔG_D value 3.3±0.1 kcal·mol^{-1} or 4.5±0.1 kcal·mol^{-1} at 37 and 25°C, respectively. The latter value is identical to that estimated from Gnd-HCl induced denaturation of N-DmI at the same temperature. It is interesting to note that both $[\text{Gnd-HCl}]_{1/2}$ and T_m values determined for N-DmI are very similar to those previously estimated for the full-length β2GpI (i.e., $[\text{Gnd-HCl}]_{1/2} \sim 2.5$ M and T_m = 63.5±0.1°C) (8,35). These findings reflect the internal sequence and structural similarity of β2GpI and suggest that the protein domains behave independently during unfolding, in keeping with the inherent interdomain flexibility of β2GpI (13).

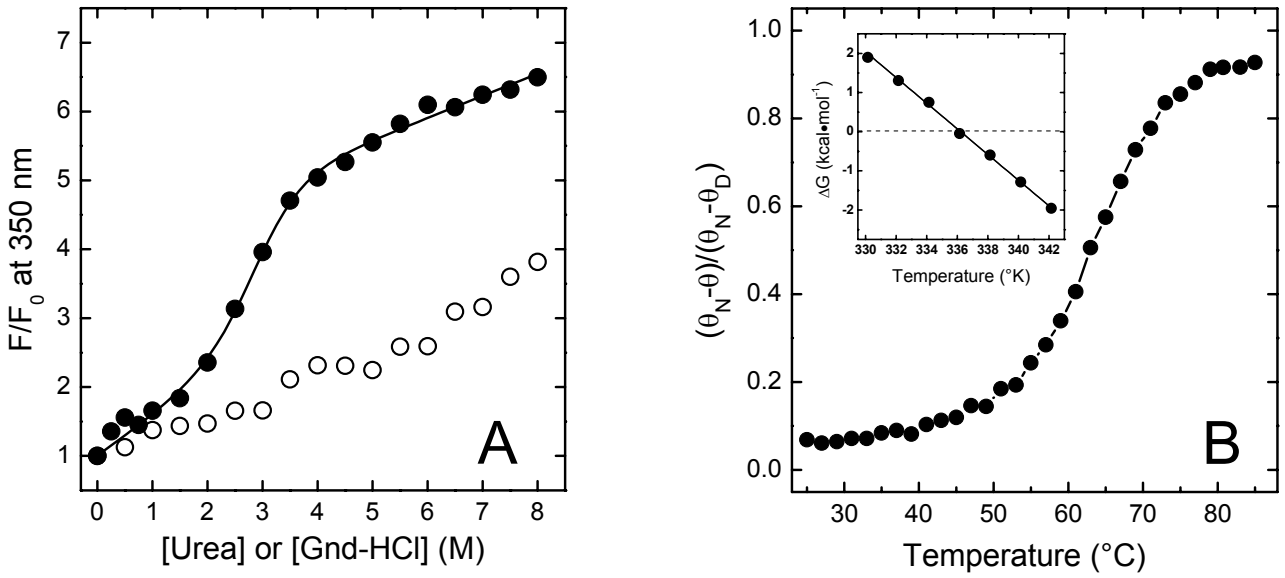

Figure 8. Stability of N-DmI. A: Denaturation of N-DmI induced by Gnd-HCl (●-●) and urea (○-○). Protein samples (1.5 ml, 0.5 μM) were excited at 280 nm and the fluorescence intensity was recorded at 350 nm as a function of denaturant concentration. Fluorescence data are expressed as the ratio F/F_0, where F_0 and F are the fluorescence intensities of DmI in the absence or in the presence of denaturant. Continuous line represents the best fit of data points to equation 1, yielding a $[Gnd\text{-}HCl]_{1/2}$ value of 2.8±0.1 M. **B**: Thermal denaturation of N-DmI (●-●). Denaturation was followed by recording the CD signal of the protein (2 μM) at 230 nm as a function of the sample temperature. CD signal is expressed as the ratio $(\theta_N\text{-}\theta)/(\theta_N\text{-}\theta_D)$, where θ is the ellipticity at a given temperature, while θ_N and θ_D are the ellipticity values recorded at the lowest and highest temperature explored, respectively. **Inset**: Temperature dependence of the free energy change of denaturation, ΔG_D, of N-DmI (●-●). All measurements were carried out at 25±0.1°C in 20 mM sodium phosphate buffer, pH 7.5, containing 0.15 M NaCl. The thermodynamic data derived from thermal denaturation curve were calculated within the approximation of a two-state model (see Methods) and van't Hoff analysis yielded ΔH_m and ΔS_m values of 47±2 kcal·mol^{-1} and 138±5 cal/(mol·K), respectively, and a ΔC_p value of 390±50 cal/(mol·K).

Despite the relatively high resistance to chemical and thermal denaturation, the difference in free energy between the denatured and native state, ΔG_D, of N-DmI is only 6-7 fold larger than the energy due to thermal motion of molecules at 37°C (i.e., R·T ~0.6 kcal/mol). This behaviour is quite common in small-size globular proteins and arises from the low values of the denaturation index, *m*, and heat capacity change of unfolding, ΔC_p, that characterize their chemical or thermal denaturation (36). In the case of N-DmI, however, two additional factors contribute to protein stability: the presence of disulfide bridges and high proline content. In N-DmI structure, Cys4-Cys47 and Cys32-Cys60 cross-link the N- and C-terminal ends to the central β-sheet and thus can stabilize local interactions in the native state. On the other hand, the two disulfides can also stabilize N-DmI by reducing the conformational entropy of the polypeptide in the unfolded state, with a resulting lower entropy change of unfolding, ΔS_D (37). Similar considerations apply for the presence in N-DmI of nine Pro-residues, which account for a relative abundance of 14%, much higher than the frequency of Pro found in natural proteins (i.e., 4.8%). The pyrrolidine ring, in fact, imposes severe steric constrains to the polypeptide chain preferentially in the unfolded state, with a resulting decrease of ΔS_D and an increase in ΔG_D (38).

ELISA competition experiments

The ability of N-DmI to competitively inhibit binding of anti-β2GpI Abs to natural β2GpI was investigated by absorbing purified β2GpI onto hydrophilic plates and then incubating the plates with increasing concentrations of N-DmI. Natural β2GpI and RC-DmI (i.e., Cys-reduced and carboxamidomethylated DmI) were used as a positive and negative control, respectively. A fixed volume of plasma from three patients affected by APS was added in all experiments and the residual amount of aPL-Abs remaining on the plate was quantified by using a secondary alkaline phosphatase-conjugated anti-human IgG antibody detection method. The selected patients (P1, P2, and P3) displayed triple positivity in specific assays for Lupus Anticoaglant (LAC^+), anticardiolipin antibodies (IgG aCL^+), and anti-β2GpI antibodies (IgG $a\beta2GpI^+$). Fitting of data points shown in Fig. 9 allowed us to estimate the IC_{50} values reported in Table 3. Altogether, our data can be summarized as follows: firstly, free β2GpI competes with plate-bound β2GpI for binding to anti-β2GpI Abs, with a mean IC_{50} value of 6.4 μM, similar to that reported by others (39). This finding seems to argue against the existence of a cryptic epitope in DmI and suggests that the major antigenic epitope is constitutively expressed in the full-length protein in solution, accessible for binding to anti-β2GpI autoantibodies (18). Secondly, the synthetic N-DmI can effectively compete with immobilized β2GpI for binding to anti-β2GpI aAbs, with a mean IC_{50} value only 30% lower than that of full-length β2GpI. Thirdly, the unfolded RC-DmI was unable to inhibit binding of antibodies from plasma patients to immobilized β2GpI, up to the highest concentration of RC-DmI tested (i.e., 48 μM), in agreement with previous results obtained with full-length β2GpI. These results indicate that the antigenic epitope on DmI is nonlinear and is formed only after the protein domain folds into the native-like structure.

Table 3. IC_{50} values (μM) obtained by ELISA competition binding experiment [a]

Patient	β_2GpI	N-DmI	RC-DmI
P1	5.1 ± 0.8	7.1 ± 0.6	n.d. [b]
P2	7.1 ± 1.1	11.7 ± 2.7	n.d. [b]
P3	7.0 ± 2.1	7.8 ± 1.7	n.d. [b]

[a] IC_{50} values were obtained by fitting the data of Figure 8 to equation 4.
[b] n.d.: not determinable in the concentration range explored.

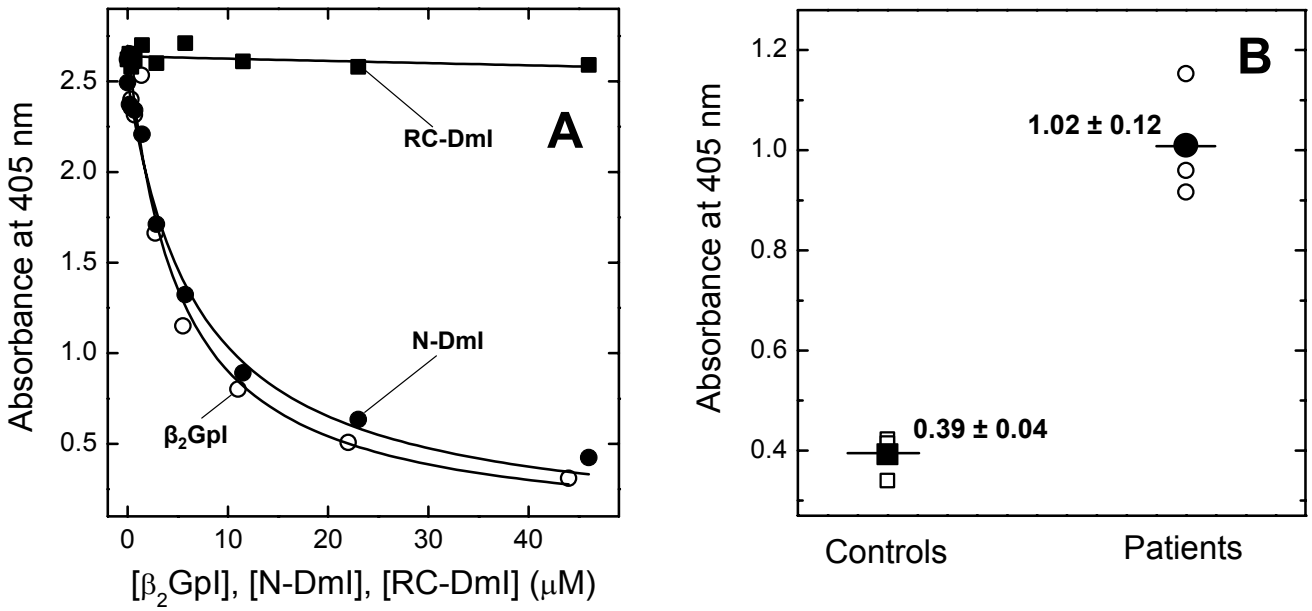

Figure 9. ELISA experiments. **A**: Competitive inhibition experiments with plate-bound β2GpI were carried out by mixing diluted plasma from APS patients with an equal volume of a solution at increasing concentrations of competitor: β2GpI (○), N-DmI (●), and RC-DmI (■). The resulting solution was added to β2GpI-coated wells and incubated for 1 hr at 37°C. After washing, quantification of anti-β2GpI Abs still bound to the microplate-absorbed β2GpI was performed by using a secondary alkaline phosphatase-conjugated anti-human IgG antibody in the presence of pNPP. The release of p-nitrophenol was determined by measuring the absorbance of the solution at 405 nm, after incubation for 30 min at 25°C. Fitting of data points to equation 4 yielded the IC_{50} values reported in Table 1. **B**: Direct binding ELISA experiments were carried out by incubating streptavidin-coated microtiter plates with a solution of Biotin-N-DmI. Thereafter, a fixed volume of plasma from selected APS patients was added and quantification of anti-β2GpI Abs bound to Biotin-N-DmI was carried out as detailed in A. Open symbols (○, □) refer to the experimental values, whereas filled symbols (●, ■) are the average values together with the standard deviation.

Synthesis and Characterization of N-biotinyl-NH-$(PEG)_2$-N-DmI

To demonstrate the utility of the chemical accessibility to β2GpI domain I, we produced by solid-phase peptide synthesis a biotinylated N-terminal derivative of N-DmI (Biotin-N-DmI) (Fig. 1B), to be used for developing novel avidin-biotin ELISA systems in the diagnosis of APS. Biotin-N-DmI was refolded and purified as detailed for wild-type N-DmI. The chemical identity and homogeneity of biotin-N-DmI was established by RP-HPLC (Fig. 3B) and mass spectrometry (Table 1), that yielded a molecular mass of 7701.9±0.6 a.m.u, consistent with the incorporation of the N-biotinyl-NH-$(PEG)_2$-CO-moiety (Fig. 1B). Of note, biotin-N-DmI elutes in RP-HPLC later than N-DmI, in agreement with the apolar nature of biotin (Fig. 3B). The comparative analysis of the CD spectra in the far- and near-UV region well documents that N-terminal extension with N-biotinyl-NH-$(PEG)_2$-CO- does not alter neither the secondary nor tertiary structure of N-DmI (Fig. 7).

Finally, a direct ELISA system was developed to test whether plate-immobilized Biotin-N-DmI was able to recognize anti-β2GpI aAbs in the plasma of APS patients. With this aim, a Biotin-N-DmI solution (200 μl, 25 μg/ml) was incubated with strepatvidin-coated 96-wells plates. Thereafter, a fixed volume of plasma from the triple positive P1, P2 and P3 APS patients, previously selected, was added in

each well and the residual amount of aPL-Abs remaining on the plate was quantified by using the secondary alkaline phosphatase-conjugated anti-human IgG antibody detection method previously described. Strikingly, the data shown in Fig. 9B clearly indicate that biotin-N-DmI can effectively discriminate between the plasma of APS patients and the plasma of healthy subjects, used as controls. Notably, when the synthetic wild-type N-DmI was coated onto a plastic plate it failed to recognize anti-β2GpI aAbs in direct ELISA experiments (not shown), likely because the plate-bound N-DmI was poorly accessible for interaction with aAbs (40). In the case of biotin-N-DmI, instead, N-DmI is properly spaced (within ~ 24 Å distance) form the biotin-streptavidin complex on the plate by a 20-atom linker (see Fig. 1B) and thus it is ready for interaction.

DISCUSSION

Arterial and venous thrombosis are the most frequent clinical manifestations of APS (2), which strongly associate to high titers of autoantiboidies directed against domain I of β2GpI (6,22). To date, the only treatment proven to reduce the risk of thrombosis in APS is life-long anticoagulation, which often has severe side effects (3). Despite antithrombotic therapy, a significant proportion of patients with APS undergo re-thrombosis (41), likely because anticoagulant therapy affects only the final outcome, without interfering with the early biochemical events from which thrombotic events originates, that is production of anti-β2GpI Abs and binding to β2GpI (19,22,42). Hence, the possibility to identify a molecule which is able to block anti-β2GpI Abs activities could disclose new therapeutic strategies in APS. With respect to this, the recombinant N-terminal β2GpI domain I (rDmI) has been expressed in submilligram quantities in *E. coli* as a C-terminally -Gly-$(His)_6$-tagged derivative to facilitate purification (43). More recently, rDmI has been shown to inhibit the activity of pathogenic anti-β2GpI Abs in mice (44).

Here we have demonstrated that large quantities (>30 mg) of correctly folded and functionally active DmI can be produced in high yields in a fast (<2 weeks) and convenient way by chemical methods for future structural (i.e., NMR) and functional studies. The purity of the synthetic DmI was ascertained by RP-HPLC, SDS-PAGE and mass spectrometry, while its chemical identity and the correctness of disulfide pairing was established by peptide mass fingerprint analysis with trypsin and chymotrypsin. All spectroscopic data herein reported are fully consistent with the crystal structure of DmI in natural β2GpI and concurrently indicate that the synthetic N-DmI has a native-like structure (11). This finding is particularly important and allows us to interpret antibody binding properties of N-DmI on the basis of the structure it assumes in the natural β2GpI (11). The results of ELISA competition experiments (Fig. 9A and Table 3) indicate that the synthetic N-DmI is able to effectively inhibit

binding of anti-β2GpI aAbs to plate-immobilized β2GpI with an affinity similar to that exhibited by full-length β2GpI. The versatility of solid-phase peptide synthesis will be also exploited in structure-activity-relationship studies for improving the affinity of DmI for anti-β2GpI Abs by incorporating coded and noncoded amino acids with tailored side chains (45).

Besides the typical clinical manifestations of APS, the diagnosis of this autoimmune disease greatly depends upon laboratory diagnostics that, however, is complicated by the limited specificity of existing assays for detecting clinically relevant antiphospholipid antibodies (19,46). Plasma of APS patients, in fact, contain pathogenic anti-β2GpI aAbs predominantly recognizing DmI (4), and non-pathogenic anti-β2GpI aAbs, recognizing β2GpI domains different from DmI (18). Therefore, ELISA systems based on direct interaction of aAbs with immobilized β2GpI do not allow us to safely take high titers of anti-β2GpI aAbs as a reliable risk factor of thrombosis in APS patients (19,46).

The data shown in Fig. 9B clearly demonstrate that streptavidin-bound Biotin-N-DmI can selectively recognize in direct ELISA experiments anti-β2GpI aAbs from APS patients with a history of thrombosis and displaying triple positivity for Lupus Anticoaglant (LAC^+), anticardiolipin antibodies (IgG aCL^+), and anti-β2GpI antibodies (IgG $a\beta2GpI^+$) (Table 4). These results are unprecedented and disclose novel opportunities for developing reliable diagnostic tools based on avidin/biotin ELISA systems. With respect to this, systematic experiments are undergoing in our laboratories to reduce the background signal of plasma samples in control subjects and to validate our data with a much larger set of patients displaying different clinical manifestations of APS. Preliminary results also indicate that pathogenic aAbs can be easily purified form APS plasma patients by immunoaffinity chromatography using Biotin-N-DmI bound to a streptavidin-linked column (unpublished). In conclusion, we have shown here that large quantities of correctly folded and functionally active DmI can be conveniently produced by chemical methods for potential therapeutic and diagnostic applications in APS.

Table 4. Serological Features of Tested Patients

Patient	LA mix 1:1/ctrl*	aCL IgG/IgM	anti-β2 IgG/IgM
P1	1.04	148/0	218/4
P2	2.04	60/12	340/4
P3	2.02	224/3	392/3

* Ratio of the dRVVT (diluted Russel Venom Time) calculated by dividing the dRVVT obtained by a mixture 1:1 patient:control for the dRVVT of the control

REFERENCES

1. Wilson WA, Piette JC, Brey R, Derksen RH, Harris EN, Hughes GRV, Triplett DA, Khamashta MA (1999) International consensus statement on preliminary classification criteria for definite antiphospholipid syndrome: report of an international workshop. Arthritis Rheum 4:1309–1311.
2. Levine JS, Branch DW, Rauch, J. (2002) The antiphospholipid syndrome. *N. Engl J Med* 346:752-763.
3. Giannakopoulos B, Krilis SA (2009) How I treat the antiphospholipid syndrome. *Blood* 114:2020-2030.
4. de Laat B, Pengo V, Pabinger I, Musial J, Voskuyl AE, Bultink IE, Ruffatti A, et al. (2009) The association between circulating antibodies against domain I of beta2-glycoprotein I and thrombosis: an international multicenter study. *J Thromb Haemost* Aug 19.
5. Lee NS, Brewer HB Jr, Osborne JC Jr (1983) Beta 2-Glycoprotein I. Molecular properties of an unusual apolipoprotein, apolipoprotein H. *J. Biol. Chem*. 258:4765-4770.
6. de Laat B, Derksen RH., de Groot, PG (2004) Beta(2)-Glycoprotein I, the playmaker of the antiphospholipid syndrome. *Clin Immunol* 112:161-168.
7. de Laat B, Derksen RH, Urbanus RT, de Groot PG (2005) IgG antibodies that recognize epitope Gly40-Arg43 in domain I of beta 2-glycoprotein I cause LAC, and their presence correlates strongly with thrombosis. *Blood* 105:1540-1545.
8. Lozier J, Takahashi N, Putnam FW (1984) Complete amino acid sequence of human plasma beta 2-glycoprotein I. *Proc Natl Acad Sci USA* 81:3640-3644.
9. Bendixen E, Halkier T, Magnusson S, Sottrup-Jensen L, Kristensen T (1992) Complete primary structure of bovine beta 2-glycoprotein I: localization of the disulfide bridges. *Biochemistry* 31:3611-3617.
10. Bork P, Downing AK, Kieffer B, Campbell ID (1996) Structure and distribution of modules in extracellular proteins. *Q Rev Biophys* 29:119-167.
11. Bouma B, de Groot PG, van den Elsen JM, Ravelli RB, Schouten A, Simmelink MJ, Derksen RH, Kroon J, Gros P (1999) Adhesion mechanism of human beta(2)-glycoprotein I to phospholipids based on its crystal structure. *EMBO J* 18:5166-5174.
12. Schwarzenbacher R, Zeth K, Diederichs K, Gries A, Kostner GM, Laggner P, Prassl R (1999) Crystal structure of human beta2-glycoprotein I: implications for phospholipid binding and the antiphospholipid syndrome. *EMBO J* 18:6228-6239.
13. Hammel M, Kriechbaum M, Gries A, Kostner GM, Laggner P, Prassl R (2002) Solution structure of human and bovine beta(2)-glycoprotein I revealed by small-angle X-ray scattering. *J Mol Biol* 321:85-97.

14. Hoshino M, Hagihara Y, Nishii I, Yamazaki T, Kato H, Goto Y (1998) Identification of phospholipid-binding site of human β2-Glyprotein I domain V by hereonuclear magnetic resonance. *J Mol Biol* 304:927-939.
15. Iverson GM, Victoria EJ, Marquis DM (1998) Anti-β_2 glycoprotein I autoantibodies recognize an epitope on the first domain of β_2GPI. *Proc Natl Acad Sci* USA 95:15542-15546.
16. Iverson GM, Reddel SW, Victoria EJ, Cockerill KA, Wang YX, Marti-Renom MA, et al. (2002) Use of single point mutations in domain I of β_2-glycoprotein I to determine fine antigenic specificity of antiphospholipid autoantibodies. *J Immunol* 169:7097-7103.
17. Ioannou Y, Pericleous C, Giles I, Latchman DS, Isenberg DA, Rahman A (2007) Binding of antiphospholipid antibodies to discontinuous epitopes on domain I of human beta(2)-glycoprotein I: mutation studies including residues R39 to R43. *Arthritis Rheum* 56:280-290.
18. Giles IP, Isenberg DA, Latchman DS, Rahman A (2003) How do antiphospholipid antibodies bind beta2-glycoprotein I? *Arthritis Rheum* 48:2111-2121.
19. Giannakopoulos B, Passam F, Rahgozar S, Krilis SA (2007) Current concepts on the pathogenesis of the antiphospholipid syndrome. *Blood* 109:422-430.
20. Hulstein JJ, Lenting PJ, de Laat B, Derksen RH, Fijnheer R, de Groot PG (2007) Beta2-Glycoprotein I inhibits von Willebrand factor dependent platelet adhesion and aggregation. *Blood* 110:1483-1491.
21. Sikara MP, Routsias JG, Samiotaki M, Panayotou G, Moutsopoulos HM, Vlachoyiannopoulos PG (2009) Beta2-glycoprotein I (beta-2GPI) binds platelet factor 4 (PF4): implications for the pathogenesis of antiphospholipid syndrome. *Blood*, DOI: blood-2009-03-206367v1.
22. Meroni PL (2008) Pathogenesis of the antiphospholipid syndrome: an additional example of the mosaic of autoimmunity. *J Autoimmun* 30:99-103.
23. Rand JH (2007) The antiphospholipid syndrome. Hematology Am Soc Hematol Educ Program 136-142.
24. Wurm H (1984) Beta2-glycoprotein-I (apolipoprotein H) interactions with phospholip vescicles. Int *J Biochem* 16:511-515.
25. De Filippis V, Draghi A, Frasson R, Grandi C, Musi V, Fontana A, Pastore A (2007) *o*-Nitrotyrosine and *p*-iodophenylalanine as spectroscopic probes for structural characterization of SH3 complexes. *Protein Sci* 16:1257-1265.
26. Brandts JF, Halvorson HR, Brennan M (1975) Consideration of the possibility that the slow step in protein denaturation reactions is due to cis–trans isomerism of proline residues. *Biochemistry* 14:4953–4963.
27. Vivian JT, Callis PR (2001) Mechanisms of tryptophan fluorescence shifts in proteins. *Biophys J* 80:2093-2109.

28. Lakowicz JR (1999) In *Principles of Fluorescence Spectroscopy* 2nd ed., Kluwer Academic/Plenum, New York.
29. Chen Y, Barkley MD (1998) Toward understanding tryptophan fluorescence in proteins. *Biochemistry* 37:9976-82.
30. Brahms S, Brahms J (1980) Determination of protein secondary structure in solution by vacuum ultraviolet circular dichroism. *J Mol Biol* 138:149-178.
31. De Filippis V, De Dea E, Lucatello F, Frasson R (2005) Effect of Na^+ Binding on the Conformation, Stability, and Molecular Recognition Properties of Thrombin. *Biochem J* 390:485-492.
32. Strickland EH (1974) Aromatic contributions to circular dichroism spectra of proteins, CRC *Crit Rev Biochem* 3:113-175.
33. Pace, CN (1986) Determination and analysis of urea and guanidine hydrochloride denaturation curves. *Methods Enzymol* 131:266-280.
34. Eftink MR (1994) The use of fluorescence methods to monitor unfolding transitions in proteins. *Biophys J* 66(2 Pt 1):482-501.
35. Hammel M, Schwarzenbacher R, Gries A, Kostner GM, Laggner P, Prassl R (2001) Mechanism of the interaction of beta(2)-glycoprotein I with negatively charged phospholipid membranes. *Biochemistry* 40:14173-14181.
36. Myers JK, Pace CN, Scholtz JM (1995) Denaturant m values and heat capacity changes: relation to changes in accessible surface areas of protein unfolding. *Protein Sci* 4:2138-2148.
37. Harrison PM, Sternberg MJ (1994) Analysis and classification of disulphide connectivity in proteins. The entropic effect of cross-linkage. *J Mol Biol* 244:448-463.
38. Matthews BW, Nicholson H, Becktel WJ (1987) Enhanced protein thermostability from site-directed mutations that decrease the entropy of unfolding. *Proc Natl Acad Sci USA* 84:6663-6667.
39. Tincani A, Spatola L, Prati E, Allegri F, Ferremi P, Cattaneo R, Meroni P, Balestrieri G (1996) The anti-beta2-glycoprotein I activity in human anti-phospholipid syndrome sera is due to monoreactive low-affinity autoantibodies directed to epitopes located on native beta2-glycoprotein I and preserved during species' evolution. *J Immunol* 157:5732-5738.
40. Iverson GM, Matsuura E, Victoria EJ, Cockerill KA, Linnik MD (2002) The orientation of beta2GPI on the plate is important for the binding of anti-beta2GPI autoantibodies by ELISA. *J Autoimmun* 18:289-297.
41. Cervera R, Khamashta MA, Shoenfeld Y, Camps MT, Jacobsen S, Kiss E et al. (2009) Morbidity and mortality in the antiphospholipid syndrome during a 5-year period: a multicentre prospective study of 1000 patients. *Ann Rheum Dis* 68:1428-1432.
42. Shoenfeld Y, Meroni PL, Cervera R (2008) Antiphospholipid syndrome dilemmas still to be solved: 2008 status. *Ann Rheum Dis* 67:438-442.

43. Ioannou Y, Giles I, Lambrianides A, Richardson C, Pearl LH, Latchman DS, Isenberg DA, Rahman A (2006) A novel expression system of domain I of human beta2 glycoprotein I in Escherichia coli. *BMC Biotechnol* 6:8.
44. Ioannou Y, Romay-Penabad Z, Pericleous C, Giles I, Papalardo E, Vargas G, Shilagard T, Latchman DS, Isenberg DA, Rahman A, Pierangeli S (2009) In vivo inhibition of antiphospholipid antibody-induced pathogenicity utilizing the antigenic target peptide domain I of beta2-glycoprotein I: proof of concept. *J Thromb Haemost* 7:833-842.
45. De Filippis V, Colombo G, Russo I, Spadari B, Fontana A (2002) Probing Hirudin-Thrombin Interaction by Incorporation of Noncoded Amino Acids. *Biochemistry* 41:13556-13569.
46. Urbanus RT, Derksen RH, de Groot PG (2008) Current insight into diagnostics and pathophysiology of the antiphospolipid syndrome. *Blood Rev* 22:93-105.
47. Atherton E, Sheppard RC (1989) In *Solid phase peptide synthesis*. IRL Press. Oxford, UK
48. Pace CN, Vajdos F, Fee L, Grimsley G, Gray T (1995) How to measure and predict the molar absorption coefficient of a protein. *Protein Sci* 11:2411-2423.
49. De Filippis V, De Antoni F, Frigo M, Polverino de Laureto P, Fontana A (1998) Enhanced Protein Thermostability by *Ala→Aib* Replacement *Biochemistry* 37:1686-1696.
50. Pengo V, Biasiolo A, Fior MG (1995) Autoimmune antiphospholipid antibodies are directed against a cryptic epitope expressed when beta 2-glycoprotein I is bound to a suitable surface. *Thromb Haemost* 73:29-34.
51. Pengo V, Tripodi A, Reber G, Rand JH, Ortel TL, Galli M, de Groot PG (2009) Update of the guidelines for lupus anticoagulant detection. *J Thromb Haemost* 7:17

4. VON WILLEBRAND FACTOR

CHAPTER 4.1

Von Willebrand Factor and ADAMTS-13: It's All About Dimension

Von Willebrand factor (VWF) is a blood glycoprotein that circulate as covalent multimers (up to 200 monomers, up to 50 x 106 Da) and is required for normal haemostasis. Deficiency of VWF, or von Willebrand disease (VWF), is the most common inherited disorder. VWF mediates the adhesion of platelets to sites of vascular damage by binding specific platelet membrane glycoprotein (GpIbα), and to constituents of the exposed connective tissue. Haemostasis depends on the balanced participation of VWF, and this balance reflects a competition between the biosynthesis of large VWF multimers and their degradation by the ADAMTS-13 metalloprotease. In other words, the pro-thrombotic potential of VWF is the result of a dynamic equilibrium between the concentration of large VWF multimers and the proteolytic activity of ADAMTS-13.

VWF multimers are the product of a complex pathway that can be divided into following steps. Endothelial cells and megakaryocytes make proVWF subunits that form dimers within the endoplasmatic reticulum (ER) though disulphide bonds between their C-terminal cysteine knot (CK) domains (1). The ProVWF dimers are transported to the Golgi apparatus where the propeptide facilitates the formation of disulfide-linked VWF multimers. Briefly in the ER, the propeptide forms a disulfide-linked intermediate with the D'D3 domain of VWF. This transient species rearranges into the Golgi to make multimers (2), and multimerization fails if the Golgi is made less acidic with chloroquine or ammonium chloride (3). Thus, the propeptide may function as an endogenous pH-sensitive oxidoreductase, converting intrasubunit disulfide bonds into intersubunit disulfide-bonded multimers. In the *trans* Golgi, the propeptide is cleaved from most subunits, and the multimeric product is secreted immediately or packaged into secretory granules – Weibel-Palade bodies in endothelium or α-granules in platelets- for later secretion (1) (Fig.1).

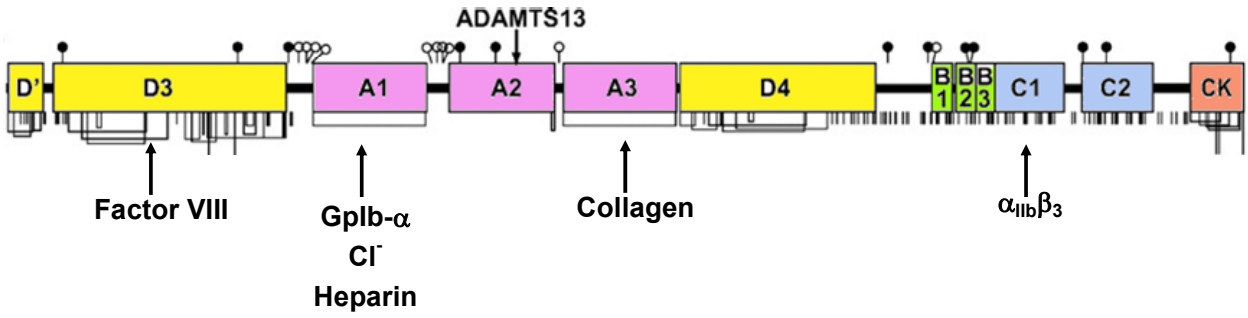

Figure 1. VWF monomeric structure. vWF is a large multidomain protein (2050 AA per monomer) highly glycosylated (10 *O*-linked and 12 *N*-linked sugar chains, indicated as lollipops) and expressed in endothelial cells (EC) and megakaryocytes (see text). In order VWF domain D3 binds to FVIII and its presence accelerate the rate of hydrolysis by ADAMTS-13. VWF domain A1 binds to platelet receptor GpIbα, chloride ions or heparin. VWF A3 doamin binds to exposed exposed connective tissue and VWF domain C1 binds to the $\alpha_{IIb}\beta$3-integrin.

Once in the bloodstream, VWF multimers are cleared with a half-life of 12-40 h (4,5) by a mechanism that may not depend strongly on multimer size (6). At the same time, large multimers are converted into smaller species by ADAMTS-13, which cleaves the Tyr^{1605}-Met^{1606} bond in domain A2 when the VWF multimer is subjected to sufficient fluid shear stress (7-9). The large multimers of VWF are much more pro-thromotic than the lower molecular size species.

ADAMTS-13 is a multidomain protease that is remarkably specific for VWF (Fig.2) (12,16). The structure of ADAMTS-13 is conserved throughout vertebrates, indicating that each of its domain has an important function. Mutagenesis of ADAMTS-13 indicates that the Cys-rich and spacer domains contribute to recognition of VWF (18-20). Conversely, mutagenesis of VWF indicates that part of the C-terminal helix of the VWF A2 domain, 25-30 Å away form the cleavable bond Tyr1605-Met1606, is required for rapid binding and cleavage by ADAMTS-13 (21). Thus it has been first hypothesized and then verified (22,23) the presence of at least one auxiliary binding site on VWF A2 domain. ADAMTS-13 also appears to be regulated by VWF structures outside of the A2 domain. For example, the VWF A1 domain inhibited the cleavage of adjacent A2 domain of several recombinant ADAMTS-13 substrates, and inhibition was relieved when heparin of fragment of GpIbα was bound to the A1 domain (22). Similar regulatory functions have been proposed for VWF domain A3 and the CUB domains of ADAMTS-13. Altogether these studies suggested that binding of VWF to platelets or collagen may promote the cleavage of domain A2 by ADAMTS-13, thereby enhancing the feedback inhibition of VWF-dependent platelet thrombosis.

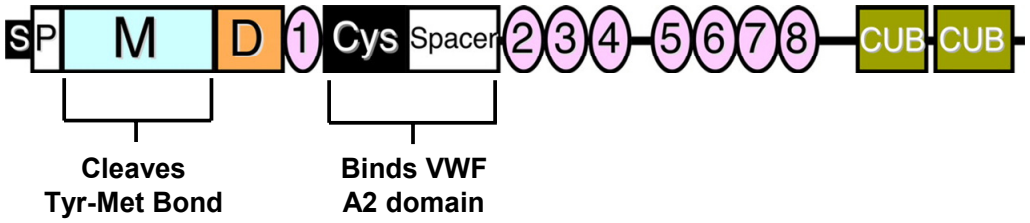

Figure 2. Structure of ADAMTS-13. The primary translation product of ADAMTS-13 consists of a signal peptide (S), a short propeptide (P), a metalloprotease domain (M), a disintegrin-like domain (D), 8 thrombospondin-1 repeats (numbered 1-8), a Cys-rich (Cys) and spacer domain that are characteristic of the ADAMTS family, and two CUB domains. The metalloprotease cleaves Tyr^{1605}-Met^{1606} bond within the unfolded VWF domainA2; the Cys-rich and spacer domain make additional contacts with VWF domain A2. Adapted from (25)

REFERENCES

1. Wagner DD. Cell biology of vonWillebrand factor. *Annu Rev Cell Biol* 1990; 6: 217–46.
2. Purvis AR, Sadler JE. A covalent oxidoreductase intermediate in propeptide-dependent von Willebrand factor multimerization. *J Biol Chem 2004*; 279: 49982–8.

3. Mayadas TN, WagnerDD. In vitro multimerization of vonWillebrand factor is triggered by low pH. Importance of the propolypeptide and free sulfhydryls. *J Biol Chem* 1989; 264: 13497–503.
4. Dobrkovska A, Krzensk U, Chediak JR. Pharmacokinetics, efficacy and safety of Humate-P in von Willebrand disease. *Haemophilia* 1998; 4: 33–9.
5. Menache D, Aronson DL, Darr F, Montgomery RR, Gill JC, Kessler CM, Lusher JM, Phatak PD, Shapiro AD, Thompson AR, White GC II. Pharmacokinetics of von Willebrand factor and factor VIIIC in patients with severe vonWillebrand disease (type 3 VWD): estimation of the rate of factor VIIIC synthesis. *Br J Haematol* 1996; 94: 740–5.
6. Lenting PJ,Westein E, TerraubeV,Ribba AS,Huizinga EG, MeyerD, de Groot PG, Denis CV. An experimental model to study the in vivo survival of vonWillebrand factor. Basic aspects and application to the R1205H mutation. *J Biol Chem* 2004; 279: 12102–9.
7. Tsai HM, Sussman II, Nagel RL. Shear stress enhances the proteolysis of von Willebrand factor in normal plasma. *Blood* 1994; 83: 2171–9.
8. Furlan M, Robles R, La¨mmle B. Partial purification and characterization of a protease from human plasma cleaving von Willebrand factor to fragments produced by in vivo proteolysis. *Blood* 1996; 87: 4223–34.
9. Tsai H-M. Physiologic cleavage of vonWillebrand factor by a plasma protease is dependent on its conformation and requires calcium ion. *Blood* 1996; 87: 4235–44.
10. Dent JA, Galbusera M, Ruggeri ZM. Heterogeneity of plasma von Willebrand factor multimers resulting from proteolysis of the constituent subunit. *J Clin Invest* 1991; 88: 774–82.
11. Furlan M, Robles R, Affolter D, Meyer D, Baillod P, Lammle B. Triplet structure of von Willebrand factor reflects proteolytic degradation of high molecular weight multimers. *Proc Natl Acad Sci USA* 1993; 90: 7503–7.
12. FujikawaK, Suzuki H,McMullen B, ChungD. Purification of human vonWillebrand factor-cleaving protease and its identification as a new member of the metalloproteinase family. *Blood* 2001; 98: 1662–6.
13. Gerritsen HE, Robles R, Lammle B, Furlan M. Partial amino acid sequence of purified von Willebrand factor-cleaving protease. *Blood* 2001; 98: 1654–61.
14. Zheng X, Chung D, Takayama TK, Majerus EM, Sadler JE, Fujikawa K. Structure of von Willebrand factor-cleaving protease (ADAMTS-13), a metalloprotease involved in thrombotic thrombocytopenic purpura. *J Biol Chem 2001*; 276: 41059–63.
15. Levy GG, Nichols WC, Lian EC, Foroud T, McClintick JN, McGee BM, Yang AY, Siemieniak DR, Stark KR, Gruppo R, Sarode R, Shurin SB, Chandrasekaran V, Stabler SP, Sabio H, Bouhassira EE, Upshaw Jr JD, Ginsburg D, Tsai HM. Mutations in a member of the ADAMTS gene family cause thrombotic thrombocytopenic purpura. *Nature* 2001; 413: 488–94.

16. Soejima K, Mimura N, Hirashima M, Maeda H, Hamamoto T, Nakagaki T, Nozaki C. A novel \human metalloprotease synthesized in the liver and secreted into the blood: possibly, the von Willebrand factor-cleaving protease? *J Biochem* 2001; 130: 475–80.
17. Sadler JE. A new name in thrombosis, ADAMTS-13. *Proc Natl Acad Sci USA 2002*; 99: 11552–4.
18. Kokame K, Matsumoto M, Soejima K, Yagi H, Ishizashi H, Funato M, Tamai H, Konno M, Kamide K, Kawano Y, Miyata T, Fujimura Y. Mutations and common polymorphisms in ADAMTS-13 gene responsible for von Willebrand factor-cleaving protease activity. *Proc Natl Acad Sci USA* 2002; 99: 11902–7.
19. Zheng X, Nishio K, Majerus EM, Sadler JE. Cleavage of von Willebrand factor requires the spacer domain of the metalloprotease ADAMTS-13. *J Biol Chem 2003*; 278: 30136–41.
20. SoejimaK,Matsumoto M,Kokame K, YagiH, Ishizashi H,MaedaH, Nozaki C, Miyata T, FujimuraY,Nakagaki T.ADAMTS-13 cysteinerich/ spacer domains are functionally essential for von Willebrand factor cleavage. *Blood* 2003; 102: 3232–7.
21. Kokame K, MatsumotoM, Fujimura Y, Miyata T. VWF73, a region from D1596 to R1668 of von Willebrand factor, provides a minimal substrate for ADAMTS-13. *Blood* 2004; 103: 607–12.
22. Nishio K, Anderson PJ, Zheng XL, Sadler JE. Binding of platelet glycoprotein Iba to von Willebrand factor domain A1 stimulates the cleavage of the adjacent domain A2 by ADAMTS-13. *Proc Natl Acad Sci USA* 2004; 101: 10578–83.
23. Dong JF, Moake JL, Bernardo A, Fujikawa K, Ball C, Nolasco L, Lopez JA, Cruz MA. ADAMTS-13 metalloprotease interacts with the endothelial cell-derived ultra-large vonWillebrand factor. *J Biol Chem* 2003; 278: 29633–9.

CHAPTER 4.2.

Formation of Methionine-sulfoxide by Peroxynitrite at Position 1606 of von Willebrand Factor Inhibits its Cleavage by ADAMTS-13. a New Prothrombotic Mechanism in Diseases Associated with Oxidative stress

Stefano Lancellotti[1#], Vincenzo De Filippis[2#], **Nicola Pozzi**[2], Flora Peyvandi[3], Roberta Palla[3], Bianca Rocca[4], Sergio Rutella[5,6], Dario Pitocco[7], Pier Mannuccio Mannucci[3], and Raimondo De Cristofaro[1,*]

[1]Institute of Internal Medicine and Geriatrics, and Haemostasis Research Centre, Catholic University School of Medicine, Rome, Italy;

2Department of Pharmaceutical Sciences, University of Padua, Italy;

3A. Bianchi Bonomi Hemophilia and Thrombosis Center, University of Milan and Department of Medicine and Medical Specialties, IRCCS Maggiore Hospital, Mangiagalli and Regina Elena Foundation, Luigi Villa Foundation, Milan, Italy;

4 Institute of Pharmacology, Catholic University School of Medicine, 00168 Rome, Italy

5.Department of Hematology, Catholic University School of Medicine, Rome, Italy

6IRCCS San Raffaele Pisana, Rome, Italy;

7Diabetes Care Unit, Department of Internal Medicine, Catholic University School of Medicine, Rome, Italy

Published in Free Radic Biol Med. 2009 Dec 4. [Epub ahead of print]

INTRODUCTION

ADAMTS-13 is a member of the ADAMTS family of metalloproteases (1) composed by a multi-domain enzyme that cleaves VWF exclusively at the peptide bond between Tyr1605 and Met1606 in the A2 domain (1-4). Modulation of the ADAMTS-13/VWF interaction is critical for setting a physiological pattern of VWF multimers. The inhibition of the ADAMTS-13/VWF proteolytic interaction by pathologic autoantibodies is associated with pathological conditions, such as thrombotic microangiopathies (5-7). VWF multimers are cleaved by ADAMTS-13 under physiological conditions of arterial shear stress (≥30 dynes/cm2), where VWF multimers are stretched and expose the buried Tyr1605–Met1606 peptide bond, in the A2 domain for cleavage (3,8-13). Likewise, binding of VWF to its platelet receptor, that is glycoprotein Ibα (GpIbα), is able to stabilize the VWF conformation which becomes suitable for cleavage by the metalloprotease (14,15). By contrast, binding of chloride ions to the A1 domain of VWF and pH values >8.0 can also inhibit proteolysis by ADAMTS-13 (5,16-18)

Thus, only specific biophysical or biochemical factors stabilize in the VWF molecule a conformation suitable to proteolytic attack by ADAMTS-13. After its synthesis, VWF is stored in the Weibel-Palade bodies of the endothelial cell, where a low pH and a proper disulfide bonding drive the packaging of the protein to form highly ordered, rod-like structures (19). Furthermore, the ultra large VWF multimers secreted by endothelial cells are more sensitive than low molecular weight multimers to shear-promoted unfolding (20). Consequently, Tyr1605 and Met1606 of the scissile peptide bond of circulating VWF become more exposed to solvent and, potentially, to oxidizing agents. These modifications may be particularly relevant in several pathological settings, where oxidative stress is exalted and the physiological scavengers defective. Several conditions, including atherogenesis, heart failure, septic shock, coronary artery diseases, and diabetes are associated with an increase of reactive oxygen species (ROS) production, in particular O2•−. Nitric oxide produced by endothelial cells can interact with O2•− and generate peroxynitrite, following the reaction NO + O2•− → ONOO-. This reaction is close to the diffusion-controlled limit, with an average rate constant of about 1010 M-1 s-1 (21). The rates of peroxynitrite production in vivo in selected sub-cellular compartments have been estimated to be as high as 50–100 μM min-1 (22). The steady-state concentrations are estimated to be in the low micromolar concentration range, which, however, can persist for a long intervals (up to hours) (23). Thus, underparticular conditions, the exposure to peroxynitrite can be biologically relevant. Despite the short half-life of peroxynitrite at physiological pH (k=0.9 sec-1 (t1/2= 0.8 sec)), its ability to cross cell membranes (24) implies that this reactive species generated from a cell can influence neighbouring cells or molecules within one to two cell diameters (5–20 μm). Peroxynitrite easily oxidizes some amino acids such as cysteine, methionine and tryptophan. Other amino acids that do not react directly with peroxynitrite (e.g. tyrosine, phenylalanine and histidine) can nevertheless be indirectly modified, through intermediary species, as hydroxyl, carbonate and nitrogen dioxide radicals. All the above mentioned amino acids have indeed the fastest reactivity with oxidants (25). The nucleophilic sulfur atom in the side chain of methionine reacts with peroxynitrite with a second-order rate constant in the range 102-103 M-1 s-1, forming methionine sulfoxide (MetSO) and nitrite (26-28). The oxidation of methionine by peroxynitrite has been observed in many proteins, perturbing their functions (29,30). On the other hand, tyrosine exposure to peroxynitrite leads to formation of 3-nitrotyrosine (NT), 3-hydroxytyrosine and, when the amino acid is free in solution, to 3,3'-dityrosine (31).

As mentioned above, ADAMTS-13 cleaves VWF only at a single Tyr-Met peptide bond in the A2 domain. Based on their high susceptibility to oxidation by peroxynitrite, Tyr1605 and Met 1606 may indeed represent vulnerable sites within the VWF molecule, potentially affecting their cleavage by ADAMTS-13. In the present study, we investigated the effect of peroxynitrite on VWF oxidation, cleavage by ADAMTS-13 and on VWF capacity to interact with its platelet receptor.

MATERIALS AND METHODS

Synthesis of pseudo wild-type VWF74 and its analogs containing NT and MetSO Nα-Fmoc protected amino acids, solvents and reagents for peptide synthesis were purchased from Applied Biosystems (Foster City, CA) or Bachem AG (Bubendorf, Switzerland). All other reagents and solvents were of analytical grade and purchased from Fluka.

The pseudo wild-type peptide VWF74 (NH2-DREQAPNLVYMVTGNPASDEIKRLPGD IQVVPIGVGPNANVQELERIGWPNAPILIQDFETLPREAPDLVLQRA-COOH), encompassing the VWF A2 domain sequence 1596-1669, was synthesized by the solid-phase method using the fluorenyl-methyloxycarbonyl (Fmoc) chemistry (32) on a model PS3 automated synthesizer from Protein Technologies International (Tucson, AZ). In the VWF74 peptide, the C-terminal Cys1669 was replaced by Ala, to avoid any possible disulfide-coupled dimerization. The peptide chain was assembled stepwise on a NovaSyn TGA resin (Novabiochem, Darmstadt, Germany) derivatized with Fmoc-Ala (0.22 mequiv/g). The crude peptide was fractionated by RP-HPLC on a Zorbax (Agilent Technologies, Santa Clara, CA) C18 analytical column, eluted with a linear acetonitrile-0.1% TFA gradient from 25 to 45% in 30 min. The absorbance of the effluent was recorded at 226 nm. The peptide material was analyzed by mass spectrometry on a Mariner ESI-TOF instrument from Perseptive Biosystems (Stafford, TX), which yielded mass values in agreement with the theoretical mass deduced from the amino acid composition of VWF74. The purified peptide was stored at -20°C under nitrogen. Very similar procedures were used for the synthesis, purification and characterization of the two singly substituted analogs of VWF74, in which Tyr1605 was replaced by 3-nitrotyrosine (VWF74-NT) and Met1606 by methionine sulfoxide (VWF74-MetSO).

Spectroscopic measurements on VWF74 peptides. Peptide concentration was determined by UV absorption at 280 nm (33) on a Lambda-2 spectrophotometer from Perkin-Elmer using a molar absorptivity value of 6970 M-1·cm-1, for both VWF74 and VWF74-MetSO. For VWF74-NT, the peptide concentration was determined by UV absorption at 381 nm, using a molar extinction coefficient of 2200 M-1·cm-1 (34). Far-UV CD spectra were recorded on a Jasco (Tokyo, Japan) model J-810 spectropolarimeter equipped with a water-jacketed cell holder. Fluorescence spectra were recorded on a Jasco model FP-6500 spectropolarimeter, equipped with a Peltier temperature control system. Peptide samples (0.5 μM) were excited at 280 or 295 nm, using excitation and emission slits of 10 nm. All spectra were taken at 25 ± 0.1°C in 10 mM in sodium phosphate buffer, pH 7.4, containing 150 mM NaCl.

Oxidation of VWF74 by peroxynitrite The concentration of peroxynitrite was determined measuring the absorbance of the solution at 302 nm (ε=1670 M−1 cm−1) (35). The frozen stock solution was

stored for 4 weeks at −80°C with negligible changes in its concentration. Immediately before use, the stock solution was diluted in sodium hydroxide 100 mM and, during the experiments, was maintained in an ice bath. Because of the very short half-life of peroxynitrite under physiological pH and the reported second order rate constant of reaction with methionine, peroxynitrite was added to VWF74 solution either by a "single shot" (2 µl in 0.1 N NaOH, at final concentrations of 10, 100, 250 and 500 µM) or by "multiple-shot" addition of 10 µM peroxynitrite at a rate of one shot per min. up to 60 min. The VWF74 solution contained 2.5% dimethylformamide instead of DMSO to avoid ROS scavenging. The reference VWF74 solution was treated similarly with NaOH alone. Oxidation products of the VWF peptide substrate were identified by liquid chromatography coupled to mass spectrometry (LC-MS), using a micro pump 200 HPLC system from Perkin-Elmer (Norwalk, CT) connected to a Mariner mass spectrometer. Specifically, 5 µl of a 48 µM VW74 solution in 25 mM Hepes buffer, pH 7.50, containing 75 mM NaCl and 2.5% (v/v) dimethylformamide, were loaded onto a C4 Grace-Vydac microbore column (1 x 50 mm, 5µm granulometry), equilibrated for 20 min at a flow-rate of 20 µl/min with H2O:CH3CN (95:5), containing 1% HCOOH.

Oxidation of VWF multimers by peroxynitrite. VWF from human plasma, was purified as previously described (16). The purity and integrity of this material was checked by SDS-agarose gel (1.5%) for non-reduced samples and by SDS-PAGE gradient gel (4-12%) for reduced samples. The concentration of purified VWF was measured spectrophotometrically at 280 nm, using an extinction coefficient, ε 0.1%, = 0.846 mg-1 cm2, calculated according to the method of Pace et al. (33) and based on the amino acid sequence of VWF monomer. Furthermore, the concentration of VWF as antigen and ristocetin-cofactor was also measured using immunoturbidometric assays ("VWF antigen" and "VWF activity") from Instrumentation Laboratory (Milano, Italy) performed on automatic spectrophotomers ("Top"TM, Instrumentation Laboratory). The VWF preparation was characterized by an activity/antigen ratio = 0.81, thus showing a good protein quality and function. This VWF preparation (0.4 mg/ml) was treated with peroxynitrite (concentration range: 50-250 µM), as detailed above for VWF peptides. Oxidation of this preparation was assessed by western blot analysis using a rabbit polyclonal anti-nitrotyrosine antibodies from Upstate Biotechnology (lot #12-348) and peroxidase-conjugated secondary antibodies purchased from Dako (Milano, Italy). The peroxynitrite-treated VWF was reduced and analyzed by SDS-PAGE on 4-12% polyacrylamide gels. The protein bands were then transferred onto nitocellulose blotting paper (GE Healthcare, Milano, Italy). The electrophoretic bands were detected by enhanced chemi-luminescence technique (ECL, GE Healthcare).

LC-MS analysis of the full-length non-treated or peroxynitrite-treated VWF. Plasma non-treated VWF (125 µl, 0.4 mg/ml) in Tris 0.1M pH 7.5 150 mM NaCl was first reduced for 20 min at 80°C with

a buffer containing 4 mM DTT (5 µl, 120 mM) and then alkylated with 10 mM iodoacetamide (5 µl, 280 mM) for 15 min at 37°C. The reduced and alkylated protein was digested for 24h at 37°C with *Staphylococcus aureus V8* (11 µl, 0.234 mg/ml) (enzyme:substrate ratio 1:20 w/w). To determine if the ADAMTS13 cleavage site –YM is accessible to peroxynitrite even when VWF is in its native multimer state, it was first oxidized by adding 25 µl of a $ONOO^-$ solution (1.59 mM) under continuous stirring. Oxidized VWF was then reduced, alkylatedas and then digested for 24h at 37°C with *Staphylococcus aureus V8*(11 µl, 0.234 mg/ml) (enzyme:substrate ratio 1:20 w/w), as previoulsy described. The reaction mixtures were directly analyzed by LC-MS using the following procedure. Immediately before loading the sample into a Vydac C18 microbore column, 20-25 µl of the proteolysis reaction (7-8 µg = 32 pmols) were added to an acidic solution of 6M Gnd-HCl in H_2O-HCOOH 1% (50-60 µl). The column was extensively washed with H_2O:CH_3CN 1%-HCOOH 1% to desalt the sample and then eluted using an exponential gradient from 1% to 80% of CH_3CN at a flow rate of 10 µl/min. Analysis were performed using a micro pump 200 HPLC system from Perkin-Elmer (Norwalk, CT) connected to a Mariner eletrospray-ionization time of flight (ESI-TOF) mass spectrometer from PerSeptive Biosystems (Stafford, TX).

MS/MS analysis of the peptide containing oxidized methionine. To definitely assign the chemical identity of the peptides that are supposed to contain the sequence of interest (i.e. ^{1599}QAPNLVYMVTGNPASDE^{1615}) we performed MS/MS sequencing experiments. Briefly, 6.4 µl (0.68 pmol/µl) of the previous proteolysis reaction or of a model peptide encompassing exactly the researched sequence, were desalted and then loaded into a Nanoease Waters Atlantis dC18 column (75 µM x 150 mm, 3 µM) at a flow rate of 200 nl/min. The sample was then eluted using a liner gradient from 5 to 70% of CH_3CN-HCOOH 0.1% in 42 min. Experiments were carried out on a tandem mass spectrometer Q-TOF Micro (Micromass, U.K.) equipped with a Z-spray ESI interface. MS/MS spectra were taken only considering chemical species having a m/z ratio of 903.4 ± 0.1 (2+) and 911.4 ± 0.1 (2+) a.m.u. for the native and oxidized peptide, respectively.

Hydrolysis by ADAMTS-13 of genuine VWF74, peroxynitrite-treated VWF74, and the analogs VWF74-NT and VWF74-MetSO. The Michaelis parameters of the hydrolysis of genuine VWF74, peroxynitrite-oxidized VWF74, VWF74-NT and VWF74-MetSO were calculated using 1 or 5 nM recombinant human ADAMTS-13. The latter was expressed in HEK293 cell lines and purified to homogeneity (m.w..≅190 kDa under reducing conditions) using Zn++-agarose affinity chromatography and DEAE-HPLC, as previously described (16). The catalytic specificity of ADAMTS-13 for genuine VWF74 and its derivatives was studied by analyzing the cleavage products by RP-HPLC. The VWF74 peptides were dissolved in 10 mM Hepes, 150 mM NaCl, 2% DMSO, pH 7.50 at 25 °C. Five different concentrations of these peptide substrates, ranging from 2.5 to 40 µM, were incubated in the above

buffer solution with 1 nM ADAMTS-13. At various time intervals (2, 4, 8, and 16 min), aliquots of these solutions were sampled and the hydrolysis reaction stopped using 10 mM EDTA. Sample aliquots (100 μl) were analyzed on a ReproSil-Pur C18-AQ RP-HPLC column (Dr. Maisch GmbH, Ammerbuch-Entringen, Germany), using a double-pump mod. 2080 HPLC apparatus from Jasco (Tokyo, Japan) equipped with a mod. 2070 UV spectrophotometric and FP-2020 fluorescence detectors. The chromatographic peaks were detected by simultaneously recording UV absorbance at 226 nm and emission fluorescence at 350 nm, after excitation at 280 nm. The column was eluted with a linear actenitrile-0.078% TFA gradient from 20 to 60% in 30 min The concentration of the uncleaved species was measured as a function of time (between 0 and 16 min) to derive the initial velocity of peptide hydrolysis by linear regression ($r > 0.95$ in all cases). Then, the hydrolysis rate by ADAMTS-13 was analyzed as a function of VWF74 concentration to calculate the Michaelis-Menten parameters kcat and Km.

Hydrolysis of peroxynitrite-treated VWF samples by ADAMTS-13 Genuine and peroxynitrite-treated VWF samples at a concentration of 20 μg/ml were incubated with 5 nM recombinant ADAMTS-13 (final concentration) in 1.5 mg/ml ristocetin (sulphate-free), 5 mM Tris-HCl, 3 mM CaCl2, pH 8.0 at 37 °C. At 0, 1, and 2 hr, an aliquot (50 μl) of this solution was sampled and the reaction stopped by adding 10 mM EDTA. In separate experiments, VWF was hydrolyzed under shear stress by continuously vortexing the samples at 2500 rpm for 20 min. at room temperature, according to the method of Zhang et al. (36). In these experiments, the samples contained 20 μg/ml VWF and 10 nM ADAMTS-13. In all cases, the hydrolysis of the samples were assessed by SDS-agarose electrophoresis in 1.5% agarose gel and using rabbit anti-human VWF polyclonal antibody and a HRP-conjugated secondary anti-rabbit antibody purchased from Dako, as previously detailed (16).

VWF multimers from human plasma samples. Healthy subjects (n=13) were blood donors from the institutional blood bank of the "A. Gemelli" hospital of the Catholic University School of Medicine, Rome, Italy. They were between 38 and 55 years of age, were in good health, non-smokers and had no risk factors for cardiovascular disease. Subjects with type 2 diabetes mellitus (T2DM, n=16) were consecutively enrolled at the time of diagnosis by the Diabetes Care Unit of the Catholic University School of Medicine of Rome and were not on chronic medications including NSAIDs, vitamin E or statin preparations. Diabetic subjects were age- and sex-matched with controls. Blood samples were collected in 3.8% citrate and rapidly stored at -80 °C. The plasma level of VWF was measured as antigen, using an immunoturbidometric assay (HemosIL von Willebrand Factor, Instrumentation Laboratory) and the automatic coagulometer model Top from Instrumentation Laboratory. The ristocetin cofactor was measured using ristocetin from Helena Laboratories (Beaumont, TX) at a final concentration of 1.5 mg/ml. The ristocetin-induced platelet agglutination was studied with lyophilized

platelets (BC VWF reagent kit, Siemens, Milano, Italy) in a BCS automatic coagulometer (Siemens). The protocols for all clinical studies were scrutinized and approved by the Institutional Review Board of the Catholic University School of Medicine of Rome. All subjects gave their informed consent to the study.

Analysis of VWF multimers from clinical samples. VWF was isolated from plasma using a rabbit polyclonal anti-VWF antibody from Dako. The antibody was covalently coupled to Affi-Gel 10 agarose beads (Bio-Rad, Milano, Italy). The protein-gel ratio was 2 mg protein/ml of gel. Briefly, 100 µl of conjugated agar beads were mixed with 1 ml of plasma sample and incubated at 25 °C under mild agitation for 1 hr. After 1 min centrifugation at 1000 rpm in a bench microfuge, the supernatant was discarded and a cycle of 3 washes with 10 mM Hepes, 0.15 M NaCl, pH 7.40 was performed. Finally, the settled agarose gel beads, containing the bound VWF, were treated with 0.1 ml of 6 M guanidine hydrochloride for 15 min under mild agitation to dissociate VWF multimers from agarose beads. The protein content was measured by the bicinchoninic acid method, using the Bio-Rad protein assay. The resulting solution was used to measure the carbonyl content of VWF as a marker of oxidative protein damage (37). The VWF carbonyl content was measured according to the low-protein procedure of the Biocell PC EIA test (Alexis Biochemical, Vinci-Biochem, Vinci, Italy), which quantifies carbonyls by derivatizing proteins with dinitrophenylhydrazine (DNP). Then, the protein was nonspecifically adsorbed overnight at 4 °C to an ELISA microplate. The adsorbed protein was probed with biotinylated anti-DNP antibody followed by streptavidin-linked horseradish peroxidase. After addition of a peroxidase substrate, the reaction was stopped with H2SO4 and the absorbance, proportional to the DNP-bound protein, was read at 450 nm. The concentration of the DNP-bound protein was measured using a standard curve prepared with serum albumin at known content of carbonyl group. The assay allowed us to obtain a reproducible sensitivity down to 1 pmol carbonyl/mg of protein, with an inter-assay variation of 13%.

In experiments performed to test the sensitivity of VWF purified from diabetics and control subjects, one pool of purified VWF from 5 T2DM patients and one pool from 5 control subjects were used in the presence of 5 nM ADAMTS-13 for 1 hr in 5 mM Tris-HCl, 3 mM CaCl2, 1.5 mg/ml ristocetin (sulphate-free), pH 8.0 at 37 °C. The SDS-agarose electrophoresis was carried out in 0.8 % (stacking gel)-1% (running gel). The western blot analysis was performed as detailed above.

Effect of ADAMTS-13 oxidation by peroxynitrite Purified ADAMTS-13 was treated with 100-250 µM peroxynitrite, as described above for VWF peptides. After treatment, the protease activity for a synthetic peptide was tested as follows. The substrate used for the enzymatic assays was DRE-A2pr(Nma)-APNLVYMVTG-A2pr(Dnp)-PASDEIKRLPGDIQVVPIGVGPNANVQELERIGWPNAPILIQDFETLPREAPDLVLQR, corresponding to the region from D1596 to R1668 of the von Willebrand factor (VWF) A2 domain.

Called FRETS-VWF73, the substrate was synthesized by Thermo Electron Corporation GmbH (Ulm, Germany) and supplied in a highly pure form (> 95%). The hydrolyzed peptide was monitored by exciting the substrate at 340 nm and measuring the fluorescence at 450 nm, as previously described (18). Assays were performed in 10 mM Bis-Tris, 150 mM NaCl, 25 mM CaCl2, 0.005% Tween 20, pH 6.0 and T=25 °C. The Michaelis parameter kcat/Km of FRETS-VWF73 hydrolysis were calculated under pseudo-first order conditions using FRETS-VWF73 at 1 μM concentration, that is <Km value, and 1-2 nM recombinant human ADAMTS-13. The kinetic parameter kcat/Km was determined as previously described (16), using the mean of at least two independent measurements in a 1-cm quartz cell and an Eclipse spectrofluorometer (Varian, Leini, Italy), equipped with a thermostated cell holder.

Ristocetin-induced platelet agglutination by untreated and peroxynitrite-treated VWF multimers. Ristocetin from Helena Laboratories (Beaumont, TX, USA) was used at a final concentration of 1.5 mg/ml. The ristocetin-induced platelet agglutination was studied as described above. The untreated VWF solution at 20 μg/ml was used as reference (100% activity). The velocity of platelet agglutination measured with VWF preparations treated with peroxynitrite (20-200 μM) was expressed as per cent of the velocity obtained by using untreated VWF.

RESULTS

Chemical synthesis of pseudo wild-type VWF74, oxidation by peroxynitrite and hydrolysis by ADAMTS-13. Earlier studies have demonstrated that the 73-amino acid segment 1596-1668 is the minimal peptide sequence of VWF efficiently cleaved by ADAMTS-13 (38). On this basis, we synthesized the pseudo wild-type peptide VWF74, corresponding to the sequence 1596-1669 of the VWF A2 domain in which the C-terminal Cys1669 was replaced by Ala, to avoid possible disulfide-coupled dimerization. VWF74 was purified (>98% pure) by semi-preparative RP-HPLC and its chemical identity established by high-resolution mass spectrometry, which yielded mass values in agreement with the theoretical mass within 50 ppM accuracy (Fig. 1A).

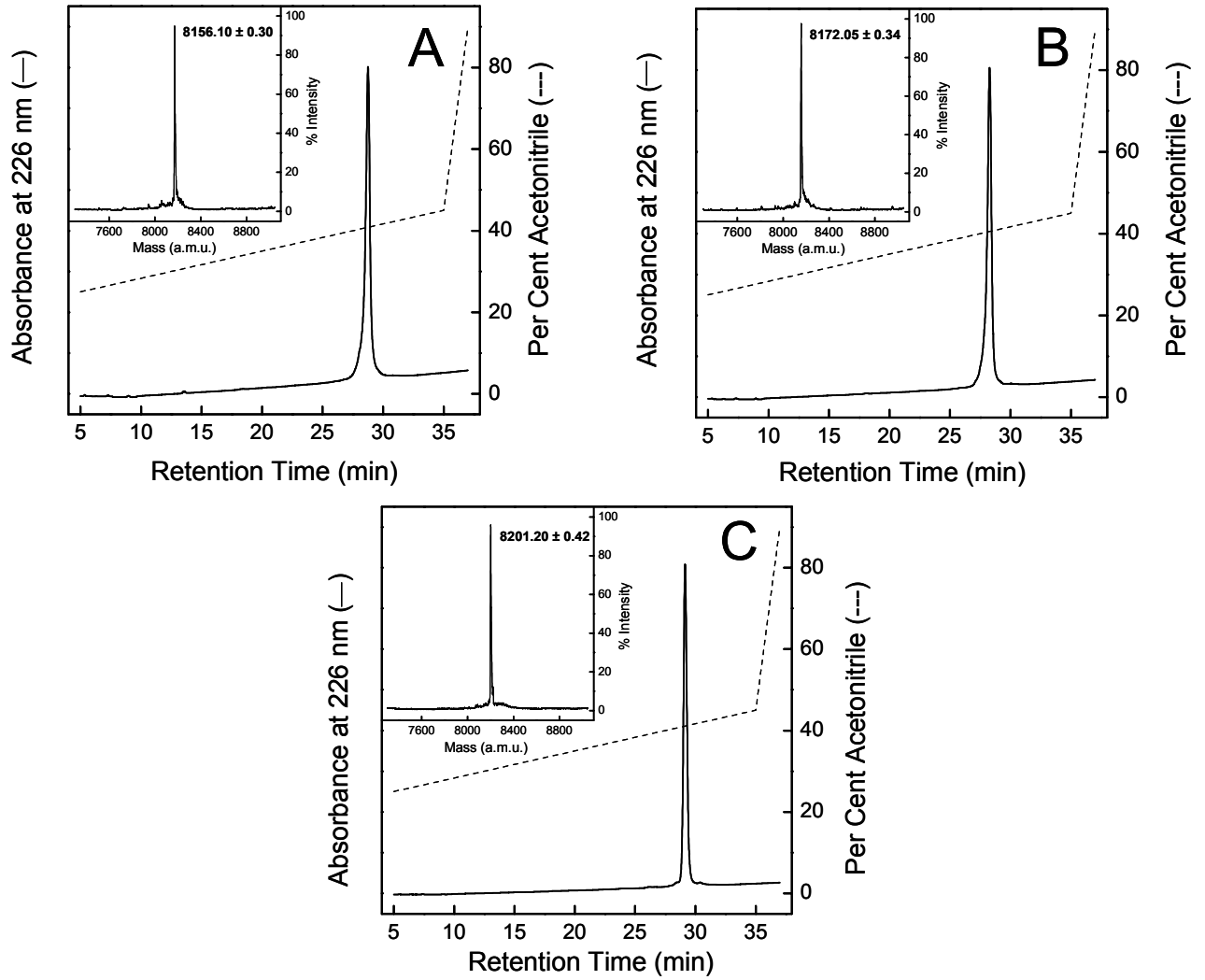

Figure 1. Purity check of the synthetic peptides VWF74 (A) VWF74-MetSO (B), and VWF74-NT (C). The peptides were synthesized as detailed in the Methods and purified by semi-preparative RP-HPLC. The homogeneity of the purified material was established by analytical RP-HPLC. An aliquot (10 μg) of each peptide was loaded onto a C18 Zorbax analytical column (4.6 x 150 mm), eluted with an acetonitrile-0.1% TFA gradient (dotted line) from 25 to 45 % in 30 min. (Inset) ESI-TOF mass spectrum of the RP-HPLC purified VWF74 peptides

Notably, we considered the high rate of peroxynitrite decomposition under physiological pHs (k=0.3-0.9 sec-1) and the relatively low magnitude of its second order rate constant of reaction with methionine (102-103 M-1 sec-1) (27). Hence, the yield of sulfoxy-methionine formation by a fixed concentration of ONOO- (10 μM) progressively increased up to 70% as a function of "multiple shot" addition of the oxidant at the same final concentration (1 addition per min. up to 60 min, see Fig. 2, panel C). Thus, the yield of MetSO formation in VWF74 substrate was about the same if either the peptide was oxidized by 100 μM peroxynitrite by a single shot or by 10 shots of 10 μM peroxynitrite (see Fig. 2, panel A-C). Notably, similar results were obtained also at pH = 6, that is under moderate acidic conditions occurring in intra-cellular Weibel-Palade granules (19,39). Using 10 μM ONOO- in

sixty shots VWF74 undergoes progressive and potentially saturable oxidation at its methionine residue (see Fig. 2, panel C).

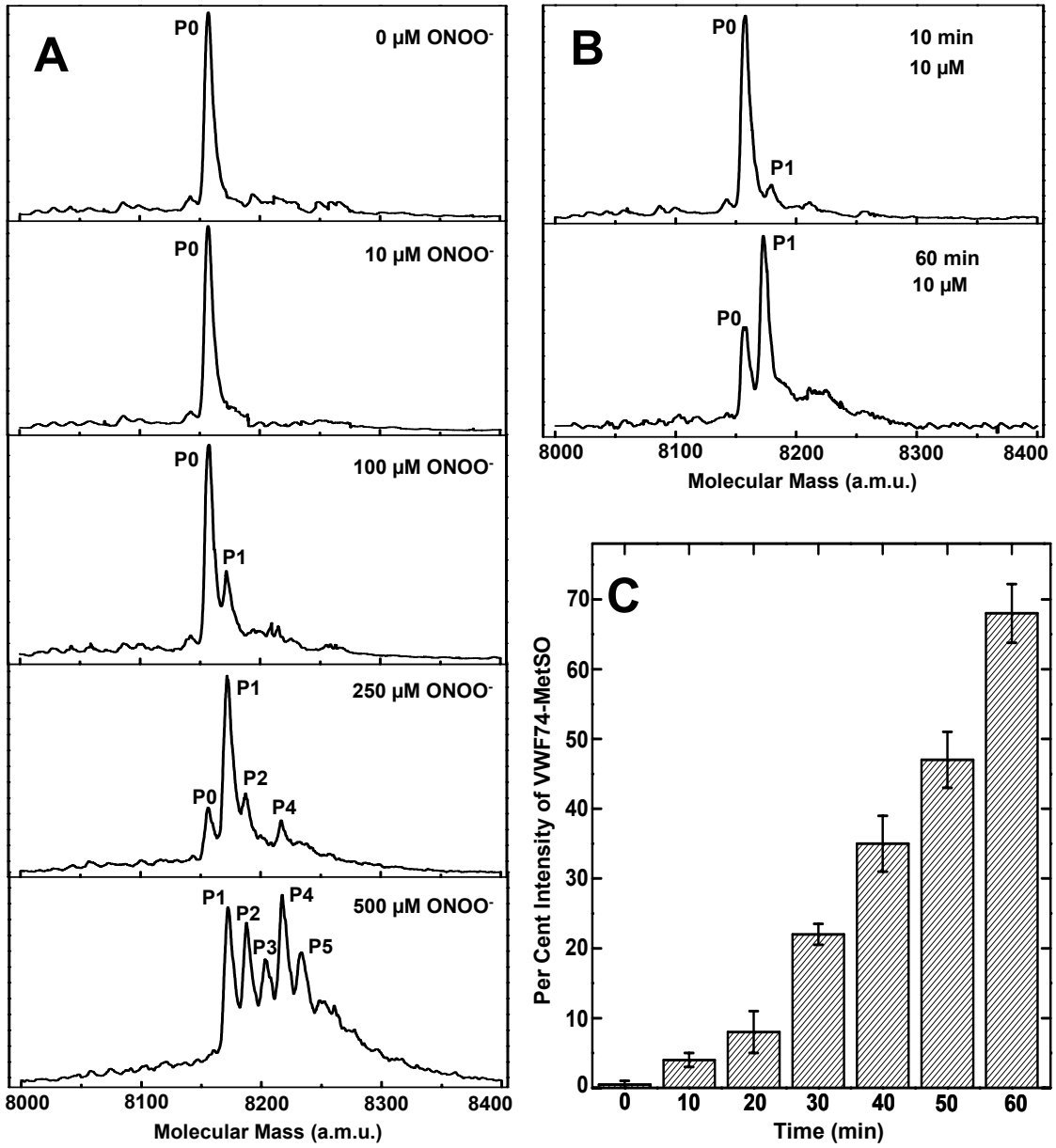

Figure 2. LC-MS analysis of peroxynitrite-treated VWF74. (A) Mass spectra of oxidized vWF74 after "single-shot" addition of increasing concentrations of peroxynitrite (0-500 mM). Labels P0-P5 identify the oxidation products of VWF74. **(B)** Mass spectra of oxidized VWF74 after "multiple-shot" addition of 10 mM peroxynitrite (one shot per min). **(C)** Plot of the intensity of the VWF74-MetSO oxidized species at +16 a.m.u. as a function of time. Each value was obtained from the mass spectra recorded using "multiple-shot" addition of peroxynitrite, as reported in panel B. Error bars correspond to the standard deviation resulting from three measurements. The assignment of the P0-P5 species to the molecular to the chemical modification(s) generated by peroxynitrite treatment is reported in Table 1.

Although precise quantitative determination of the oxidation products is impaired by their different ionization/vaporization efficiency during mass spectrometric analysis, LC-MS spectra shown in Fig. 2A and the data reported in Table 1 indicate that oxidation by 250 μM peroxynitrite predominantly induced the formation of a species at +16 a.m.u., assigned to the formation of the MetSO derivative (i.e., P1), in

keeping with the higher oxidant sensitivity of Met-residues (26-28), whereas oxidation of the single Trp1644 (P2) and nitration of Tyr1605 (P4) were very poor. Oxidation of either Met to MetSO and Trp to oxindolylalanine resulted in a mass increment of +16 a.m.u. The chemical identity of the P1 species was unequivocally established by peptide mass fingerprint analysis of genuine and peroxynitrite-treated VWF74 with leukocyte elastase (data not shown). At 500 μM peroxynitrite, instead, the combined oxidation/nitration reaction of the most sensitive amino acids in the primary structure of VWF74, namely Tyr1605, Met1606, and Trp1644, became predominant (Fig. 2A and Table 1). The formation of Tyr-nitrated species was also confirmed by the appearance of a diagnostic band at 430 nm (34) in the absorption UV-VIS spectrum of oxidized VWF74.

Table 1. LC-MS Analysis of Synthetic VWF74 Oxidized with 250-500 μM Peroxynitrite[a]

Oxidation Products [b]	Experimental Mass (a.m.u.) [c]	Chemical Modification [d]	Δm (a.m.u.) [e]
P0	8156.3 (8156.0)	Unmodified VWF74	-
P1	8172.1 (8172.0)	Met1606→MetSO	+15.7 (+16.0)
P2	8188.2 (8188.0)	Met1606→MetSO + Trp1644→Oxy-Indolyl-Ala	+31.8 (16+16 = +32.0)
P3	8201.8 (8201.0)	Tyr1605→TyrNO2	+45.5 (+45.0)
P4	8217.5 (8217.0)	Met1606→MetSO + Tyr1605→TyrNO2	+61.2 (16+45 = +61.0)
P5	8233.9 (8233.0)	Met1606→MetSO + Tyr1605→TyrNO2 + Trp1644→Oxy-Indolyl-Ala	+77.5 (16+45+16 = +77.0)

[a] The reaction of VWF74 with peroxynitrite and analysis with LC-MS was conducted as detailed in Methods. b P0–P5 identify the oxidation products of VWF74, as obtained from the mass spectra in Fig. 2A and B. c Experimental and theoretical (in parenthesis) average molecular mass values of VWF74 oxidation products. d Chemical modifications assigned to the oxidation products. e Experimental and theoretical (in parenthesis) mass increments corresponding to the chemical modifications present in the oxidation products.

In proteolysis experiments with 5 nM ADAMTS-13, the genuine VWF74 peptide was hydrolyzed with the best-fit Michaelis-Menten parameter values k_{cat}=0.72±0.023 sec^{-1} and K_m= 6.62±0.64 μM. On the contrary, no kinetic parameter could be calculated for the peroxynitrite-treated VWF74 peptide under the same experimental conditions over a concentration range from 2.5 to 40 μM (see Fig. 3). This finding indicates that oxidation of the VWF substrate caused a strong decrease of the ADAMTS-13 catalytic specificity.

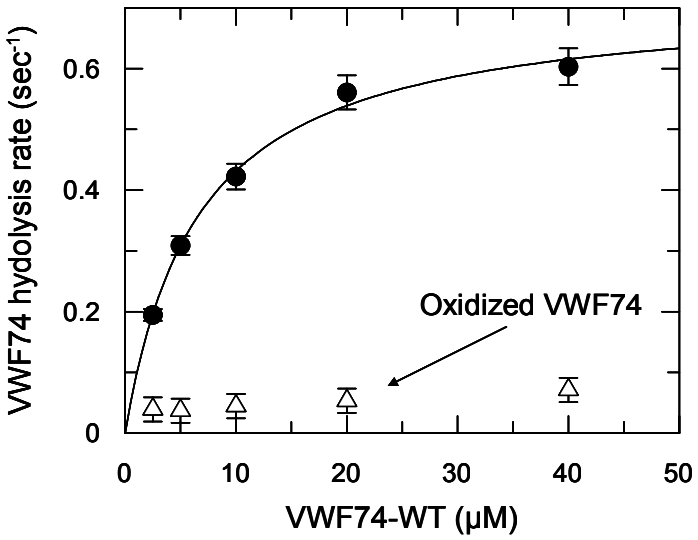

Figure 3. Steady state kinetic parameters of untreated (●) and peroxynitrite-treated VWF74 (Δ). VWF74 was treated with 250 μM peroxynitrite. The continuous line was drawn according to the Michaelis-Menten equation with the best-fit parameter values k_{cat}= 0.72±0.023 sec^{-1} and K_m= 6.62±0.64 μM. No kinetic parameter could be calculated for the peroxynitrite-treated VWF74 peptide. The vertical bars show average and S.D. of 2 independent measurements.

Hydrolysis by ADAMTS-13 of VWF74 analogs containing 3-nytrotyrosine and methionine-sulfoxide Based on the observation that oxidative reaction involves Met and, at higher peroxynitrite concentration, Tyr residue (Table 1), besides the pseudo wild-type peptide VWF74 we synthesized two singly substituted analogs in which Tyr1605 and Met1606 were replaced by NT and MetSO, to yield the synthetic peptides VWF74-NT and VWF74-MetSO, respectively (see Fig. 1B-C). These substitutions provided unequivocal information to assess which residue, either Tyr or Met, accounted for the reduced proteolysis by ADAMTS-13 after exposure to peroxynitrite.

In this experiment, VWF74 and VWF74-NT were hydrolyzed with similar steady-state kinetic parameters: VWF74 had a kcat value of 0.64±0.04 sec^{-1} and K_m of 6.0 ±1.3 μM, while VWF74-NT had a k_{cat} of 1.2±0.02 sec^{-1} and K_m of 6.3 ±0.3 μM (best-fit and standard error values, see Fig. 4). Thus, VWF74-NT showed specificity for ADAMTS-13 even slightly higher than that of the unmodified peptide. By contrast, VWF74-MetSO was almost fully resistant to cleavage, such that determination of the catalytic rate constants was not possible. Only at the highest concentration tested, i.e. 40 μM, VWF74-MetSO showed some proteolysis (Fig. 4).

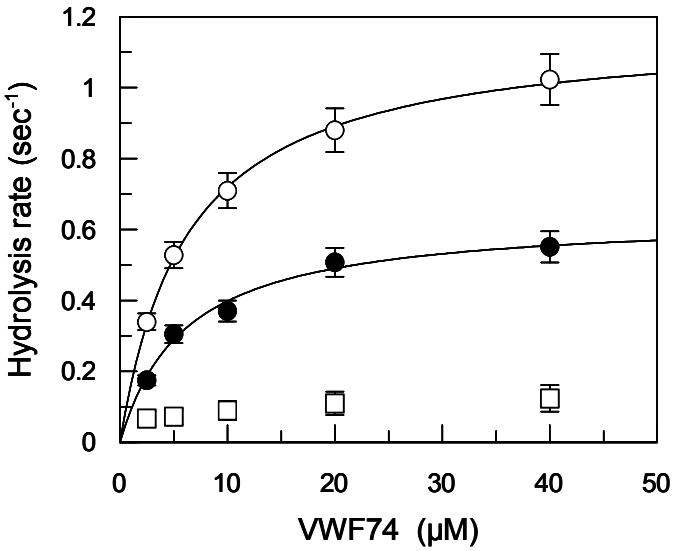

Figure 4. Michaelis-Menten parameters of hydrolysis by ADAMTS-13 of VWF74 (●), VWF74-NT (○) and VWF-MetSO (□). The continuous lines were drawn according to the Michaelis-Menten equation with the best-fit parameter values k_{cat}=0.64±0.04 sec-1 and K_m=6 ±1.3 μM for VWF74, and k_{cat}=1.2±0.02 sec-1 and K_m=6.3 ±0.3 μM for for VWF74-3NT. No kinetic parameter could be obtained for the VWF74-MetSO substrate analog, because of its resistance to ADAMTS-13 cleavage under the same experimental conditions.

Spectroscopic properties of VWF74 and its analogs VWF74-NT and VWF74-MetSO. Spectroscopic measurements were carried out to ascertain whether the effect of methionine oxidation on the cleavage by ADAMTS-13 were caused directly by a change in the physico-chemical properties (e.g., side-chain volume, polarizability, and hydrophobicity) of Met1606, or the presence of MetSO indirectly affected proteolysis by inducing some conformational alteration in the VWF74 structure in solution. Hence, the conformational properties of VWF74 and its analogs VWF74-NT and VWF74-MetSO were investigated by circular dichroism (CD) and fluorescence spectroscopy (see Fig. 5). For the three peptides tested, the CD spectra in the far-UV region were nearly superimposable and typical of a polypeptide chain in a disordered conformation (40). Similar conclusions could be drawn from the fluorescence spectra, which displayed λmax values centred at 357 nm and poor energy transfer, both spectral features being typical of disordered polypeptides (41). Our data indicate that VWF74 is largely unfolded in solution, in agreement with earlier preliminary NMR data obtained with FRETS-VWF73 (42), and provide evidence that, within the limits of the experimental techniques used, both Tyr→NT and Met→MetSO substitutions do not appreciably alter the conformation of VWF74.

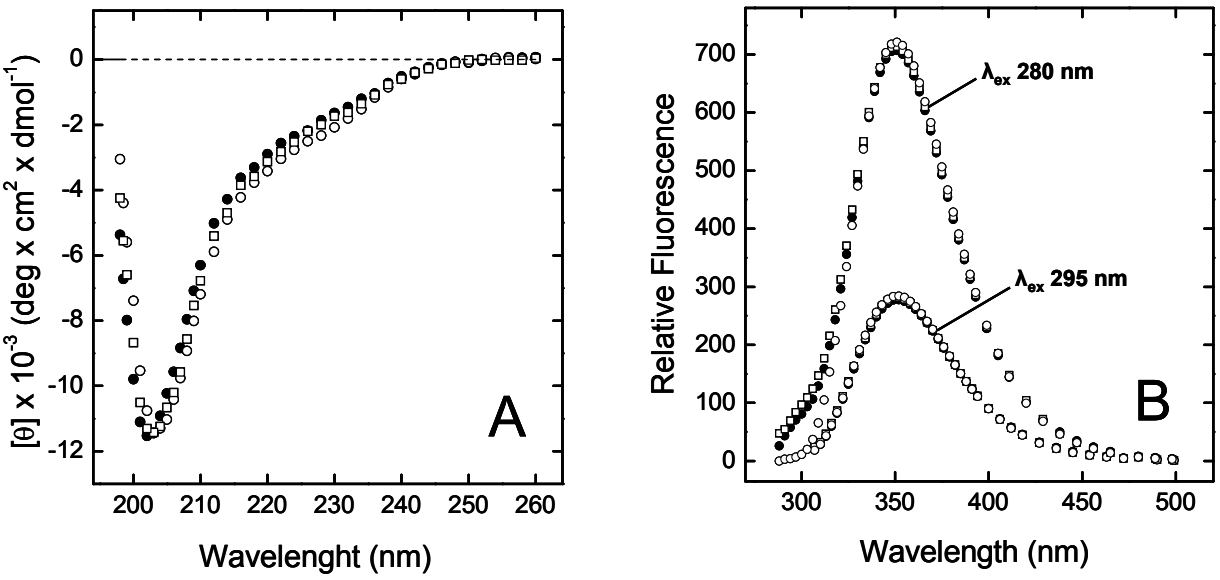

Figure 5. Conformational characterization of VWF74 (●),VWF74-NT (○) and VWF-MetSO (□) peptides by far-UV circular dichroism (A) and fluorescence spectroscopy (B). CD spectra were obtained at a peptide concentration of 0.15 mg/ml in a 1-mm pathlength cuvette. Fluorescence spectra of VWF74 peptides were obtained by exciting the sample (1.5 ml, 0.5 μM) at 280 or 295 nm. All measurements were carried out at 25 ± 0.1°C in 10 mM Na2HPO4 buffer, pH 7.4, in the presence of 150 mM NaCl.

In vitro oxidation of VWF multimers and their hydrolysis by ADAMTS-13. The treatment with peroxynitrite of VWF caused the formation of NT, whereas no NT was detected in the untreated protein, as obtained by Western blot analysis with anti-NT monoclonal antibodies (see Fig. 6A). Tyr nitration is significantly less efficient than Met oxidation (26-28) and therefore the presence of NT can be taken as a strong, albeit indirect, proof also for the presence of MetSO-residues in VWF monomers. The results shown in Fig. 6B clearly indicate that peroxynitrite-treated VWF multimers are significantly more resistant to proteolysis by ADAMTS-13 and that this inhibitory effect increases with oxidant concentrations. Qualitatively comparable results were obtained under shear stress conditions (not shown). Although the inhibitory effect was qualitatively similar to that obtained with the synthetic peptides, a quantitative comparison could not be done in terms of reaction kinetics, due to the multimeric nature of VWF and the obvious difference in the stoichiometry of oxidant:substrate ratio present in the two experimental settings.

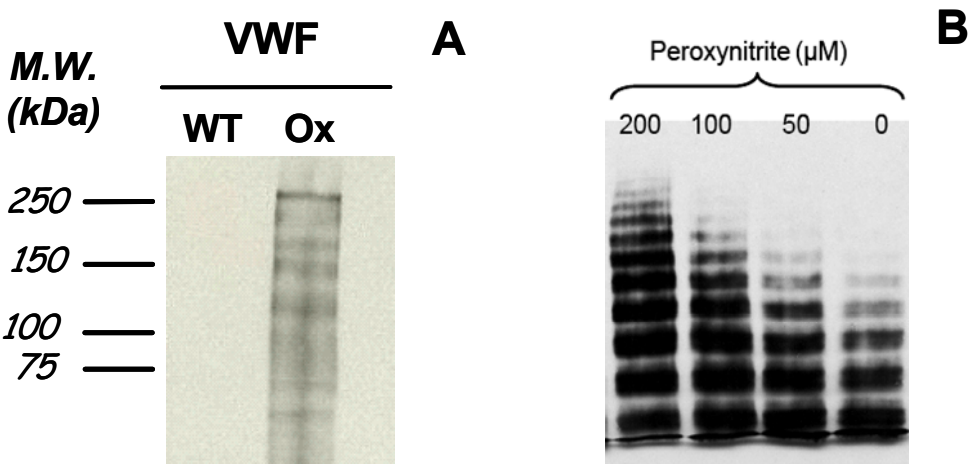

Figure 6. (A) Western blot of both untreated VWF and VWF oxidized with 250 μM peroxynitrite (ONOO-). The samples (in duplicate) were then reduced and underwent electrophoresis. The bands corresponding to oxidized proteins were detected by polyclonal anti-NT antibodies. On the left the molecular weight of the protein standards are shown. The main band with m.w. of 250 kDa corresponds to VWF monomers. (B) Determination of ADAMTS-13 (5 nM, final concentration) activity on VWF multimers (20 μg/ml, final concentration) oxidized in vitro by the indicated concentration of peroxynitrite in a single shot. After 1 hr incubation, the reaction was stopped, the samples were diluted 1:20 and were subjected to electrophoresis and immunoblotting.

LC-MS and MS/MS analysis of the full-length untreated or peroxynitrite-treated VWF. The proteolysis of the reduced and alkilated plasma VWF by *Staphylococcus aureus V8* (enzyme:substrate ratio 1:20 w/w) showed an extremely complex LC-MS analysis for either untreated or peroxynitrite-treated sample (see Fig. 7A and 7B). Even if this behavior was expected because of the heterogeneity and the complexity of the biological sample (i.e. 2050 AA, M.W. 250 kDa), the chromatographic profile made almost impossible to detect unequivocally a single peptide that contains the cleavable sequence ^{1605}Y-M^{1606}. Thus a "pick and choose" approach was adopted to resolve the problem. Working on the theoretic pattern fragmentation expected from the proteolysis of VWF by *Staphylococcus aureus V8* (www.expesy.org), we identified suitable peptides that contain the cleavable sequence ^{1605}Y-M^{1606} (i.e. ^{1599}QAPNLVYMVTG NPASDE^{1615}, called VWF17) having a m/z ratio of 903.4 ± 0.1 (2+) and 911.4 ± 0.1 (2+) a.m.u. for native and oxidized species, respectively (Fig. 7). First (1) we produced these model peptides, (i.e. VWF17 and VWF17(MSO)) by cleaving VWF74 synthetic peptide with *Staphylococcus aureus V8*; (2) we then characterized VWF17 and VWF17(MSO) by LC-MS and MS/MS analysis and finally (3) we investigated the presence of the expected peptides in the plasma VWF samples, just focusing our attention next to the retention time observed with the models. Following this workflow we successfully detected both peptides into the LC-MS analysis of the full-length plasma VWF (Fig 7A,7B, 8A, 8B). Notably, as observed for the models, the non-treated peptide, VWF17, was eluted around 30 min whereas the peroxynitrite-treated peptide, VWF17(MSO) was eluted with a lower retention time, in close agreement with the substitution of an hydrophobic aminoacid such as methionine with to an hydrophilic aminoacid such as methionine sulfoxide. To definitely assign the chemical identity of the

peptides derived form the proteolysis of the full-length plasma VWF, we performed MS/MS sequencing experiments. The fragmentation pattern obtained for either the untreated peptide or the peroxnityte-treated peptide, permitted us to cover more than 90% of the sequence (see Fig. 8C) concluding that the proteolytic peptides generated were chemically correct.

To better elucidate whether the oxidation of the VWF could happen only in drastic denaturing condition or in a more physiological relevant environment, we first oxidized the plasma VWF under simulated shear stress conditions with peroxynitrite and then we reduced, alkilated and proteolyzed it. Also in these experimental conditions we obtained the VWF17(MSO), indicating that peroxynitrite can freely diffuse in between the native multimer plasma VWF. Reasonably in this latter case the oxidation resulted not quantitative, however methionine was oxidized more than 60%.

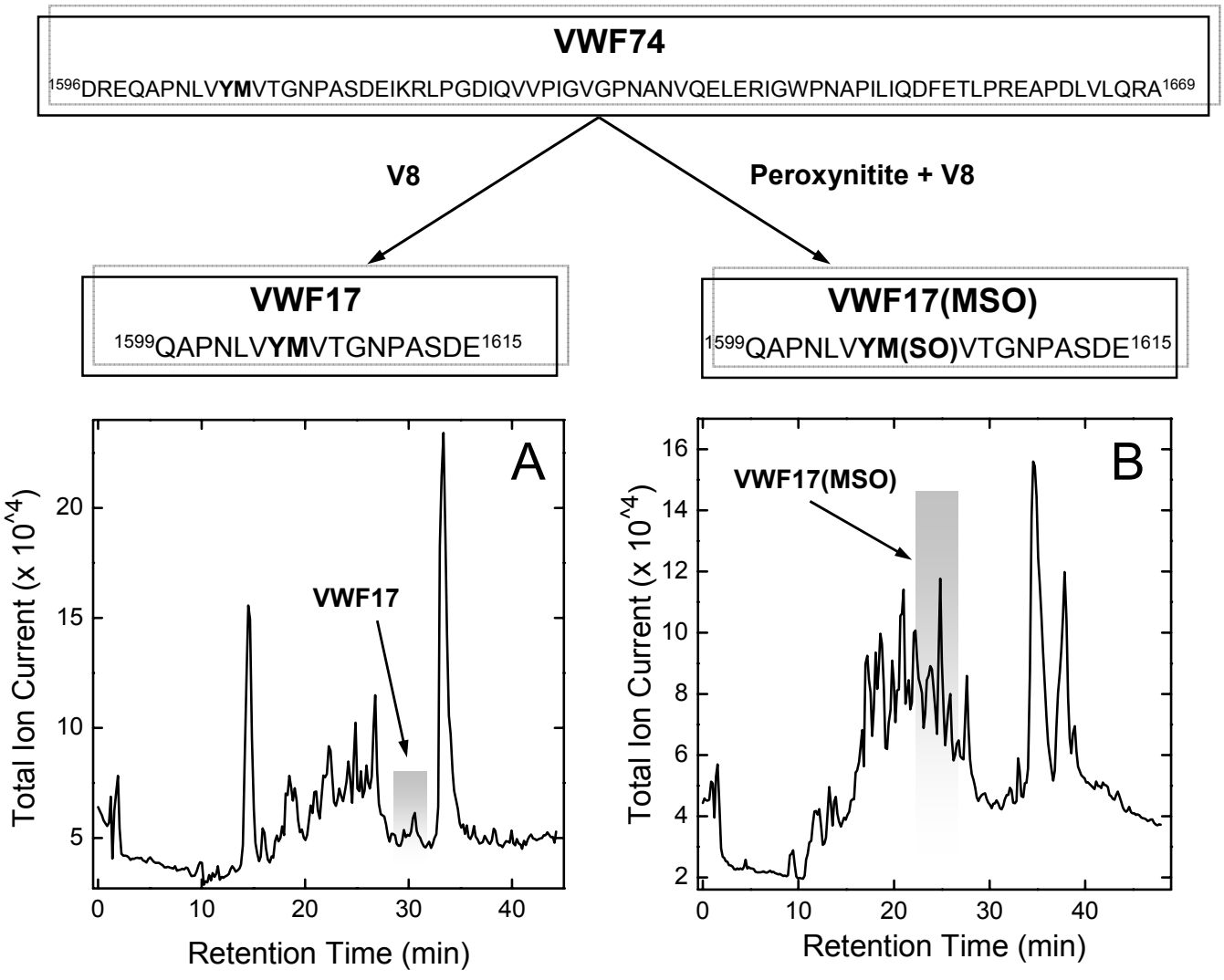

Figure 7. LC-MS analysis of the full-length non-treated (A) or peroxynitrite-treated (B) VWF. Natural or oxidized VWF sample (7-8 μg = 32 pmols), coming from the proteolysis reaction with *Staphylococcus aureus V8*, was loaded onto a Vydac C18 microbore column. The column was desalted and then eluted using an exponential gradient from 1% to 80% of CH_3CN at a flow rate of 10 μl/min. Notably the natural peptide, having a m/z ratio of 903.4 a.m.u. is eluted at 30 min whereas the peroxynitrite-treated peptide, having a m/z raito of 911.4 a.m.u., is eluted at 25 min.

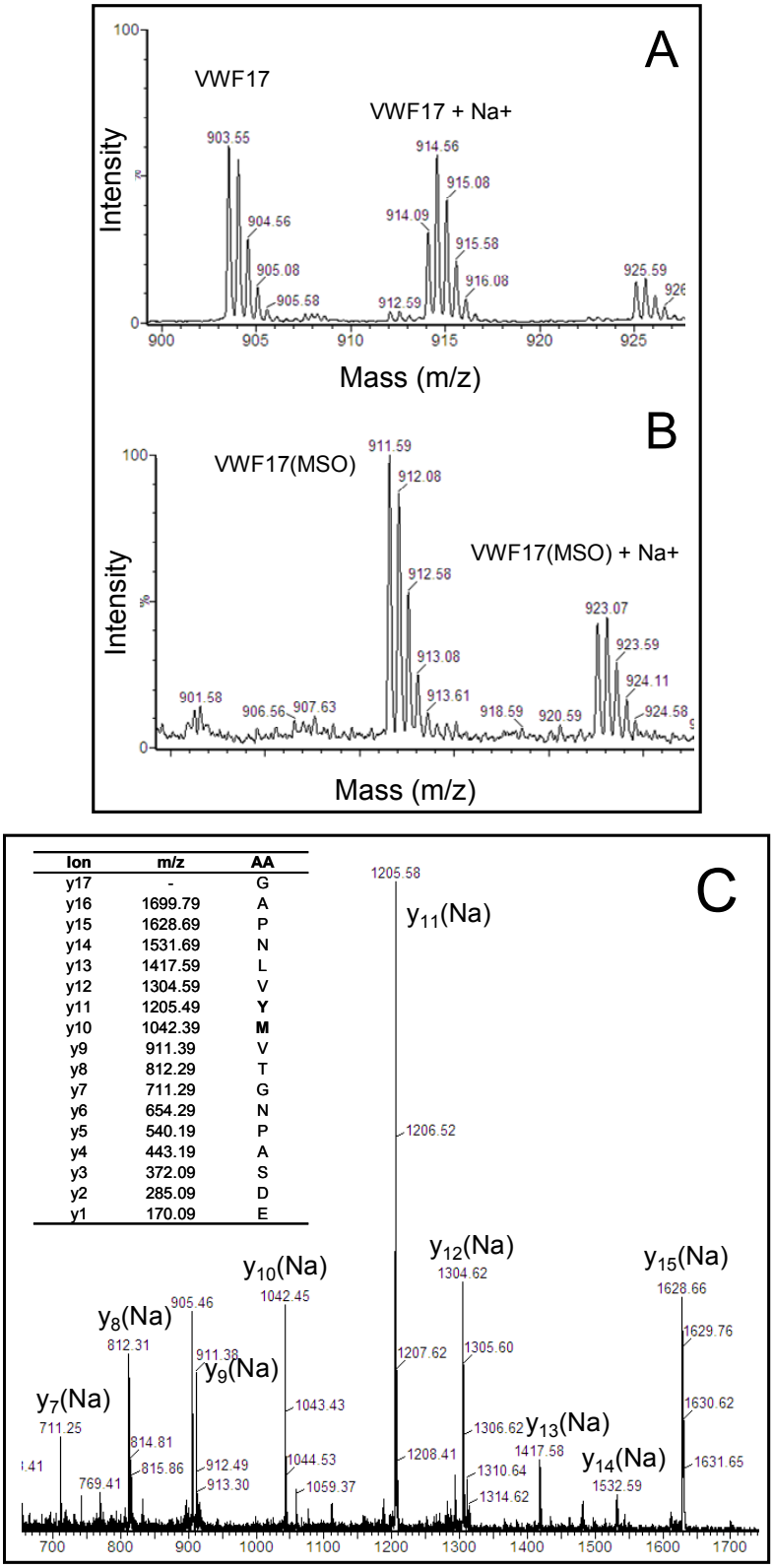

Figure 8. MS spectra of the non-treated (A) or peroxynitrite-treated (B) peptide. Peptide spectra here reported contain adducts of a Na^+ ion. Sodium, as well-known reported for V8 proteolytic fragments, easily binds to the peptides especially when vicinal acid amioacids are localized at the C-terminal. **MS/MS sequencing of the non treated peptide (C).** The MS/MS spectrum of VWF17 + Na+ is reported. The theoretic fragmentation of the y-series is reported in the inset and it was obtained considering the expected VWF17 sequence plus Na+. The presence of several predicted y-series fragments permitted us to cover more than the 90% of the sequence.

Analysis of VWF multimers from healthy and diabetic subjects. Previous studies showed that type 2 diabetes mellitus (T2DM) is characterized by oxidative stress, which involves lipids, and proteins, causing perturbation of vascular endothelium (43-46). We evaluated the oxidative modification of VWF purified from samples of T2DM patients. In particular, the carbonyl content of plasma VWF was measured as a realistic marker of oxidative modification of the protein. Compared to healthy donors, these patients showed a significantly increased plasma level of VWF (VWF:RiCof 187±77% vs 102±23%, respectively, $p<0.001$). Notably, the higher VWF levels in T2DM patients occurred in the majority of cases despite the blood groups were of type "0", a condition associated with plasma VWF levels 25% lower than in "non-0" subjects (47) The carbonyl content of VWF was significantly higher in T2DM than in controls (66.7±128 vs 1.74±0.631 pmol/mg of protein, respectively, $p<0.01$), as shown in Fig. 9A.

SDS-agarose electophoresis and western blot analysis showed that VWF multimers from T2DM samples with the highest carbonyl content were particularly rich of ultra large multimers, as emerging from comparison with VWF multimers from healthy subjects (see Fig. 9B). This ex-vivo finding was in agreement with the hypothesis that oxidative modification of VWF, and particularly of Met1606, causes resistance to proteolysis by ADAMTS-13, favoring the accumulation of UL-VWF multimers. This hypothesis was further validated by purification of VWF from diabetic subjects and by performing its proteolysis by ADAMTS-13 in vitro. Thus, the purified VWF preparations with the highest carbonyl content were used to assess their specificity of interaction with ADAMTS-13. Compared to VWF purified from control subjects, VWF preparations from T2DM patients showed a relative resistance to ADAMTS-13 hydrolysis, as shown in Fig. 9C.

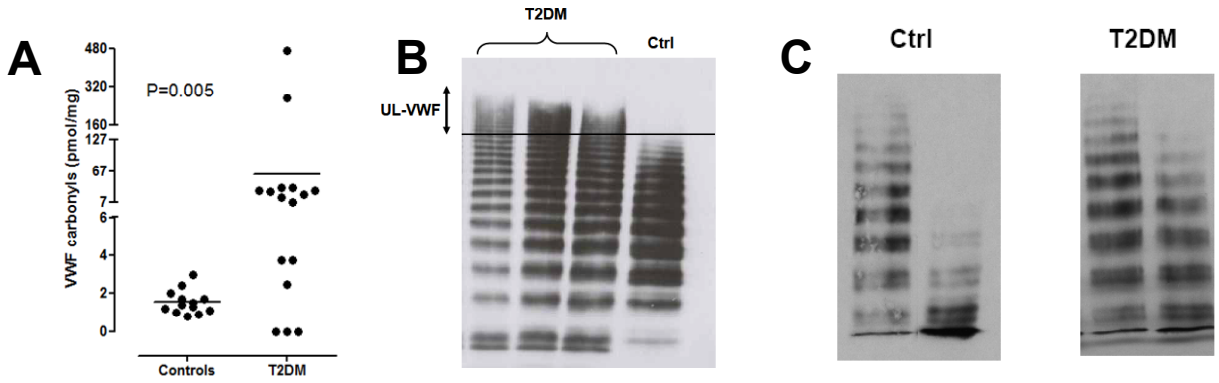

Figure 9. (A) Plot of the carbonyl content of VWF in control subjects and in T2DM patients. The horizontal lines represent the means of the corresponding data set; B) Western blot of VWF multimers from three diabetic patients with high carbonyl content (T2DM) and a pool from 5 healthy subjects (Ctrl). The straight line indicates the limit of high molecular weight VWF multimers in healthy subjects. Above this line UL-VWF multimers are seen only in T2DM samples. C) Cleavage by ADAMTS-13 of VWF multimers in a pool obtained from five diabetics (T2DM) and five healthy subjects (Ctrl). Purified VWF multimers were digested by 5 nM ADAMTS-13 for 2 hr in the presence of 1.5 mg/ml ristocetin. under the experimental conditions detailed in the text. The same protein amount was loaded on the gels. The samples from diabetic patients had the highest VWF carbonyl content (44-480 pmol/mg), whereas the controls had a carbonyl content ranging from 1.3 and 1.8 pmol/mg.

Ristocetin-induced platelet agglutination by genuine and peroxynitrite-treated VWF multimers Oxidation of VWF multimers by peroxynitrite (from 20 to 200 μM), did not significantly alter the ristocetin-induced platelet agglutination (Fig. 10). This finding showed that treatment of VWF with peroxynitrite over a 20-200 μM concentration range did not significantly alter the structure/conformation of both the binding site for ristocetin and that one for GpIb in the A1 domain of VWF.

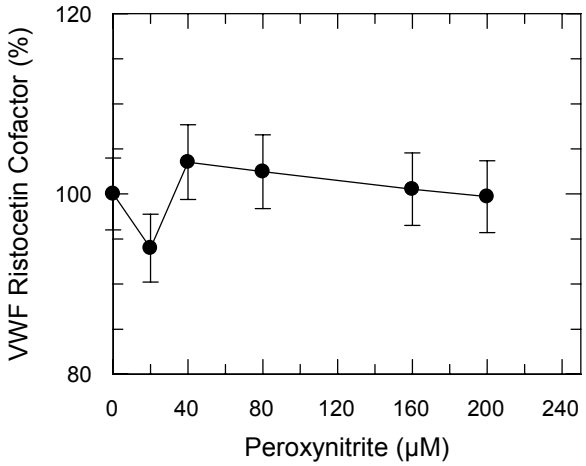

Figure 10. Ristocetin-induced platelet agglutination by VWF multimers oxidized by peroxynitrite. The vertical bars show average and S.D. of 2 independent experiments.

Effect of peroxynitrite on ADAMTS-13 protease activity. In vitro treatment of ADAMTS-13 with peroxynitrite over a concentration ranging from 50 to 250 μM caused a complete inhibition of the protease activity of the enzyme, as determined using the fluorescence substrate FRETS-VW73 (18) (data not shown). This drastic effect did not allow to measure any kinetic parameter at low concentration of the FRET substrate used in these experiments.

DISCUSSION

Several studies have indicated a strong association between high levels of circulating VWF and some thrombotic diseases, such as myocardial infarction, stroke and sudden death in some clinical settings such as coronary artery disease and diabetes (48-50). However, beside a quantitative abnormality of VWF, the qualitative composition of its multimers appears also relevant for inducing a pro-thrombotic state, as clearly shown in thrombotic microangiopathies (7). In this study, we have tested how oxidative stress induced by peroxynitrite could affect VWF structure and its interaction with ADAMTS-13 and platelet receptor. VWF multimers showed to be sensitive to peroxynitrite-driven oxidation, even under static conditions, where the folded/globular conformation of the protein is predominant and the Tyr1605-Met1606 peptide bond is buried in the core of the A2 domain (51).

Moreover, ultra large VWF multimers secreted by endothelial cells are more sensitive than low molecular weight multimers to shear-promoted unfolding, as recently reported (20). Hence, Tyr1605 and Met1606 of the scissile peptide bond of circulating VWF become more exposed to solvent and, potentially, to oxidizing agents. Thus, peroxynitrite-treated VWF showed increased levels of NT, a marker of protein (nitro)oxidation, found in many oxidative stress-related disorders and particularly in atherothrombotic cardiovascular diseases (26,52-62). Among the proteins of the coagulation system, oxidation of a single methionine residue in the thrombomodulin protein (Met388) severely impairs the capacity of the thrombomodulin-thrombin complex to activate protein C (63,64). Other coagulation proteins affected by methionine oxidation include fibrinogen (65), thrombin (66), and the serine protease inhibitors plasminogen-activator inhibitor (67), α2-antiplasmin and antithrombin (68).

This study showed that oxidation by peroxynitrite of Met1606 in the A2 domain of VWF severely inhibits the ability of ADAMTS-13 to cleave the peptide bond between Tyr1605 and Met1606. On the contrary, peroxynitrite-driven oxidation of Tyr1605 with formation of NT does not significantly alter the same cleavage process, which is even slightly accelerated. The inhibition observed also in the peroxynitrite-oxidized VWF multimers may be attributed to oxidation of that particular Met-residue, although other residues of the protein likely undergo oxidative modifications. Peroxynitrite can still diffuse quite far on a cellular scale, crossing cell membranes in part through anion channels (24,69,70). We showed that VWF purified from T2DM patients, a clinical setting characterized by oxidative stress, contains carbonyl residues, not detectable in VWF samples from normal subjects. The elucidation of the mechanism responsible for the formation of these oxidized species in VWF molecules is not in the realm of this study. However, we can speculate that the kinetics of peroxynitrite reactivity with aminoacids could determine VWF oxidation during the synthesis and storage of VWF in endothelial cells, a typical site of peroxynitrite formation. The steady state flux of peroxynitrite formation can oxidize Met1606, although this residue is buried in the hydrophobic core of VWF A2 domain (51). Thus, similar oxidative modifications of VWF multimers can be induced not only by high peroxynitrite concentrations for a very short time but also by steady-state fluxes at lower concentrations for longer time periods. This hypothesis is strongly suggested by the in vitro experiments based on multiple shots of peroxynitrite addition (Fig. 2). Our experimental data globally showed indeed that Met1606 undergoes oxidative modification by peroxynitrite. We hypothesized that also other oxidants, such as anion superoxide or hypochlorous acid, mostly generated by blood polymorphonuclear cells (PMNs) during inflammatory reactions could be involved in the formation of MetSO in the VWF molecule, as very recently reported during the revision phase of the present study (71). Experimental data obtained by our group showed that purified myeloperoxidase-H2O2-Cl- system was able indeed to oxidize in vitro VWF multimers (data not shown). However, when superoxide radical was generated in vitro by PMNs stimulated by 50 ng/ml phorbol myristate acetate, we observed a severe VWF multimers degradation by cell-derived proteases, such as elastase, proteinase 3, cathepsin G and metalloprotease 9,

as recently reported (72). This phenomenon could in practice cancel out the inhibiting effect by PMNs-derived ROS on ADAMTS-13 hydrolysis. These findings strongly supported the hypothesis that peroxynitrite plays in vivo a major role in inducing in VWF oxidative modifications and resistance to ADAMTS-13 activity.

Although the ability of oxidized VWF multimers to be cleaved by ADAMTS-13 is strongly inhibited, their platelet agglutinating activity is not significantly affected by peroxynitrite over the same concentration range. Only at high concentrations (>200 μM) a slight inhibition of ristocetin-induced platelet agglutination was observed, likely because of oxidation of VWF residues involved in GpIb binding or partial denaturation of oxidized VWF multimers. However, no major effects were observed on GpIb/VWF-dependent platelet agglutination in the range of peroxynitrite concentration blunting the VWF-ADAMTS-13 interaction. Furthermore, peroxynitrite was found in vitro to exert also a strong inhibitory effect on ADAMTS-13. This effect may be caused by the well known reactivity of peroxynitrite with Zn-ion centers in proteins (70), the oxidation of methionine residues present in the S1' recognition site of the enzyme or the oxidation of the histidine residues that coordinate the catalytic zinc ion in the protease. Further studies are needed to localize the target of the oxidative reactions responsible for ADAMTS-13 inhibition.

Overall, peroxynitrite-driven oxidative stress could favor accumulation of ultralarge VWF multimers without altering their interaction with platelets. The findings reported in the present study suggest a novel pro-thrombotic effect of oxidative stress, centered on heightened haemostatic functions of UL-VWF multimers.

We have shown here that Met→MetSO and Tyr→NT exchanges do not appreciably alter the conformational properties of the VWF substrate VWF74 (Fig. 5), within the limits of our experimental techniques. Hence, from a mechanistic point of view, we can only speculate on how the changes in the physico-chemical properties (e.g., size, polarity, and local conformational propensity) of the modified side-chains upon oxidation of Tyr1605 and Met1606 could diversely affect the hydrolytic reaction of ADAMTS-13 in the two analogs VWF74-NT and VWF74-MetSO. In particular, the conversion of Met to MetSO only slightly increases the side-chain volume (i.e., 6-8 Å3), but converts a hydrophobic amino acid like Met into a polar and partially charged amino acid like MetSO (60). Hence, we propose that the drastic chemical perturbation introduced at position 1606 of VWF74 by methionine oxidation disrupts the continuous apolar surface formed by the N-terminal hydrophobic region ^{1599}QAPNLVY-MVTGNPA^{1612} of the cleaved peptide, thus impairing productive interaction with ADAMTS-13. Molecular modeling of the catalytic domain of ADAMTS-13 and in silico docking simulations of ADAMTS-13/VWF74 interaction showed indeed that the S1' site of the protease is hydrophobic in nature and structurally constrained, forming a narrow and deep apolar pocket (manuscript in preparation). Thus, the presence of the highly polar MetSO at the P1' site of VWF is expected to dramatically reduce the affinity for the apolar S1' pocket of the protease. Concluding remarks.

In conclusion, oxidative damage on Met1606, renders VWF resistant to proteolysis by ADAMTS-13, and thus ultra-large VWF multimers undergo a low proteolytic processing. Oxidized VWF can still normally trigger platelet aggregation. Altogether, these effects in vivo may lead to a qualitative, in addition to a quantitative alteration of circulating VWF. The present study may pave the way to alternative anti-platelet strategies in clinical settings where traditional anti-platelet therapies show a lower-than-expected efficacy, such as diabetes and chronic renal failure (73-75). High levels of VWF have been reported as an independent risk factor for cardiovascular diseases in insulin resistance or overt type-2 diabetes mellitus, possibly indicating that these conditions are associated with endothelial dysfunction and prothrombotic state leading to cardiovascular disease events, as shown in the recent Framingham Offspring Study (50). Binding of VWF multimers to platelet GpIb induces indeed intraplatelet signaling independent from the arachidonic acid pathway or ADP receptor signaling (76,77). The inhibition of the proteolytic processing of VWF by oxidative damage of Met1606, beside increased release of VWF by damaged endothelium, may be one of the mechanisms involved in the pathogenesis of ischemic microangiopathies only partially sensitive to traditional antithrombotic drugs.

REFERENCES

1. Chung, D.W.; Fujikawa, K. Processing of von Willebrand factor by ADAMTS-13. *Biochemistry*. 41:11065-11070; 2002.
2. Dent, J.A.; Berkowitz, S.D.; Ware, J.; Kasper, C.K.; Ruggeri, Z.M. Identification of a cleavage site directing the immunochemical detection of molecular abnormalities in type IIA von Willebrand factor. *Proc Natl Acad Sci U S A*. 87:6306-6310; 1990.
3. Tsai, H.M. Physiologic cleavage of von Willebrand factor by a plasma protease is dependent on its conformation and requires calcium ion. *Blood*. 87:4235-4244; 1996.
4. Fischer, B.E.; Thomas, K.B.; Schlokat, U.; Dorner, F. Triplet structure of human von Willebrand factor. *Biochem J*. 331 (Pt 2):483-488; 1998.
5. Furlan, M.; Robles, R.; Lamie, B. Partial purification and characterization of a protease from human plasma cleaving von Willebrand factor to fragments produced by in vivo proteolysis. *Blood*. 87:4223-4234; 1996.
6. Levy, G.G.; Nichols, W.C.; Lian, E.C.; Foroud, T.; McClintick, J.N.; McGee, B.M.; Yang, A.Y.; Siemieniak, D.R.; Stark, K.R.; Gruppo, R.; Sarode, R.; Shurin, S.B.; Chandrasekaran, V.; Stabler, S.P.; Sabio, H.; Bouhassira, E.E.; Upshaw, J.D., Jr.; Ginsburg, D.; Tsai, H.M. Mutations in a member of the ADAMTS gene family cause thrombotic thrombocytopenic purpura. *Nature*. 413:488-494; 2001.
7. Moake, J.L. Thrombotic microangiopathies. *N Engl J Med*. 347:589-600; 2002.

8. O'Brien, L.A.; Sutherland, J.J.; Weaver, D.F.; Lillicrap, D. Theoretical structural explanation for Group I and Group II, type 2A von Willebrand disease mutations. *J Thromb Haemost*. 3:796-797; 2005.
9. Dong, J.F. Cleavage of ultra-large von Willebrand factor by ADAMTS-13 under flow conditions. *J Thromb Haemost*. 3:1710-1716; 2005.
10. Sutherland, J.J.; O'Brien, L.A.; Lillicrap, D.; Weaver, D.F. Molecular modeling of the von Willebrand factor A2 Domain and the effects of associated type 2A von Willebrand disease mutations. *J Mol Model (Online)*. 10:259-270; 2004.
11. O'Brien, L.A.; James, P.D.; Othman, M.; Berber, E.; Cameron, C.; Notley, C.R.; Hegadorn, C.A.; Sutherland, J.J.; Hough, C.; Rivard, G.E.; O'Shaunessey, D.; Lillicrap, D. Founder von Willebrand factor haplotype associated with type 1 von Willebrand disease. *Blood*. 102:549-557; 2003.
12. Dong, J.F.; Moake, J.L.; Nolasco, L.; Bernardo, A.; Arceneaux, W.; Shrimpton, C.N.; Schade, A.J.; McIntire, L.V.; Fujikawa, K.; Lopez, J.A. ADAMTS-13 rapidly cleaves newly secreted ultralarge von Willebrand factor multimers on the endothelial surface under flowing conditions. *Blood*. 100:4033-4039; 2002.
13. Tsai, H.M.; Sussman, II; Nagel, R.L. Shear stress enhances the proteolysis of von Willebrand factor in normal plasma. *Blood*. 83:2171-2179; 1994.
14. von Willebrand factor domain A1 stimulates the cleavage of the adjacent domain A2 by ADAMTS13. *Proc Natl Acad Sci U S A*. 101:10578-10583; 2004.
15. Shim, K.; Anderson, P.J.; Tuley, E.A.; Wiswall, E.; Sadler, J.E. Platelet-VWF complexes are preferred substrates of ADAMTS13 under fluid shear stress. *Blood*. 111:651-657; 2008.
16. De Cristofaro, R.; Peyvandi, F.; Palla, R.; Lavoretano, S.; Lombardi, R.; Merati, G.; Romitelli, F.; Di Stasio, E.; Mannucci, P.M. Role of chloride ions in modulation of the interaction between von Willebrand factor and ADAMTS-13. *J Biol Chem*. 280:23295-23302; 2005.
17. Peyvandi, F.; Lavoretano, S.; Palla, R.; Valsecchi, C.; Merati, G.; De Cristofaro, R.; Rossi, E.; Mannuccio Mannucci, P. Mechanisms of the interaction between two ADAMTS13 gene mutations leading to severe deficiency of enzymatic activity. *Hum Mutat*. 27:330-336; 2006.
18. Di Stasio, E.; Lancellotti, S.; Peyvandi, F.; Palla, R.; Mannucci, P.M.; De Cristofaro, R. Mechanistic studies on ADAMTS13 catalysis. *Biophys J*. 95:2450-2461; 2008.
19. Huang, R.H.; Wang, Y.; Roth, R.; Yu, X.; Purvis, A.R.; Heuser, J.E.; Egelman, E.H.; Sadler, J.E. Assembly of Weibel-Palade body-like tubules from N-terminal domains of von Willebrand factor. *Proc Natl Acad Sci U S A*. 105:482-487; 2008.
20. Zhang, X.; Halvorsen, K.; Zhang, C.Z.; Wong, W.P.; Springer, T.A. Mechanoenzymatic cleavage of the ultralarge vascular protein von Willebrand factor. *Science*. 324:1330-1334; 2009.
21. Huie, R.E.; Padmaja, S. The reaction of no with superoxide. *Free Radic Res Commun*. 18:195-199; 1993.

22. Alvarez, M.N.; Piacenza, L.; Irigoin, F.; Peluffo, G.; Radi, R. Macrophage-derived peroxynitrite diffusion and toxicity to Trypanosoma cruzi. *Arch Biochem Biophys*. 432:222-232; 2004.
23. Quijano, C.; Romero, N.; Radi, R. Tyrosine nitration by superoxide and nitric oxide fluxes in biological systems: modeling the impact of superoxide dismutase and nitric oxide diffusion. *Free Radic Biol Med*. 39:728-741; 2005.
24. Denicola, A.; Souza, J.M.; Radi, R. Diffusion of peroxynitrite across erythrocyte membranes. *Proc Natl Acad Sci U S A*. 95:3566-3571; 1998.
25. Alvarez, B.; Ferrer-Sueta, G.; Freeman, B.A.; Radi, R. Kinetics of peroxynitrite reaction with amino acids and human serum albumin. *J Biol Chem*. 274:842-848; 1999.
26. Pryor, W.A.; Jin, X.; Squadrito, G.L. One- and two-electron oxidations of methionine by peroxynitrite. *Proc Natl Acad Sci U S A*. 91:11173-11177; 1994.
27. Perrin, D.; Koppenol, W.H. The quantitative oxidation of methionine to methionine sulfoxide by peroxynitrite. *Arch Biochem Biophys*. 377:266-272; 2000.
28. Alvarez, B.; Radi, R. Peroxynitrite reactivity with amino acids and proteins. *Amino Acids*. 25:295-311; 2003.
29. Moreno, J.J.; Pryor, W.A. Inactivation of alpha 1-proteinase inhibitor by peroxynitrite. *Chem Res Toxicol*. 5:425-431; 1992.
30. Berlett, B.S.; Levine, R.L.; Stadtman, E.R. Carbon dioxide stimulates peroxynitrite-mediated nitration of tyrosine residues and inhibits oxidation of methionine residues of glutamine synthetase: both modifications mimic effects of adenylylation. *Proc Natl Acad Sci U S A*. 95:2784-2789; 1998.
31. Gow, A.J.; Duran, D.; Malcolm, S.; Ischiropoulos, H. Effects of peroxynitrite-induced protein modifications on tyrosine phosphorylation and degradation. *FEBS Lett*. 385:63-66; 1996.
32. Fields, G.B.; Noble, R.L. Solid phase peptide synthesis utilizing 9-fluorenylmethoxycarbonyl amino acids. *Int J Pept Protein Res*. 35:161-214; 1990.
33. Pace, C.N.; Vajdos, F.; Fee, L.; Grimsley, G.; Gray, T. How to measure and predict the molar absorption coefficient of a protein. *Protein Sci*. 4:2411-2423; 1995.
34. De Filippis, V.; Frasson, R.; Fontana, A. 3-Nitrotyrosine as a spectroscopic probe for investigating protein protein interactions. *Protein Sci*. 15:976-986; 2006.
35. Beckman, J.S.; Chen, J.; Ischiropoulos, H.; Crow, J.P. Oxidative chemistry of peroxynitrite. *Methods Enzymol*. 233:229-240; 1994.
36. Zhang, P.; Pan, W.; Rux, A.H.; Sachais, B.S.; Zheng, X.L. The cooperative activity between the carboxyl-terminal TSP1 repeats and the CUB domains of ADAMTS13 is crucial for recognition of von Willebrand factor under flow. *Blood*. 110:1887-1894; 2007.
37. Reznick, A.Z.; Packer, L. Oxidative damage to proteins: spectrophotometric method for carbonyl assay. *Methods Enzymol*. 233:357-363; 1994.

38. Kokame, K.; Matsumoto, M.; Fujimura, Y.; Miyata, T. VWF73, a region from D1596 to R1668 of von Willebrand factor, provides a minimal substrate for ADAMTS-13. *Blood*. 103:607-612; 2004.
39. Ewenstein, B.M.; Warhol, M.J.; Handin, R.I.; Pober, J.S. Composition of the von Willebrand factor storage organelle (Weibel-Palade body) isolated from cultured human umbilical vein endothelial cells. *J Cell Biol*. 104:1423-1433; 1987.
40. Gokce, I.; Woody, R.W.; Anderluh, G.; Lakey, J.H. Single peptide bonds exhibit poly(pro)II ("random coil") circular dichroism spectra. *J Am Chem Soc*. 127:9700-9701; 2005.
41. Lakowicz, J.R. Principles of fluorescence spectroscopy; Springer: New York: 2006.
42. Sadler, J.E.; Moake, J.L.; Miyata, T.; George, J.N. Recent advances in thrombotic thrombocytopenic purpura. *Hematology Am Soc Hematol Educ Program*. 407-423; 2004.
43. De Cristofaro, R.; Rocca, B.; Vitacolonna, E.; Falco, A.; Marchesani, P.; Ciabattoni, G.; Landolfi, R.; Patrono, C.; Davi, G. Lipid and protein oxidation contribute to a prothrombotic state in patients with type 2 diabetes mellitus. *J Thromb Haemost*. 1:250-256; 2003.
44. Orasanu, G.; Plutzky, J. The pathologic continuum of diabetic vascular disease. *J Am Coll Cardiol*. 53:S35-42; 2009.
45. Hink, U.; Li, H.; Mollnau, H.; Oelze, M.; Matheis, E.; Hartmann, M.; Skatchkov, M.; Thaiss, F.; Stahl, R.A.; Warnholtz, A.; Meinertz, T.; Griendling, K.; Harrison, D.G.; Forstermann, U.; Munzel, T. Mechanisms underlying endothelial dysfunction in diabetes mellitus. *Circ Res*. 88:E14-22; 2001.
46. Davi, G.; Ciabattoni, G.; Consoli, A.; Mezzetti, A.; Falco, A.; Santarone, S.; Pennese, E.; Vitacolonna, E.; Bucciarelli, T.; Costantini, F.; Capani, F.; Patrono, C. In vivo formation of 8-iso-prostaglandin f2alpha and platelet activation in diabetes mellitus: effects of improved metabolic control and vitamin E supplementation. *Circulation*. 99:224-229; 1999.
47. Gill, J.C.; Endres-Brooks, J.; Bauer, P.J.; Marks, W.J., Jr.; Montgomery, R.R. The effect of ABO blood group on the diagnosis of von Willebrand disease. *Blood*. 69:1691-1695; 1987.
48. Franchini, M.; Mannucci, P.M. Von Willebrand factor: another janus-faced hemostasis protein. *Semin Thromb Hemost*. 34:663-669; 2008.
49. Spiel, A.O.; Gilbert, J.C.; Jilma, B. von Willebrand factor in cardiovascular disease: focus on acute coronary syndromes. *Circulation*. 117:1449-1459; 2008.
50. Frankel, D.S.; Meigs, J.B.; Massaro, J.M.; Wilson, P.W.; O'Donnell, C.J.; D'Agostino, R.B.; Tofler, G.H. Von Willebrand factor, type 2 diabetes mellitus, and risk of cardiovascular disease: the framingham offspring study. *Circulation*. 118:2533-2539; 2008.
51. Zhang, Q.; Zhou, Y.F.; Zhang, C.Z.; Zhang, X.; Lu, C.; Springer, T.A. Structural specializations of A2, a force-sensing domain in the ultralarge vascular protein von Willebrand factor. *Proc Natl Acad Sci U S A*. 2009.

52. Sacksteder, C.A.; Qian, W.J.; Knyushko, T.V.; Wang, H.; Chin, M.H.; Lacan, G.; Melega, W.P.; Camp, D.G., 2nd; Smith, R.D.; Smith, D.J.; Squier, T.C.; Bigelow, D.J. Endogenously nitrated proteins in mouse brain: links to neurodegenerative disease. *Biochemistry*. 45:8009-8022; 2006.
53. Souza, J.M.; Peluffo, G.; Radi, R. Protein tyrosine nitration--functional alteration or just a biomarker? *Free Radic Biol Med*. 45:357-366; 2008.
54. 54 Fuentes-Prior, P.; Iwanaga, Y.; Huber, R.; Pagila, R.; Rumennik, G.; Seto, M.; Morser, J.; Light, D.R.; Bode, W. Structural basis for the anticoagulant activity of the thrombin-thrombomodulin complex. *Nature*. 404:518-525; 2000.
55. Gellman, S.H. On the role of methionine residues in the sequence-independent recognition of nonpolar protein surfaces. *Biochemistry.* 30:6633-6636; 1991.
56. Parastatidis, I.; Thomson, L.; Burke, A.; Chernysh, I.; Nagaswami, C.; Visser, J.; Stamer, S.; Liebler, D.C.; Koliakos, G.; Heijnen, H.F.; Fitzgerald, G.A.; Weisel, J.W.; Ischiropoulos, H. Fibrinogen beta-chain tyrosine nitration is a prothrombotic risk factor. *J Biol Chem*. 283:33846-33853; 2008.
57. Vogt, W. Oxidation of methionyl residues in proteins: tools, targets, and reversal. *Free Radic Biol Med*. 18:93-105; 1995.
58. Burns, E.R.; Lou, Y.; Pathak, A. Morphologic diagnosis of thrombotic thrombocytopenic purpura. *Am J Hematol*. 75:18-21; 2004.
59. Lowther, W.T.; Brot, N.; Weissbach, H.; Matthews, B.W. Structure and mechanism of peptide methionine sulfoxide reductase, an "anti-oxidation" enzyme. *Biochemistry*. 39:13307-13312; 2000.
60. Levine, R.L.; Mosoni, L.; Berlett, B.S.; Stadtman, E.R. Methionine residues as endogenous antioxidants in proteins. *Proc Natl Acad Sci U S A*. 93:15036-15040; 1996.
61. Stadtman, E.R.; Moskovitz, J.; Berlett, B.S.; Levine, R.L. Cyclic oxidation and reduction of protein methionine residues is an important antioxidant mechanism. *Mol Cell Biochem*. 234-235:3-9; 2002.
62. Leopold, J.A.; Loscalzo, J. Oxidative risk for atherothrombotic cardiovascular disease. *Free Radic Biol Med*. 2009.
63. Glaser, C.B.; Morser, J.; Clarke, J.H.; Blasko, E.; McLean, K.; Kuhn, I.; Chang, R.J.; Lin, J.H.; Vilander, L.; Andrews, W.H.; et al. Oxidation of a specific methionine in thrombomodulin by activated neutrophil products blocks cofactor activity. A potential rapid mechanism for modulation of coagulation. *J Clin Invest*. 90:2565-2573; 1992.
64. Wood, M.J.; Becvar, L.A.; Prieto, J.H.; Melacini, G.; Komives, E.A. NMR structures reveal how oxidation inactivates thrombomodulin. *Biochemistry*. 42:11932-11942; 2003.
65. Shacter, E.; Williams, J.A.; Levine, R.L. Oxidative modification of fibrinogen inhibits thrombin-catalyzed clot formation. *Free Radic Biol Med*. 18:815-821; 1995.
66. De Cristofaro, R.; Landolfi, R. Oxidation of human alpha-thrombin by the myeloperoxidase-H2O2-chloride system: structural and functional effects. *Thromb Haemost*. 83:253-261; 2000.

67. Lawrence, D.A.; Loskutoff, D.J. Inactivation of plasminogen activator inhibitor by oxidants. *Biochemistry*. 25:6351-6355; 1986.
68. Stief, T.W.; Aab, A.; Heimburger, N. Oxidative inactivation of purified human alpha-2-antiplasmin, antithrombin III, and C1-inhibitor. *Thromb Res*. 49:581-589; 1988.
69. Macfadyen, A.J.; Reiter, C.; Zhuang, Y.; Beckman, J.S. A novel superoxide dismutase-based trap for peroxynitrite used to detect entry of peroxynitrite into erythrocyte ghosts. *Chem Res Toxicol*. 12:223-229; 1999.
70. Pacher, P.; Beckman, J.S.; Liaudet, L. Nitric oxide and peroxynitrite in health and disease. *Physiol Rev*. 87:315-424; 2007.
71. Chen, J.; Fu, X.; Wang, Y.; Ling, M.; McMullen, B.; Kulman, J.; Chung, D.W.; Lopez, J.A. Oxidative modification of von Willebrand factor by neutrophil oxidants inhibits its cleavage by ADAMTS13. *Blood*. 2009.
72. Raife, T.J.; Cao, W.; Atkinson, B.S.; Bedell, B.; Montgomery, R.R.; Lentz, S.R.; Johnson, G.F.; Zheng, X.L. Leukocyte proteases cleave von Willebrand factor at or near the ADAMTS13 cleavage site. *Blood*. 114:1666-1674; 2009.
73. Ogawa, H.; Nakayama, M.; Morimoto, T.; Uemura, S.; Kanauchi, M.; Doi, N.; Jinnouchi, H.; Sugiyama, S.; Saito, Y. Low-dose aspirin for primary prevention of atherosclerotic events in patients with type 2 diabetes: a randomized controlled trial. *Jama*. 300:2134-2141; 2008.
74. Anfossi, G.; Russo, I.; Trovati, M. Resistance to aspirin and thienopyridines in diabetes mellitus and metabolic syndrome. *Curr Vasc Pharmacol*. 6:313-328; 2008.
75. Ando, K.; Fujita, T. Metabolic syndrome and oxidative stress. *Free Radic Biol Med*. 47:213-218; 2009.
76. Yin, H.; Liu, J.; Li, Z.; Berndt, M.C.; Lowell, C.A.; Du, X. Src family tyrosine kinase Lyn mediates VWF/GPIb-IX-induced platelet activation via the cGMP signaling pathway. *Blood*. 112:1139-1146; 2008.
77. Yin, H.; Stojanovic, A.; Hay, N.; Du, X. The role of Akt in the signaling pathway of the glycoprotein Ib-IX induced platelet activation. *Blood*. 111:658-665; 2008

APPENDIX

Appendix A

Abbreviations and Symbols

Å	Angstrom
aa	amino acid
Da	Dalton
DTT	Dithiothreitol
EDTA	Ethylene Diamino Tetracetic Acid
IPTG	IsoPropyl-β-D-ThioGalactopyranoside
LB	Luria Bertani liquid medium
MW	Molecular Weight
PEG	PolyEthylene Glycol
SDS	Sodium Dodecyl Sulfate
SDS-PAGE	SDS-PolyAcrylamide Gel Electrophoresis
ESI	Electrospray ionization
GlcNAc	N-Acetylglucosamine
HPLC	High-pressure liquid chromatography
m/z	Mass to charge ratio
MS	Mass spectrometry
RP	Reverse-phase
HPLC	High-pressure liquid chromatography
SEC	Size-exclusion chromatography
TFA	Trifluoroacetic acid
TOF	Time-of-flight
w/v	Weight/volume
UV	ultraviolet
Tris	Tris(hydroxymethyl)aminomethane
Pre2	Recombinant prethrombin-2
rThb	Recombinant human α-thrombin
hThb	Plasma-derived human α-thrombin
D102N	α-Thrombin containing the Asp102 → Asn mutation

Amino Acids

Ala	A	Alanine
Arg	R	Arginine
Asp	D	Aspartic acid
Asn	N	Asparagine
Cys	C	Cysteine
Gly	G	Glycine
Gln	Q	Glutamine
Glu	E	Glutamic acid
His	H	Histidine
Ile	I	Isoleucine
Lys	K	Lysine
Leu	L	Leucine
Met	M	Methionine
Phe	F	Phenylalanine
Pro	P	Proline
Ser	S	Serine
Thr	T	Threonine
Tyr	Y	Tyrosine
Trp	W	Tryptophan
Val	V	Valine

Appendix B

Thrombin Numbering Scheme

Chym	T1h	F1g	G1f	S1e	G1d	E1c	A1b	D1a	C1	G2	L3	R4
Ch-A	1	2	3	4	5	6	7	8	9	10	11	12
Ch-B	-	-	-	-	-	-	-	-	-	-	-	-
ProT	285	286	287	288	289	290	291	292	293	294	295	296

Chym	P5	L6	F7	E8	K9	K10	S11	L12	E13	D14	K14a	T14b
Ch-A	13	14	15	16	17	18	19	20	21	22	23	24
Ch-B	-	-	-	-	-	-	-	-	-	-	-	-
ProT	297	298	299	300	301	302	303	304	305	306	307	308

Chym	E14c	R14d	E14e	L14f	L14g	E14h	S14i	Y14j	I14k	D14l	G14m	R15
Ch-A	25	26	27	28	29	30	31	32	33	34	35	36
Ch-B	-	-	-	-	-	-	-	-	-	-	-	-
ProT	309	310	311	312	313	314	315	316	317	318	319	320

Chym	I16	V17	E18	G19	S20	D21	A22	E23	I24	G25	M26	S27
Ch-A	37	38	39	40	41	42	43	44	45	46	47	48
Ch-B	1	2	3	4	5	6	7	8	9	10	11	12
ProT	321	322	323	324	325	326	327	328	329	330	331	332

Chym	P28	W29	Q30	V31	M32	L33	F34	R35	K36	S36a	C37	Q38
Ch-A	49	50	51	52	53	54	55	56	57	58	59	60
Ch-B	13	14	15	16	17	18	19	20	21	22	23	24
ProT	333	334	335	336	337	338	339	340	341	342	343	344

Chym	E39	L40	L41	C42	G43	A44	S45	L46	I47	S48	D49	R50
Ch-A	61	62	63	64	65	66	67	68	69	70	71	72
Ch-B	25	26	27	28	29	30	31	32	33	34	35	36
ProT	345	346	347	348	349	350	351	352	353	354	355	356

Chym	W51	V52	L53	T54	A55	A56	H57	C58	L59	L60	Y60a	P60b
Ch-A	73	74	75	76	77	78	79	80	81	82	83	84
Ch-B	37	38	39	40	41	42	43	44	45	46	47	48
ProT	357	358	359	360	361	362	363	364	365	366	367	368

Chym	P60c	W60d	D60e	K60f	N60g	F60h	T60i	E61	N62	D63	L64	L65
Ch-A	85	86	87	88	89	90	91	92	93	94	95	96
Ch-B	49	50	51	52	53	54	55	56	57	58	59	60
ProT	369	370	371	372	373	374	375	376	377	378	379	380

Chym	V66	R67	I68	G69	K70	H71	S72	R73	T74	R75	Y76	E77
Ch-A	97	98	99	100	101	102	103	104	105	106	107	108
Ch-B	61	62	63	64	65	66	67	68	69	70	71	72
ProT	381	382	383	384	385	386	387	388	389	390	391	392

Chym	R77a	N78	I79	E80	K81	I82	S83	M84	L85	E86	K87	I88
Ch-A	109	110	111	112	113	114	115	116	117	118	119	120
Ch-B	73	74	75	76	77	78	79	80	81	82	83	84
ProT	393	394	395	396	397	398	399	400	401	402	403	404

Chym	Y89	I90	H91	P92	R93	Y94	N95	W96	R97	E97a	N98	L99
Ch-A	121	122	123	124	125	126	127	128	129	130	131	132
Ch-B	85	86	87	88	89	90	91	92	93	94	95	96
ProT	405	406	407	408	409	410	411	412	413	414	415	416

Chym	D100	R101	D102	I103	A104	L105	M106	K107	L108	K109	K110	P111
Ch-A	133	134	135	136	137	138	139	140	141	142	143	144
Ch-B	97	98	99	100	101	102	103	104	105	106	107	108
ProT	417	418	419	420	421	422	423	424	425	426	427	428

Chym	V112	A113	F114	S115	D116	Y117	I118	H119	P120	V121	C122	L123
Ch-A	145	146	147	148	149	150	151	152	153	154	155	156
Ch-B	109	110	111	112	113	114	115	116	117	118	119	120
ProT	429	430	431	432	433	434	435	436	437	438	439	440

Chym	P124	D125	R126	E127	T128	A129	A129a	S129b	L129c	L130	Q131	A132
Ch-A	157	158	159	160	161	162	163	164	165	166	167	168
Ch-B	121	122	123	124	125	126	127	128	129	130	131	132
ProT	441	442	443	444	445	446	447	448	449	450	451	452

Chym	G133	Y134	K135	G136	R137	V138	T139	G140	W141	G142	N143	L144
Ch-A	169	170	171	172	173	174	175	176	177	178	179	180
Ch-B	133	134	135	136	137	138	139	140	141	142	143	144
ProT	453	454	455	456	457	458	459	460	461	462	463	464

Chym	K145	E146	T147	W148	T149	A149a	N149b	V149c	G149d	K149e	G150	Q151
Ch-A	181	182	183	184	185	186	187	188	189	190	191	192
Ch-B	145	146	147	148	149	150	151	152	153	154	155	156
ProT	465	466	467	468	469	470	471	472	473	474	475	476

Chym	P152	S153	V154	L155	Q156	V157	V158	N159	L160	P161	I162	V163
Ch-A	193	194	195	196	197	198	199	200	201	202	203	204
Ch-B	157	158	159	160	161	162	163	164	165	166	167	168
ProT	477	478	479	480	481	482	483	484	485	486	487	488

Chym	E164	R165	P166	V167	C168	K169	D170	S171	T172	R173	I174	R175
Ch-A	205	206	207	208	209	210	211	212	213	214	215	216
Ch-B	169	170	171	172	173	174	175	176	177	178	179	180
ProT	489	490	491	492	493	494	495	496	497	498	499	500

Chym	I176	T177	D178	N179	M180	F181	C182	A183	G184	Y184a	K185	P186
Ch-A	217	218	219	220	221	222	223	224	225	226	227	228
Ch-B	181	182	183	184	185	186	187	188	189	190	191	192
ProT	501	502	503	504	505	506	507	508	509	510	511	512

Chym	D186a	E186b	G186c	K186d	R187	G188	D189	A190	C191	E192	G193	D194
Ch-A	229	230	231	232	233	234	235	236	237	238	239	240
Ch-B	193	194	195	196	197	198	199	200	201	202	203	204
ProT	513	514	515	516	517	518	519	520	521	522	523	524

Chym	S195	G196	G197	P198	F199	V200	M201	K202	S203	P204	F204a	N204b
Ch-A	241	242	243	244	245	246	247	248	249	250	251	252
Ch-B	205	206	207	208	209	210	211	212	213	214	215	216
ProT	525	526	527	528	529	530	531	532	533	534	535	536

Chym	N205	R206	W207	Y208	Q209	M210	G211	I212	V213	S214	W215	G216
Ch-A	253	254	255	256	257	258	259	260	261	262	263	264
Ch-B	217	218	219	220	221	222	223	224	225	226	227	228
ProT	537	538	539	540	541	542	543	544	545	546	547	548

Chym	E217	G219	C220	D221	R221a	D222	G223	K224	Y225	G226	F227	Y228
Ch-A	265	266	267	268	269	270	271	272	273	274	275	276
Ch-B	229	230	231	232	233	234	235	236	237	238	239	240
ProT	549	550	551	552	553	554	555	556	557	558	559	560

Chym	T229	H230	V231	F232	R233	L234	K235	K236	W237	I238	Q239	K240
Ch-A	277	278	279	280	281	282	283	284	285	286	287	288
Ch-B	241	242	243	244	245	246	247	248	249	250	251	252
ProT	561	562	563	564	565	566	567	568	569	570	571	572

Chym	V241	I242	D243	Q244	F245	G246	E247
Ch-A	289	290	291	292	293	294	295
Ch-B	253	254	255	256	257	258	259
ProT	573	574	575	576	577	578	579

In the first row the chymotrypsinogen numeration of thrombin is indicated; in the second row the numeration in which the first residue of the A-chain is designated as 1 is indicated.; in the third row the numeration in which the first residue of the B-chain is designated as 1 is indicated; finally, the last row show the numeration of prothrombin.

ACKNOWNLEDGMENTS.....

When I started this journey almost four years ago, I could not imagine to meet such special colleagues and friends. Consequently these acknowledgments are dedicated to all people who helped me to reach this important target.

First I'm very grateful to my supervisor, prof. Vincenzo De Filippis either as a mentor but especially as a man. Working in his lab I could grow as a researcher and further widen my passion for science. Thanks a lot.

A special acknowledgment goes to Dr. Daniele Dalzoppo for his thousands suggestions and for his never satisfactory willing to teach me every single, sometime strange, aspect of science.

Thanks to the only big universe boss Dr. Roberta Frasson, my "friend in thrombin trouble" or more simply a special friend.

Thanks to my lab family Daniela Galla, Fabio Maset, Davide Zaramella, Samuele Bettin, Laura Acquasaliente, Chiara D'Orlando, Isabella Perissinotto, Silvia Baiguera, Francesca Martorina and Marco Daniele for everything we spent together. It was really a nice ride.

Thanks to Dr. Stefano Lancellotti and Prof..Raimondo De Cristofaro for the wonderful collaborations and for the scientific projects we could join together.

Thanks to Dr. Alessandra Banzato, Dr. Elisa Bison and Dr.Vittorio Pengo for hosting me in their laboratory and for the trust they had in me. Dear Dr. Pengo next football match I promise you I will score....

Thanks to Dr. Barbara Spolaore for have performing some MS spectra.

And finally.....my best thanks go to my mum Lucia, my dad Fabrizio, my brother Stefano and especially to Wanna who supported and encouraged me every single day of my life. This thesis belongs to you, too.